UNIVERSITY OF CALIFORNIA, SAN DIEGO

Foraging ecology, biogeography, and population biology of seabird and toothed whale predators in the Anthropocene.

A dissertation submitted in partial satisfaction of the requirements for the degree Doctor of Philosophy

in

Oceanography

by

Trevor William Joyce

Committee in charge:

Professor Lisa Ballance, Co-Chair
Professor Paul Dayton, Co-Chair
Professor Carolyn Kurle
Professor Brice Semmens
Professor Jonathan Shurin
Professor Lynne Talley

2016

The Dissertation of Trevor William Joyce is approved, and it is acceptable in quality and form for publication on microfilm and electronically:

_____

_____

_____

_____

_____
Co-Chair

_____
Co-Chair

University of California, San Diego

2016

DEDICATION

To my mother, Lynn, and my wife, Maxine

TABLE OF CONTENTS

LIST OF TABLES

LIST OF FIGURES

ACKNOWLEDGEMENTS

I would first like to express my deep gratitude to my two advisors, Lisa Ballance and Paul Dayton. Each has provided me with support, encouragement, and deep insights throughout my doctoral program. Lisa has been a wonderful mentor, and despite her incredibly busy schedule, has always carved out time to help me with strategic decisions, funding applications, manuscript revisions, and regular check-ins. Paul has also contributed his vast knowledge of natural history, insightful feedback, and guidance in navigating the doctoral process. I would also like to gratefully acknowledge the members of my doctoral committee: Carolyn Kurle, Brice Semmens, Jonathan Shurin, Lynne Talley. Each has been very generous with their time and thoughtful in their feedback. My coauthors on the manuscripts presented in this dissertation and in particular John Durban, Diane Claridge, Holly Fearnbach and Robert Pitman have each contributed valuable data and provided great feedback.

I would also like to acknowledge the foundation in marine ecology instilled by the great Biological Oceanography (BO) faculty at SIO, and in particular Lisa Levin, Mark Ohman, Peter Franks, Jim Leichter, Paul Dayton, and Lisa Ballance. I would further like to thank the Gilbert Bretado, Joshua Reeves, Adam Peterson, Denise Darling, Maureen McGreevy, and Maureen Mccormack from the SIO graduate department for their help in navigating the Ph.D. process and for their friendly support of my many adventures.

Chapter 1, in full, is a reprint of the material as it appears in Marine Mammal Science 2016. Joyce, Trevor W.; Durban, John W.; Fearnbach, Holly; Claridge, Diane

E.; Ballance, Lisa T. The dissertation author was the primary investigator and author of this material.

Chapter 2, in full, is currently being prepared for submission for publication of the material. Joyce, Trevor W.; Durban, John W.; Claridge, Diane E.; Fearnbach, Holly; Andrews, Russel; Ballance, Lisa T. The dissertation author was the primary investigator and author of this material.

Chapter 3, in full, is currently being prepared for submission for publication of the material. Joyce, Trevor W.; Durban, John W.; Claridge, Diane E.; Ylitalo, Gina; Fearnbach, Holly; Ballance, Lisa T. The dissertation author was the primary investigator and author of this material.

Chapter 4, in full, is currently being prepared for submission for publication of the material. Joyce, Trevor W.; Pitman, Robert L.; Ballance, Lisa T. The dissertation author was the primary investigator and author of this material.

Chapter 5, in full, is currently being prepared for submission for publication of the material. Joyce, Trevor W.; Moore, Jeffrey E.; Pitman, Robert L.; Ballance, Lisa T. The dissertation author was the primary investigator and author of this material.

VITA

1999	Bachelor of Science, University of Alaska Southeast
2015	Master of Science, University of California, San Diego
2016	Doctor of Philosophy, University of California, San Diego

PUBLICATIONS

Joyce, T.W., Durban J.W., Fearnbach H., Claridge D.E. and Ballance L.T. 2016. Use of time-at-temperature data to describe dive behavior in five species of sympatric deep-diving toothed whales. Marine Mammal Science.

Troy, J.R., Holmes N.D., Joyce T.W., Behnke J. and Green M.C. 2016. Characteristics Associated with Newell's Shearwater (Puffinus newelli) and Hawaiian Petrel (Pterodroma sandwichensis) Burrows on Kauai, Hawaii, USA. Waterbirds.

Joyce, T.W., Eifler D.A. and Powell R. 2010. Variable habitat use influences the mating system of a Lesser Antillean anole. Amphibia-Reptilia. 31: 395-401

Joyce, T.W. 2013. Abundance estimates of the Hawaiian Petrel (Pterodroma sandwichensis) and Newell's Shearwater (Puffinus newelli) based on data collected at sea, 1998-2011. Technical Report to US Fish and Wildlife Service (pp. 31).

FIELDS OF STUDY

Major Field: Biological Oceanography (Marine Ecology)

Studies in Field Ecology
Studies in Animal Behavior
Professor Paul Dayton

Studies in Biologging and Biotelemetry
Studies in Seabird Biology
Studies in Marine Mammal Biology
Studies in Population Biology
Professor Lisa Ballance

ABSTRACT OF THE DISSERTATION

Foraging ecology, biogeography, and population biology of seabird and toothed whale predators in the Anthropocene

by

Trevor William Joyce

Doctor of Philosophy in Oceanography

University of California, San Diego, 2016

Professor Lisa Ballance, Co-Chair
Professor Paul Dayton, Co-Chair

The human capacity to expand niche breadth through cultural evolution has propelled humans into keystone ecological roles in many ecosystems. In particular terrestrial animal assemblages have experienced radical reductions in diversity and size distribution. Oceanic habitats have experienced shorter histories of exploitation and typically retain faunal assemblages that more closely resemble pre-human

Pleistocene assemblages. Although the direct harvest of many marine mammal and seabird species has diminished in recent decades, these assemblages now face an onslaught of novel human impacts in marine and oceanic island habitats. Stressors range from noise and chemical pollution to the introduction of invasive mammalian predators on oceanic islands. To develop a better understanding of how these disparate effects will impact the ecologies and conservation statuses of wide-ranging, dynamic, and patchy seabird and marine mammal populations, this dissertation leveraged the use of two extensive observational datasets collected by and in collaboration with the NOAA-NMFS Southwest Fisheries Science Center. In the first section (Chapters 1-3) I used satellite tag and biopsy sampling 1) to describe vertical habitat use and biogeographic distribution patterns, and 2) to develop a systematic framework to better understand foraging ecology trade-offs in seven species of toothed whales from the Bahamas. In the second section (Chapters 4-5) I have applied innovative modeling techniques to estimate population abundance and growth rate parameters using an extensive time series of seabird transect surveys. These parameters play critical roles in assessing population status and developing strategic management decisions.

INTRODUCTION

The capacity of anatomically and culturally modern humans to rapidly expand into novel niches and habitats through the cultural evolution of technological and social adaptations (Henrich and McElreath 2003) has led humans to assume keystone ecological roles in numerous ecosystems across the planet (O'Neill and Kahn 2000). One of the major impacts of the expansion of human technology, population, and range has been a reduction in the diversity and a rearrangement of the size distribution in many terrestrial animal assemblages relative to those that existed prior to human occupation (McCauley et al. 2015). Terrestrial and near-shore ecosystems on the African and Eurasian continents shared millions of years of co-evolutionary history with the ancestors of anatomically modern humans (Lyons et al. 2004, Surovell et al. 2005). However the expansion of humans beyond the range of earlier hominid ancestors brought anatomically modern humans with advanced toolkits and novel social organizations into contact with faunal assemblages lacking long histories of co-evolutionary adaptation (e.g., Australia/New Guinea, North and South America, New Zealand, Madagascar; Barnosky et al. 2004). This succession of contacts resulted in "a serial loss of mammals, birds, reptiles, and invertebrates" and radical modifications of terrestrial ecosystem function (McCauley et al. 2015). Since the advent of settled agricultural and coastal communities the pace of human population growth and technological advances (Kremer 1993), as well as the scale of terrestrial

and near-shore ecosystem modification have all rapidly increased (Sherratt 1983, Gignoux et al. 2011).

Over much of this geologically brief history of human range expansion and terrestrial ecosystem modification, oceanic ecosystems generally, though not exclusively (e.g., O'Connor et al. 2011), remained beyond the technological reach of intensive human resource use (McCauley et al. 2015). As a result of this comparatively short history of exploitation, oceanic habitats have typically experienced overall lower rates of known diversity loss when compared with terrestrial habitats at a global level (McCauley et al. 2015). With notable exceptions of a few marine mammal species (e.g., Caribbean monk seal, *Monachus tropicalis*, Steller's sea cow, *Hydrodamalis gigas*) and a substantially larger number of seabird species (e.g., great auk, *Pinguinus impennis*, large St. Helena petrel *Pterodroma rupinarum*, small St. Helena petrel *Bulweria bifax*; Scofield 2009), oceanic communities generally retain complements of medium to large animal species that more closely resemble pre-human assemblages, relative to the majority of terrestrial ecosystems outside of fragmentary habitats in Africa and Eurasia (McCauley et al. 2015). Despite this relatively limited number of known extinction events for marine megafuana, the relatively recent encounters of many oceanic animal assemblages with technologically advanced humans has resulted in numerous population declines, local extirpations, and reductions in previous ecological roles (Clapham et al. 2007, Worm and Tittensor 2011).

Historically the major human impacts on many marine mammal populations have resulted primarily from direct harvesting for food and other commodities (e.g., furs, lighting oils, industrial lubricants; Gambell 1976, Doroff et al. 2003, Turvey 2009).

This exploitation began as an extension of coastal marine animal harvesting dating to at least 164,000 years BP (Marean et al. 2007). Although the use of stranded cetaceans by coastal communities (Martin 1981) and some subsistence hunting likely go back hundreds to thousands of years (Reeves 2002), the intentional harvest of fully-aquatic cetaceans at a scale sufficient to demographically impact populations, likely began with the Bay of Biscay harvest of North Atlantic right whales by the Basque whalers in the 11th century (Aguilar 1986). Intensification and geographic expansion of cetacean exploitation coinciding with introduction of commercial and subsequently industrial whaling technologies, has brought a succession of cetacean populations to commercial extinction (Gambell 1976, Hilborn et al. 2003), if not outright demographic collapse and extirpation (Clapham et al. 2007).

Direct harvesting by humans has also played a role in the declines and extirpations of many seabird populations (Scofield 2009). However a potentially even greater impact on seabird populations, derives from our role as vectors for the dispersal of domesticated and commensal mammal species to oceanic islands (Scofield 2009). Over millions of years, some groups of seabirds have evolved body morphologies (e.g., limited terrestrial mobility), breeding ecologies (e.g., burrow or ground nesting), and life history adaptations (e.g., long lifespan, low reproductive

output) consistent with the isolation from terrestrial mammal dispersal offered by many oceanic islands (Lavers et al. 2010, Croxall et al. 2012). Like the initial contact of humans with novel continental faunal assemblages, the introductions of many mammalian predators (e.g., cats, rats, dogs, mongooses, pigs) and habitat modifiers (e.g., rabbits, goats, pigs) to island ecosystems, have rapidly scrambled these millions of years of co-evolutionary history. Because of high rates of endemism, these introductions have resulted in waves of extinction and extirpation events particularly during the Melanesian and Polynesian expansions into the islands of the Pacific, followed globally by the European Age of Exploration (Scofield 2009).

As the availability of alternative food stuffs, insulative clothing, lighting sources (Bopp 1983, Coleman 1995), and lubricants (Ackman et al. 1972, Gisser et al. 1975) have generally supplanted the broad societal use of marine mammal and seabird products (although these products are still locally very important in some subsistence economies; Reeves 2002), the direct harvest of many of these species has generally diminished to the point where it has a minimal impact on the demographic stability of populations (Reeves 2002). However, today marine mammals and seabirds face an exponential onslaught of novel human activities in marine and oceanic island habitats fueled by rapid technological changes and the expansion of a globalized economy (Kraus et al. 2005).

In contrast to the earlier phases of direct exploitation, many of the current impacts are inadvertent byproducts of 1) fisheries targeting non-cetacean and non-seabird species (Kraus et al. 2005), 2) industrial development of marine mineral and gas

infrastructure (Mate et al. 1994, Di Iorio and Clark 2010), 3) expansion of marine cargo transportation networks (Laist et al. 2001), and 4) military use and testing of acoustic detection technologies and underwater weaponry (D'Amico et al. 2009). In addition the marine habitats of seabirds and cetaceans are also being affected by spill-over effects from terrestrial land-use changes and industrial activities including: 1) increases in non-native mammal populations on islands, 2) dispersal of chemical and plastic pollutants (Law et al. 2010, Ericksen et al. 2013), and 3) anthropogenic CO_2 emissions (Humlum et al. 2012). Many species, though certainly not all, may lack the behavioral flexibility or sufficient time to co-evolve adaptations to these accelerating impacts.

Our understanding of the ecological impacts of these disparate technologies on impact seabird and marine mammal populations has lagged behind their deployment in marine ecosystems. To make concerted progress in conserving and facilitating the recovery of depleted populations we need to develop a better understanding of the foraging ecology, biogeography, and population biology of oceanic seabirds and marine mammals. However, these fields have historically been difficult to quantify for many oceanic seabirds and marine mammals because of 1) logistical barriers to accessing remote oceanic habitats, 2) wide-ranging, dynamic, patchy, and sparse distributions (McCauley et al. 2015), and 3) difficulty directly observing sub-surface foraging dynamics (Aoki et al. 2015) and seabird breeding sites on islands. Large, dynamic, and often trans-boundary ranges also generally limit the applicability of controlled experimental ecological approaches (exceptions: DeRuiter

et al. 2013). Large observational datasets encompassing extensive geographic areas and long time-series, such as those collected by and in collaboration with the NOAA-NMFS Southwest Fisheries Science Center, offer unique opportunities to develop better understandings of these fields of seabird and marine mammal biology.

Objectives

In the first section of my dissertation (chapters 1-3), I leverage a substantial set of satellite tag and biopsy sampling data collected from seven species of toothed whales in Bahamas to: 1) provide an improved description of vertical habitats and biogeographic distributions; 2) improve our understanding of morphological, physiological, and behavioral constraints and trade-offs affecting the foraging ecology of different toothed whale species. The results of these chapters will help to systematically understand the vulnerabilities and potentially the capacities of different tooth whale species to adapt to 1) acute acoustic disturbance (e.g., naval mid-frequency active sonar and percussive seismographic surveys, D'Amico et al. 2009) 2) chronic acoustic disturbance (e.g., vessel engine noise; e.g., Aguilar de Soto et al. 2006) 3) vessel strike hazard (Laist et al. 2001), 4) depth stratified pollution (e.g., heavy metals; Peterson et al. 2015).

In the second section of my dissertation (chapters 4-5), I leverage an extensive set of seabird transect surveys to develop a better understanding of the population biology of several seabird species in the order Procellariiformes endemic to the eastern and central Pacific. Specifically I estimated abundance and trend parameters

using Generalized Additive Models and Bayesian hierarchal (or mixed effects) state space models. These parameters play critical roles in assessing risk of extinction for listing decisions (IUCN 2001), and in strategically targeting limited conservation resources for these vulnerable seabirds

REFERENCES

Ackman, R.G., Hooper, S.N., Epstein, S. & Kelleher, M. (1972) Wax esters of barracudina lipid: a potential replacement for sperm whale oil. *Journal of the American Oil Chemists Society*, **49**, 378–382.

Aguilar, A. 1986. A review of old Basque whaling and its effect on the right whales (*Eubalaena glacialis*) of the North Atlantic. *Report to the International Whaling Commission*, **10**, 191-199.

Aguilar de Soto, N., Johnson, M., Madsen, P.T., Tyack, P.L., Bocconcelli, A. & Fabrizio Borsani, J. (2006) Does intense ship noise disrupt foraging in deep-diving cuvier's beaked whales (Ziphius cavirostris)? *Marine Mammal Science*, **22**, 690–699.

Aoki, K., Amano, M., Kubodera, T., Mori, K., Okamoto, R. & Sato, K. (2015) Visual and behavioral evidence indicates active hunting by sperm whales. *Marine Ecology Progress Series*, **523**, 233–241.

Barnosky, A.D., Koch, P.L., Feranec, R.S., Wing, S.L. & Shabel, A.B. (2004) Assessing the Causes of Late Pleistocene Extinctions on the Continents. *Science*, **306**, 70–75.

Bopp, A.E. (1983) The demand for kerosene: a modern Giffen good. *Applied Economics*, **15**, 459–468.

Clapham, P.J., Aguilar, A. & Hatch, L.T. (2008) Determining spatial and temporal scales for management: lessons from whaling. *Marine Mammal Science*, **24**, 183–201.

Coleman Jr, J.L. (1995) The American whale oil industry: A look back to the future of the American petroleum industry? *Nonrenewable Resources*, **4**, 273–288.

Croxall, J.P., Butchart, S.H., Lascelles, B.E.N., Stattersfield, A.J., Sullivan, B.E.N., Symes, A. & Taylor, P. (2012) Seabird conservation status, threats and

priority actions: a global assessment. *Bird Conservation International*, **22**, 1–34.

Di Iorio, L. & Clark, C.W. (2010) Exposure to seismic survey alters blue whale acoustic communication. *Biology letters*, **6**, 51–54.

Dirzo, R., Young, H.S., Galetti, M., Ceballos, G., Isaac, N.J. & Collen, B. (2014) Defaunation in the Anthropocene. *Science*, **345**, 401–406.

Doroff, A.M., Estes, J.A., Tinker, M.T., Burn, D.M. & Evans, T.J. (2003) Sea otter population declines in the Aleutian archipelago. *Journal of Mammalogy*, **84**, 55–64.

Gambell, R. (1976) World whale stocks. *Mammal Review*, **6**, 41–53.

Gignoux, C.R., Henn, B.M. & Mountain, J.L. (2011) Rapid, global demographic expansions after the origins of agriculture. *Proceedings of the National Academy of Sciences*, **108**, 6044–6049.

Gisser, H., Messina, J. & Chasan, D. (1975) Jojoba oil as a sperm oil substitute. *Wear*, **34**, 53–63.

Henrich, J. & McElreath, R. (2003) The evolution of cultural evolution. *Evolutionary Anthropology: Issues, News, and Reviews*, **12**, 123–135.

Hilborn, R., Branch, T.A., Ernst, B., Magnusson, A., Minte-Vera, C.V., Scheuerell, M.D. & Valero, J.L. (2003) State of the world's fisheries. *Annual review of Environment and Resources*, **28**, 359.

Kraus, S.D., Brown, M.W., Caswell, H., Clark, C.W., Fujiwara, M., Hamilton, P.K., Kenney, R.D., Knowlton, A.R., Landry, S., Mayo, C.A. & others. (2005) North Atlantic right whales in crisis. *Science*, **309**, 561–562.

Kremer, M. (1993) Population growth and technological change: one million BC to 1990. *The Quarterly Journal of Economics*, 681–716.

Laist, D.W., Knowlton, A.R., Mead, J.G., Collet, A.S. & Podesta, M. (2001) Collisions between ships and whales. *Marine Mammal Science*, **17**, 35–75.

Lavers, J.L., Wilcox, C. & Donlan, C.J. (2010) Bird demographic responses to predator removal programs. *Biological Invasions*, **12**, 3839–3859.

Lyons, S.K., Smith, * Felisa A. & Brown, J.H. (2004) Of mice, mastodons and men: human-mediated extinctions on four continents. *Evolutionary Ecology Research*, **6**, 339–358.

Marean, C.W., Bar-Matthews, M., Bernatchez, J., Fisher, E., Goldberg, P., Herries, A.I.R., Jacobs, Z., Jerardino, A., Karkanas, P., Minichillo, T., Nilssen, P.J., Thompson, E., Watts, I. & Williams, H.M. (2007) Early human use of marine resources and pigment in South Africa during the Middle Pleistocene. *Nature*, **449**, 905–908.

Martin, J. (1981) *Tonga Islands: William Mariner's Account: An Account of the Natives of the Tonga Islands in the South Pacific Ocean, with an Original Grammar and Vocabulary of Their Language*. Vava'u Press.

Mate, B.R., Stafford, K.M. & Ljungblad, D.K. (1994) A change in sperm whale (Physeter macroephalus) distribution correlated to seismic surveys in the Gulf of Mexico. *The Journal of the Acoustical Society of America*, **96**, 3268–3269.

McCauley, D.J., Pinsky, M.L., Palumbi, S.R., Estes, J.A., Joyce, F.H. & Warner, R.R. (2015) Marine defaunation: Animal loss in the global ocean. *Science*, **347**, 1255641.

O'Connor, S., Ono, R. & Clarkson, C. (2011) Pelagic Fishing at 42,000 Years Before the Present and the Maritime Skills of Modern Humans. *Science*, **334**, 1117–1121.

O'neill, R.V. & Kahn, J.R. (2000) Homo economus as a Keystone Species. *BioScience*, **50**, 333–337.

Reeves, R.R. (2002) The origins and character of "aboriginal subsistence" whaling: a global review. *Mammal Review*, **32**, 71–106.

Scofield, R.P. (2009) Procellariform extinctions in the Holocene: threat processes and wider ecosystem-scale implications. *Holocene extinctions*, 151–166.

Sherratt, A. (1983) The secondary exploitation of animals in the Old World. *World Archaeology*, **15**, 90–104.

Surovell, T., Waguespack, N. & Brantingham, P.J. (2005) Global archaeological evidence for proboscidean overkill. *Proceedings of the National Academy of Sciences*, **102**, 6231–6236.

Turvey, S.T. (2009) *Holocene Extinctions*. Oxford University Press.

Worm, B. & Tittensor, D.P. (2011) Range contraction in large pelagic predators. *Proceedings of the National Academy of Sciences*, **108**, 11942–11947.

CHAPTER 1:

Use of time-at-temperature data to describe dive behavior in five species of sympatric deep-diving toothed whales

TREVOR W. JOYCE, JOHN W. DURBAN, HOLLY FEARNBACH, DIANE CLARIDGE, LISA T. BALLANCE

Abstract

This paper develops and validates a method of using time-at-temperature (TAT) histograms from satellite transmitter tags to describe the dive activity patterns and approximate depth distributions of five deep-diving toothed whale species in the northern Bahamas. TAT histograms represent a bandwidth-conserving method of recovering a long-term proxy record of dive activity. However, using temperature to interpret TAT on a scale of approximate depths required the complex estimation of depths associated with the temperature boundaries separating TAT histogram bins in a dynamic oceanographic region. Here we evaluated the relative performance of four interpolation methods and a global reanalysis data assimilation model in estimating climatological isotherm depth surfaces and uncertainty within our study area. TAT-derived approximate time-at-depth (TAD) distributions aligned closely with directly observed TAD distributions from a smaller sample of depth-recording satellite tags deployed on separate individuals of each species. TAT-derived approximate depth distributions were also consistent with various published accounts for this suite of species. Estimating dive ranges and time budgets are important components of 1) understanding habitat overlap between species, 2) evaluating the potential role of these predators in meso- and bathypelagic ecosystems, and 3) assessing vulnerability

and exposure to anthropogenic impacts.

Introduction

Deep-diving toothed whales (Suborder: *Odontoceti*) elicit considerable interest due to their exceptional diving capacity and potential ecological importance as apex predators in meso- and bathypelagic ecosystems (Noren and Williams 2000, Tyack *et al.* 2006, Lavery *et al.* 2010). Direct examination of the diverse niches occupied by different species in the deep-diving toothed whale foraging guild have been hampered to date by difficulties in directly observing their foraging activities at depths (Macleod *et al.* 2003, Tyack *et al.* 2006, Hazen *et al.* 2011, Aoki *et al.* 2015). With minimal direct observations, vertical profiles of time spent at different depth and/or temperature strata in the water column can provide useful information to deduce differences in dive strategy and habitat use between species and sexes, as well as over diurnal cycles (Johnson *et al.* 2009). Moreover, deep-diving toothed whales in many regions are exposed to a range of potentially deleterious anthropogenic activities (Frantzis 1998, Laist *et al.* 2001, Cox *et al.* 2006, D'Amico *et al.* 2009). Thus, vertical distributions of time spent in the water column can also help monitor the relative exposures and responses of different species to anthropogenic threats.

Archival biologging instruments developed over the last 15 yr have considerably improved the understanding of the niche-spaces occupied by a growing number of deep-diving odontocete species. In particular, time-depth recording tags (TDR, *e.g.*, Hooker and Baird 1999), and digital acoustic recording tags (DTAG, *e.g.*,

Johnson and Tyack 2003) have contributed to detailed descriptions of time spent at different depths in the water column, and in the case of DTAGs descriptions of habitat use included the localization of search effort and prey capture attempts (Madsen *et al.* 2002, Miller *et al.* 2004*a*, Tyack *et al.* 2006, Watwood *et al.* 2006, Aguilar de Soto *et al.* 2008, Teloni *et al.* 2008). However, the close proximity required for deployment, and the lengthy follows necessary for the recovery of these platforms requires extensive investment and labor input, which ultimately limits sample sizes. Moreover the non-invasive attachment and high-sampling frequency of these technologies limits their deployment duration to short time windows (typically <24 h), constraining analyses of lower-frequency variations in behavioral patterns such as shifts over diurnal or lunar cycles. Here we explore the complementary use of a satellite-linked telemetry platform that can provide relatively long and continuous, though indirect, proxy records of dive patterns and approximate depth ranges.

Smart Position Only Tags (SPOT, Wildlife Computers, Inc., Redmond, Washington) and more recently developed depth-recording satellite transmitter tags (SPLASH, Wildlife Computers, Inc., Redmond, Washington), both provide satellite telemetry estimates of animal position through time using the Argos-satellite system (www.Argos-system.org). These small tags (49g & 63g, respectively) have become particularly useful for studies of cetaceans when implemented in the Limited Impact Minimally Percutaneous External Electronic Transmitters configuration (LIMPET; Andrews *et al.* 2008), because they can be reliably projected onto the dorsal fins of cetaceans from distances up to 25m, greatly increasing the range of species that can

be monitored using telemetry (Baird *et al.* 2011, Schorr *et al.* 2010, Durban and Pitman 2012). In addition to returning position information, SPOT tags can also be programmed to transmit highly compressed periodic records of the proportion of time that diving animals spend in different user specified temperature strata within the water column. These summaries, in the form of time-at-temperature (TAT) frequency histograms, can be interpreted directly in terms of the thermoregulatory costs imposed by exposure to different water temperatures. However, in regions where the gradient of water-temperature with depth has been measured and is relatively consistent temporally, TAT summaries can also be used as proxies for time-at-depth, providing a useful source of information on diving behavior and time budgets.

In this study we developed and validated an approach for using TAT summaries to describe and compare the diving activity of five odontocete species within the Great Bahama Canyon, in the northern Bahamas. Considerable research interest has been focused in this region in response to a mass stranding event of beaked whales in 2000, coincident with naval sonar exercises (Balcomb and Claridge 2001, Cox *et al.* 2006), and subsequent research showing behavioral responses Blainville's beaked whales (*Mesoplodon densirostris*) to sonar exposure at the US Navy's Atlantic Test and Evaluation Center (AUTEC) within this canyon system (McCarthy *et al.* 2011, Tyack *et al.* 2011, Moretti *et al.* 2014). A number of other species of deep-diving whales regularly occur in this region and are also potentially exposed to sonar sources, highlighting the need to fill key gaps in our understanding of their behavioral ecology in order to manage their vulnerabilities.

Here, we compare a range of approaches to empirically describe the depths of isotherms separating TAT histogram categories across our study region and use temperature as a proxy to describe the proportion of time these animals spend in different estimated depth strata. Subsequently, we validate the approximate depth distributions derived from TAT by comparing the estimated vertical habitat use patterns with directly observed depth distributions from a small sample of SPLASH model LIMPET tags. These SPLASH tags were deployed in parallel with SPOT tag deployments in the later years of the study on the same suite of species in the same habitats. Due to their lighter weight, lower battery consumption, and limited transmission bandwidth requirements, SPOT tags typically provided longer and more continuous record of dive activity than SPLASH tags in this study. TAT derived approximate depth distributions thus complemented the direct descriptions of dive behavior from SPLASH tags. Additionally, developing and validating this method allowed us to make use of a substantial legacy data set from SPOT tags that had accrued before SPLASH models became commercially available, and thus to more fully use all available data to fill key information gaps for deep-diving cetaceans in this strategic region.

Methods

Study Area

This study was conducted in the Great Bahama Canyon region of the Bahamas archipelago in the western North Atlantic Ocean, between 23ºN and 27ºN, and 76ºW

and 79ºW. Tagging of five odontocete species was carried out in the deep-water channels of the NE and NW Providence Channels and Tongue of the Ocean (Fig. 1). Importantly for the estimation of isotherm depths, this study area is embedded within the western boundary current system of the North Atlantic Subtropical Gyre (Hamilton *et al.* 2005), and is situated between the Antilles Current (Lee *et al.* 1996, Olson *et al.* 1984) flowing along the eastern slope of the Bahamas archipelago, and the Florida Current flowing through the Florida Strait to the west of the study area (Hamilton *et al.* 2005, Wang and Mooers 1997). The northeast and northwest Providence Channels are open to both of these currents, although constricted by a shallow sill (664 m) near the western end of the NW Providence Channel, and thus a time-varying volume transport of 0.9-1.3 Sv (10^6 m^3/s) has been estimated to flow from east to west through this channel (Wang and Mooers 1997, Hamilton *et al.* 2005, Beal *et al.* 2008). Below ~800 m, along the eastern slope of Little Bahama Bank at 26.5ºN, a deep western boundary current with a highly variable net southward flow has been measured from the shelf slope out to the eastern edge of the study area (Johns *et al.* 2008).

Study Species and Tagging

The telemetry data used in this analysis were collected over a 5-year period (2009-2014) and comprised deployments of small Argos satellite transmitters on five species of odontocetes: melon-headed whale (*Peponocephala electra*), short-finned pilot whale (*Globicephala macrorhynchus*), sperm whale (*Physeter macrocephalus*),

Cuvier's beaked whale (*Ziphius cavirostris*), and Blainville's beaked whale (*Mesoplodon densirostris*). Whales were located using visual search effort following a mixture of line transect and *ad hoc* survey techniques from platforms ranging from small boats to large research ships, as well as passive acoustic monitoring using either a towed hydrophone array (Gillespie *et al.* 2009) or a fixed array on the AUTEC range (McCarthy *et al.* 2011). Two models of LIMPET satellite transmitting tags were used: SPOT (AM-S240A-C, Wildlife Computers Inc.; *e.g.*, Andrews *et al.* 2008) and SPLASH (Mk-10, Wildlife Computers Inc.; *e.g.*, Schorr *et al.* 2014). These tags were attached on or near the dorsal fins of free-ranging cetaceans using two minimally-invasive 4.5-6.5 cm surgical grade titanium darts that were projected using a crossbow bolt from distances of 5-25 m. During intervals when these animals surfaced to breathe and exposed their dorsal fins above the surface, the tags transmitted a series of messages to overhead Argos satellites (www.Argos-system.org) which allowed the calculation of location estimates with associated error ellipse estimates. These messages also delivered a limited quantity of dive behavior data collected and summarized internally within the tag.

Dive information transmitted by SPOT tags were derived from a thermistor, whereas SPLASH tags combined pressure sensor and thermistor measurements. SPOT tag models transmitted a condensed summary of temperature readings collected at 10-second intervals, typically over a 6-hour period (29/36 tags returned partial 1-5 h summaries at the beginnings of deployments). SPOT temperature summaries were transmitted in the bandwidth-conserving format of TAT histograms,

in which the proportion of time spent within 12 user-defined temperature categories (<4ºC, 4-6ºC, 6-8ºC, 8-10ºC, 10-12ºC, 12-14ºC, 14-16ºC, 16-18ºC, 18-20ºC, 20-22ºC, 22-24ºC and ≥24ºC) was represented as a percentage of all observations within the sampling period. We compared TAT data sets from each species with small samples (see below) of dive depth observations from more expensive (1.64x cost) SPLASH tags. As Argos bandwidth-allowed, these SPLASH tags uploaded time series of depth observations with a sampling interval of 2.5-minutes. In addition to dive data, SPLASH tags occasionally transmitted coarse resolution profiles of depth and temperature (PDT), each containing minimum and maximum of temperature observations over a 12-hour sampling period on 8 depth levels evenly spaced over the dive range of each specific tagged animal over this sampling period. The midpoints between minimum and maximum PDT temperature readings on each depth level were employed in conjunction with hydrographic survey data in estimating the depths of isotherms defining the boundaries of TAT histogram categories (see Isotherm Depth Estimation).

Location Estimation

Estimating the movements of tagged cetaceans through space proved to be an important initial step both in incorporating PDT data into spatial models of isotherm depths, and in predicting isotherm boundaries at the mean locations of TAT histograms. To estimate the maximum likelihood path of each tracked individual through space, while accounting for Argos location estimates of varying precision, we

used the R package *crawl* (Johnson *et al.* 2013) to fit a Continuous Time Correlated Random Walk (CTCRW, Johnson *et al.* 2008) assuming the estimated error radii represented the standard deviations of normally distributed errors about each location (*e.g.*, Ford *et al.* 2013). Following initial model fitting, the measurement error shock diagnostic of de Jong and Penzer (1998) was used to eliminate significant outliers (*P*-value ≤0.01), and the model was refitted to estimate a movement track for each whale. Tags for this study were scheduled to transmit up to 700 times during 12-18 h of each day, timed to coincide with passes of satellites from the Argos satellite system. Location estimates from Argos system were therefore irregularly spaced, and we used the second run of CTCRW to predict locations at regular hourly increments over the duration of the track. The mean location of tags over TAT (6 h) and PDT (12 h) summary periods were calculated as the mean of hourly maximum likelihood CTCRW location predictions (Figs. 1 & 2).

Isotherm Depth Analysis

To interpret TAT summaries of cetacean dive behavior on a biologically meaningful and intercomparable scale of depth, we applied a range of statistical methods to estimate the climatological (*i.e.*, long-term mean) depth of isotherms defining the temperature boundaries of TAT histogram categories. To simultaneously account for spatial and temporal components of isotherm depth variability, we compared these climatological estimates based on direct observations to time and location specific potential temperature outputs from the Hybrid Coordinate Ocean

Model (HYCOM) 1/12º global reanalysis. This reanalysis employed Navy Coupled Ocean Data Assimilation and an ocean generalized circulation model to produce daily estimates of ocean state variables (*e.g*., potential temperature, potential salinity) on 40 standard depth levels over the period 1992 to 2014 (Chassignet *et al*. 2007). The observational data used in estimating isotherm depths included coarse depth-resolution PDT profiles from SPLASH tags as well as moderate to high vertical-resolution, quality-controlled hydrographic profile data from vessel-based conductivity-temperature-depth instruments (CTD), and drifting neutrally buoyant profiling floats (PFL) that were both extracted from the World Ocean Database (WOD) online repository on 7 July 2014 (http://www.nodc.noaa.gov/OC5/SELECT/dbsearch/dbsearch.html). Although extensive CTD sampling dating to 1968 was available within the study area, we avoided sampling conducted prior to the advent of civilian GPS technology (~1990) because of the insufficient precision of CTD locations based on pre-GPS navigation tools.

A two-step process was applied in estimating the climatological depths of the relevant isotherms (4-24ºC in 2ºC increments). First the depth of each isotherm was estimated in the vertical *z*-dimension within each profile using a linear approximation between the temperature/depth observations bracketing the i^{th} isotherm. An identical procedure was applied to estimate the depth of the i^{th} isotherm from 40 standard depth levels of potential temperature predictions (0 m, 2 m, 4 m, 6 m, 8 m, 10 m, 12 m, 15 m, 20 m, 25 m, 30 m, 35 m, 40 m, 45 m, 50 m, 60 m, 70 m, 80 m, 90 m, 100 m, 125

m, 150 m, 200 m, 250 m, 300 m, 350 m, 400 m, 500 m, 600 m, 700 m, 800 m, 900 m, 1,000 m, 1,250 m, 1,500 m, 2,000 m, 2,500 m, 3,000 m, 4,000 m, and 5,000 m) in each cell of HYCOM reanalysis (GLBu0.08) raster outputs. Using the observational data, the i^{th} isotherm was subsequently interpolated in *x*- and *y*-dimensions over the study area using 1) an overall mean depth, 2) grid cell mean depths at 0.1º, 0.5º, and 1.0º latitude and longitude resolutions, and 3) spatial models of isotherm depth. This two-step approach reduced the dimensions and complexity of isotherm depth interpolation and limited the degrees of freedom needed to fit isotherm depth models with respect to a three-dimensional model of thermal structure. However, in low-resolution PDT profiles which contained only eight temperature-depth observations per profile, linear approximation between widely spaced data points introduced artifacts (see Fig. 2) where the slope of the thermocline abruptly changed, such as at the 18-20ºC subtropical mode water thermostad and at the 6ºC base of the thermocline. To reduce this potential source of bias, PDT observations were excluded from spatial interpolations of the 20ºC and 6ºC isotherms, but were maintained in the remaining isotherm interpolations where they supplemented CTD and PFL sampling coverage within the otherwise sparsely sampled NW Providence Channel and Tongue of the Ocean (Fig. 2).

The goal of implementing interpolation methods more complex than a single overall mean isotherm depth in the study area (calculated using all available observational data), was to improve the precision of isotherm depth predictions by accounting for the spatial and/or temporal processes affecting the climatological

depth field of each isotherm. To account for the spatial component of the isotherm depth field variability, we first applied a grid-averaging approach, in which point observations were organized into grids covering the study area with cell dimensions of 1.0º, 0.5º, and 0.1º of latitude and longitude. Where present, the mean of all observations was calculated in each grid cell.

Using the linearly approximated depth of the i^{th} isotherm (z_i) within each profile as a response variable, we fitted initial quadratic linear (LM) and generalized additive models (GAM) including five covariates, as well as interactions between each pair of covariates (Trossman *et al.* 2011). We used latitude (y), longitude (x), and Julian date (t, *i.e.*, numerical day within year) as initial covariates to explicitly model the spatial and seasonal components of variability in climatological z_i. We also evaluated the use of several proxy covariates to improve the representation of narrow topography-following features in LM and GAM based on the example of Roemmich and Gilson (2009). These covariates included distance-across-the-Providence-Channel (d_{chan}) and distance-from-the-Florida- Straight (d_{flst}) in the upper water column (>24ºC to 10ºC). Distance across the Providence Channel (d_{chan}) provided a proxy for a gradient of isotherm depths within the thermocline (10-18ºC) across the NE and NW Providence Channels resulting from a mean geostrophic flow of 0.9-1.3 Sv between the Antilles Current and Gulf Stream (Wang and Mooers 1997, Hamilton *et al.* 2005, Beal *et al.* 2008). Distance to the Florida Strait (d_{flst}) was similarly introduced as a proxy representing a time-varying recirculation of the Florida Current in the NW Providence Channel. The proxy variables d_{chan} and d_{flst} were calculated as

minimum geodesic distances from the 50 m isobath surrounding Little Bahama Bank (Fig 1.), and a line traversing the western mouth of the NW Providence Channel (79.25W 25.96N to 79.20W 27.10N, Fig 1), respectively. These distances were calculated using the function *gdist* in the *R* library *Imap* (Wallace *et al.* 2012) and a geographic coordinate system based on the World Geodetic Survey 1984 datum. Distance-across-the-Providence-Channel (d_{chan}) was capped at the maximum breadth of the NE and NW Providence Channels (84.3km). In modeling isotherms at depths of 10ºC and colder, simplified initial specifications of GAMs did not include day-of-year or either of the distance proxies due to insufficient degrees of freedom given the relatively small number of profiles reaching these isotherms.

The optimal specification of quadratic LM for each isotherm was selected on the basis of Akaike's Information Criterion (AIC) score through a stepwise forward and backward covariate selection process implemented in the function *StepAIC* from the R library *MASS* (Venables and Ripley 2002). GAMs of the i^{th} isotherm depth were fitted using univariate cubic shrinkage splines with a maximum of 3 degrees of freedom (df) and bivariate thin-plate shrinkage splines with a maximum of 20 df in the R library *mgcv* (Wood 2006). Shrinkage splines permit the effective degrees of freedom assigned by the *gam* algorithm to any smooth term to be penalized to 0, allowing *mgcv* to select an additive combination of predictors that minimizes generalized cross validation scores without resorting to a stepwise forward/backward variable selection process (Wood 2006). After fitting the quadratic linear model, Objective Analysis (OA) was implemented to interpolate the residual spatial

autocorrelation left over after accounting for model covariates (Thomson and Emery 2014). This approach applies a Gauss-Markov function (Roemmich 1983), with parameters of decorrelation length scales in *x*- and *y*-dimensions and a signal-to-noise ratio, to weight the influence of nearby points as a function of proximity to the interpolation location (Mcintosh 1990, Trossman *et al.* 2011). Decorrelation length scales were set at 84.3 km, which corresponded to the maximum perpendicular width of the NE and NW Providence Channels and Tongue of the Ocean.

To compare the relative predictive performance of various interpolation methods, we applied a 10-fold cross-validation to the overall mean, grid cell means, spatial models of isotherm depth, and objective analysis interpolations to determine which method provided the most accurate, general, and precise prediction of the i^{th} isotherm depth as well as an estimate of the uncertainty at the specific location and time of each TAT histogram. Point observations of each isotherm were randomly sorted into 10 subsets and subsequently an overall mean, grid means, LM, GAM, and OA models were fitted on the basis of nine out of 10 subsets. Predicted isotherm depths from these models were then compared with observed isotherm depth in the remaining subset, and this process was repeated such that each subset was used once as test data and 9 times as training data. We compared five interpolation methods based on their utility in reducing the mean squared cross-validation prediction error ($MSPE_i$) relative to the MSPE of an overall mean.

$$MSPE_i = \frac{1}{n} \cdot \sum_{j=1}^{n} (Observed_{i,j} - Predicted_{i,j})^2 \qquad \text{Eq. 1}$$

HYCOM-estimated isotherm depths were similarly compared to other interpolation methods based on MSPE scores. For individual TAT histograms, each representing a unique location and date combination, the depth of the i^{th} isotherm was predicted by the interpolation/reanalysis method that best minimized $MSPE_i$, while the overall range of observed depths at a given isotherm within the study area was used as an estimate of the uncertainty. When comparing two or more TAT histograms spanning multiple locations and dates, the depth of the i^{th} isotherm was estimated by calculating a median of 0.05º grid cell predictions from the best interpolation method specific to the i^{th} isotherm over the study area.

Validation of TAT

To validate the rescaling of TAT histograms from temperature to approximate depth categories, we compared the vertical distribution of dive activity inferred from TAT histograms with a small sample (see below) of time-at-depth (TAD) summaries of the directly observed depth time series data available from SPLASH tags deployed on each study species. TAD summaries were assembled from depth time series observations collected at 2.5-minute intervals and were subsequently organized into six-hour blocks starting at 0100, 0700, 1300, or 2100 local time (identical to TAT start times). From each six-hour block, a 12-category TAD histogram was calculated with depth breaks drawn from median best interpolation model predictions over the study area. Uploading full depth time series from SPLASH tags over the Argos satellite network required significantly greater transmission bandwidth than was

typically available during relatively short surface intervals, thus very few six-hour blocks contain a complete and continuous depth time series. To qualitatively compare the vertical distributions of dive activity for each species inferred from TAT histograms to the time series of TAD histograms, we generated vertically stacked horizontal box-plots. These plots generally consisted of all the TAD histograms for a given species where the time series contained at least 50% (≥72/144) of the possible observations per 6-hour block. Because this 50% threshold excluded all but one TAD sample for *P. electra*, a lower threshold of 25% (≥36/144) of observations per time block was applied to this species only. In *P. electra* and *Z. cavirostris* the limited TAD histograms data available substantially over-represented daytime and nighttime sampling, respectively. To compare these samples of TAD histograms to TAT observations that roughly overlapped in time-of-day, we restricted both TAD and TAT used in the box plot comparison for these species to only daytime and nighttime records, respectively.

TAT and TAD samples, each containing multiple histograms per species, were evaluated for dissimilarity in the distribution of time spent within different depth strata using a nonparametric mixed-effects permutational multivariate analysis of variance (perMANOVA) implemented in the program PRIMER+ (Clarke 1993). Before applying the perMANOVA test, categories representing the proportion of time spent within different temperature/depth strata were transformed into independent vectors using a centered log-ratio transformation (Aitchison 1986) implemented in the R package *compositions* (van den Boogaart and Tolosana-Delgado 2008). With two

exceptions (a female and a subadult male sperm whale), each individual animal carried only one type of instrument, thus individual variability was treated as a random effect variable nested within each tag type. We then tested whether a fixed effect of tag type (*e.g*., approximate temperature-based *vs*. directly-observed) resulted in different multivariate distributions of time-at-depth within each species.

Results

Sampling

Over a 5-year period (2009-2014), SPOT model telemetry and temperature recording tags were deployed on 46 individuals of five species of odontocete cetaceans (Table 1), with data collected widely throughout the study area (Fig. 1). From 2011-2014, 28 SPLASH model telemetry, pressure, and temperature recording tags were deployed on individuals of the same five species (Table 1). SPOT tags were attached to multiple individuals within a group on 23 occasions for four species (*P. macrocephalus*, *G. macrorhynchus*, *P. electra*, and *M. densirostris).* Tracks of these individuals show highly correlated post deployment movements suggesting at least short-term persistence of social groups in these species (maximum tag duration: 92 d). Assuming a degree of dive synchrony within social groups (Pirotta *et al.* 2012, Aoki *et al.* 2013), the number of completely independent samples of dive behavior was thus less than the total number of tags attached (Table 1). Mean transmission durations of SPOT tags varied between 8.2 d for *P. macrocephalus* and 23.7 d for *Z. cavirostris*. Over this deployment period a total of 1,539 TAT histogram summaries

were recovered, representing 9,115 h of dive activity across all species. TAT samples were primarily recovered from *P. macrocephalus*, *G. macrorhynchus*, and *P. electra* because of a programmatic emphasis on deploying SPLASH rather than SPOT tags on both beaked whale species (Table 1). Due to transmission bandwidth constraints during short surface intervals, only 216 six-hour TAD summaries that were at least 50% complete were recovered, representing 1,296 h (896 h of raw depth time series sampling) of dive activity across all species. Over the period 2011-2014, 158 PDT profiles were recovered from 20 SPLASH tags on the basis of 12 h of temperature and depth sampling per profile.

Querying WOD for hydrographic profile data within our study area on July 7, 2014 returned 920 CTD casts over the period 1990-2013 and 899 PFL profiles from 2004 through 2013. The majority of CTD casts in our study area derived from repeat hydrographic sampling of the 26.5ºN transatlantic RAPID-MOCHA transect (Fig. 2, right; *e.g.*, Smeed *et al.* 2014) in the NE corner of our study area, as well as a transect traversing the western entrance of the NW Providence Channel, with a minority of these CTD casts detailing hydrography within the interior of deep-water channels interspersed between the Bahamas banks (Fig. 2, right). The majority of PFL profiles in our study area were derived from multiple Argo floats that were advected into the eastern entrance of the NE Providence Channel and penetrated as far as the northern Tongue of the Ocean (Fig. 2, right). In addition, the 146 PDT profiles recovered *via* Argos satellites helped in filling some important gaps in the spatial coverage of our study area particularly in NW Providence Channel and in TOTO.

Location Estimation

TAT and TAD histogram locations calculated as a mean of hourly CTCRW-predicted locations are shown in Figure 1. The mean locations of *G. macrorhynchus*, *P. electra*, and *P. macrocephalus* TAT and TAD histograms reveal expansive dispersal and movement across the study area both over shelf-slope and deep-basin habitats. In contrast, tracks from SPOT tags and the more numerous SPLASH tags deployed on *Z. cavirostris* and *M. densirostris* indicate concentrations of activity over the shelf-slope and suggest moderate and limited dispersal, respectively. Tagged cetaceans, with the exception of five *G. macrorhynchus* individuals from two social groups and one *P. macrocephalus* individual, remained in the study area over the duration of tag battery and/or attachment life, and activity outside the study area was excluded from comparisons of TAT distributions due to significantly divergent thermal structure of the water column outside of the study area.

Isotherm Depth Analysis

Simultaneously plotting all of the temperature profile data with respect to depth revealed that, with the exception of the seasonally variable mixed layer (23-29ºC), the subtropical mode water (18ºC), and the North Atlantic Deep Water (NADW, <4ºC), temperature declined nearly linearly as a function of depth between 150 and 1,200 m depth (Fig. 2a). This approximately linear decline of temperature over much of the vertical range used by the five species of deep-diving odontocetes

sampled in this study provided considerable resolution to differentiate the depth ranges of TAT histograms bins. However, the overlay of boxplots at the relevant temperature boundaries between 4ºC and 24ºC on top of the aggregate profiles (Fig. 2a) illustrates the considerable variation in isotherm depth across the study area, ranging from 542.8 m (1,273.1-1,815.9 m) at the 4ºC isotherm to <172.1 m (76.9-249.0 m) at the 22ºC isotherm. At least part of this variation is related to consistent spatial and/or temporal processes. A portion of the variability in the depth of the 22 and 24ºC isotherms is attributable to seasonal variation in the depth of the mixed layer, which can extend as deep as 150 m and as cold as 23ºC in winter (Fig. 2, left). Furthermore, the vertical spreading of profiles between the 18ºC subtropical mode water thermostad and approximately 10ºC reflects geostrophic flows between these isotherms 1) along the eastern slope of Great and Little Bahama Banks and 2) through the NE and NW Providence Channels (Fig. 2a).

The interpolation approach of taking the mean of observations within grid cells begins, at a coarse resolution, to address the spatial component of variability in climatological isotherm depth fields (Fig. 3, b). Grid cell mean isotherm depths calculated at the 0.5º spatial resolution provided the greatest detail to resolve the spatial component of isotherm depth field variability (Fig. 3b), while still providing gapless coverage over almost all of the study area. This grid resolution revealed a deeper pool of warm water (14 ºC) in the western N. Atlantic subtropical gyre to the east of the study area, as well as some indication of a temperature gradient along the eastern edge of the Bahamas banks and through the NW Providence Channel. The

0.1º resolution interpolation (not shown in Fig. 3) was more accurate than the 0.5º at the scale of individual TAT histograms, but was of limited utility as a general interpolation of the isotherm depth field due to numerous missing values in grid cells where observational data was not available. Conversely, the 1.0º grid resolution (also not shown) was too coarse to resolve gradients across the narrow interior channels between Bahamas banks.

Explicitly modeling the variation in isotherm depths using LM, GAM, and Objective Analysis improved the resolution of the climatological isotherm depth fields with respect to a single overall mean (Table 2), while simultaneously accounting for both spatial and temporal components of variability. Spatial and temporal covariates including Julian date and the interaction of latitude and longitude were selected as significant correlates explaining a portion of the variation in the depth field of the 20-24ºC isotherms in both GAM and LM. Spatial covariates including the interaction of latitude and longitude, distance across the Providence Channels, and distance to the Florida Strait improved the prediction of 10-18ºC isotherm depths in GAM and LM (Table 2). Below 10ºC, the interaction of latitude and longitude proved to be the most important covariate in GAM fits. Spatial autocorrelation was indicated in the 10-18ºC LM residuals and 14-16ºC GAM residuals, thus Objective Analysis was implemented at these depths (Table 2). The comparison of isotherm depth predictions and HYCOM reanalysis climatology in Figure 3 shows a qualitative correspondence between the observed depths and the isotherm depth fields predicted by grid cell means, reanalysis outputs, and the various

model based interpolation methods. This visual correspondence is confirmed by pairwise Pearson correlation coefficients between different prediction methods ranging, for example, from 0.80 and 0.88 in the 16ºC isotherm (Table 3).

The relative utility of various interpolation models and HYCOM reanalysis outputs in improving the prediction of isotherm depths at unobserved locations and times is illustrated through the comparison of cross-validation and reanalysis prediction errors in Table 2. In particular, the increase in the precision and decrease in the MSPE using GAM, LM, and Objective Analysis depth predictions between 10ºC and 18ºC relative to an overall mean and grid cell mean at these isotherms reflects the greater utility of these models in predicting the spatial structure associated with geostrophic currents at these depths. The climatological view of HYCOM outputs reveals the same general spatial patterns of isotherm depths as the other interpolation methods, which is corroborated by relatively high correlation coefficients shown in (Table 3). However, as indicated by the generally much larger MSPE values (Table 2), as well as the depth contours in Figure 3, the HYCOM outputs exhibited a systematic shallow bias with respect to the directly observed isotherm depths. The best models selected for each isotherm of interest on the basis of MSPE (Table 2) were quadratic LM between 22ºC and 24ºC, GAM at 20ºC, and quadratic LM with objective analysis between 4ºC and 18ºC. These models were subsequently used to estimate depth and uncertainty of isotherm boundaries at TAT locations. Study-area wide medians of isotherm depth fields predicted from these models at a 0.05° grid cell resolution were subsequently used in the depth scales shown in Figures 4 and 5.

These median predicted isotherm depths (Fig. 4 *c, f*) yielded very similar behavioral patterns to spatially varying estimates of isotherm depths (Fig. 4 *b, e*), even when individuals ranged widely within the study area (Fig. 4 *d-f*).

Validation and Interpretation of TAT

Qualitatively, Figure 5 demonstrates a close correspondence for each species between the approximate dive depth distributions inferred from TAT histograms (SPOT) with TAD histogram summaries of directly observed dive depths (SPLASH), when the comparisons were constrained to samples that overlapped in terms of time of day. Additionally, mixed effects perMANOVA results summarized in Table 4 indicate that distributions of time in different depth categories did not differ significantly on the basis of sampling method (*e.g.*, TAT *vs*. TAD), when individual variation was explicitly treated by including individual random effects.

Comparing the depth ranges and patterns of time at depth using both methods reveals distinct species-specific modes of vertical habitat use (Fig. 5). However, because of the large imbalance of daytime to nighttime TAD profiles in *P. electra,* both TAT and TAD were restricted to daytime periods only in Figure 5. As a result, the distribution shown in Figure 5 poorly represents the overall pattern of dive activity in *P. electra* and the overall dive pattern for *P. electra* is more clearly shown in Figure 4 *a-c*. The proportion of time that *P. electra* and *G. macrorhynchus* spent in sequential depth/temperature strata declined monotonically with increasing depth and lacked distinct deep activity peaks at the resolution of our analysis. Based on TAT

data, the dive distributions of *P. electra* and *G. macrorhynchus* reached maxima of approximately 350-450 m (16-18ºC) and 1,000-1,500 m (4-6ºC), respectively. In both TAT and TAD, *P. macrocephalus* exhibited distinctly bimodal distributions of time at depth, with a broad peak of time spent between approximately 550-1,000 m (6-14ºC), and a highly variable amount of time spent in the uppermost depth and temperature strata ranging from <10-100%. Both beaked whales, *Z. cavirostris* and *M. densirostris*, exhibited similarly bimodal distributions of time spent as a function of depth. *M. densirostris* displayed a deep peak of time spent between approximately 750-1,500 m (4-10ºC), while *Z. cavirostris* exhibited an analogous maxima, but slightly deeper between approximately 850-1,500 m (4-8ºC) in both TAT and TAD distributions. Finally, the discrepancies in the proportion of time spent in the upper two temperature-depth strata in *Ziphius* (Fig. 5) can be attributed to small sample sizes and individual differences in near-surface "bounce" dive depths.

Discussion

Validation of TAT

The comparison of approximate TAT-derived depth distributions from SPOT tags with directly observed TAD from SPLASH tags (Fig. 5) indicates that, despite markedly different sample sizes (Table 1) and sampling rates (10 s *vs*. 2.5 min), and even after accounting for interindividual variation in dive behavior, these two approaches converged on similar descriptions of dive behavior patterns in our study species (Fig. 5, Table 4). Moreover, TAT-derived descriptions are also consistent

with published accounts of diving activities, where available, for these species. Deep peaks of *P. macrocephalus* dive activity observed in both TAT and TAD (Fig. 5, ~550-1,000 m) were comparable to the peaks of time spent at depth by a similar demographic mixture of adult female and subadult males as those tagged in the Gulf of Mexico, western Atlantic Ocean, and Mediterranean Sea (Watwood *et al*. 2006). Animal-borne acoustic sensor data in Watwood *et al.* (2006) showed a peak of prey capture attempts, inferred from "buzz" vocalizations, at 700-800 m, which falls within the center of the TAT-derived approximate depth distribution. Similarly, the deep peaks of time spent by *Z. cavirostris* between ~850-1,500 m and by *M. densirostris* between ~750-1,500 m in TAT, closely overlapped the depth strata where maximum dive depths (*Z.c*.: 1,450 m and *M.d*.: 890-1,408 m) were reported from TDR studies by Baird *et al.* (2006) in Hawaii, and also contained the mean maximum foraging dive depth in 11 of 14 *M. densirostris* dive records from 9 individuals in the Canary Islands (Arranz *et al.* 2011). The approximate depth range of the deep activity peak estimated for *Z. cavirostris* in this study also overlapped the peak of echolocation buzzes recorded in a DTAG study of *Z. cavirostris* in the Ligurian Sea (Tyack *et al.* 2006). However, the diving range identified from TAT histograms in our study only overlapped the peak of benthic boundary layer buzzes and not the shallower open water mesopelagic peak of buzzes recorded in a DTAG study of *M. densirostris* in the Canary Islands (Arranz *et al.* 2011). Although the maximum dive depth of *Ziphius* reported in the Southern California Bight (2,992 m, Schorr *et al.* 2014) considerably exceeded the maximum recorded in our study (1,722

m), the mean deep dive duration and mean maximum dive depth in our SPLASH tag data were both consistent with the values reported by Schorr *et al.* (2014). Preliminary examination showed that *Z. cavirostris* dives ranged close to the benthos in the areas where tagged animals occurred within our study area, and thus the discrepancy between our deepest observation and Schorr *et al.* (2014) may relate to the capacity of this species to dive deeper when not constrained by the relatively shallow bottom depths found in much of our study area. Dive patterns of *G. macrorhynchus* in both TAT and TAD distributions reached a similar maximum depth strata (TAT: ~1,000-1,500 m, TAD: 840 m) to those reported by Aguilar de Soto *et al.* (2008; 1,019 m). Additionally, the gradual decline in time spent as a function of depth (Fig. 5), and the lack of a deep activity peak in this species, also reflected a similar dive pattern to the highly-aerobic deep daytime foraging dives and relatively shallower nighttime foraging dives exhibited by *G. macrorhynchus* in the Canary Islands (Aguilar de Soto *et al.* 2008). To the best of our knowledge this is the first biologging effort to describe the distribution of subsurface activity in *P. electra*.

Interpretation of TAT

TAT histograms interpreted on a scale of approximate depths provided a relatively coarse but useful means of differentiating dive depth ranges and time budgets between species and sexes, particularly when interpreted in conjunction with complementary information from SPLASH tags and published high resolution DTAG and TDR data. For example these tools allowed the description of *P. electra* as a

nearly exclusively nocturnal upper-mesopelagic diver (~150-400m, Fig. 4). This pattern of habitat use showed elements of commonality with the dive behavior of its closest relative in our study *G. macrorhynchus*, which also dove more frequently during nighttime periods. However as shown by Aguilar de Soto *et al.* (2008), *G. macrorhynchus,* unlike *P. electra*, also dove during daytime periods though typically less frequently and to deeper lower-mesopelagic depths. The interpretation of TAT on a scale of approximate depths also allowed the confirmation of a broad differentiation within our study area between the central to lower mesopelagic peak of dive activity in *P. macrocephalus*, and the lower mesopelagic and upper bathypelagic dive activity peaks of *M. densirostris* and *Z. cavirostris* (Fig.5). Calculating the proportion of time that different species spent below species-specific foraging depth thresholds identified from DTAG acoustic, depth, and accelerometry data (Tyack *et al*. 2006, Watwood *et al*. 2006, Aguilar de Soto *et al.* 2008), further allowed comparisons of the minimum proportion of time that different species spent foraging. Time series of TAT histograms from SPOT tags also provided a useful complement to the typically shorter duration (due to higher battery consumption) and more discontinuous records of dive behavior produced by SPLASH tags in this study, allowing the identification and confirmation of diurnal and even lunar patterns of variation in vertical habitat use (Baird *et al*. 2008). That said, pressure recording SPLASH tags can be programmed to optimize satellite data acquisition by prioritizing data packages of different sizes ranging from full and summarized dive profiles to time-at-depth histograms. The relatively discontinuous depth time series records collected in this study thus reflected

the prioritization of other data types at the expense of a continuous time series, rather than an innate limitation of the SPLASH tag. Finally, the larger sample sizes afforded by incorporating legacy SPOT data with SPLASH tag data allowed wider perspectives on intra-population variation and particularly, on inter-sexual differences in dive behaviors, and thus allowed a more full use of all available data to fill key information gaps for these deep-diving cetaceans.

Limitations of Thermal Proxy For Depth

Because of the dynamic nature of oceanic temperature fields in space and time, using temperature as a proxy for depth presented a range of limitations and required a number of estimation assumptions. Deriving model estimates of climatological isotherm depth fields and of the uncertainty surrounding these depth surfaces, particularly in a hydrodynamically complex region such as our study area, first required 1) a robust oceanographic data set, 2) an assumption of residual normality, and 3) persistent spatial- and/or temporal-variability in the climatological mean state that could be effectively modeled as a function of random variables (*e.g.*, $x, y, d_{flst}, d_{chan}, t$). In the first estimation requirement, our study benefited from temperature profile data from the animal-borne sensors on SPLASH tags, as well as a relatively dense program of hydrographic sampling in our study area, due primarily to an interest in quantifying the Atlantic Meridional Overturning Circulation (AMOC) transport (Wang and Mooers 1997, Hamilton *et al.* 2005, Beal *et al.* 2008, Kanzow *et al.* 2010). The second assumption of approximate residual normality was evaluated

and supported in the model validation step through the examination of Q-Q plots. The third assumption, that a portion of the variability in the climatological isotherm depths was attributable to persistent spatial processes and structures, was supported by the relatively low variability of flow through the NW Providence channel shown in Figures 4 *e*, 5 *e* from Hamilton *et al.* (2005), as well as the reduction in MSPE and model residual standard deviation achieved by LM and GAM interpolations, particularly between 10ºC and 18ºC (Table 2). Seasonal variation in the vertical mixing affecting the depths of the 22ºC and 24ºC isotherms, as well as a small seasonal cycle in AMOC (Kanzow *et al.* 2010), were similarly captured by the inclusion of day-of-year (*t*), which is reflected in a reduction in MSPE of both LM and GAM interpolations with respect to an overall mean encompassing all depth observations at these isotherms. The descriptions of isotherm depth achieved in this study were also consistent with the isotherm and isopycnal structures identified along transects across the NW Providence Channel that were used in estimates of volume transport from the NW Providence Channel into the Florida Current (Leaman *et al.* 1995, Wang and Mooers 1998, Hamilton *et al.* 2005, Beal *et al.* 2008).

Both the use of temperature as a proxy for depth and the vertical and temporal binning inherent in TAT summaries limited the interpretation of finer resolution dive behavior in several important respects. To simultaneously interpret multiple TAT histograms in terms of approximate time-at-depth distributions, we primarily report isotherm depths using climatological estimates derived from optimal model interpolations that incorporated all the available hydrographic sampling over the last

24 yr (1990-2014). However, the instantaneous isotherm depths at any given TAT location and time may have differed from these climatological isotherm depth surfaces, although they are likely contained within the overall ranges of observed values at each isotherm (Fig. 2). This divergence of the instantaneous values from the climatological state is indicated by the spread of model residuals and cross-validation prediction errors after accounting for spatial and seasonal processes. Specifically, we considered daily HYCOM reanalysis outputs to simultaneously account for the spatial and temporal components of isotherm depth variability. However, the global HYCOM data assimilation model outputs performed relatively poorly as predictors of the observed temperature-depth data (Table 2) and also exhibited a systematic shallow bias. Thus, the HYCOM reanalysis was not used to interpret TAT histograms (Table 2), and the use of climatological estimates required us to refer to time-at-depth distributions inferred from TAT histograms as *approximate* depth distributions throughout this paper (Figs. 4, 5). Defining the approximate depth axis of box-plots (Figs. 4, 5) that compared multiple TAT histograms across different locations and times further necessitated the use of median predicted isotherm depths over the entire study area or a subregion of interest, as opposed to a location- and time-specific estimate of climatological isotherm depths specific to any single TAT histogram. As an alternative to defining a single vector of overall median climatological isotherm depth estimates along this axis, we developed a graphical representation in which multiple TAT histograms are shown as time-series where the depth axis is fixed and colored boxes represent the proportion of time spent in particular temperature/depth

strata that vary in vertical dimension in response to model predicted local climatological isotherm depths (Fig. 4 *b*, *e*). The comparison of this depth-varying time series plot with an analogous time-series plot defined by median isotherm depths from the entire study area (Fig. 4 *c*, *f*) indicates little qualitative difference between these contrasting descriptions of dive activity patterns. We were also able to specify dive depth distributions and time allocations from TAT with greater precision, for example by stating that "on average $\geq a\%$ of species *b* time is spent between $z_{min,T1}$ and $z_{max,T2}$ depth (*i.e.*, maximum depth range) over a geographic region of interest."

Alternatively, TAT frequency histograms could alternatively have been interpreted directly based on the thermoregulatory demands and constraints imposed by ambient water temperatures. However, approximate depth ranges likely provide greater insight into the potential drivers of depth distribution patterns in odontocetes. As homeothermic endotherms with efficient insulation and counter-current heat exchange (Ryg *et al.* 2003), the depth distributions of odontocetes are likely more sensitive to variables related to depth rather than external temperatures, such as the tradeoffs between the vertical distributions of preferred prey in the water column, the physiological limits of diving capacity (Noren and Williams 2000), and potentially neutral buoyancy thresholds (Miller *et al.* 2004*b*, Tyack *et al.* 2006). The distributions of many mesopelagic and some bathypelagic prey in the water column, although ultimately constrained by physiological oxygen and thermal tolerances, are also likely most directly influenced by variables such as particulate organic matter concentration and flux (Martin *et al.* 1987) and downwelling light intensity (Ohman *et al.* 1983),

which attenuate as functions of depth. Thus, interpreting TAT histograms as approximate depth distributions likely provides greater insight into the diving behavior and habitats of deep-diving odontocete cetaceans compared to interpreting this information stream directly in terms of time-at-temperature.

Recommendations for Future Use

Despite the limitations and complexities of interpretation outlined above, our approach of estimating isotherm depths to interpret the dive behavior information transmitted in TAT histograms succeeded in describing vertical habitat use patterns and approximate dive depth ranges that converged with direct dive depth measurements in our case study species. This study thus demonstrates that, even under complex oceanographic regimes, summarized temperature outputs from SPOT tags can serve as a useful complementary tool to augment more direct measurements of dive behavior from SPLASH telemetry tags, TDRs, and DTAGs. In particular, this approach will be valuable in recovering under-utilized dive information from prior studies that employed SPOT telemetry technology with a primary focus on ranging and spatial habitat use patterns. Tag technology is in a constant state of evolution, and in particular the incorporation of lightweight, relatively inexpensive, and low power consumption pressure sensors has become standard in more recent models of satellite telemetry tags. While the choice of telemetry technology will always remain dependent on the specific questions addressed by each study, using less precise but still informative SPOT model tags may become harder to justify in future studies of

protected species such as cetaceans, where from an ethical standpoint data quality takes precedence over the total number of tags deployed. However, there remain several advantages to using SPOT tags unrelated to their lower cost. In particular these tags can provide longer battery life relative to SPLASH tags, which can extend both duration and strength of transmission. SPOT tags are also smaller and lighter than SPLASH tags (49 g *vs*. 63 g), which leads to moderately better flight characteristics and placement precision when remotely projected from longer distances. Therefore, a range of tradeoffs must be weighed in choosing between tag models, and in cases where high resolution and longer term tracks of spatial movement represents the primary focus of the study, the TAT interpretation approach outlined here can allow some additional inference to be gleaned on diving. Furthermore given the cost difference between SPOT and SPLASH models at the time of this study (*i.e.*, SPOT were 61% of the cost of SPLASH in the LIMPET configuration), SPOT models may also be widely applicable in studies of non-protected species such as highly migratory fishes (*e.g.*, scombrids and elasmobranchs) where the precision of dive behavior estimates is balanced by the large number of tag deployments necessary to recover information.

Oceanographic regimes and hydrographic sampling densities in potential study areas are also critically important considerations in assessing the applicability of the methods outlined in this study. This study benefitted from a nearly linear decline from 23-28ºC in the surface mixed layer to <4ºC over the upper 1,200 m of the water column in our study area (Fig. 1 *a*). This allowed temperature categories

spaced at 2ºC intervals (*i.e.*, 20x greater than the ±0.1ºC reported accuracy of SPOT thermistor, Wildlife Computers 2013) to define relatively narrow (~70-200 m) depth intervals, providing sufficient resolution to differentiate the dive ranges exhibited by most of the deep-diving species in our case study (Fig. 5). The relative stability of thermal structure over a 24-year period of hydrographic sampling (Fig. 1 *a*) in our study area also enabled the use of a climatological mean (1990-2014) as a useful approximation of the depth of the temperature strata. To maximize the granularity of dive patterns that can be resolved, careful thought and planning must be applied in tailoring the SPOT temperature bins to the thermal regime in the study area of interest, as well as the behavioral questions of interest.

The results in this study also benefitted from the relatively high density of hydrographic sampling in our study, which enabled the characterization of climatological thermal structure at a fine spatial resolution. This fine scale characterization was necessary given the complex bathymetry and the dynamic flow regime within our study area. However, the interpolation methods applied in this study could also be effectively implemented in study areas with less dense and/or frequent hydrographic sampling, where the thermal structure varies less in space and time. Areas with relatively low spatiotemporal variation in thermal structure and sufficient temperature contrast between surface and deep waters occur primarily over large areas of the northern and southern hemisphere subtropical gyres away from boundary currents. Moreover, with the continuing expansion of the global Argo profiling float array since the early 2000s, spatial and temporal sampling of

temperature within the interiors of oceans worldwide is rapidly expanding. Thus, these approaches may be applicable in many areas where research on cetaceans and other large oceanic predators is conducted using SPOT tags (*e.g.*, Hawaii, Azores, Canary Islands, Mediterranean Sea, and sub-tropical Australia).

Acknowledgements

We are grateful to Charlotte Dunn and Leigh Hickmott at the Bahamas Marine Mammal Research Organisation (BMMRO) for their contributions to field research and project planning. We would also like to thank Dean Roemmich, Cesar Rocha, and Nick Cavanaugh of Scripps Institution of Oceanography for their guidance in sourcing physical oceanographic data and implementing an Objective Analysis interpolation approach. We would like to thank Brice Semmens, Lynn Talley, and Paul Dayton for their valuable input on the manuscript. We also thank dedicated field biologists Robert Pitman, Olivia Patterson, Aaron Banks, Marie Guilpin, Kendria Ferguson, Eric Lewallen and Edward Adderley for their contribution to field efforts. We made use of data collected and made freely available by the International Argo Program and the national programs that contribute to it (http://www.argo.ucsd.edu, http://argo.jcommops.org). Finally, we are also very grateful to the captains and crews of the R/V *Walton Smith* and M/V *Slumber Venture* for their outstanding support of our research efforts. Funding for tagging efforts in the Bahamas was supported by the US Navy Office of Naval Research (grant N000140710120), NAVFAC (grants N002441110021, N002441210007 and contract N6660413P2671), and the Strategic Environmental Research and Development Program (award RC-

2114). Tagging was conducted under Bahamas Marine Mammal Protection Permit #12A. Tag types, methods of deployment, and sample sizes were all reviewed and approved by BMMRO's Institutional Animal Care and Use Committee (IACUC).

Chapter 1, in full, is a reprint of the material as it appears in Marine Mammal Science 2016. Joyce, Trevor W.; Durban, John W.; Fearnbach, Holly; Claridge, Diane E.; Ballance, Lisa T. The dissertation author was the primary investigator and author of this materia

References

Aguilar Soto, N., Johnson, M.P., Madsen, P.T., Díaz, F., Domínguez, I., Brito, A. & Tyack, P. (2008) Cheetahs of the deep sea: deep foraging sprints in short-finned pilot whales off Tenerife (Canary Islands). *Journal of Animal Ecology*, 77, 936–947.

Aitchison, J. (1986) *The statistical analysis of compositional data*. Blackburn Press, Caldwell, New Jersey, USA.

Andrews, R.D., Pitman, R.L. & Ballance, L.T. (2008) Satellite tracking reveals distinct movement patterns for Type B and Type C killer whales in the southern Ross Sea, Antarctica. *Polar Biology*, 31, 1461–1468.

Aoki, K., Amano, M., Kubodera, T., Mori, K., Okamoto, R. & Sato, K. (2015) Visual and behavioral evidence indicates active hunting by sperm whales. *Marine Ecology Progress Series*, 523, 233–241.

Aoki, K., Sakai, M., Miller, P.J., Visser, F. & Sato, K. (2013) Body contact and synchronous diving in long-finned pilot whales. *Behavioural processes*, 99, 12–20.

Arranz, P., De Soto, N.A., Madsen, P.T., Brito, A., Bordes, F. & Johnson, M.P. (2011) Following a foraging fish-finder: Diel habitat use of Blainville's beaked whales revealed by echolocation. *PloS one*, 6, e28353.

Baird, R.W., Schorr, G.S., Webster, D.L., McSweeney, D.J., Hanson, M.B. & Andrews, R.D. (2011) Movements of two satellite-tagged pygmy killer whales (Feresa attenuata) off the island of Hawai 'i. *Marine Mammal Science*, 27, E332–E337.

Baird, R.W., Webster, D.L., McSweeney, D.J., Ligon, A.D., Schorr, G.S. & Barlow, J. (2006) Diving behaviour of Cuvier's (Ziphius cavirostris) and Blainville's (Mesoplodon densirostris) beaked whales in Hawai'i. *Canadian Journal of Zoology*, 84, 1120–1128.

Baird, R.W., Webster, D.L., Schorr, G.S., McSweeney, D.J. & Barlow, J. (2008) Diel variation in beaked whale diving behavior. *Marine Mammal Science*, 24, 630–642.

Balcomb III, K.C. & Claridge, D.E. (2001) A mass stranding of cetaceans caused by naval sonar in the Bahamas. *Bahamas Journal of Science*, 8, 2–12.

Beal, L.M., Hummon, J.M., Williams, E., Brown, O.B., Baringer, W. & Kearns, E.J. (2008) Five years of Florida Current structure and transport from the Royal Caribbean Cruise Ship Explorer of the Seas. *Journal of Geophysical Research: Oceans*, 113.

van den Boogaart, K.G. & Tolosana-Delgado, R. (2008) "Compositions": a unified R package to analyze compositional data. *Computers & Geosciences*, 34, 320–338.

Chassignet, E.P., Hurlburt, H.E., Smedstad, O.M., Halliwell, G.R., Hogan, P.J., Wallcraft, A.J., Baraille, R. & Bleck, R. (2007) The HYCOM (hybrid coordinate ocean model) data assimilative system. *Journal of Marine Systems*, 65, 60–83.

Clarke, K.R. (1993) Non-parametric multivariate analyses of changes in community structure. *Australian journal of ecology*, 18, 117–143.

Cox, T.M., Ragen, T.J., Read, A.J., Vos, E., Baird, R.W., Balcomb, K., Barlow, J., Caldwell, J., Cranford, T. & Crum, L. (2006) *Understanding the Impacts of Anthropogenic Sound on Beaked Whales*. DTIC Document.

D'Amico, A., Gisiner, R.C., Ketten, D.R., Hammock, J.A., Johnson, C., Tyack, P.L. & Mead, J. (2009) Beaked whale strandings and naval exercises. *Aquatic Mammals*, 35, 452.

De Jong, P. & Penzer, J. (1998) Diagnosing shocks in time series. *Journal of the American Statistical Association*, 93, 796–806.

Durban, J.W. & Pitman, R.L. (2011) Antarctic killer whales make rapid, round-trip movements to subtropical waters: evidence for physiological maintenance migrations? *Biology Letters*, rsbl20110875.

Ford, J.K., Durban, J.W., Ellis, G.M., Towers, J.R., Pilkington, J.F., Barrett-Lennard, L.G. & Andrews, R.D. (2013) New insights into the northward migration route of gray whales between Vancouver Island, British Columbia, and southeastern Alaska. *Marine Mammal Science*, 29, 325–337.

Frantzis, A. (1998) Does acoustic testing strand whales? *Nature*, 392, 29.

Gillespie, D., Dunn, C., Gordon, J., Claridge, D., Embling, C. & Boyd, I. (2009) Field recordings of Gervais' beaked whales Mesoplodon europaeus from the Bahamas. *The Journal of the Acoustical Society of America*, 125, 3428–3433.

Hamilton, P., Larsen, J.C., Leaman, K.D., Lee, T.N. & Waddell, E. (2005) Transports through the Straits of Florida. *Journal of physical oceanography*, 35, 308–322.

Hazen, E.L., Nowacek, D.P., Laurent, L.S., Halpin, P.N. & Moretti, D.J. (2011) The relationship among oceanography, prey fields, and beaked whale foraging habitat in the Tongue of the Ocean. *PloS one*, 6, e19269.

Hooker, S.K. & Baird, R.W. (1999) Deep–diving behaviour of the northern bottlenose whale, Hyperoodon ampullatus (Cetacea: Ziphiidae). *Proceedings of the Royal Society of London B: Biological Sciences*, 266, 671–676.

Johns, W.E., Beal, L.M., Baringer, M.O., Molina, J.R., Cunningham, S.A., Kanzow, T. & Rayner, D. (2008) Variability of shallow and deep western boundary currents off the Bahamas during 2004-05: Results from the 26 N RAPID-MOC array. *Journal of Physical Oceanography*, 38, 605–623.

Johnson, D.S. (2013) *Crawl: Fit Continuous-Time Correlated Random Walk Models to Animal Movement Data. R Package Version 1.4-1*.

Johnson, D.S., London, J.M., Lea, M.-A. & Durban, J.W. (2008) Continuous-time correlated random walk model for animal telemetry data. *Ecology*, 89, 1208–1215.

Johnson, M., de Soto, N.A. & Madsen, P.T. (2009) Studying the behaviour and sensory ecology of marine mammals using acoustic recording tags: a review. *Marine Ecology Progress Series*, 395, 55–73.

Johnson, M.P. & Tyack, P.L. (2003) A digital acoustic recording tag for measuring the response of wild marine mammals to sound. *IEEE journal of oceanic engineering*, 28, 3–12.

Kanzow, T., Cunningham, S.A., Johns, W.E., Hirschi, J.J., Marotzke, J., Baringer, M.O., Meinen, C.S., Chidichimo, M.P., Atkinson, C., Beal, L.M. & others. (2010) Seasonal variability of the Atlantic meridional overturning circulation at 26.5 N. *Journal of Climate*, 23, 5678–5698.

Laist, D.W., Knowlton, A.R., Mead, J.G., Collet, A.S. & Podesta, M. (2001) Collisions between ships and whales. *Marine Mammal Science*, 17, 35–75.

Lavery, T.J., Roudnew, B., Gill, P., Seymour, J., Seuront, L., Johnson, G., Mitchell, J.G. & Smetacek, V. (2010) Iron defecation by sperm whales stimulates carbon export in the Southern Ocean. *Proceedings of the Royal Society of London B: Biological Sciences*, rspb20100863.

Leaman, K.D., Vertes, P.S., Atkinson, L.P., Lee, T.N., Hamilton, P. & Waddell, E. (1995) Transport, potential vorticity, and current/temperature structure across Northwest Providence and Santaren Channels and the Florida Current off Cay Sal Bank. *Journal of Geophysical Research: Oceans*, 100, 8561–8569.

Lee, T.N., Johns, W.E., Zantopp, R.J. & Fillenbaum, E.R. (1996) Moored observations of western boundary current variability and thermohaline circulation at 26.5 in the subtropical North Atlantic. *Journal of Physical Oceanography*, 26, 962–983.

MacLeod, C.D., Santos, M.B. & Pierce, G.J. (2003) Review of data on diets of beaked whales: evidence of niche separation and geographic segregation. *Journal of the Marine Biological Association of the UK*, 83, 651–665.

Madsen, P.T., Payne, R., Kristiansen, N.U., Wahlberg, M., Kerr, I. & Møhl, B. (2002) Sperm whale sound production studied with ultrasound time/depth-recording tags. *Journal of Experimental Biology*, 205, 1899–1906.

Martin, J.H., Knauer, G.A., Karl, D.M. & Broenkow, W.W. (1987) VERTEX: carbon cycling in the northeast Pacific. *Deep Sea Research Part A. Oceanographic Research Papers*, 34, 267–285.

McCarthy, E., Moretti, D., Thomas, L., DiMarzio, N., Morrissey, R., Jarvis, S., Ward, J., Izzi, A. & Dilley, A. (2011) Changes in spatial and temporal distribution and vocal behavior of Blainville's beaked whales (Mesoplodon densirostris) during multiship exercises with mid-frequency sonar. *Marine Mammal Science*, 27, E206–E226.

McIntosh, P.C. (1990) Oceanographic data interpolation: Objective analysis and splines. *Journal of Geophysical Research: Oceans*, 95, 13529–13541.

Miller, P.J., Johnson, M.P. & Tyack, P.L. (2004a) Sperm whale behaviour indicates the use of echolocation click buzzes "creaks" in prey capture. *Proceedings of the Royal Society of London B: Biological Sciences*, 271, 2239–2247.

Miller, P.J., Johnson, M.P., Tyack, P.L. & Terray, E.A. (2004b) Swimming gaits, passive drag and buoyancy of diving sperm whales Physeter macrocephalus. *Journal of Experimental Biology*, 207, 1953–1967.

Moretti, D., Thomas, L., Marques, T., Harwood, J., Dilley, A., Neales, B., Shaffer, J., McCarthy, E., New, L., Jarvis, S. & others. (2014) A risk function for behavioral disruption of Blainville's beaked whales (Mesoplodon densirostris) from mid-frequency active sonar. *PloS one*, 9, e85064.

Noren, S.R. & Williams, T.M. (2000) Body size and skeletal muscle myoglobin of cetaceans: adaptations for maximizing dive duration. *Comparative Biochemistry and Physiology Part A: Molecular & Integrative Physiology*, 126, 181–191.

Ohman, M.D., Frost, B.W. & Cohen, E.B. (1983) Reverse diel vertical migration: an escape from invertebrate predators. *Science*, 220, 1404–1407.

Olson, D.B., Schott, F.A., Zantopp, R.J. & Leaman, K.D. (1984) The mean circulation east of the Bahamas as determined from a recent measurement program and historical XBT data. *Journal of Physical Oceanography*, 14, 1470–1487.

Pirotta, E., Milor, R., Quick, N., Moretti, D., Di Marzio, N., Tyack, P., Boyd, I. & Hastie, G. (2012) Vessel noise affects beaked whale behavior: results of a dedicated acoustic response study. *PLoS One*, 7, e42535.

Roemmich, D. (1983) Optimal estimation of hydrographic station data and derived fields. *Journal of Physical Oceanography*, 13, 1544–1549.

Roemmich, D. & Gilson, J. (2009) The 2004–2008 mean and annual cycle of temperature, salinity, and steric height in the global ocean from the Argo Program. *Progress in Oceanography*, 82, 81–100.

Ryg, M., Lydersen, C., Knutsen, L., Bjørge, A., Smith, T.G. & Øritsland, N.A. (1993) Scaling of insulation in seals and whales. *Journal of Zoology*, 230, 193–206.

Schorr, G.S., Baird, R.W., Hanson, Mb., Webster, D.L., McSweeney, D.J. & Andrews, R.D. (2009) *Movements of Satellite-Tagged Blainville's Beaked Whales Off the Island of Hawaii*. DTIC Document.

Schorr, G.S., Falcone, E.A., Moretti, D.J. & Andrews, R.D. (2014) First long-term behavioral records from Cuvier's beaked whales (Ziphius cavirostris) reveal record-breaking dives. *PLoS One*, 9, e92633.

Smeed, D.A., McCarthy, G., Cunningham, S.A., Frajka-Williams, E., Rayner, D., Johns, W.E., Meinen, C.S., Baringer, M.O., Moat, B.I., Duchez, A. & others. (2014) Observed decline of the Atlantic meridional overturning circulation 2004–2012. *Ocean Science*, 10, 29–38.

Teloni, V., Mark, J.P., Patrick, M.J. & Peter, M.T. (2008) Shallow food for deep divers: Dynamic foraging behavior of male sperm whales in a high latitude habitat. *Journal of Experimental Marine Biology and Ecology*, 354, 119–131.

Thomson, R.E. & Emery, W.J. (2014) *Data Analysis Methods in Physical Oceanography*. Third ed., Elsevier Publishing, Amsterdam, The Netherlands.

Trossman, D.S., Thompson, L. & Hautala, S.L. (2011) Application of thin-plate splines in two dimensions to oceanographic tracer data. *Journal of Atmospheric and Oceanic Technology*, 28, 1522–1538.

Tyack, P.L., Johnson, M., Soto, N.A., Sturlese, A. & Madsen, P.T. (2006) Extreme diving of beaked whales. *Journal of Experimental Biology*, 209, 4238–4253.

Tyack, P.L., Zimmer, W.M., Moretti, D., Southall, B.L., Claridge, D.E., Durban, J.W., Clark, C.W., D'Amico, A., DiMarzio, N., Jarvis, S. & others. (2011) Beaked whales respond to simulated and actual navy sonar. *PloS one*, 6, e17009.

Venables, W.N. & Ripley, B.D. (2002) Random and mixed effects. *Modern Applied Statistics with S*, pp. 271–300. Springer.

Wallace, J.R. (2012) *Imap: Interactive Mapping. R Package Version 1.32*.

Wang, J. & Mooers, C.N. (1998) Three-dimensional perspectives of the Florida Current: transport, potential vorticity, and related dynamical properties. *Dynamics of atmospheres and oceans*, 27, 135–149.

Watwood, S.L., Miller, P.J., Johnson, M., Madsen, P.T. & Tyack, P.L. (2006) Deep-diving foraging behaviour of sperm whales (Physeter macrocephalus). *Journal of Animal Ecology*, 75, 814–825.

Wildlife Computers. 2013. Wildlife Computers Data Analysis Programs. Available: http://wildlifecomputers.com/downloads.aspx

Wood, S. (2006) *Generalized Additive Models: An Introduction with R*. CRC press, Boca Raton, Florida, USA.

Tables

Table 1-1. Summary of Argos satellite LIMPET tag deployments on five species of deep-diving odontocete cetaceans in the NW Bahamas. SPOT model tag deployments were conducted over the period 2009-2014, while SPLASH model tag deployments were conducted over the period 2011-2014. The number of groups signifies the number of independent encounters with groups of odontocetes in which one or more animals were tagged. The number of Time-at-Temperature (TAT) recovered represents the number of six-hour summary histograms successfully downloaded from SPOT tags, while the number of Time-at-Depth (TAD) recovered represents the number of six-hour periods in which ≥50% (≥25% for *P. electra*) of depth time series observations were downloaded from SPLASH tags.

Species	SPOT Deployments	SPLASH Deployments	Number of Groups	TAT Recovered	TAD Recovered	Mean Deployment Duration (d, Min-Max)
Melon-headed whale *Peponocephala electra*	9	4	6	274	5	9.51 (0.02-38.79)
Short-finned pilot whale *Globicephala macrorhynchus*	12	3	6	612	53	15.67 (0.37-40.80)
Sperm whale *Physeter macrocephalus*	21	6	13	563	23	8.20 (0.01-17.76)
Blainville's beaked whale *Mesoplodon densirostris*	3	9	9	28	119	16.41 (0.01-45.64)
Cuvier's beaked whales *Ziphius cavirostris*	1	6	6	24	20	23.72 (8.53-90.14)

Table 1-2. Summary of depth and temperature (N_{PDT}) profiles from SPLASH tags, conductivity-temperature-depth (N_{CTD}) profiles, and neutrally buoyant profiling float (N_{PFL}) profiles used in isotherm depth analyses. Additionally, estimated isotherm depths, and cross-validation mean squared prediction errors (MSPE) for various interpolation methods are reported at the temperature boundaries of Time-at-Temperature histogram categories. Isotherm depths are reported as an overall mean depth (Depth Overall), including the range of observed depths (Depth Min., Depth Max.), as well as the median of predicted depths (Depth Best) within the study area from the best interpolation model for each temperature level. The best interpolation method for each isotherm (shown in bold) were selected on the basis of the lowest MSPE score from the overall mean, a 0.5° Latitude x 0.5° Longitude grid mean, linear model (LM), linear model with subsequent optimal interpolation (LM OA), generalized additive model (GAM), and HYCOM reanalysis.

Isotherm	N PDT	N CTD	N PFL	Depth Overall	Depth Min.	Depth Max.	Depth Best	MSPE Overall	MSPE Grid 0.5°	MSPE LM	MSPE LM OA	MSPE GAM	MSPE HYCOM
24°C	146	237	192	100.59	2.33	172.11	109.02	1389	1160	769	816	**766**	740
22°C	146	269	226	169.67	76.92	248.97	174.98	814	516	442	434	**429**	990
20°C	144	263	226	229	129.81	336.69	233.54	800	600	**485**	491	505	1274
18°C	144	235	225	347.4	191.23	462.97	342.33	1488	690	636	**571**	590	4783
16°C	141	219	224	463.51	261.27	629.32	452.07	2663	951	912	**657**	672	4971
14°C	139	200	223	554.43	414.45	708.56	548.8	2243	985	800	**572**	627	4739
12°C	133	190	220	645.61	545.11	784.3	642.21	1699	904	678	**587**	630	5039
10°C	121	183	220	746.36	657.19	871.05	753.31	1367	1003	759	**709**	715	3882
8°C	110	164	216	863.37	747.96	968.18	878.46	1342	1197	888	**833**	936	3840
6°C	87	155	202	1013.77	883.21	1193.07	1030.14	2838	2639	1845	**1742**	1985	5712
4°C	9	116	55	1577.45	1273.1	1815.87	1573.35	10150	9789	**8667**	9101	9153	28020

Table 1-3. Pearson correlation coefficients (*r*) of isotherm depths predicted by each pair of interpolation or reanalysis methods at the temperature boundaries of Time-at-Temperature histogram categories.

Isotherm	LM	GAM	LM OA	HYCOM	GAM	LM OA	HYCOM	LM OA	HYCOM	HYCOM
24°C	0.29	0.25	0.28	0.34	0.53	0.79	0.78	0.08	0.88	0.76
22°C	0.79	0.83	0.77	0.66	0.92	0.87	0.61	0.91	0.71	0.66
20°C	0.69	0.80	0.72	0.35	0.81	0.89	0.41	0.82	0.29	0.40
18°C	0.85	0.88	0.82	0.01	0.89	0.85	0.19	0.95	0.11	0.19
16°C	0.83	0.85	0.82	0.32	0.88	0.86	0.45	0.98	0.45	0.50
14°C	0.78	0.80	0.74	0.23	0.89	0.89	0.43	0.96	0.37	0.48
12°C	0.75	0.84	0.76	0.10	0.84	0.91	0.37	0.91	0.22	0.39
10°C	0.63	0.74	0.65	0.16	0.79	0.85	0.48	0.84	0.24	0.43
8°C	0.52	0.62	0.56	0.31	0.58	0.60	0.53	0.76	0.28	0.46
6°C	0.31	0.42	0.30	0.08	0.29	0.63	0.03	0.71	0.11	0.03
4°C	0.25	0.77	0.24	0.14	0.17	0.92	0.05	0.10	0.04	0.08

Table 1-4. Results of mixed-effects permutational multivariate analysis of variance (perMANOVA) comparison of centered log-ratio transformed time-at-depth (TAD) and time-at-temperature (TAT) distributions within each species implemented in the program PRIMER+. After accounting for individual variability as a random effect variable nested within each tag type, none of these comparisons indicate a significant multivariate difference between summary types (*e.g.*, TAT and TAD).

Species	**Variable**	**Effect Type**	**df**	**F**	p
Melon-headed whale	Individual	Random	9	2.8653	0.001
Peponocephala electra	Summary Type	Fixed	1	0.4894	0.684
Short-finned pilot whale	Individual	Random	10	2.5533	0.001
Globicephala macrorhynchus	Summary Type	Fixed	1	1.3464	0.311
Sperm whale	Individual	Random	19	5.5137	0.001
Physeter macrocephalus	Summary Type	Fixed	1	0.8948	0.470
Blainville's beaked whale	Individual	Random	5	3.5048	0.001
Mesoplodon densirostris	Summary Type	Fixed	1	0.9719	0.280
Cuvier's beaked whales	Individual	Random	2	3.6920	0.002
Ziphius cavirostris	Summary Type	Fixed	1	1.6730	0.188

Figures

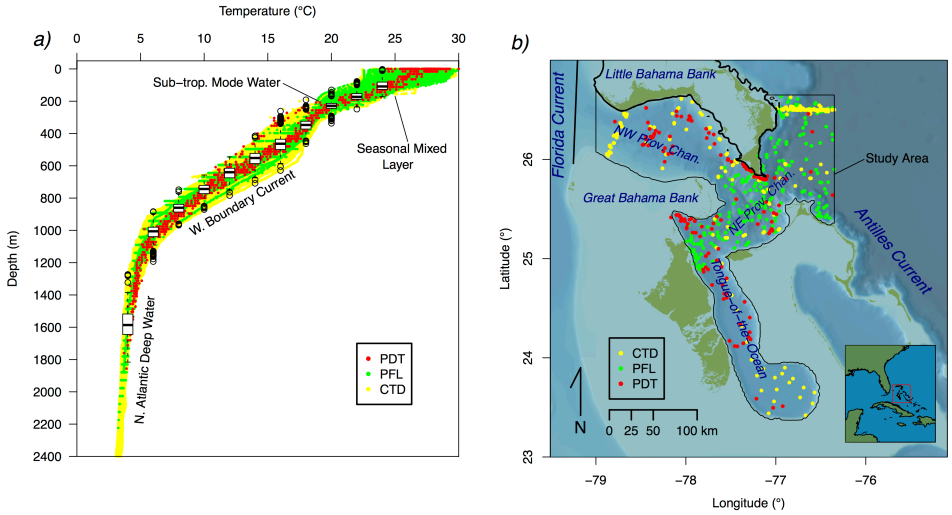

Fig. 1-1. *a*) Plot of temperature as a function of depth across all types of profiles within the study area. Temperature profile types included coarse-resolution profiles of depth and temperature (PDT, 2011-2014) recovered from SPLASH tag deployments on 4 species of cetaceans, as well as moderate- to high-resolution sampling from neutrally-buoyant Argo profiling floats (PFL, 2004-2013) and conductivity temperature depth instruments (CTD, 1990-2013) from the World Ocean Database (WOD). Modified box plots have been overlaid on these profiles showing the central tendency (median) and depth variation of the even numbered isotherms between 4-24ºC. *b*) Map showing sampling locations of these three types of temperature profile data that were employed in statistical descriptions of thermal structure in the NW Bahamas. The study area boundary and major geographic and oceanographic features are also labeled. The line features used to calculate the distance proxies across the Providence Channels (d_{chan}) and distance from the Florida Strait ($d_{flst.}$) are highlighted in bold.

Fig. 1-2. Mean locations of time-at-temperature (TAT) histograms and time-at-depth (TAD) histograms from transmitter tags deployed on each of five species in the Great Bahama Canyon: *a*) melon-headed whale (*Peponocephala electra*, N_{SPOT}=9, N_{SPLASH}=4), *b*) short-finned pilot whale (*Globicephala macrorhynchus*, N_{SPOT}=12, N_{SPLASH}=3), *c*) sperm whales (*Physeter macrocephalus*, N_{SPOT}=21, N_{SPLASH}=6), *d*) Blainville's beaked whale (*Mesoplodon densirostris*, N_{SPOT}=3, N_{SPLASH}=9) and *e*) Cuvier's beaked whale (*Ziphius cavirostris*, N_{SPOT}=1, N_{SPLASH}=6). The mean locations were derived by fitting a movement model (Johnson et al. 2008) to smooth and filter irregularly spaced Argos Telemetry estimates from SPOT and SPLASH tags, respectively. The study area boundary and US Navy's Atlantic Test and Evaluation Center (AUTEC) are also shown.

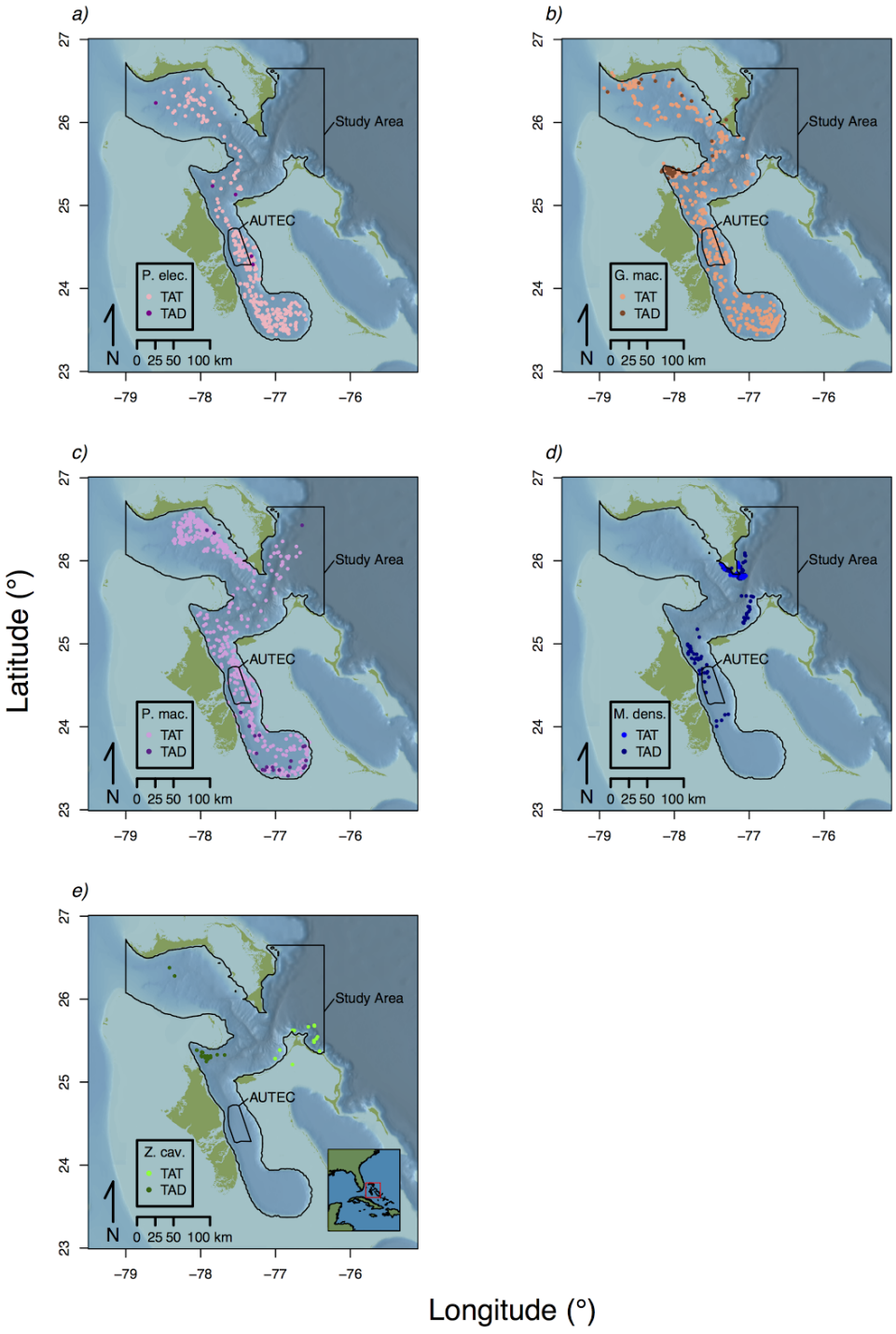
a)
b)
c)
d)
e)
Study Area
AUTEC
P. elec.
G. mac.
P. mac.
M. dens.
Z. cav.
TAT
TAD
N
0 25 50 100 km
Latitude (°)
Longitude (°)

Fig. 1-3. Prediction surfaces of the *a*) linearly approximated depth observations and estimated mean depth field of three example isotherms (8ºC, 14ºC, and 20ºC), that were predicted using 5 interpolation methods: *b*) 0.5º grid cell mean, *c*) HYCOM reanalysis, *d*) quadratic linear model, *e*) objective analysis based on the quadratic linear model, and *f*) generalized additive model. The color scale in each panel represents a 250 m range centered on median observed depth of each displayed isotherm, thus the relatively muted color contrast in the 20ºC series of plots reflects the lower total variability in isotherm depth at this temperature level when compared with the 8ºC and 14ºC series of plots.

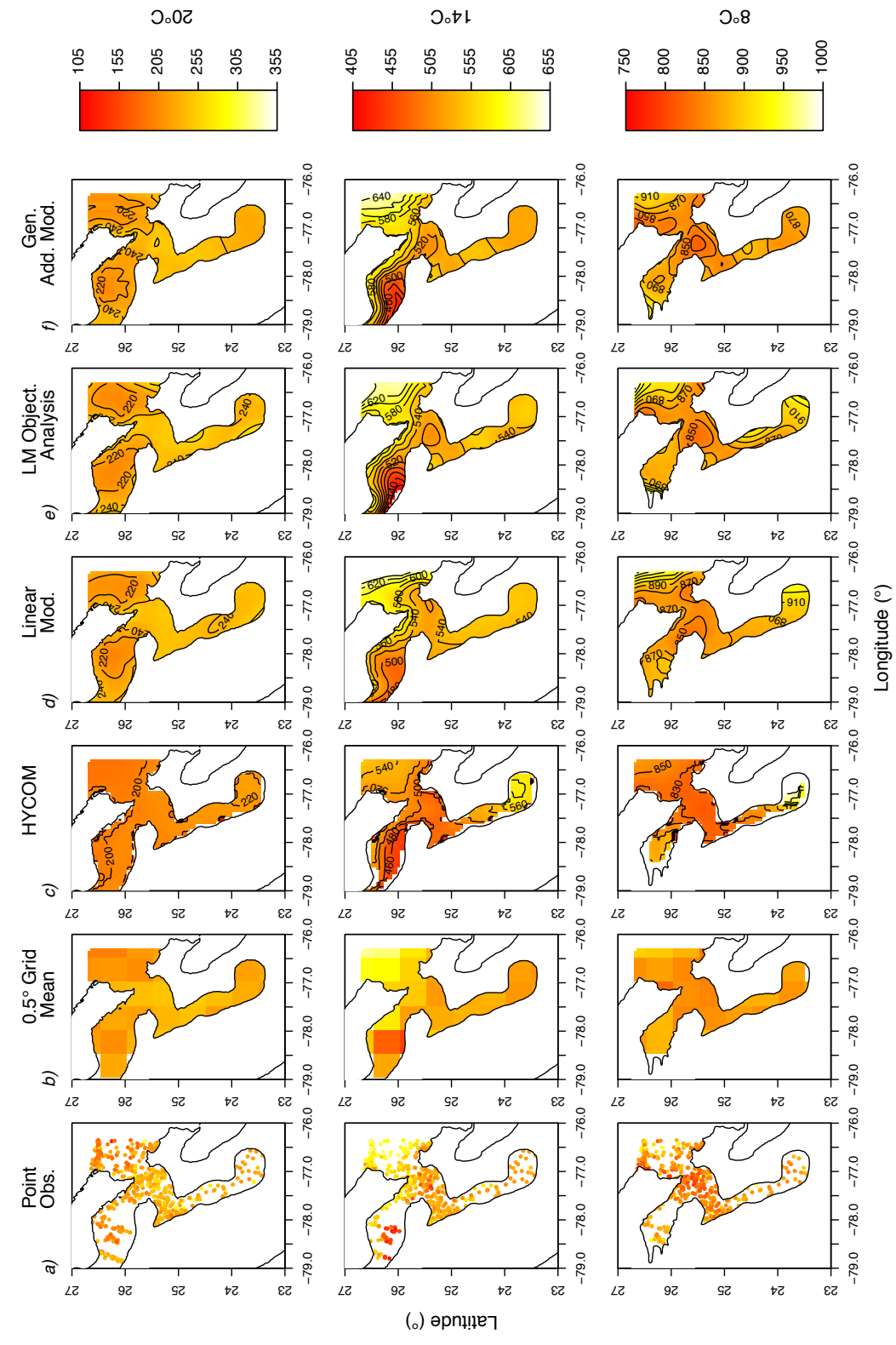
a) Point Obs.
b) 0.5° Grid Mean
c) HYCOM
d) Linear Mod.
e) LM Object. Analysis
f) Gen. Add. Mod.
20°C
14°C
8°C
Latitude (°)
Longitude (°)

Fig. 1-4. Illustrating three representations of 8.5-day time series of melon-headed whale (*Peponocephala electra*, *a-c*), and sperm whale (*Physeter macrocephalus*, *d-f*) time-at-temperature (TAT) histograms. Column 1 shows the median and variability in the proportion of time spent in 12 depth/temperature strata in a box-plot representation. Column 2 shows a time series representation with a fixed depth scale and variable box dimensions representing the local estimated depths of TAT strata. Column 3 shows the same data in an analogous representation, but with a depth scale that indicates the study-area wide central tendency of isotherm depths and internal box dimensions that remain fixed.

a)
b)
c)
d)
e)
f)
Depth (m)
Date–Time
Temperature (°C)
P. electra
TAT (n=34)
P. macrocephalus
TAT (n=34)
MBD:1219.7
MBD:1049.1

Fig. 1-5. Boxplots comparing approximate dive depth distributions derived using time-at-temperature (TAT) data from SPOT satellite tags, to time-at-depth (TAD) summaries, generated from directly observed dive depth time series from SPLASH satellite tag deployments on *a*) melon-headed whales (*Peponocephala electra*), *b*) short-finned pilot whales (*Globicephala macrorhynchus*), *c*) sperm whales (*Physeter macrocephalus*), *d*) Blainville's beaked whales (*Mesoplodon densirostris*) and *e*) Cuvier's beaked whales (*Ziphius cavirostris*). Mean of bottom depths (MBD) at the continuous time correlated random walk (CTCRW) maximum likelihood estimated locations of TAT histograms are shown on each plot.

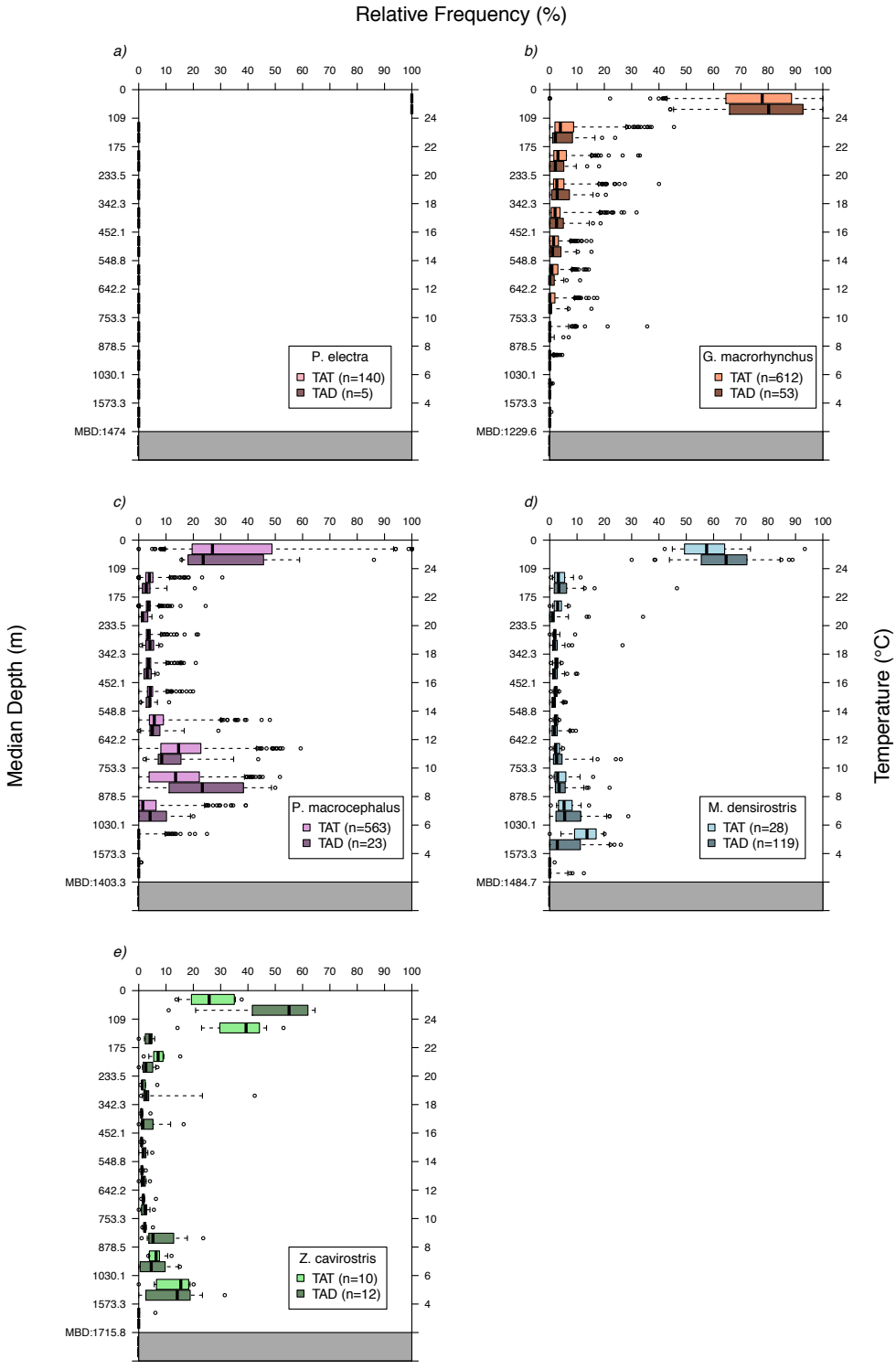
Relative Frequency (%)
Median Depth (m)
Temperature (°C)
a)
P. electra
TAT (n=140)
TAD (n=5)
MBD:1474
b)
G. macrorhynchus
TAT (n=612)
TAD (n=53)
MBD:1229.6
c)
P. macrocephalus
TAT (n=563)
TAD (n=23)
MBD:1403.3
d)
M. densirostris
TAT (n=28)
TAD (n=119)
MBD:1484.7
e)
Z. cavirostris
TAT (n=10)
TAD (n=12)
MBD:1715.8

CHAPTER 2:

Comparisons of dive behavior in a sympatric assemblage of deep-diving toothed-whales from the Bahamas

TREVOR W. JOYCE, JOHN W. DURBAN, HOLLY FEARNBACH, DIANE CLARIDGE, RUSSEL ANDREWS, LISA T. BALLANCE

Abstract

This study examined physiological, morphological, behavioral, and ecological tradeoffs influencing vertical habitat in five deep-diving toothed whale species from the northern Bahamas using dive profile and tracking data collected via small satellite transmitter tags. Tagged species included 1) two species in the family Delphinidae: the melon-headed whale (*Peponocephala electra*, n=13), short-finned pilot whale (*Globicephala macrorhynchus*, n=15); 2) one species in the family Physeteridae: the sperm whale (*Physeter macrocephalus*, n=27); and 3) two species in the family Ziphiidae: the Cuvier's beaked whale (*Ziphius cavirostris*, n=7), and Blainville's beaked whale (*Mesoplodon densirostris*, n=12). Allometric power law functions fitted using generalized linear models (GLM) with terms accounting only for body mass and muscular myoglobin concentration explained comparatively low proportions of variation in maximum dive durations ($R^2 = 0.36$) relative to previous research findings. Much of the deviation from previous studies was driven by two beaked whale species, which were exceptional in both the duration and depth of foraging dives (*M. densirostris* mean 46.1 min & 1129 m; *Z. cavirostris* mean 65.4 min & 1179 m), as well as in length of time between successive deep dives, termed inter-deep-dive intervals (IDDI; *M. densirostris* med. 62 min; *Z. cavirostris* med. 68

min). The inclusion of IDDI as a covariate in allometric GLM models of dive duration and dive depth substantially improved goodness-of-fit metrics for both model types ($R^2 = 0.92$). We hypothesize that the beaked whales extended foraging dives by exceeding aerobic dive capacity, requiring the extension of IDDI to metabolize accumulations of lactic acid. Information theory inference from this study points to an array of intriguing tradeoffs between body size, access to prey at different depths, and time allocated to foraging, commuting, and recovery between dives. These trade-offs have important implications in terms of impacts of toothed whales as apex predators in meso- and bathypelagic ecosystems, as well as in the relative vulnerabilities of different species to anthropogenic impacts.

Introduction

With a few notable exceptions, such as the surface copepod aggregations exploited by *Eubaleana* spp. (Mayo and Marx 1990), the prey resources of cetaceans are often found at depths from the ocean surface ranging from 10s to 1000s of meters (Arranz *et al.* 2011, Watwood *et al.* 2006, Aguilar de Soto *et al.* 2008, Benoit-Bird *et al.* 2004). Due to the retention of air breathing in the secondary aquatic transition of cetaceans, accessing these prey resources requires commuting and limits the duration of each bout of access (Houston and Carbone 1992). The vertical separation between prey resources and the surface imposes a complex array of energetic, physiological, and ecological tradeoffs (Carbone and Houston 1996, Mori 1999) that have played important evolutionary roles in shaping cetacean biology. These tradeoffs may have

been particularly influential among lineages of specialist deep-diving toothed whales from the sub-order *Odontoceti*, which undertake extensive vertical travel to reach mesopelagic (200-1000 m) and bathypelagic (1000-3000 m) prey resources.

One important set of tradeoffs in diving balances the time and energy invested in commuting, with the time available for prey search and energy acquisition at a given target depth (Houston and Carbone 1992, Mori 1999, Costa *et al.* 2001). Different depth strata offer different potential opportunities for energy and nutrient acquisition based on 1) the heterogeneous distribution of prey density with depth (Johnson 1948, Marshall 1965), 2) variation in nutritional quality of prey with depth (Stickney and Torres 1989, Bailey and Robison 1986, Childress and Nygaard 1973), 3) differences in the capacities of prey to evade capture with depth (Childress 1995), and 4) potential vertical differences in the strength of competitive interactions with other cetacean and non-cetacean predators (Waring *et al.* 2001). These energetic and ecological tradeoffs play out as morphological, physiological, and behavioral tradeoffs that constrain the dive duration sustained by different odontocete species and individuals (Mirceta *et al.* 2013, Halsey *et al.* 2006, Noren and Williams 2000).

Dive duration, or the amount of time cetaceans can sustain dive apnea, plays an important role in vertical habitat use tradeoffs, effectively determining the absolute range of accessible dive depths based on vertical commuting velocities and two-way travel times (Georges *et al.* 2000, Costa *et al.* 2001). Longer dives can also enable more efficient access to prey at a given depth within this overall range, by increasing the proportion of dive time spent within the target foraging depth strata relative to the

proportion of dive time spent commuting (Houston and Carbone 1992). Given the important role of dive duration in cetacean vertical habitat use, we first consider in this paper how morphology, physiology, and behavioral factors interact to constrain the length of breath-hold dives.

A range of previous studies have noted a positive relationship of dive duration with body mass, specifically among the toothed whales (Noren and Williams 2000), and more broadly among cetaceans, mammals, and other tetrapods (Noren and Williams 2000, Mirceta *et al.* 2013, Halsey *et al.* 2006). A hypothesized mechanism underpinning this relationship proposes that both oxygen reservoirs and oxygen demand increase as a function of body mass. However oxygen reservoirs scale approximately isometrically (*i.e.*, linearly) with increasing body mass, while oxygen demand scales non-linearly as a function of body mass, based on the allometric scaling of metabolic rates (Kooyman *et al.*, 1983, Castellini *et al.*, 1992, Schreer and Kovacs, 1997). The divergence between these two curves is hypothesized to allow larger species to sustain longer dives (Butler and Jones 1982, Halsey *et al.* 2006). The added dive duration and increased energetic efficiency of a larger body mass, may however be counter-balanced in certain spatial habitats and/or depth strata by the challenges of supporting the metabolic demands of a large body mass under conditions of consistent resource limitation (Lomolino 1985, McClain *et al.* 2006).

In addition to body mass, red blood cell counts and the concentration of myoglobin ([Mb]) in the muscle tissues represent additional dimensions over which body tissue oxygen reservoirs and hence dive duration may vary (Snyder 1983, Noren

and Williams 2000, Ponganis *et al.* 2011). Noren and Williams *et al.* (2000) showed a positive though comparatively weak correlation of maximum dive duration with muscle myoglobin concentrations across a range of taxa within Odontoceti. Mirceta *et al.* (2013) found a similar relationship overall within a broader suite of diving and non-diving mammals. However, boosting body oxygen reservoirs by increasing red blood cell counts and/or increasing concentrations of muscle myoglobin both face upper limits and tradeoffs, due to the increasing viscosity of blood with elevated red blood cell counts (Wells and Merrill 1962), and the potential for self-adhesion and denaturization as myoglobin units become more closely spaced within muscle fibers (Mirceta *et al.* 2013, Lawrence *et al.* 2007).

Finally, dive duration may also be extended by tolerating imbalances between total oxygen reservoirs and oxygen consumption during dives, through a transition from aerobic to anaerobic glycolysis pathways in muscle tissues following the depletion of muscular oxygen reservoirs (Tyack *et al.* 2006, Mori 1999, Carbone and Houston 1996, Kooyman *et al.* 1980). Extending dive time beyond aerobic dive limits (ADL) faces an ultimate ceiling set by the aerobic metabolic demands of critical organ systems and avoiding tissue damage from lactic acid accumulation (Castellini and Somero 1981). However within these ultimate boundaries, exceeding ADL represents an additional potential evolutionary or facultative behavioral strategy for increasing the range of accessible habitats or reducing the ratio of commuting time to foraging time within a dive (Tyack *et al.* 2006, Mori 1999, Carbone and Houston 1996). In one of the few species in which ADL has been empirically measured,

Weddell seals (*Leptonychotes weddellii*) completed >92% of dives within ≤26 min necessitating minimal recovery time (<10 min) between dives during which gasses were exchanged (Kooyman *et al.* 1980). By contrast, infrequent and opportunistic extended dives undertaken by *L. weddellii*, ranged from 26 min up to a maximum of 61.4 min. Extended dives (>26 min) coincided with near exponential increases arterial blood lactate concentrations and the linear extension of recovery periods from ~10 min to ~120min (Kooyman *et al.* 1980). This change in the duration of recovery periods highlights a "time efficiency" tradeoff of extending dives beyond ADL, whereby the proportion of total time budget time available for foraging within deep prey layers is substantially reduced (Mori 2002, Carbone and Houston 1996).

In this study we collected and analyzed an extensive multi-species satellite telemetry and biologging data set in the northern Bahamas archipelago. This data set allowed us to describe where different species and individuals in a sympatric assemblage of deep-diving toothed whales foraged in both the vertical and spatial dimensions of the complex underwater canyon and basin topography of this habitat. We first examined the potential roles of morphological (*e.g.*, body mass), physiological (*e.g.*, myoglobin concentration, [Mb]), and behavioral (*e.g.*, recovery period duration) traits in dive duration capacities and vertical habitat use patterns. Temporal variation in vertical habitat use over diel cycles and spatial distribution patterns with respect to bathymetry were subsequently investigated within the context of inter-specific and inter-individual differences in dive duration and dive depth capacities. Finally, we have attempted to place inter-specific differences in habitat use

within a context of diving efficiency tradeoffs and ecological variation in the vertical and spatial dimensions of oceanic prey fields.

Methods

Field Data Collection

Tagging and biopsy sampling of deep-diving odontocete cetaceans was conducted from a small boat (6.8m rigid hull inflatable) in the NE and NW Providence Channels and Tongue-of-the-Ocean regions of the Great Bahama Canyon system between 23ºN and 27ºN, and 76ºW and 79ºW (Fig. 1). Between 2009 and 2014, cetaceans were located for tagging using visual search from ship and small boat platforms, following line transect and *ad hoc* survey protocols, and passive acoustic monitoring using towed and fixed hydrophone arrays (Gillespie *et al.* 2009, McCarthy *et al.* 2011).

Two models of small (49-55g) Limited Impact Minimally Percutaneous External Electronic Transmitter (LIMPET) satellite telemetry and dive behavior recording tags were successfully attached to five odontocete species: melon-headed whale (*Peponocephala electra*, Family Delphinidae), short-finned pilot whale (*Globicephala macrorhynchus*, Family Delphinidae); sperm whale (*Physeter macrocephalus*, Family Physeteridae), Cuvier's beaked whale (*Ziphius cavirostris*, Family Ziphiidae), and Blainville's beaked whale (*Mesoplodon densirostris*, Family Ziphiidae). Both SPOT (AM-S240A-C, Wildlife Computers Inc.; *e.g.*, Andrews *et al.* 2008) and SPLASH (Mk-10, Wildlife Computers Inc.; *e.g.*, Schorr *et al.* 2014) model

satellite transmitting tags were affixed to free-ranging cetaceans using 4-6.5cm surgical grade titanium darts that were propelled into the connective tissue on or near the base of cetacean dorsal fins using a crossbow (*e.g.*, Pitman and Durban 2012) or black powder gun (*e.g.*, Tyack *et al.* 2011) from a range of 5-25m.

Morphometrics

The body masses of the individual free-ranging cetaceans tagged in this study could not be measured directly in the field. Therefore estimates of median body masses corresponding to the species, sex-, and age-classes of individuals in our tagging dataset were used in the subsequent models examining morphological, physiological, and behavioral factors influencing dive duration and depth (see below). Sexes and age-classes of tagged individuals were assigned with varying degrees of certainty using sexually dimorphic characteristics where present (*i.e.*, *G. macrorhynchus*, *Z. cavirostris*, *M. densirostris*) and when possible assigning genetic sex based on the PCR amplification of the SRY and ZFX genes (*e.g.*, Rosel 2003). Skin biopsy samples were collected using a remote dart biopsy technique (*e.g.*, Hooker *et al.* 2001) and stored frozen in salt-saturated dimethyl sulfoxide (DMSO) solution until the time of processing. Total genomic DNA was isolated from skin biopsy subsamples using either silica-based filter membranes (Qiagen, Valencia, CA) or lithium chloride (Gemmell and Akiyama 1996) standard extraction procedures. Otherwise genders were treated as unknown.

The masses of our study species were also inconsistently reported across the literature in a variety of formats (*e.g.*, maximum, mean, approximation). We therefore estimated median body masses of each species, sex, and age-class using body mass and standard length data from strandings and historic whaling that were retrieved from the National Museum of Natural History (NMNH) whale collection database (downloaded from http://collections.nmnh.si.edu/search/ mammals/ on July 13, 2015), as well as a variety of primary literature sources not included in the NMNH database (Miyazaki *et al.* 1998, Kasuya and Matsui 1989, Heyning 1989, Mead 1989, Lockyer 1976). The mass data provided by all these sources was relatively sparse and often biased towards the smaller end of the size spectrum in many species, presenting challenges in estimating representative median masses for each species, sex, and age class based directly on the mass measurements. To overcome this challenge we estimated power law relationships of body mass to standard length for each species. Following the approach of Kasuya and Matsui (1984) this relationship was modeled as a linear function of log-transformed body mass and standard length measurements using *lm* command from the R library *stats*. The extensive standard length measurement data from NMNH and other sources (*e.g.*, Heyning 1989, Mead 1989) were then used to estimate the median standard length of each species, sex, and age class, and then the median estimated mass of each species, sex, and age-class was predicted from these power law relationships. Threshold lengths separating sub-adult from adult age classes in the standard length dataset were defined based on literature reported values (Heyning 1989, Mead 1989), as well as on

the minimum length at which sexual maturity characteristics, such as evidence of pregnancies and increases in gonad mass, were described in necropsy notes.

Spatial Distributions and Location-specific Covariates

During surface intervals, both SPOT and SPLASH tags transmitted a series of messages to any overhead satellites in the Argos network (www.Argos-system.org), which permitted the estimation of two-dimensional positions with error ellipse estimates. The movement track for each tagged cetacean over the transmission life of each tag was estimated from irregularly spaced Argos position fixes using a Continuous Time Correlated Random Walk (CTCRW, Johnson *et al.* 2008) model fitted in the R package *crawl* (Johnson *et al.* 2013), modified to include an observation model for the full extent and shape of the Argos error ellipses (McClintock *et al.* 2015). Location estimates were predicted from fitted CTCRW models at regular one-hour date-time stamps within each track, and were subsequently used to 1) calculate solar and lunar rise and set times, 2) estimate bathymetric depth, and 3) predict the isotherm boundaries at the mean locations of SPOT time-at-temperature histograms (see *Dive Patterns*). Bathymetric depths were extracted from a 0.0083 º latitude and longitude resolution bathymetric digital elevation model at predicted locations using the function *extract* from the R library *raster* (Hijmans and van Etten 2012). Sunrise and sunset times as well as solar angular elevations were calculated at the predicted locations and corresponding date-time stamps using the function *sunriset* from the R library *maptools*.

Dive Depth, Dive Duration, and Inter-Deep-Dive Intervals

The transmitted messages from tags used in location estimation included moderate-resolution dive behavior data. They were summarized from raw high-resolution environmental sensor time series onboard the tags (*e.g.*, temperature, pressure, wet/dry) in order to facilitate transmission over a bandwidth and time-limited connection with the Argos satellite system. In SPLASH tags, a pressure sensor allowed the direct measurement of dive depth and dive duration. Pressure transducer observations (accuracy: ±1% of depth reading) from SPLASH tags were summarized internally within the tag and uploaded in the form of 1) a behavior log which summarized pressure and wet-dry measurements into sequences of dives and surface intervals, and 2) a time series log that recorded depth observations at either 2.5 or 5 minute intervals. Each dive in the behavior log was defined by the deepest depth reached and time interval between successive dry measurements. In contrast to SPLASH tags, SPOT tags carried a thermistor and transmitted time-at-temperature (TAT) histogram summaries, which required the use of temperature profile information to interpret this proxy in terms of the depths of dive activity (Joyce *et al.* 2016). These TAT summaries consisted of the proportion of thermistor readings, collected at 10-second intervals over 6-hour sampling periods, that fell into 12 temperature categories (<4ºC, 4-6ºC, 6-8ºC, 8-10ºC, 10-12ºC, 12-14ºC, 14-16ºC, 16-18ºC, 18-20ºC, 20-22ºC, 22-24ºC and ≥24ºC). Sampling periods of TAT were programmed to begin at 01:00, 07:00, 13:00, or 21:00 local time, which were selected

so that the majority (>80%) of sampling contributing to each TAT histogram fell within either daytime or nighttime periods over the course of seasonal variation in daylight periods.

"Foraging" dives were defined as dives falling within a set of species-specific depth ranges where foraging activity was known or inferred to occur. Dive distributions were principally interpreted using published digital acoustic recording tag (DTAG) dive profiles that described the vertical distribution of echolocation clicks and/or "buzz" vocalizations associated with prey capture attempts (Aguilar de Soto *et al.* 2008, Tyack *et al.* 2006, Watwood *et al.* 2006, Arranz *et al.* 2011, Miller *et al.* 2004a). Published DTAG profiles were available for all tagged study species except *P. electra*. Species-specific foraging depth range definitions were developed using the best available information and were principally used to distinguish "foraging" dives from shorter and comparatively shallow dives. In the beaked whales, these short and relatively shallow so-called "bounce" dives have been shown to be non-foraging in nature based on the absence of echolocation clicks and feeding buzz cues (Tyack *et al.* 2006). In species where the distribution of dive depths was distinctly bimodal in nature, we selected depth thresholds that classified the deeper of the two peaks as foraging activity, to separate out this near-surface dive behavior. The time intervals between successive "foraging" dives in the behavior log, are referred to in this paper as inter-deep-dive intervals (IDDI, *sensu* Tyack *et al.* 2006). These were calculated for all species as the sum of surface period durations and the duration of any short and comparatively shallow dives that did not meet the foraging dive criteria

interspersed between deeper dives. We further defined "time efficiency" in this paper as the proportion of each tagged individual's time budget engaged in foraging dives (behavior log) or spent within foraging depth strata (TAT and time series).

Models of Dive Duration and Depth

Several previous inter-specific comparative analyses of mammalian dive behaviors (Noren and Williams 2000, Halsey *et al.* 2006, Mirceta *et al.* 2013) have examined factors influencing maximum dive duration (T_{max}) as a response variable. As an initial step in examining the morphological, physiological, and behavioral factors influencing dive behavior variation in the odontocete assemblage of our study area we first evaluated the predictive performance of the odontocete-specific allometric model (eq. 2) from Noren and Williams (2000).

$$T_{max} = 0.68\, m^{0.47} \qquad (1)$$

The coefficient of determination, R^2, indicating the proportion of variance in T_{max} explained by this model was calculated across individuals of all species tagged in this study, and also within specific family-level sub-groupings.

For comparability with previous modeling efforts, we further developed models of T_{max} using dive information from the tagged individuals in this study. In developing models at the individual level we had to contend with the phylogenetic non-independence of dive behaviors both between individuals within species, as well as between species. The random effects structure in a mixed model framework is often applied to account for non-independence in model residuals (Villemereuil and

Nakagawa 2014). Villemereuil and Nakagawa (2014) have further elaborated an approach to explicitly account for the evolutionary interdependencies between species by incorporating a phylogenetic tree model with divergence time estimate into the mixed model framework in an analysis termed phylogenetic generalized linear mixed models (PGLMM). The PGLMM of T_{max} developed in this paper incorporated the cetacean phylogenetic tree hypothesis of McGowen *et al.* (2009) as well as fixed effects covariates including estimates of median body mass (*m*, see Morphometrics), literature-derived myoglobin concentration ([*Mb*]), and median IDDI from individuals in the behavior log dataset.

Following the mixed-effects model selection guidance outlined by Zuur *et al.* (2009), we undertook an initial model comparison phase in which we contrasted different random effects structures with a full complement of fixed effects covariates. Bayesian posterior probability distributions for a fixed-effects only log-log (*i.e.*, power law) generalized linear model (GLM) and a log-log PGLMM model of T_{max}, were implemented in the R function *MCMCglmm*. Bayesian Markov Chain Monte Carlo (MCMC) simulations used the default Gaussian fixed effects prior (mean = 0 and variance = 10^{10}) implemented in *MCMCglmm*, and an inverse-Gamma random effects priors with shape and scale parameters of 0.01 (Villemereuil and Nakagawa 2014). MCMC simulations were repeated over 10^5 iterations, discarding a burn-in phase of 1000 iterations and applying a further thinning of 1 in every 50 iterations. In this initial phase of comparing model random effects structures, the fixed-effects and mixed-effects log-log models were evaluated on the basis of Deviance Information

Criterion (DIC) scores, and a model weighting metric, *w*DIC, that was developed based on the Akaike's weight metric (*w*AIC, eq. 2) from Burnham and Anderson (2002).

$$wDIC = \frac{e^{-0.5(DIC_i - DIC_{min})}}{\sum_{i=1}^{n} e^{-0.5(DIC_i - DIC_{min})}} \qquad (2)$$

After the selection of a random-effects structure (in this case the fixed-effects-only model), log-log PGLMM with the different combinations of fixed-effects terms were estimated, and a second phase of model selection was undertaken on the basis of DIC and *w*DIC.

To provide a broader phylogenetic context for the dive behaviors observed among the tagged species in this study area, we also developed phylogenetic generalized least squares (PGLS, Grafen 1989) models of T_{max}. This analysis incorporated a range of other odontocete species for which literature reported values of T_{max}, m, $[Mb]$, and IDDI were available or could be extracted from supplemental materials. Additional species included: beluga (*Delphinapterus leucas*), narwhal (*Monodon monoceros*), harbour porpoise (*Phocoena phocoena*), killer whale (*Orcinus orca*), pantropical spotted dolphin (*Stenella attenuata*), pygmy sperm whale (*Kogia breviceps*), and northern bottlenose whale (*Hyperoodon ampullatus*) (Westgate *et al.* 1995, Martin and Smith 1999, Hooker and Baird 1999, Noren and Williams 2000, Baird *et al.* 2001, Scott *et al.* 2001, Laidre *et al.* 2002, Kielhorn *et al.* 2013, Durban and Pitman unpublished data). Like PGLMM, PGLS models in this analysis incorporated the McGowen *et al.* (2009) phylogenetic tree into the variance-

covariance matrix of a generalized least squares model using a Brownian motion model of trait evolution (Grafen 1989).

Finally, models of T_{max}, which were developed for comparability to previous modeling efforts, collapsed the variability of each individual's dive behavior to a single number, which may not have described the typical dive behaviors of that individual or species. We therefore also developed log-log PGLMM models of dive duration (T) and dive depth (Z) using all of the unique dives for which IDDI was available. These versions of PGLMM models contained a random effect of species (SPP) that incorporated a phylogenetic correlation structure, and also random effects of individual variability (PTT) nested within species. The choice between different random- and fixed-effects structures in these models followed the same model selection procedure described above for T_{max}.

Foraging Depth and Bathymetric Depth

We used dive depth and spatial distribution information from tagging to examine the relative geographic affinities of different deep-diving species for various benthic habitats accessible within the observed dive ranges. This was examined for each species by overlaying the CTCRW predicted movement tracks on the distribution of bathymetric habitat that fell within the foraging dive depth range. We also calculated the average proportion of coordinate fixes that were recorded over habitats falling within the foraging dive depth range of each species detailed above. Because the number of position fixes recovered varied widely between tagged

individuals, species averages were calculated as a grand mean of averages across individuals. For particular species that showed sex and/or ontogenetic differences in spatial distribution patterns we also calculated a sex-specific average spatial overlap with bathymetric habitats within dive ranges. Finally, we also calculated correlation coefficients between maximum depth of dives recorded in the behavior log for each species and the bathymetric depth corresponding to the predicted CTCRW location at the midpoint of each dive.

Results

Tagging

Over the period 2009-2014, 75 Argos tags were successfully deployed on five deep-diving odontocete cetacean species commonly encountered within our study area, yielding 7752 position fixes and 12,204 h of dive data (Table 1). Both SPOT and SPLASH tags were successfully deployed on all five species (Table 1), however SPLASH tags were deliberately deployed in a higher proportion of tagging attempts on the two beaked whales species (75% and 86%). The tagging of the delphinids and physeterids emphasized SPOT tags (Table 1). A total of 24 individuals were tagged and biopsied simultaneously; with long-term photo identification catalogues allowing the linkage of a further 15 biopsied records from individuals that were tagged on separate occasions. The overlap between tagging and biopsy datasets allowed the genetic identification of sex in 52% of the tagged individuals.

Morphometrics

Across the five tagged species, we compiled 175 simultaneous measurements of mass and standard length from the literature and unpublished sources, and compared with 1,912 records in which standard length alone was measured (Table 2). This revealed a systematic bias towards smaller individuals being measured for mass (Fig. 1) and skewed direct estimates of mean and median body mass based on body mass data alone. Estimates of median body mass from power law models relating body mass and standard length (Table 2) yielded a body mass range spanning nearly two orders of magnitude from *P. electra* (169.6 kg) to *P. macrocephalus* (11774.5 kg). Adult *P. macrocephalus* typically exhibited extreme sexual size dimorphism (male:female body mass ratio of 2.3), however no adult males were tagged in this study. In the subsequent modeling of dive duration and dive depth sub-adult male body mass values were used (Fig. 1), and the sub-adult male and adult female *P. macrocephalus* regularly observed in this study area were much closer in body mass (Table 2).

Dive Depth and Duration

The tagged species occupied partially overlapping foraging ranges (Fig. 2) in the vertical dimension. Dives of the two delphinid species, *P. electra* (mean 310.1 ± s.d. 100.6 m) and *G. macrorhynchus* (mean 203.7 ± s.d. 220.7m) were generally distributed within the upper- to the central-mesopelagic (~200 - 800m), although *G. macrorhynchus* also occupied depths <200m (*i.e.*, epipelagic) at night. *P.*

macrocephalus (mean 899.9 ± s.d. 104.7 m) dove relatively consistently to lower mesopelagic depths (~600-1000m). The two beaked whales, *M. densirostris* (mean 1128.8 ± s.d. 229.6 m) and *Z. cavirostris* (mean 1179.8 ± s.d. 225.3 m) generally occupied the lower mesopelagic and upper-bathypelagic (Fig. 2). Overall, dive depths were positively related to dive duration in each species, although the relationship was non-linear in many species. Power law functional forms provided the best fits for *P. electra* and *P. macrocephalus*, and linear and exponential formulations provided better fits for *M. densirostris*, *Z. cavirostris*, and *G. macrorhynchus* (Fig. 3).

Models of Maximum Dive Duration

In examining the morphological, physiological, and behavioral factors influencing maximum dive duration in our study species, we found that models employing *m* and [*Mb*] provided inadequate explanations of the observed variation in T_{max} among the tagged individuals in this study. The allometric model (eq. 2) from Noren and Williams (2000) relating T_{max} with *m*, explained less variance ($R^2 < 0$) than an overall mean ($\overline{T_{max}}$). In particular this model substantially underestimated maximum dive duration in the two ziphiid species *M. densirostris* and *Z. cavirostris* (Fig. 4a). However, it did perform considerably better when predicting maximum dive duration of individuals in the delphinid (*P. electra* and *G. macrorhynchus*), and physeterid (*P. macrocephalus*) families (R^2=0.90, Fig. 4a). This divergence from model expectations of allometric scaling of T_{max} was particularly highlighted by the maximum dive duration of *M. densirostris*, which on average exceeded the maximum

dive durations of *G. macrorhynchus* females by a factor of 6.2x, despite their similar median masses (*M. densirostris*: 842.9 kg, *G. macrorhynchus*: 868.0 kg). Additionally, despite weighing 7.6x less than *P. macrocephalus*, on average *Z. cavirostris* dove for 17.6 min longer per deep dive. Because of these large disparities, a simple allometric GLM model (Mod. 5b) did not fare substantially better than the Noren and Williams allometric model in predicting T_{max} of tagged individuals, which can be seen in a relatively poor trend line fit (Fig. 4b), and in an R_m^2 value of 0.31 (Table 3). The log-log GLM model with [*Mb*] as covariate (Mod. 6b) likewise explained only 26% of the variance in T_{max} (Table 3), which is similarly indicated by a weak trend line fit (Fig. 4c). Together *m* and [*Mb*] accounted for <37% the variance in T_{max}.

Including IDDI along with *m* in log-log GLM models (Mod 2b, Table 3) explained a substantially greater proportion of the variance in T_{max} ($R_m^2 = 0.92$) relative to models with just *m* and [*Mb*], and provided a considerably closer alignment of the model predictions to the observed data (Fig. 4d). This improvement in model fit was demonstrated by 1) the selection of Model 2b (IDDI and *m*) as the most parsimonious model fit (Table 3), and 2) by the trend lines in Figure 4d, which show the different functional relationships of T_{max} to *m*, with input values of IDDI corresponding to the median IDDI of the delphinids and physeterids (8 min), and ziphiids (65 min). In addition to the IDDI of the two ziphiids being comparatively long in absolute terms (Fig. 5), these IDDI were also long in proportion to dive

duration (Fig. 6b), with median IDDI : T_{max} ratios of 1.41 and 1.01 among the ziphiids compared to ratios of 0.39, 0.38, and 0.17 among the delphinids and physeterids.

The comparison of PGLS models in Table 4 further supported the importance IDDI in the prediction of T_{max}, in this case over a wider range of taxonomic diversity than the species tagged in the present study. This analysis included representative species from all six primarily marine families of Odontoceti. Figure 7 also shows a clustering of species belonging to the Delphinoidea (Families: Monodontidae, Phocoenidae, Delphinidae) and Physeteroidea (Families: Kogiidae, and Physeteridae) superfamilies in m and T_{max} space, while the Ziphioidea (Family: Ziphiidae) were clearly clustered apart from these two families. The PGLS Mod. 2 functional relationships between m and T_{max} with different IDDI input values corresponding to the median IDDI values of Delphinoidea, Physeteroidea, and Ziphioidea (Fig. 7), illustrate that this inter-familial variation could be readily explained by differences in *IDDI* within and between families (Fig. 7).

Models of Dive Duration and Depth

Figures 8a and 8b illustrate that variation in the duration (T) and depth (Z) of individual dives was considerably greater than the variation in T_{max} between individuals, which was reflected in the outcome of the initial phase of mixed-effects model selection. In both cases a PGLMM structure with random effects of species including phylogenetic correlations and random effects of individuals within species were selected on the basis of wDIC values over models that explained the variation in

T and *Z* solely on the basis of fixed effects covariates *m*, [*Mb*], and IDDI. As demonstrated by the relatively low marginal coefficients of determination (R_m^2) for the PGLMM in Tables 5 and 6, the fixed effects components of these models contributed minimally to the explanation of variation in *T* and *Z* after accounting for phylogenetic and random individual effects. This is illustrated by the large random effects offsets of the delphinid, physeterid, and ziphiid families from the main effect of the fixed effects covariates shown in Figure 8a and 8b, and the relatively small coefficient of the log(IDDI) term when compared to the log(IDDI) coefficient in models of T_{max}. Although not selected in the initial phase of model comparison, the R_m^2 values of 0.56 and 0.75 in the fixed-effects only GLM models of *T* and *Z* (Mod. 1d and 1f) demonstrate that these fixed effects could explain a substantial portion of the variance in both response variable. Overall, Figures 8a and 8b illustrate that the same general patterns observed in T_{max} also hold in T and Z.

Time Budgets

Due to the comparatively long IDDI for ziphiids, the delphinids and physeterids spent a lower proportion of their time budgets at or near the surface during foraging periods and consequently a higher proportion of their time at foraging depths. This effect is illustrated by the maxima of only 37.0% and 34.2% of 6-hour TAT histogram time blocks that *M. densirostris* and *Z. cavirostris* in temperature/approximate depth ranges thought to be associate with foraging (Fig. 6a). This contrasted with upwards of 84.1%, 89.2%, and 72.3% that *P. electra*, *G.*

macrorhynchus, and *P. macrocephalus* were able to spend in their respective foraging temperature/approximate depth ranges (Fig. 6a). In part this reflected the shorter commuting distances and consequently shorter commuting times exhibited by the delphinids and physeterids relative to the ziphiids. However, when comparing bouts of *P. macrocephalus* and *M. densirostris* dives that reached similar depths of approximately 800m, on average *P. macrocephalus* were able to spend 2.05x more of their time engaged in foraging dives relative to *M. densirostris*. When averaged over an entire diel cycle, the two delphinid species spent on average 27.2% and 31.6% of their respective time budgets within target foraging strata, only moderately higher than the 24.0% and 22.6% spent by the two ziphiids. However, the low median values and large variability in time efficiency exhibited by these two delphinid species (Fig. 6a) predominately reflected the large portions of daylight periods spent at or near the surface not engaged in foraging behaviors.

Diurnal Patterns

The tagged species in this study showed divergent responses to daytime and nighttime light levels, both in terms of dive depth and dive frequency (Fig. 8). The shallowest diving species, *P. electra*, showed a binary response in which no daytime dives were recorded below 25m or the 24°C isotherm (median depth 117 m) in over 869 hours of daytime behavior log and TAT data, respectively. Foraging dive activity in this species appears to be exclusively confined to nighttime periods. *G. macrorhynchus*, with the second shallowest median dive depths, undertook daytime

dives that were on average 417 m deeper than nighttime dives, but also 69.9% less frequent, and appear to be concentrated during hours of lower incident light angles during the early morning and late afternoon periods. Uniquely among the species tagged in this study, the distribution of nighttime dives in *G. macrorhynchus* ranged from the central mesopelagic zone to the near-surface without a clear distinction (bi-modality). This nighttime dive pattern however varied between the sexes in this highly sexually dimorphic species with males that were 2.05x larger by mass and able to dive 5.3% longer than females. Males continued to dive to consistently deeper depths at night, while the dive depths of females varied to a greater extent between day and night. Overall *P. macrocephalus* displayed small diurnal differences between median daytime (920 m) and nighttime (888 m) dive depths. This pattern also varied between the different sexes and age-classes of *P. macrocephalus*: females and juvenile males that were tagged within matrilineal social groups dove on average to 3.5% shallower depths and exhibited a 26.4% larger diurnal difference in dive depths when compared with sub-adult males tagged either solitarily or in bachelor groups. *M. densirostris* exhibited daytime dives that were on average 142.3m shallower than nighttime dives. This diurnal dive pattern was not observed in all tagged *M. densirostris* but was detectable in 5 of 7 individuals. *Z. cavirostris*, the deepest diving species, showed little to no difference in foraging dive depths between day and night.

Spatial Habitat Use

Considering the bathymetric topography within our study area, we observed interspecific differences in spatial distribution as reflected in overlap of CTCRW-predicted position fixes with different bathymetric depths (Figure 9). In general the CTCRW-predicted locations of the deeper diving species *P. macrocephalus*, *M. densirostris*, and *Z. cavirostris* were more frequently localized over areas where the bottom was within reach of their dives (Fig. 9 c, d, e) while shallower diving delphinids, *P. electra* and *G. macrorhynchus* were proportionally less frequently localized over habitats where the benthos fell within their respective dive depth ranges (Fig. 9 a, b).

There was also some intra-specific variation in these patterns. In particular, *M. densirostris* showed considerable inter-individual variation. Nine of 11 *M. densirostris* individuals exhibited consistent associations with areas where the bathymetric depth were less than the maximum recorded dive depth of this species (1888m), while two other *M. densirostris* individuals ranged widely over a variety of benthic depths that were beyond the range of their dive capacities (Fig. 9d). In this habitat *P. macrocephalus* exhibited gender differences in spatial affinity for different bathymetric habitats. A group of females and dependent calves was consistently localized along the northern slope of the Great Bahama Canyon in an area where the benthos fell within their dive range and the shape of this distribution pattern also appears to reflect the bathymetric topography which becomes shallower from east to west. By contrast sub-adult males *P. macrocephalus* encountered solitarily or in small groups were found to range widely over a range of bathymetric habitats with both

shallower and deeper than their maximum dive depth (1344 m). Finally, the dive depths of *Z. cavirostris* showed a relatively high correlation of with bottom depths ($\rho = 0.62$), across the wide range of bathymetric depths occupied by this species (90% central quantile: 851.2- 2247m). The other species all showed low overall correlations of dive depths with bottom depths ($\rho = 0.16$- 0.27).

Discussion

Dive behavior and body mass

As in previous efforts (Noren and Williams 2000, Halsey *et al.* 2006, Mirceta *et al.* 2013), this study found an overall positive relationship of dive duration with estimated body mass. In particular, the relatively strong performance of the Noren and Williams (2000) Eq. 2 model among the delphinids and physeterids suggested that variation in body mass did underlie an important component of the variation in dive duration, dive depth, and the proportion of time available for foraging. The difference in dive duration between *M. densirostris* (med. 843 kg) and *Z. cavirostris* (med. 1557 kg) also pointed to the relevance of body mass as a predictor of dive capacities. However, the comparatively low proportion of variance in maximum dive duration explained by body mass alone, suggested a need for additional covariates, especially to explain the dive durations of the two beaked whales species.

Considering variation in body mass solely in a context of dive duration and dive efficiency may also have omitted other potential factors. For example, larger size likely decreased the per-unit-mass metabolic rate and external surface-area-to-

volume ratios fostering greater overall efficiency of energy use and thermoregulation (Kleiber 1975, Hayssen and Lacy 1985). Greater size may also have increased the efficiency of locomotion in a viscous fluid medium by reducing drag at higher Reynolds numbers (Lang 1966, Sato *et al.* 2007). Larger size may additionally have conferred the ability to capture a greater volume of prey during each dive, endure longer periods of fasting (Lindstedt and Boyce 1985), and subsist on lower quality forage by increasing gastro-intestinal surface area and processing time (Demment and Van Soest 1985). Conversely, larger size could have limited maneuverability in the pursuit of prey (Miller *et al.* 2004b, Aguilar de Soto *et al.* 2008, Aoki *et al.* 2012). Odontocete size may also have come under selection for reasons unrelated to foraging and energetic efficiency, such as minimizing risk from predators (Sinclair *et al.* 2003) or competing for mates (Clutton-Brock 1988). Finally, although body mass correlated with dive duration, it is unlikely that this variable directly determines diving ability, and instead it represents a proxy for the quantity of oxygen stored in various tissue reservoirs (*e.g.*, blood, muscle, lungs), relative to metabolic rate (Halsey *et al.* 2006),

Dive behavior and myoglobin concentration

The quantity of oxygen stored in various tissue reservoirs may also have varied based on the concentrations of oxygen storing molecules in these tissues. However, in this study, which focused particularly on deep-diving specialist taxa, [Mb] accounted for only a minimal additional proportion of the variance in maximum

dive duration, dive duration, and depth, and its inclusion could not be justified in models of T_{max}, T, and Z. Compared to epipelagic odontocetes, baleen whales (Mysticeti) and non-diving mammals (Mirceta *et al.* 2013), taxa in this study exhibit relatively high values of [Mb]. We suggest that this potentially reflected a physiological ceiling on myoglobin concentrations ([Mb]), possibly due to self-adhesion and denaturation as myoglobin units become more densely concentrated in muscle fibers (Mirceta *et al.* 2013, Lawrence *et al.* 2007).

One potential evolutionary response to this constraint is the genome-level modification of peptide sequences to increase myoglobin net surface charge, Z_{Mb}, a property which increases the repulsion and decreases the adhesion of adjacent myoglobin units (Mirceta *et al.* 2013). These authors noted elevated Z_{Mb} within the ziphiids (Z_{Mb} = 4.80) relative to delphinids (Z_{Mb} = 4.03), physeterids (Z_{Mb} = 4.15), and kogiids (Z_{Mb} = 4.24). However, despite this elevated Z_{Mb} value, empirical measurements of [Mb] among ziphiids did not appear to be exceptional relative to other specialist deep-diving odontocete taxa based on literature reported values (Sharp and Marsh 1953, Noren and Williams 2000, Velten *et al.* 2013). To us this suggested a need for additional covariates to explain the extended dive duration and deep dive depth of ziphiids with respect to their body masses.

Dive behavior and Aerobic Dive Limits

The limits of dive duration related to body mass and muscle myoglobin concentrations both presuppose that diving occurs within dive time windows and/or

energetic expenditure budgets within which oxygen reservoirs match or exceed oxygen consumption. However, transitioning from aerobic to anaerobic glycolysis pathways after the depletion of muscular oxygen reservoirs may have offered a alternative strategy that could enable the substantial extension of dive duration with respect to body mass (Carbone and Houston 1996, Mori 1999, Tyack *et al.* 2006). Using the Aerobic Dive Limit (ADL) of *Leptonychotes weddellii* (Kooyman *et al.* 1980), one of the only marine mammals for which the diving metabolic rate and ADL have been empirically measured, Tyack *et al.* (2006) derived Calculated Aerobic Dive Limit (cADL) values of 25 min and 33 min for *M. densirostris* and *Z. cavirostris*, taking into account their respective masses.

$$cADL = \frac{body\ O_2\ reservoirs}{dMR} \qquad (3)$$

Both estimates of cADL were substantially less than the observed mean dive duration of *M. densirostris* and *Z. cavirostris* (46.2 min and 65.3 min, respectively). This led to a hypothesis that, at their respective body masses, these species partially relied on muscular anaerobic glycolysis to access prey resources beyond the reach of aerobic dives. As an alternative hypothesis (Velten *et al.* 2013) proposed that economical diving locomotion (including substantial gliding) and some distinct histological characteristics could combine to decrease diving metabolic rates (dMR) in ziphiids, thus allowing the substantial extension of cADL relative to the cADL estimates that were proposed by Tyack *et al.* (2006).

During this study we lacked the technical capacity to empirically test these alternative hypotheses with field measurements of dMR or blood lactate

concentrations in free ranging beaked whales. However, the dMR values used by Velten *et al.* (2013) (to compute cADL values that exceeded *M. densirostris* mean dive duration) were 18% and 37% lower than the basal metabolic rate (bMR) values estimated for this species based on general allometric relationships of body mass to bMR in mammals (Kleiber 1975). Several empirical findings have shown that dMR values in other diving species generally exceeded bMR by a factor of ~2x (Castellini *et al.* 1992, Ponganis *et al.* 1993), raising questions regarding the reliability these estimates of cADL.

In addition to the exceptional length of ziphiid dives relative to their body masses, the protracted IDDI exhibited by the ziphiids in this study may also have indicated the extension of dive durations beyond ADL. Tyack *et al.* (2006) interpreted these extended IDDI as periods of recovery from lactate debt, mirroring the extension of recovery periods and concomitant increases in lactate concentration observed in *L. weddellii* after it exceeds the ~26 min ADL threshold. The behavior log dive profiles from *M. densirostris* (695.91 hr) and *Z. cavirostris* (365.65 hr) in this study, confirmed these patterns of extended IDDI documented by Tyack *et al.* (2006) over a more extensive time series. Furthermore, the information theory inference from the PGLMM models of T_{max}, T, and Z, pointed to the importance of extended IDDI (Tables 3, 5, and 6; Figs. 4, 7, and 8) as a key variable in accounting for a significant component of dive duration variability within our study species. Our PGLS analysis further extended this inference to a wider range of odontocete taxonomic diversity.

However, one important caveat to consider is that both *M. densirostris* and *Z. cavirostris* exhibited very infrequent (≤1.46% of IDDI) but notable "back-to-back" deep foraging dives with an intervening IDDI of <10 min. These were exceedingly rare, however these short IDDI raised a question of whether prolonged IDDI represented an absolute necessity, based on the physiological need to immediately metabolize excess lactate? This question hinges on whether ziphiids were diving at or near their physiological capacity as proposed by Tyack *et al.* (2006), or whether they might have been able to pursue two or more extended dives in short succession by tolerating and buffering accumulated lactic acid and metabolizing it at a later time (Hazen *et al.* 2015). Comparing buffering capacities of muscle and blood tissues between ziphiids and others odontocetes represents an intriguing potential future line of research. As alternative hypotheses, the temporal partitioning of metabolically costly food digestion from oxygen-constrained food acquisition (Rosen *et al.* 2015), and/or engaging in social behaviors (Sparling *et al.* 2007), could potentially account for these extended IDDI among ziphiids. However, if these alternative hypotheses were true, it is intriguing that neither the delphinids nor physeterids exhibited a similar need to pause between dives. Taken together with the cADL calculated by Tyack *et al.* (2006), we contend that a preponderance of evidence, including model inferences from this study, supported an overall hypothesis that the small to medium tagged species of ziphiids rely at least partially on anaerobic metabolism to extend the duration of most dives. This may have allowed these species to access prey resources that would otherwise lie

beyond the economical reach of their dive capacities given on their relatively small body sizes.

Moreover, even taking into account the as yet unresolved mechanism underpinning these extended ziphiid IDDI, our data showed that these extended IDDI had important consequences in terms of the proportion of time available for foraging in different species. After having accounted for differences in commuting times necessary to reach different depths, the ziphiids spent a much lower proportion of time at their target foraging depths (max. 34-37% vs. 72-89%) relative to other sympatric species. This discrepancy warranted the consideration of the ecological context in which this reduction in time efficiency occurred.

Ecological Context

The context for the morphological, physiological, and behavioral tradeoffs detailed above was a complex northern Bahamas marine ecosystem, in which prey abundance, nutritional quality, and capacities for evasion varied heterogeneously with respect to depth. Despite this heterogeneity there are general physical properties of oceanic habitats that combine to produce dynamic yet typically persistent structuring of prey fields with depth (Marshall 1965). One key property is the exponential attenuation of down-welling photosynthetically-active radiation over the euphotic zone (Jerlov 1968). This along with the remineralization of sinking particulate organic matter (POM), results in a roughly exponential decline of POM flux from near-surface to the abyssal ocean (Martin *et al.* 1987). With the

important exception of vertically migratory deep scattering layer (DSL) organisms and the mesopelagic trophic web that they support, this decline typically reduces the caloric inputs to trophic webs with depth (Gage and Tyler 1991). There is also a decrease in visual detectability of prey with depth (Warrant 2000), providing some species with a refuge from visual predators. As a result, DSL organisms in oligotrophic subtropical ecosystems tend to form a distinct biomass peak within the mesopelagic twilight depths ranging from approximately 200-600m (Barham 1966). During nighttime, and other low-light periods (*e.g.*, eclipses, Ohman 1984), a vertically migratory component of the DSL shifts upwards to forage closer to the source of POM production in the euphotic zone, leaving behind deeper concentrations of non-migratory or minimally-migratory species (Childress 1995).

With increasing depth, the meso- and bathypelagic fish, cephalopod, and crustacean prey of deep-diving marine mammals also exhibit greater sedentism and less locomotory performance (Childress 1995). In parallel, deeper dwelling organisms may also increase in water content and decrease in protein content (Childress and Nygaard 1973, Bailey and Robison 1986, Stickney and Torres 1989).

The settlement and resulting concentration of sinking POM flux at the benthos also supports a larger community of benthic boundary layer (BBL) recyclers and consumers than would be found in mid-waters at comparable depths (Angel and Boxshall 1990). Thus the densities, caloric values, and relative difficulties of capturing prey all vary substantially in vertical and temporal

dimensions, as well as to a lesser but still significant extent in the spatial dimension (Benoit-Bird *et al.* 2001). In the subsequent taxa-specific sections, we explore how the different species of odontocetes in our study area appear to deal with these ecological, physiological, morphological, and behavioral tradeoffs, and propose hypotheses for how the adaptations observed in each group match the specific ecological contexts of their typical foraging habitats.

Ziphiid Synthesis Hypothesis

Our synthesis hypothesis for the dive duration, IDDI, dive depth and body mass in the beaked whales proposes that these species have adopted a seemingly inefficient strategy of relying on anaerobic respiration to access lower-mesopelagic and bathypelagic prey layers. Cephalopod, fish, and crustacean prey at these depths may have been less abundant and less nutritionally rewarding relative to shallower prey, however this prey was also likely less evasive and the beaked whales likely faced fewer competitors in these niches. Importantly they have accomplished this balance of diving for sufficiently long to energetically recoup the costs of commuting and profit from dives, while maintaining relatively small body masses. Smaller body masses may have been particularly important in these deeper habitats, since the total metabolic demand of a larger body mass may have been difficult sustain given calorically-restricted lower mesopelagic and bathypelagic food webs (Gage and Tyler 1991).

We also hypothesize that a regular reliance on anaerobic respiration among the beaked whales could also have accounted for two interesting findings in the analyses of Velten *et al.* (2013) and Mirceta *et al.* (2013). Velten *et al.* (2013) proposed that the "high proportion (76-83%) of Type II glycolytic muscle fibers in *Mesoplodon* spp. represent a metabolically inexpensive oxygen store within the muscle for use of less abundant Type I fibers." An alternative interpretation of this histological finding might be that this high proportion of Type II glycolytic fibers represented an adaptation to sustained anaerobic muscular function. Furthermore, the comparatively high net surface charge ($Z_{Mb} = 4.80$) among the beaked whales relative to bulk *Mb* concentrations, which were otherwise broadly similar to other deep divers (Mirceta *et al.* 2013, Noren and Williams 2000), might have represented an adaptation to allow the tight spacing of myoglobin units within proportionally rare aerobically metabolizing Type I fibers. Consequently, the higher proportional representation of glycolytic Type II fibers, which in other mammals typically had lower [Mb] (Drews and Engel 1961, Peter *et al.* 1972, Nemeth and Lowry 1984), could explain the overall similarity observed between the bulk [Mb] of the beaked whales and other deep divers.

There was also evidence among these small and medium beaked whales of other adaptations for economizing metabolically, including anatomically reapportioning from metabolically expensive tissues (*e.g.*, brain and visceral tissues) to metabolically inexpensive tissues (*e.g.*, adipose, bone, and inactive muscles) (Pabst *et al.* 2015). Relative to *G. macrorhynchus,* the larger diameter of

Mesoplodon spp. muscle fibers also decreased the cellular surface-area-to-volume ratio and reduced the metabolic demand of the active ion pumps needed to maintain muscle fiber membrane potential (Johnston *et al.* 2004, Jimenez *et al.* 2011, Velten *et al.* 2013). Finally, *Mesoplodon* spp. exhibited considerably lower mitochondrial densities in muscle tissues relative to *G. macrorhynchus* (Velten *et al.* 2013). This strategy may have allowed longer and thus more efficient dives, but was also ecologically consistent with the more limited evasive capacities of prey species inhabiting the lower-mesopelagic and bathypelagic depth strata targeted by the two beaked whale species in our study area.

Physeterid Synthesis Hypothesis

In sharp contrast to the beaked whales, we suggest that large body masses of sperm whales enabled them to aerobically access (Fig. 6a) prey resources over a wide range of depths. This flexibility was reflected in the wide range of prey reported from stomach contents (Evans and Hindell 2004, Smith and Whitehead 2000, Clarke *et al.* 1993), and reports of diving/foraging activity in the bathypelagic (Watkins *et al.* 2003), mesopelagic (Watwood *et al.* 2006) and epipelagic (Teloni *et al.* 2008) over the nearly global distribution of this species. In our study area *P. macrocephalus* appeared to exploit central and lower mesopelagic layers, in which prey were likely moderately more abundant and more nutritionally rewarding, compared to the deeper habitats occupied by the beaked whales. Larger body mass may also have consistently required large caloric inputs, which may

have limited their ability to sustain themselves on sparser food webs below a mesopelagic prey optimum in this oligotrophic habitat. Larger size and also potentially positive buoyancy (Miller *et al.* 2004b) may also have limited the ability of sperm whales to pursue more maneuverable and evasive prey at shallower depths in the upper mesopelagic of this highly oligotrophic ecosystem with high light transmittance.

Delphinid Synthesis Hypothesis

The sub-family Globicephalinae, to which *G. macrorhynchus* and *P. electra*, belong, represents a comparatively recent (Late Miocene - early Pliocene, 7.35MA, 95% CI: 5.11–9.74MA) branch of the predominately neritic, estuarine, and/or epipelagic family Delphinidae (McGowen *et al.* 2009). Our synthesis hypothesis for these globicephaline delphinids posits that smaller body masses and other retained delphinid traits such as a high mitochondrial densities (Kielhorn *et al.* 2013, Velten *et al.* 2013), may have limited the duration of *G. macrorhynchus* and *P. electra* dives (Fig. 5) and thus their access to lower mesopelagic and bathypelagic niches (Fig. 2). However, these retained traits may also have enabled them to pursue more evasive and but also nutritionally valuable components of the DSL (Childress and Nygaard 1973). The size differences between *G. macrorhynchus* and *P. electra* may have reflected prey utilization from different components of the DSL. Specifically, *P. electra* did not undertake any deep dives during the day (Fig. 8), indicating energetically advantageous prey may have been

too deep during daylight periods and only became accessible as they migrated towards the surface during lower light periods. By contrast *G. macrorhynchus* pursued a mixed strategy: less frequent, but deeper (maximum 984 m; Figs. 2 and 8) and more highly aerobic daytime sprint pursuit dives (Aguilar de Soto *et al.* 2008), and more frequent, on-average shallower nighttime dives potentially overlapping the prey pursued by *P. electra* (Fig. 2)

Spatial and temporal habitat use patterns

Our data for the overlap between movement tracks and bathymetry provided insights into how differential prey layer access may in turn influence interspecific patterns of spatial habitat use. The aggregated telemetry information suggested two general distribution patterns: 1) wide-ranging benthic depths consistent with broadly distributed DSL prey resources, and 2) more localized distribution patterns consistent with predators targeting benthic boundary layer prey resources. Benthic echoes, recorded by digital acoustic recording tags (DTAG) deployed on *M. densirostris*, have already directly shown that this species often maintains close proximity to the benthos along the steep underwater slopes of Tenerife in the Canary Islands (Arranz *et al.* 2011). This species also showed some flexibility in their foraging strategy, switching between mid-water lower mesopelagic, and benthic boundary layer prey (Arranz *et al.* 2011). Although more circumstantial, our inter-specific and inter-individual position data also suggested that *M.d., Z.c.*, and *P. macrocephalus*, to varying degrees, interacted with prey

layers tied geographically to the benthos. A specific example was the close match between the spatial distribution of accessible benthic habitats and the wedge-shaped westward spreading of tracks for a matrilineal group of female *P. macrocephalus* that were observed consistently over the northern slope of the Great Bahama Canyon. The inter-individual variation in geographic affinity noted in *M. densirostris*, was also mirrored in the on-average shallower nighttime and deeper daytime dives exhibited by *M. densirostris.* This diurnal dive depth variability may have indicated either the pursuit of prey that undertook a reverse diel vertical migration, or as shown by Arranz *et al.* (2011) potentially a switching between mid-water lower mesopelagic resources and benthopelagic resources as prey densities varied within these layers between day and night. The geographic affinity and the correlation of *Z. cavirostris* dive depths with benthic depths at estimated dive locations also circumstantially supported a hypothesis of benthopelagic prey layer use.

By contrast, distributions of *P. electra*, *G. macrorhynchus*, and sub-adult male *P. macrocephalus* individuals ranged widely over a variety of habitats, even where the benthos was deeper than their dive depth range. This pointed to a potentially important distinction for any place-based management of these populations. Some typically shallower-diving individuals, classes, and/or species of deep-diving odontocetes may have been targeting widely distributed DSL prey resources, while other deeper-diving individuals and/or species may have been more dependent on localized benthopelagic prey resources.

Conclusions and Conservation Implications

In conclusion, this study confirmed body mass as an important correlate of dive duration capacities in toothed whales and consequently their ability to access prey at different depths. However substantial evidence supported the hypothesis of Tyack *et al.* (2006) that the small and medium beaked whales investigated in this study employed a mix of aerobic and anaerobic respiration to extend dive duration during deep foraging dives. We suggest that this represented an alternative strategy for accessing these deeper prey without growing large, and that this strategy may be related to limited prey availability below the mesopelagic deep scattering layers, where the relative importance of benthopelagic prey also increased for ziphiids.

Overall we contend that a better understanding of the morphological, physiological, and behavioral constraints that each of these cetacean groups faced in accessing deep oceanic prey will reveal novel insights into meso- and bathypelagic trophic webs. This comparative analysis provided an improved, though incomplete, understanding of the evolutionary tradeoffs that have helped shape the bodies and behaviors of deep-diving toothed whales. Finally, this information was also highly relevant in detailing the vulnerabilities and relative exposures of different toothed whale species to a variety of anthropogenic impacts including particularly acoustic disturbances and vessel strikes. In particular, the findings of this analysis may point to a special vulnerability of beaked whales to chronic acoustic disturbances from naval sonar, seismic mapping, and even

potentially vessel engine noise, since these species likely subsisted on relatively nutritionally marginal prey resources (Childress and Nygaard 1973) and invested a comparatively much greater proportion of their time and energy into each foraging dive relative to other deep-diving cetaceans. The interruption of normal foraging behaviors, which have been observed during experimental disturbance events (McCarthy *et al.* 2011, Tyack *et al.* 2011, Moretti *et al.* 2014), may therefore have had a greater impact on stress, reproduction, and potentially survival of these beaked whales (New *et al.* 2013). Additionally, the apparent use of localized benthopelagic prey resources among the beaked whales may also have important implications for the space-based management of these species (Hooker *et al.* 1999). Finally, the additional time spent in the near surface due to the extended IDDI of the beaked whales, may also have exposed these species to elevated vessel strike risk (Laist *et al.* 2001) and acute exposure to high-intensity thermally ducted sound (D'Spain *et al.* 2006).

Acknowledgements

We appreciate the large contribution of Charlotte Dunn and Leigh Hickmott at the Bahamas Marine Mammal Research Organisation (BMMRO) to the field research and planning of this project. Brice Semmens, Lynne Talley, and Paul Dayton all provided valuable input on this manuscript. We would also like to thank the many biologists, including Robert Pitman, Olivia Patterson, Aaron Banks, Marie Guilpin, Kendria Ferguson, Eric Lewallen and Edward Adderley who contributed to the field

efforts. In addition we appreciate the support of the the captains and crews of the R/V Walton Smith and M/V Slumber Venture for their support of these research efforts. Funding for tagging efforts in the Bahamas and FA analyses at the NOAA-NMFS Northwest Fisheries Science Center were supported by the US Navy Office of Naval Research (grant N000140710120), NAVFAC (grants N002441110021, N002441210007 and contract N6660413P2671), and the Strategic Environmental Research and Development Program (award RC-2114). All tagging was conducted under Bahamas Marine Mammal Protection Permit #12A. Tag types, methods of deployment, and sample sizes were all reviewed and approved by BMMRO's Institutional Animal Care and Use Committee (IACUC).

Chapter 2, in full, has been submitted for publication of the material. Joyce, Trevor W.; Durban, John W.; Fearnbach, Holly; Claridge, Diane E.; Andrews, Russel; Ballance, Lisa T. The dissertation author was the primary investigator and author of this material.

References

Aguilar de Soto, N., Johnson, M.P., Madsen, P.T., Díaz, F., Domínguez, I., Brito, A. & Tyack, P. (2008) Cheetahs of the deep sea: deep foraging sprints in short-finned pilot whales off Tenerife (Canary Islands). *Journal of Animal Ecology*, **77**, 936–947.

Angel, M.V. & Boxshall, G.A. (1990) Life in the benthic boundary layer: connections to the mid-water and sea floor [and Discussion]. *Philosophical Transactions of the Royal Society of London A: Mathematical, Physical and Engineering Sciences*, **331**, 15–28.

Aoki, K., Amano, M., Mori, K., Kourogi, A., Kubodera, T. & Miyazaki, N. (2012) Active hunting by deep-diving sperm whales: 3D dive profiles and maneuvers during bursts of speed. *Marine Ecology Progress Series*, **444**, 289–301.

Arranz, P., De Soto, N.A., Madsen, P.T., Brito, A., Bordes, F. & Johnson, M.P. (2011) Following a foraging fish-finder: Diel habitat use of Blainville's beaked whales revealed by echolocation. *PloS one*, **6**, e28353.

Bailey, T.G. & Robison, B.H. (1986) Food availability as a selective factor on the chemical compositions of midwater fishes in the eastern North Pacific. *Marine Biology*, **91**, 131–141.

Baird, R.W., Ligon, A.D., Hooker, S.K. & Gorgone, A.M. (2001) Subsurface and nighttime behaviour of pantropical spotted dolphins in Hawai'i. *Canadian Journal of Zoology*, **79**, 988–996.

Barham, E.G. (1966) Deep scattering layer migration and composition: observations from a diving saucer. *Science*, **151**, 1399–1403.

Benoit-Bird, K.J., Au, W.W., Brainard, R.E. & Lammers, M.O. (2001) Diel horizontal migration of the Hawaiian mesopelagic boundary community observed acoustically. *Marine Ecology Progress Series*, **217**, 1–14.

Benoit-Bird, K.J., Würsig, B. & Mfadden, C.J. (2004) Dusky dolphin (Lagenorhynchus obscurus) foraging in two different habitats: active acoustic detection of dolphins and their prey. *Marine Mammal Science*, **20**, 215–231.

Burnham, K.P. & Anderson, D.R. (eds). (2004) *Model Selection and Multimodel Inference*. Springer New York, New York, NY.

Butler, P.J. & Jones, D.R. (1982) The comparative physiology of diving in vertebrates. *Advances in comparative physiology and biochemistry*, **8**, 179–364.

Carbone, C. & Houston, A.I. (1996) The optimal allocation of time over the dive cycle: an approach based on aerobic and anaerobic respiration. *Animal Behaviour*, **51**, 1247–1255.

Castellini, M.A., Kooyman, G.L. & Ponganis, P.J. (1992) Metabolic rates of freely diving Weddell seals: correlations with oxygen stores, swim velocity and diving duration. *Journal of Experimental Biology*, **165**, 181–194.

Castellini, M.A. & Somero, G.N. (1981) Buffering capacity of vertebrate muscle: correlations with potentials for anaerobic function. *Journal of Comparative Physiology*, **143**, 191–198.

Childress, J.J. (1995) Are there physiological and biochemical adaptations of metabolism in deep-sea animals? *Trends in Ecology & Evolution*, **10**, 30–36.

Childress, J.J. & Nygaard, M.H. (1973) The chemical composition of midwater fishes as a function of depth of occurence off southern California. *Deep Sea Research and Oceanographic Abstracts*, pp. 1093–1109. Elsevier.

Clutton-Brock, T.H. (1988) *Reproductive Success: Studies of Individual Variation in Contrasting Breeding Systems*. University of Chicago Press.

Costa, D.P., Gales, N.J. & Goebel, M.E. (2001) Aerobic dive limit: how often does it occur in nature? *Comparative Biochemistry and Physiology Part A: Molecular & Integrative Physiology*, **129**, 771–783.

Demment, M.W. & Van Soest, P.J. (1985) A nutritional explanation for body-size patterns of ruminant and nonruminant herbivores. *American Naturalist*, 641–672.

Drews, G.A. & Engel, W.K. (1961) An attempt at histochemical localization of myoglobin in skeletal muscle by the benzidine-peroxidase reaction. *Journal of Histochemistry & Cytochemistry*, **9**, 206–207.

D'Spain, G.L., D'Amico, A. & Fromm, D.M. (2006) Properties of the underwater sound fields during some well documented beaked whale mass stranding events. *Journal of Cetacean Research and Management*, **7**, 223–238.

Gage, J.D. & Tyler, P.A. (1991) *Deep-Sea Biology*. Cambridge University Press, Cambridge, UK.

Gemmell, N.J. & Akiyama, S. (1996) An efficient method for the extraction of DNA from vertebrate tissues. *Trends in Genetics*, **12**, 338–339.

Georges, J.Y., Tremblay, Y. & Guinet, C. (2000) Seasonal diving behaviour in lactating subantarctic fur seals on Amsterdam Island. *Polar Biology*, **23**, 59–69.

Gillespie, D., Dunn, C., Gordon, J., Claridge, D., Embling, C. & Boyd, I. (2009) Field recordings of Gervais' beaked whales Mesoplodon europaeus from the Bahamas. *The Journal of the Acoustical Society of America*, **125**, 3428–3433.

Grafen, A. (1989) The phylogenetic regression. *Philosophical Transactions of the Royal Society of London. Series B, Biological Sciences*, **326**, 119–157.

Halsey, L.G., Butler, P.J. & Blackburn, T.M. (2006) A phylogenetic analysis of the allometry of diving. *The American Naturalist*, **167**, 276–287.

Hayssen, V. & Lacy, R.C. (1985) Basal metabolic rates in mammals: taxonomic differences in the allometry of BMR and body mass. *Comparative Biochemistry and Physiology Part A: Physiology*, **81**, 741–754.

Hazen, E.L., Friedlaender, A.S. & Goldbogen, J.A. (2015) Blue whales (Balaenoptera musculus) optimize foraging efficiency by balancing oxygen use and energy gain as a function of prey density. *Science advances*, **1**, e1500469.

Heyning, J.E. (1989) Cuvier's beaked whale Ziphius cavirostris G. Cuvier, 1823. *Handbook of marine mammals*, **4**, 289–308.

Hijmans, R.J. & van Etten, J. (2012) raster: Geographic analysis and modeling with raster data. R package version 2.0–12. *R Found. Stat. Comput., Vienna. http://CRAN. R-project. org/package= raster*.

Hooker, S.K. & Baird, R.W. (1999) Deep–diving behaviour of the northern bottlenose whale, Hyperoodon ampullatus (Cetacea: Ziphiidae). *Proceedings of the Royal Society of London B: Biological Sciences*, **266**, 671–676.

Hooker, S.K. & Baird, R.W. (2001) Diving and ranging behaviour of odontocetes: a methodological review and critique. *Mammal Review*, **31**, 81–105.

Houston, A.I. & Carbone, C. (1992) The optimal allocation of time during the diving cycle. *Behavioral Ecology*, **3**, 255–265.

Jerlov, N. G. (1968) *Optical oceanography*. Elsevier Publishing Company, Amsterdam.

Jimenez, A.G., Dasika, S.K., Locke, B.R. & Kinsey, S.T. (2011) An evaluation of muscle maintenance costs during fiber hypertrophy in the lobster Homarus americanus: are larger muscle fibers cheaper to maintain? *Journal of Experimental Biology*, **214**, 3688–3697.

Johnson, D.S. (2013) *Crawl: Fit Continuous-Time Correlated Random Walk Models to Animal Movement Data. R Package Version 1.4-1*.

Johnson, D.S., London, J.M., Lea, M.-A. & Durban, J.W. (2008) Continuous-Time Correlated Random Walk Model for Animal Telemetry Data. *Ecology*, **89**, 1208–1215.

Johnston, I.A., Abercromby, M., Vieira, V.L., Sigursteindóttir, R.J., Kristjánsson, B.K., Sibthorpe, D. & Skúlason, S. (2004) Rapid evolution of muscle fibre number in post-glacial populations of Arctic charr Salvelinus alpinus. *Journal of Experimental Biology*, **207**, 4343–4360.

Kasuya, T. & Matsui, S. (1984) Age determination and growth of the short-finned pilot whale off the Pacific coast of Japan. *Scientific Reports of the Whales Research Institute, Tokyo*, **35**, 57–91.

Kielhorn, C.E., Dillaman, R.M., Kinsey, S.T., McLellan, W.A., Mark Gay, D., Dearolf, J.L. & Ann Pabst, D. (2013) Locomotor muscle profile of a deep (Kogia breviceps) versus shallow (Tursiops truncatus) diving cetacean. *Journal of morphology*, **274**, 663–675.

Kleiber, M. (1975) Metabolic turnover rate: a physiological meaning of the metabolic rate per unit body weight. *Journal of Theoretical Biology*, **53**, 199–204.

Kooyman, G.L., Castellini, M.A., Davis, R.W. & Maue, R.A. (1983) Aerobic diving limits of immature Weddell seals. *Journal of Comparative Physiology B: Biochemical, Systemic, and Environmental Physiology*, **151**, 171–174.

Kooyman, G.L., Wahrenbrock, E.A., Castellini, M.A., Davis, R.W. & Sinnett, E.E. (1980) Aerobic and anaerobic metabolism during voluntary diving in Weddell seals: evidence of preferred pathways from blood chemsitry and behavior. *Journal of Comparative Physiology B: Biochemical, Systemic, and Environmental Physiology*, **138**, 335–346.

Laidre, K.L., Heide-Jørgensen, M.P. & Dietz, R. (2002) Diving behaviour of narwhals (Monodon monoceros) at two coastal localities in the Canadian High Arctic. *Canadian Journal of Zoology*, **80**, 624–635.

Laist, D.W., Knowlton, A.R., Mead, J.G., Collet, A.S. & Podesta, M. (2001) Collisions between ships and whales. *Marine Mammal Science*, **17**, 35–75.

Lang, T.G. (1966) Hydrodynamic analysis of cetacean performance. *Whales, porpoises and dolphins. University of California Press, Berkeley, California*, 410–432.

Lawrence, M.S., Phillips, K.J. & Liu, D.R. (2007) Supercharging proteins can impart unusual resilience. *Journal of the American Chemical Society*, **129**, 10110–10112.

Lindstedt, S.L. & Boyce, M.S. (1985) Seasonality, fasting endurance, and body size in mammals. *The American Naturalist*, **125**, 873–878.

Lockyer, C. (1976) Body weights of some species of large whales. *Journal du conseil*, **36**, 259–273.

Lomolino, M.V. (1985) Body size of mammals on islands: the island rule reexamined. *The American Naturalist*, **125**, 310–316.

Marshall, N.B. (1965) Systematic and biological studies of the macrourid fishes (Anacanthini-Teleostii). *Deep Sea Research and Oceanographic Abstracts*, pp. 299–322. Elsevier.

Martin, J.H., Knauer, G.A., Karl, D.M. & Broenkow, W.W. (1987) VERTEX: carbon cycling in the northeast Pacific. *Deep Sea Research Part A. Oceanographic Research Papers*, **34**, 267–285.

Martin, A.R. & Smith, T.G. (1999) Strategy and capability of wild belugas, Delphinapterus leucas, during deep, benthic diving. *Canadian Journal of Zoology*, **77**, 1783–1793.

Mayo, C.A. & Marx, M.K. (1990) Surface foraging behaviour of the North Atlantic right whale, Eubalaena glacialis, and associated zooplankton characteristics. *Canadian Journal of Zoology*, **68**, 2214–2220.

McCarthy, E., Moretti, D., Thomas, L., DiMarzio, N., Morrissey, R., Jarvis, S., Ward, J., Izzi, A. & Dilley, A. (2011) Changes in spatial and temporal distribution and vocal behavior of Blainville's beaked whales (Mesoplodon densirostris) during multiship exercises with mid-frequency sonar. *Marine Mammal Science*, **27**, E206–E226.

McClain, C.R., Boyer, A.G. & Rosenberg, G. (2006) The island rule and the evolution of body size in the deep sea. *Journal of Biogeography*, **33**, 1578–1584.

McClintock, B.T., London, J.M., Cameron, M.F. & Boveng, P.L. (2015) Modelling animal movement using the Argos satellite telemetry location error ellipse. *Methods in Ecology and Evolution*, **6**, 266–277.

McGowen, M.R., Spaulding, M. & Gatesy, J. (2009) Divergence date estimation and a comprehensive molecular tree of extant cetaceans. *Molecular Phylogenetics and Evolution*, **53**, 891–906.

Mead, J.G. (1989) *Beaked Whales of the Genus Mesoplodon*. Handbook of marine mammals.

Miller, P.J., Johnson, M.P. & Tyack, P.L. (2004a) Sperm whale behaviour indicates the use of echolocation click buzzes "creaks" in prey capture. *Proceedings of the Royal Society of London B: Biological Sciences*, **271**, 2239–2247.

Miller, P.J., Johnson, M.P., Tyack, P.L. & Terray, E.A. (2004b) Swimming gaits, passive drag and buoyancy of diving sperm whales Physeter macrocephalus. *Journal of Experimental Biology*, **207**, 1953–1967.

Mirceta, S., Signore, A.V., Burns, J.M., Cossins, A.R., Campbell, K.L. & Berenbrink, M. (2013) Evolution of mammalian diving capacity traced by myoglobin net surface charge. *Science*, **340**, 1234192.

Miyazaki, N., Fujise, Y. & Iwata, K. (1998) Biological analysis of a mass stranding of melon-headed whales (Peponocephala electra) at Aoshima, Japan. *BULLETIN-NATIONAL SCIENCE MUSEUM TOKYO SERIES A*, **24**, 31–60.

Moretti, D., Thomas, L., Marques, T., Harwood, J., Dilley, A., Neales, B., Shaffer, J., McCarthy, E., New, L., Jarvis, S. & others. (2014) A risk function for behavioral disruption of Blainville's beaked whales (Mesoplodon densirostris) from mid-frequency active sonar. *PloS one*, **9**, e85064.

Mori, Y. (1999) The optimal allocation of time and respiratory metabolism over the dive cycle. *Behavioral Ecology*, **10**, 155–160.

Mori, Y. (2002) Optimal diving behaviour for foraging in relation to body size. *Journal of Evolutionary Biology*, **15**, 269–276.

Nakagawa, S. & Schielzeth, H. (2013) A general and simple method for obtaining R2 from generalized linear mixed-effects models. *Methods in Ecology and Evolution*, **4**, 133–142.

Nemeth, P.M. & Lowry, O.H. (1984) Myoglobin levels in individual human skeletal muscle fibers of different types. *Journal of Histochemistry & Cytochemistry*, **32**, 1211–1216.

New, L.F., Moretti, D.J., Hooker, S.K., Costa, D.P. & Simmons, S.E. (2013) Using energetic models to investigate the survival and reproduction of beaked whales (family Ziphiidae). *PloS one*, **8**, e68725.

Noren, S.R. & Williams, T.M. (2000) Body size and skeletal muscle myoglobin of cetaceans: adaptations for maximizing dive duration. *Comparative Biochemistry and Physiology Part A: Molecular & Integrative Physiology*, **126**, 181–191.

Ohman, M.D., Frost, B.W. & Cohen, E.B. (1983) Reverse diel vertical migration: an escape from invertebrate predators. *Science*, **220**, 1404–1407.

Pabst, D.A. & McLellan, W.A. (2015) The extreme morphology of mesoplodonts. Presentation to the 22nd Society for Marine Mammalogy Conference.

Peter, J.B., Barnard, R.J., Edgerton, V.R., Gillespie, C.A. & Stempel, K.E. (1972) Metabolic profiles of three fiber types of skeletal muscle in guinea pigs and rabbits. *Biochemistry*, **11**, 2627–2633.

Pitman, R.L. & Durban, J.W. (2012) Cooperative hunting behavior, prey selectivity and prey handling by pack ice killer whales (Orcinus orca), type B, in Antarctic Peninsula waters. *Marine Mammal Science*, **28**, 16–36.

Ponganis, P.J., Kooyman, G.L. & Castellini, M.A. (1993) Determinants of the Aerobic Dive Limit of Weddell Seals: Analysis of Diving Metabolic Rates, Postdive End Tidal Po_2's, and Blood and Muscle Oxygen Stores. *Physiological Zoology*, 732–749.

Ponganis, P.J., Meir, J.U. & Williams, C.L. (2011) In pursuit of Irving and Scholander: a review of oxygen store management in seals and penguins. *Journal of Experimental Biology*, **214**, 3325–3339.

Rosel, P.E. (2003) PCR-based sex determination in Odontocete cetaceans. *Conservation Genetics*, **4**, 647–649.

Rosen, D.A., Gerlinsky, C.D. & Trites, A.W. (2015) Evidence of partial deferment of digestion during diving in Steller sea lions (Eumetopias jubatus). *Journal of Experimental Marine Biology and Ecology*, **469**, 93–97.

Sato, K., Watanuki, Y., Takahashi, A., Miller, P.J., Tanaka, H., Kawabe, R., Ponganis, P.J., Handrich, Y., Akamatsu, T., Watanabe, Y. & others. (2007) Stroke frequency, but not swimming speed, is related to body size in free-ranging seabirds, pinnipeds and cetaceans. *Proceedings of the Royal Society of London B: Biological Sciences*, **274**, 471–477.

Schreer, J.F. & Kovacs, K.M. (1997) Allometry of diving capacity in air-breathing vertebrates. *Canadian Journal of Zoology*, **75**, 339–358.

Scott, M., Hohn, A., Westgate, A., Nicolas, J., Whitaker, B. & Campbell, W. (2001) A note on the release and tracking of a rehabilitated pygmy sperm whale (Kogia breviceps). *J. Cetacean Res. Manage*, **3**, 87–94.

Sharp J.G. & Marsh, B.B. (1953) *Whalemeat: Production and Preservation.* UK Department of Scientific and Industrial Research, London, UK.

Sinclair, A.R.E., Mduma, S. & Brashares, J.S. (2003) Patterns of predation in a diverse predator–prey system. *Nature*, **425**, 288–290.

Snyder, G.K. (1983) Respiratory adaptations in diving mammals. *Respiration physiology*, **54**, 269–294.

Sparling, C.E., Fedak, M.A. & Thompson, D. (2007) Eat now, pay later? Evidence of deferred food-processing costs in diving seals. *Biology Letters*, **3**, 95–99.

Stickney, D.G. & Torres, J.J. (1989) Proximate composition and energy content of mesopelagic fishes from the eastern Gulf of Mexico. *Marine Biology*, **103**, 13–24.

Teloni, V., Mark, J.P., Patrick, M.J. & Peter, M.T. (2008) Shallow food for deep divers: Dynamic foraging behavior of male sperm whales in a high latitude habitat. *Journal of Experimental Marine Biology and Ecology*, **354**, 119–131.

Tyack, P.L., Johnson, M., Soto, N.A., Sturlese, A. & Madsen, P.T. (2006) Extreme diving of beaked whales. *Journal of Experimental Biology*, **209**, 4238–4253.

Tyack, P.L., Zimmer, W.M., Moretti, D., Southall, B.L., Claridge, D.E., Durban, J.W., Clark, C.W., D'Amico, A., DiMarzio, N., Jarvis, S. & others. (2011) Beaked whales respond to simulated and actual navy sonar. *PloS one*, **6**, e17009.

Velten, B.P., Dillaman, R.M., Kinsey, S.T., McLellan, W.A. & Pabst, D.A. (2013) Novel locomotor muscle design in extreme deep-diving whales. *Journal of Experimental Biology*, **216**, 1862–1871.

de Villemereuil, P. & Nakagawa, S. (2014) General quantitative genetic methods for comparative biology. *Modern Phylogenetic Comparative Methods and Their Application in Evolutionary Biology*, pp. 287–303. Springer.

Waring, G.T., Hamazaki, T., Sheehan, D., Wood, G. & Baker, S. (2001) Characterization of beaked whale (Ziphiidae) and sperm whale (Physeter macrocephalus) summer habitat in shelf-edge and deeper waters off the northeast US. *Marine Mammal Science*, **17**, 703–717.

Warrant, E. (2000) The eyes of deep–sea fishes and the changing nature of visual scenes with depth. *Philosophical Transactions of the Royal Society B: Biological Sciences*, **355**, 1155–1159.

Watkins, W.A., Daher, M.A., Fristrup, K.M., Howald, T.J., Sciara, D. & Notarbartolo, G. (1993) Sperm whales tagged with transponders and tracked underwater by sonar. *Marine mammal science*, **9**, 55–67.

Watwood, S.L., Miller, P.J., Johnson, M., Madsen, P.T. & Tyack, P.L. (2006) Deep-diving foraging behaviour of sperm whales (Physeter macrocephalus). *Journal of Animal Ecology*, **75**, 814–825.

Wells Jr, R.E. & Merrill, E.W. (1962) Influence of flow properties of blood upon viscosity-hematocrit relationships. *Journal of Clinical Investigation*, **41**, 1591.

Westgate, A.J., Head, A.J., Berggren, P., Koopman, H.N. & Gaskin, D.E. (1995) Diving behaviour of harbour porpoises, Phocoena phocoena. *Canadian Journal of Fisheries and Aquatic Sciences*, **52**, 1064–1073.

Zuur, A.F., Ieno, E.N., Walker, N.J., Saveliev, A.A. & Smith, G.M. (2009) Mixed effects modelling for nested data. *Mixed effects models and extensions in ecology with R*, pp. 101–142. Springer.

Tables

Table 2-1. Number of satellite tag deployments, 2009-2014, by tag type (SPOT model from 2009-2014, SPLASH model from 2011-2014) and gender: male (M), female (F), and unknown (U). Number of tagging events indicates the number of separate encounters with groups of odontocetes during which tagging took place; some groups may have been repeatedly encountered across multiple years. Also shown are the total hours of dive data recovered for each species in the behavior and time series logs of SPLASH tags and the time-at-temperature histograms of SPOT tags, and mean duration of tag transmission for five species of deep-diving odontocete cetaceans in the northern Bahamas.

Species	SPOT			SPLASH			Tagging	Behav.	Time	TAT	Mean Duration
	M	F	U	M	F	U	Events	Log (h)	Series (h)	Histo. (h)	(d, Min-Max)
Melon-headed whale *Peponocephala electra*	0	0	9	0	0	4	6	55.45	15.04	1605	9.51 (0.02,38.79)
Short-finned pilot whale *Globicephala macrorhynchus*	7	4	1	2	0	1	5	252.61	277.83	3639	15.67 (0.37,40.8)
Sperm whale *Physeter macrocephalus*	11	9	1	5	1	0	13	451.01	140.42	3340	8.2 (0,17.76)
Blainville's beaked whale *Mesoplodon densirostris*	3	0	0	3	6	0	10	695.91	694.75	167	16.41 (0.01,45.64)
Cuvier's beaked whales *Ziphius cavirostris*	0	1	0	4	2	0	6	365.65	139.96	139	23.72 (8.53,90.14)

Table 2-2. A summary of standard-length (m), mass (kg), and myoglobin ([Mb]; mg kg^{-1}) measurements for five species of cetacean retrieved from the National Museum of Natural History (NMNH) whale collection database, and a variety of primary literature sources not found in the NMNH database (Lockyer 1976, Kasuya and Matsui 1984, Heyning 1989, Mead 1989, Miyazaki *et al.* 1998). These mass and standard length measurements were used to calculate median length and estimate median body masses for each species, sex, and age-class represented in our tagging datasets using the models shown in Figure 1. Threshold standard-lengths were used to categorize measured individuals into age-classes within each sex and species. The sources of [Mb] measurements are 1) Mirceta *et al.* 2013, 2) Velten *et al.* 2013, 3) Noren and Williams 2000, and 4) Sharp and Marsh 1953. *note this value was not measured empirically but estimated from eq. 1 in Mirceta *et al.* (2013).

Species	Sex	N Mass	N Length	Age Class	Thresh. Lengths	Med. Length	Med. Mass	[Mb]	Mb Source
Melon-headed whale	Male	14	33	Adult	2.45-3m	2.505	179.77	25.0*	1
Peponocephala electra									
				Sub-adult	1.5-2.45m	2.23	125.48		
	Female	12	45	Adult	2.3-3m	2.41	159.51		
				Sub-adult	1.5-2.3m	2.17	115.32		
Short-finned pilot whale	Male	12	93	Adult	3.95-7m	4.65	1195.4	68.2	2
Globicephala macrorhynchus									
				Sub-adult	3-3.95m	3.48	528.25		
	Female	32	143	Adult	2.93-7m	3.6	581.58		
				Sub-adult	2-2.93m	2.615	236.46		
Blainville's beaked whale	Male	6	52	Adult	3.5-6m	4.115	817.8	69.2	2
Mesoplodon densirostris									
				Sub-adult	1.5-3.5m	3.01	306.09		
	Female	9	52	Adult	3.5-6m	4.195	868.04		
				Sub-adult	1.5-3.5m	2.195	116.4		
Cuvier's beaked whales	Male	10	179	Adult	4.9-8m	5.64	1601.3	43.2	3
Ziphius cavirostris									
				Sub-adult	2.5-4.9m	4.01	736.03		
	Female	16	178	Adult	4.6-8m	5.5	1512.1		
				Sub-adult	2.5-4.6m	3.8	651.12		
Sperm whale	Male	51	651	Adult	12-25m	14.1	25679	70	4
Physeter macrocephalus									
				Sub-adult	8-12m	10.97	12362		
	Female	11	337	Adult	8.5-14m	10.6	11186		
				Sub-adult	3-8.5m	4.215	762.53		

Table 2-3. Section (a) compares a fixed-effect only model (*i.e.*, a generalized linear model, GLM, Model 1a) with a phylogenetic generalized linear mixed model (PGLMM, Model 2a) to assess the advantage of including a random effects structure in models of maximum dive duration (T_{max}). Section (b) evaluates different combinations of the fixed effect covariates body mass (M), myoglobin concentration ([Mb]), and inter-deep-dive interval ($IDDI$) within the GLM structure indicated in section (a). The term k denotes the number of parameters estimated in each model, while the marginal (R_m^2) and conditional (R_c^2) coefficients of determination indicate the proportion of variance in T_{max} explained by the fixed effects only and the full mixed effects model, respectively (Nakagawa and Schielzeth, 2013). Model selection and information theory inference were based the absolute and relative Deviance Information Criterion scores (DIC and ΔDIC), and DIC weights (wDIC), which provided a measure of the relative probability that model$_i$ represented the most parsimonious model fit out of the list of candidate models (Burnham and Anderson 2002).

Model Formula	***k***	R_m^2	R_c^2	**DIC**	**ΔDIC**	***w*DIC**
Mod. 1a (GLM):						
$\log(T_{max}) \sim \log(M) + \log([Mb]) + \log(IDDI)$	4	0.91	-	-41.91	0	0.71
Mod. 2a (PGLMM):						
$\log(T_{max}) \sim \log(M) + \log([Mb]) + \log(IDDI) + SPP$	5	0.36	0.95	-40.15	1.76	0.29
Mod. 1b (GLM):						
$\log(T_{max}) \sim \log(M) + \log([Mb]) + \log(IDDI)$	4	0.92	-	-41.84	2.3	0.24
Mod. 2b (GLM):						
$\log(T_{max}) \sim \log(M) + \log(IDDI)$	3	0.92	-	-44.14	0	0.76
Mod. 3b (GLM)::						
$\log(T_{max}) \sim \log(M) + \log([Mb])$	3	0.36	-	8.54	52.68	0
Mod. 4b (GLM)::						
$\log(T_{max}) \sim \log(IDDI) + \log([Mb])$	3	0.69	-	-10.21	33.93	0
Mod. 5b (GLM):						
$\log(T_{max}) \sim \log(M)$	2	0.31	-	8.46	52.6	0
Mod. 6b (GLM):						
$\log(T_{max}) \sim \log([Mb])$	2	0.26	-	10.38	54.52	0
Mod. 7b (GLM):						
$\log(T_{max}) \sim \log(IDDI)$	2	0.58	-	-3.85	40.29	0

Table 2-4. A comparison of phylogenetic generalized least squares (PGLS) models of maximum dive duration (T_{max}), with covariates of body mass (M), myoglobin concentration ([Mb]), and/or inter-deep-dive interval ($IDDI$). Model selection and information theory inference were based on the number of estimated parameters (k), the absolute and relative Akaike's Information Criterion scores (AIC and ΔAIC), and Akaike's weights (wAIC), which provided a measure of the relative probability that model$_i$ represented the most parsimonious model fit out of the list of candidate models (Burnham and Anderson 2002). The top three candidate PGLS models all included IDDI (Models 1, 2, & 4), and accounted for 92% of wAIC probabilities.

Model Formula	***k***	**AIC**	**ΔAIC**	**wAIC**
Mod. 1c (PGLS): $\log(T_{max}) \sim \log(M) + \log([Mb]) + \log(IDDI)$	4	-2.06	0	0.52
Mod. 2c (PGLS): $\log(T_{max}) \sim \log(M) + \log(IDDI)$	3	-1.06	1	0.31
Mod. 3c (PGLS): $\log(T_{max}) \sim \log(M) + \log([Mb])$	3	3.65	5.71	0.03
Mod. 4c (PGLS): $\log(T_{max}) \sim \log(IDDI) + \log([Mb])$	3	1.39	3.45	0.09
Mod. 5c (PGLS): $\log(T_{max}) \sim \log(M)$	2	3.32	5.38	0.04
Mod. 6c (PGLS): $\log(T_{max}) \sim \log([Mb])$	2	9.93	11.99	0
Mod. 7c (PGLS): $\log(T_{max}) \sim \log(IDDI)$	2	5.64	7.7	0.01

Table 2-5. A comparison of a generalized linear model (GLM, Model 1a) and phylogenetic generalized linear mixed models (PGLMM, Models 2a-3a & 1b-7b) of dive duration (T) at the level of individual dives. See details and interpretation of model selection metrics (k, R_m^2, R_c^2, DIC, ΔDIC, and wDIC) in Table 3.

Model Formula	***k***	R_m^2	R_c^2	**DIC**	**ΔDIC**	***w*DIC**
Mod. 1d (GLM):						
log(*T*) ~ log(*M*) + log([*Mb*]) + log(*IDDI*)	4	0.75	-	-814.72	1426.44	0
Mod. 2d (PGLMM):						
log(*T*) ~ log(*M*) + log([*Mb*]) + log(*IDDI*) + *SPP*	5	0.07	0.98	-2141.9	99.26	0
Mod. 3d (PGLMM):						
log(*T*) ~ log(*M*) + log([*Mb*]) + log(*IDDI*) + *SPP* + *PTT*	6	0.04	0.99	-2241.16	0	1
Mod. 1e (PGLMM):						
log(*T*) ~ log(*M*) + log([*Mb*]) + log(*IDDI*) + *SPP* + *PTT*	6	0.04	0.99	-2241.09	0.03	0.2
Mod. 2e (PGLMM):						
log(*T*) ~ log(*M*) + log(*IDDI*) + *SPP* + *PTT*	5	0.10	0.98	-2241.08	0.04	0.2
Mod. 3e (PGLMM):						
log(*T*) ~ log(*M*) + log([*Mb*]) + *SPP* + *PTT*	5	0.05	0.99	-2238.78	2.34	0.06
Mod. 4e (PGLMM):						
log(*T*) ~ log(*IDDI*) + log([*Mb*]) + *SPP* + *PTT*	5	0.01	0.99	-2241.12	0	0.2
Mod. 5e (PGLMM):						
log(*T*) ~ log(*M*) + *SPP* + *PTT*	4	0.11	0.98	-2238.75	2.37	0.06
Mod. 6e (PGLMM):						
log(*T*) ~ log([*Mb*]) + *SPP* + *PTT*	4	0.01	0.99	-2238.8	2.32	0.06
Mod. 7e (PGLMM):						
log(*T*) ~ log(*IDDI*) + *SPP* + *PTT*	4	<0.01	0.99	-2241.11	0.01	0.2

Table 2-6. A comparison of a generalized linear model (GLM, Model 1a) and phylogenetic generalized linear mixed models (PGLMM, Models 2a-3a & 1b-7b) of dive depth (Z) at the level of individual dives. See details and interpretation of model selection metrics (k, R_m^2, R_c^2, DIC, ΔDIC, and wDIC) in Table 3.

Model Formula	k	R_m^2	R_c^2	**DIC**	**ΔDIC**	w**DIC**
Mod. 1f (GLM):						
$\log(Z) \sim \log(M) + \log([Mb]) + \log(IDDI)$	4	0.56	NA	-864.54	504.83	0
Mod. 2f (PGLMM):						
$\log(Z) \sim \log(M) + \log([Mb]) + \log(IDDI) + SPP$	5	0.06	0.91	-1343.58	25.79	0
Mod. 3f (PGLMM):						
$\log(Z) \sim \log(M) + \log([Mb]) + \log(IDDI) + SPP + PTT$	6	0.03	0.94	-1369.37	0	1
Mod. 1g (PGLMM):						
$\log(Z) \sim \log(M) + \log([Mb]) + \log(IDDI) + SPP + PTT$	6	0.02	0.97	-1369.33	1.31	0.1
Mod. 2g (PGLMM):						
$\log(Z) \sim \log(M) + \log(IDDI) + SPP + PTT$	5	0.07	0.9	-1369.48	1.16	0.11
Mod. 3g (PGLMM):						
$\log(Z) \sim \log(M) + \log([Mb]) + SPP + PTT$	5	0.04	0.93	-1370.54	0.1	0.19
Mod. 4g (PGLMM):						
$\log(Z) \sim \log(IDDI) + \log([Mb]) + SPP + PTT$	5	0	0.93	-1369.44	1.2	0.11
Mod. 5g (PGLMM):						
$\log(Z) \sim \log(M) + SPP + PTT$	4	0.07	0.9	-1370.64	0	0.2
Mod. 6g (PGLMM):						
$\log(Z) \sim \log([Mb]) + SPP + PTT$	4	0	0.93	-1370.6	0.04	0.19
Mod. 7g (PGLMM):						
$\log(Z) \sim \log(IDDI) + SPP + PTT$	4	0	0.91	-1369.46	1.18	0.11

Figures

Figure 2-1. Each x-y scatter plot in this panel shows the relationship of body mass and standard length in males (lighter) and females (darker) of each species represented in our tagging datasets. The histograms embedded in the upper margin of each plot indicate the distributions of male and female standard lengths recovered from stranding and historic whaling data. The median standard lengths for each species were used to estimate the median adult and sub-adult body masses for each species and sex, using the fitted power law relationship indicated in each plot.

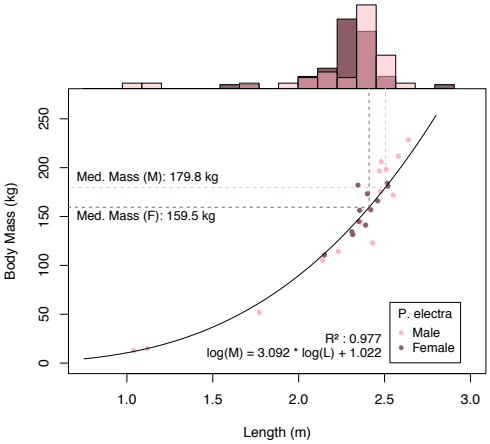
Med. Mass (M): 179.8 kg
Med. Mass (F): 159.5 kg
P. electra
Male
Female
R² : 0.977
log(M) = 3.092 * log(L) + 1.022
Body Mass (kg)
Length (m)

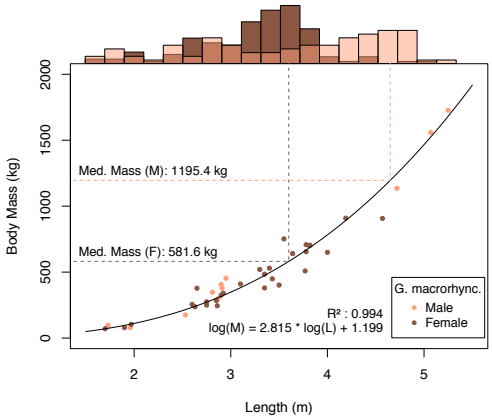
Med. Mass (M): 1195.4 kg
Med. Mass (F): 581.6 kg
G. macrorhync.
Male
Female
R² : 0.994
log(M) = 2.815 * log(L) + 1.199
Body Mass (kg)
Length (m)

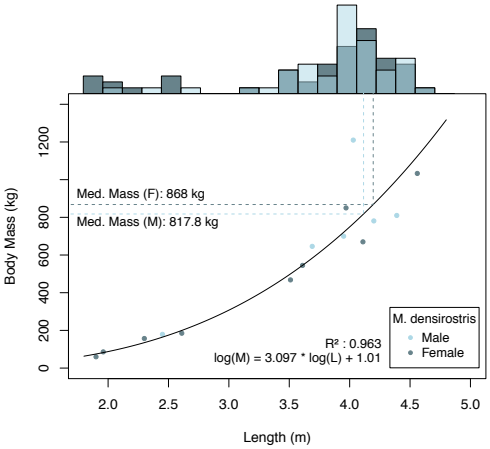
Med. Mass (F): 868 kg
Med. Mass (M): 817.8 kg
M. densirostris
Male
Female
R² : 0.963
log(M) = 3.097 * log(L) + 1.01
Body Mass (kg)
Length (m)

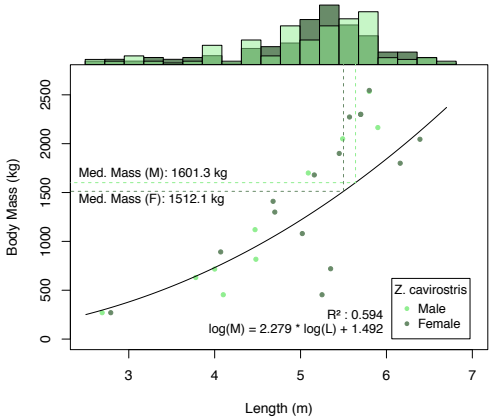
Med. Mass (M): 1601.3 kg
Med. Mass (F): 1512.1 kg
Z. cavirostris
Male
Female
R² : 0.594
log(M) = 2.279 * log(L) + 1.492
Body Mass (kg)
Length (m)

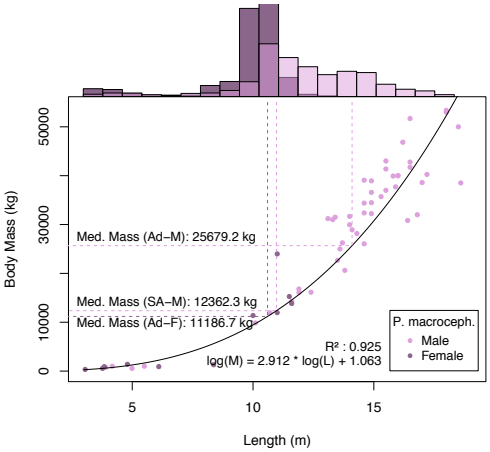
Med. Mass (Ad−M): 25679.2 kg
Med. Mass (SA−M): 12362.3 kg
Med. Mass (Ad−F): 11186.7 kg
P. macroceph.
Male
Female
R² : 0.925
log(M) = 2.912 * log(L) + 1.063
Body Mass (kg)
Length (m)

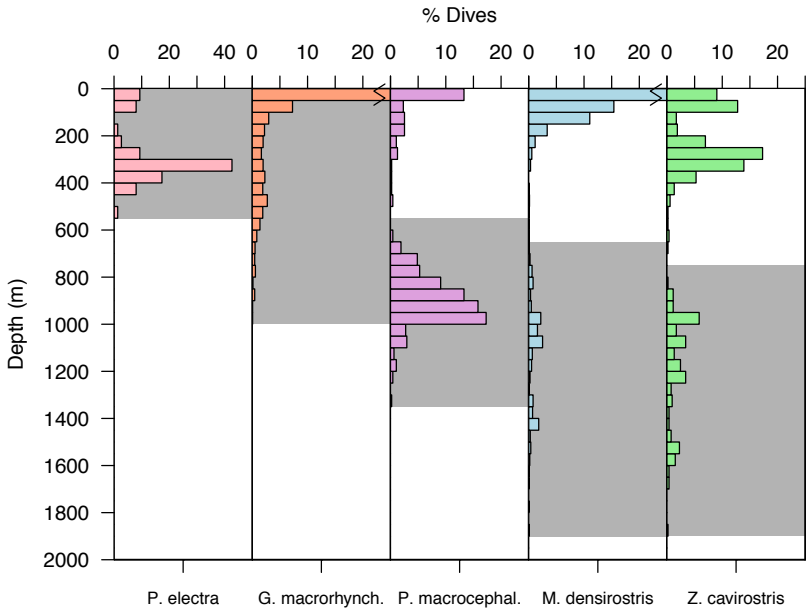

Figure 2-2. Percent frequency histograms in this plot show the cumulative distribution of foraging dive depths from all tagged individuals of each study species arranged from shallowest to deepest divers. The dives that were considered likely foraging dives on the basis of the vertical distribution of foraging buzzes recorded in previous digital acoustic recording tag studies (Arranz *et al.* 2011, Aguilar de Soto *et al.* 2008, Tyack *et al.* 2006, Watwood *et al.* 2006) are indicated by the grey background colors.

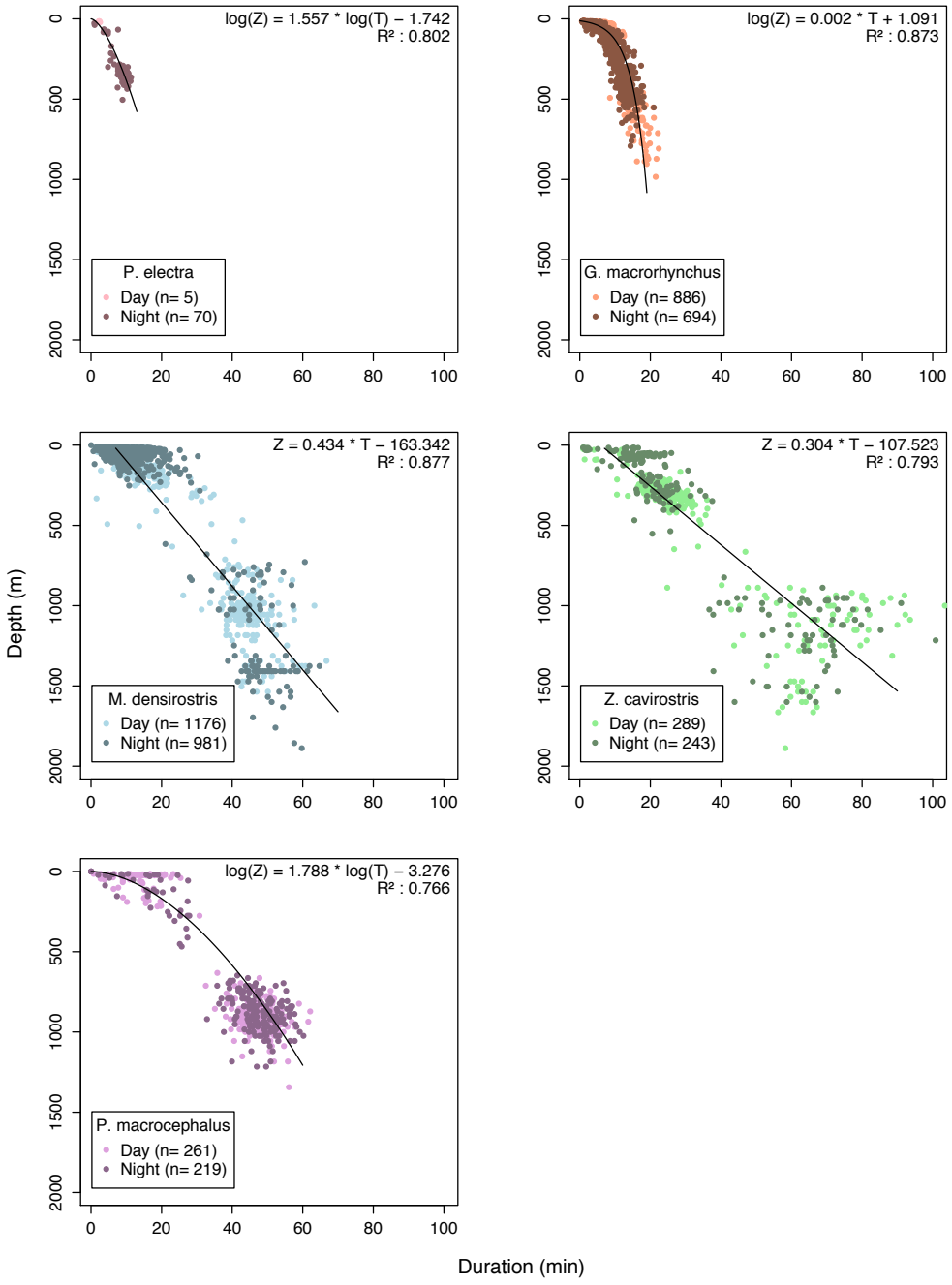

Figure 2-3. The scatter plots in this panel show that dive duration typically increases as a function dive depth in all of the species tagged in this study. Different functional forms ranging from exponential (*G.m.*), to power law (*P.e.* and *P.m.*), to linear (*M.d.* and *Z.c.*) provided the best model fits in different species. Greater variation in dive duration of deeper dives was observed particularly among the beaked whales.

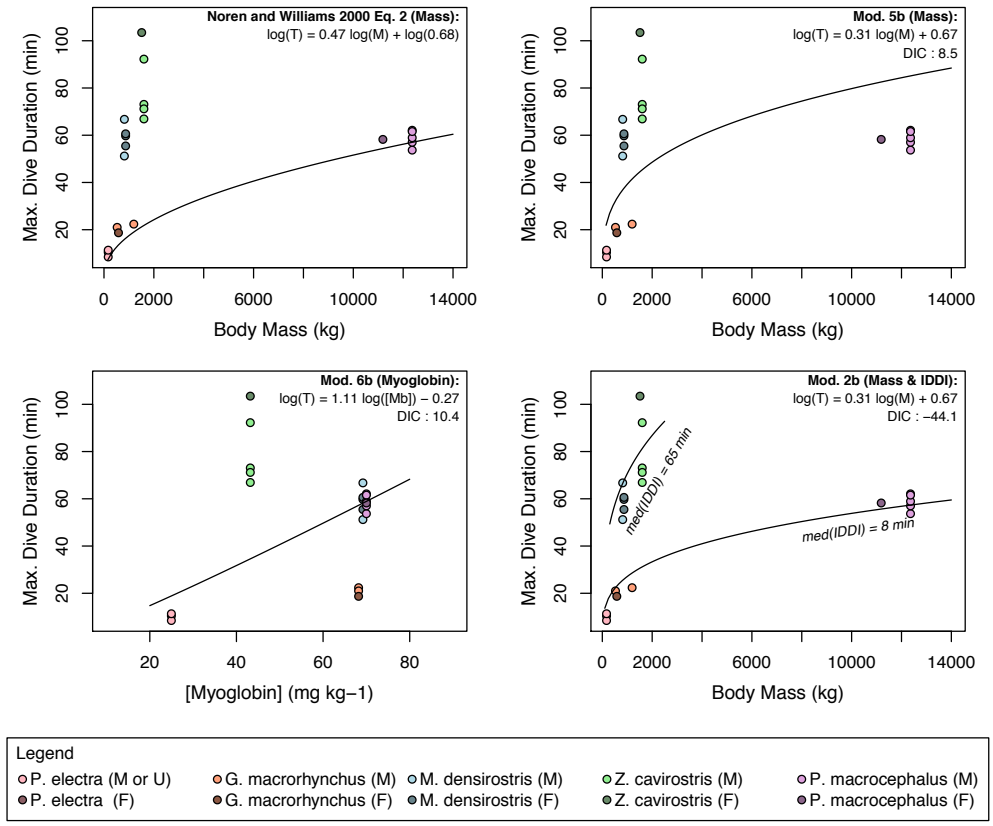

Figure 2-4. The relationship of maximum dive duration to body mass (a, b, and c) and myoglobin concentration ([Mb], d) using behavior log data from individuals tagged with SPLASH model satellite transmitters. Plot *a* shows the power law relationship fitted by Noren and Williams 2000 eq. 2, which relatively closely matches the dive duration observed in the delphinids and physeterids. The dive duration of the two ziphiids were substantially underestimated by this model (*a*), however the improvement in the model fit shown in plot *c* indicates the importance of IDDI and body mass as predictors of dive duration.

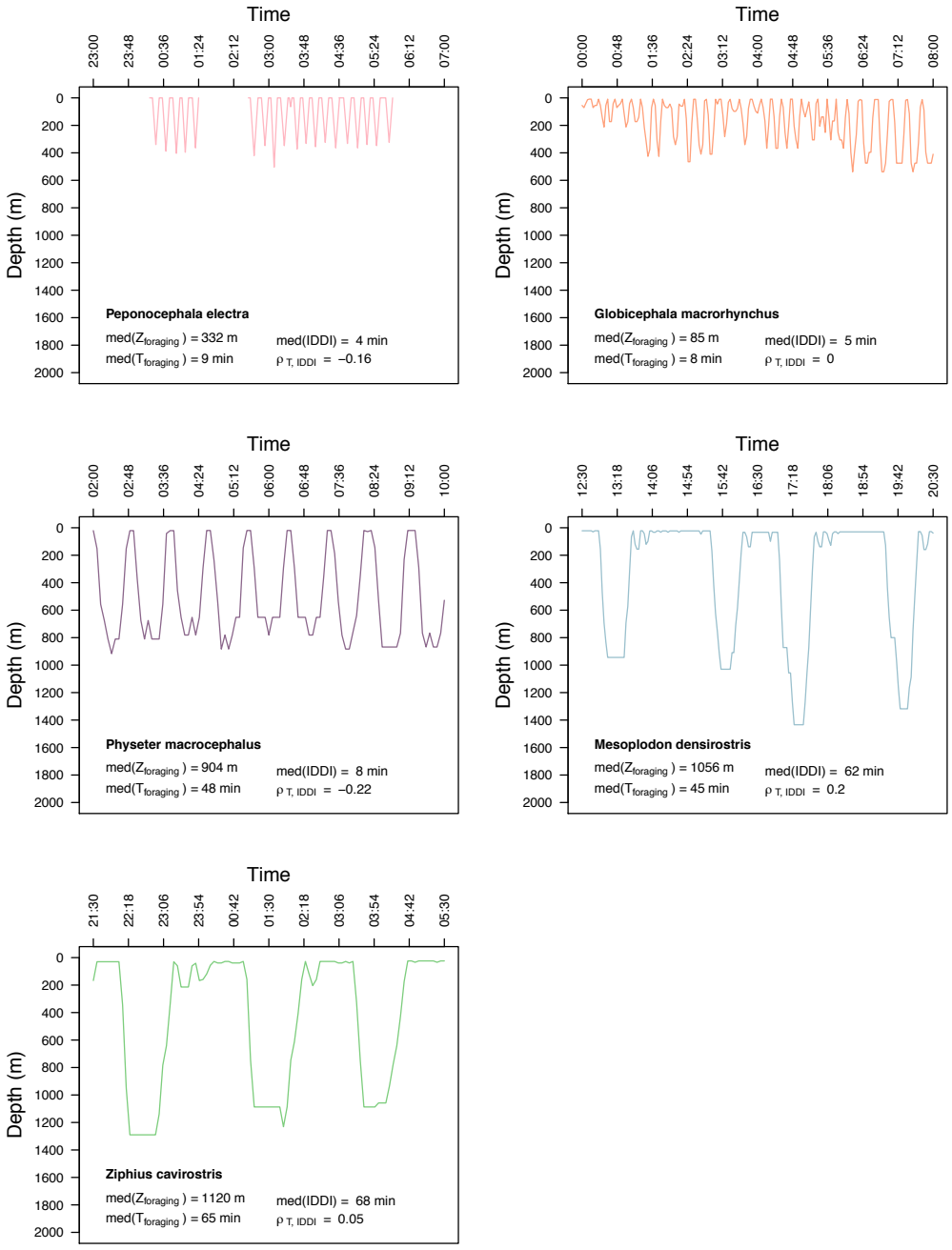

Figure 2-5. Typical time-depth dive profiles from the species in our tagging dataset, each representing an 8-hour window of dive behavior. Importantly, this plot contrasts the comparatively short inter-deep dive intervals (IDDI) and relatively continuous diving of the delphinids and physeterids, with both the extended dives and IDDI exhibited by the ziphiids. The median depth ($Z_{foraging}$), median duration ($T_{foraging}$), median surface intervals (*IDDI*), and correlation coefficients of duration and IDDI ($\rho_{T,IDDI}$) are indicated at the bottom of each plot.

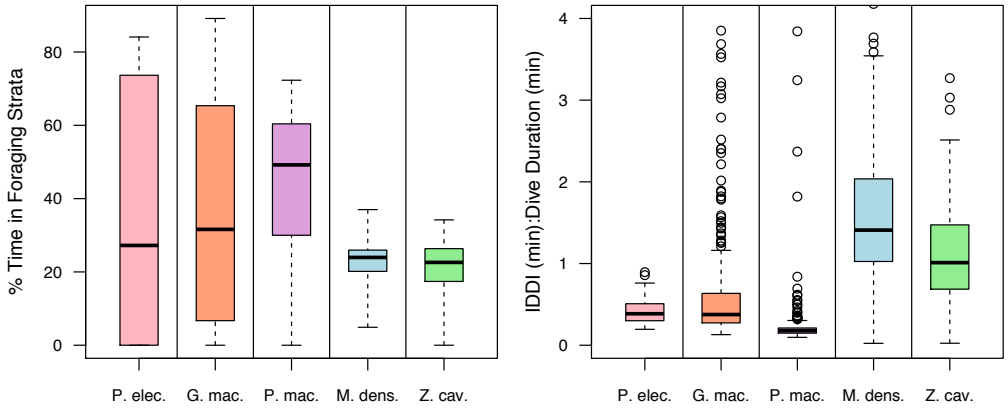

Figure 2-6. The set of boxplots on the left (*a*) illustrate different proportions of total time budgets spent within the foraging the foraging depths identified in Fig. 2, arrayed from the shallowest to deepest diving species in our tagging dataset. The proportions of time spent in foraging strata derive from SPOT tag time-at-temperature histograms that were translated units of temperature to units of depth using the hydrographic data and interpolation methods detailed in Joyce *et al.* (2016). Overall the ziphiids exhibited substantially lower proportion of time spent in foraging strata relative to the delphinids and physeterids. This difference was primarily attributable to the substantially longer inter-deep dive intervals exhibited by the beaked whales which is shown in plot (b) to exceed the duration of foraging dives.

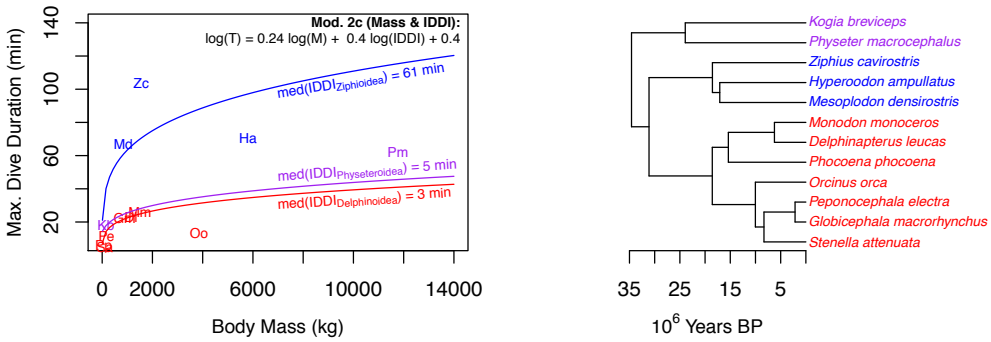

Figure 2-7. Inter-specific patterns of maximum dive duration (*T*) with respect to body mass (*m*), myoglobin concentration ([*Mb*]), and inter-deep-dive interval (IDDI) within the 12 odontocete species considered in a phylogenetic generalized least squares (PGLS) analysis. The three curves overlaid on this scatterplot represent the predictions from the PGLS Model 2 (Table 7) using the median IDDI of the *Ziphioidea* (blue), *Physeteroidea* (purple), and *Delphinoidea* (red) super-families within the sub-order *Odontoceti*. These super-families are also indicated (b) in the phylogenetic tree hypothesis of McGowen *et al.* (2009), which was used to develop the correlation structure in PGLS models.

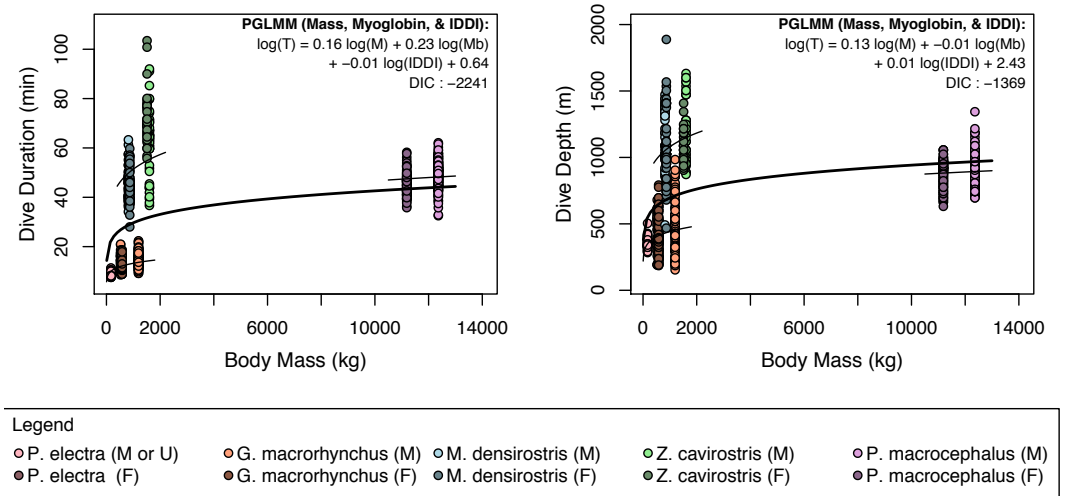

Figure 2-8. Patterns of (a) dive duration (*T*) and (b) dive depth (*Z*) with respect to body mass (*m*) at the level of individual dives. Overlaid on plots (a) and (b) are the predicted relationships from phylogenetic generalized linear mixed models (PGLMM) relating *T* and *Z* with *m*, myoglobin concentration ([*Mb*]), and inter-deep-dive interval (IDDI). The bold solid lines represent the main effect of the fixed effect parameters, while predictions including mean of random intercept parameters representing each family are shown in the stippled lines.

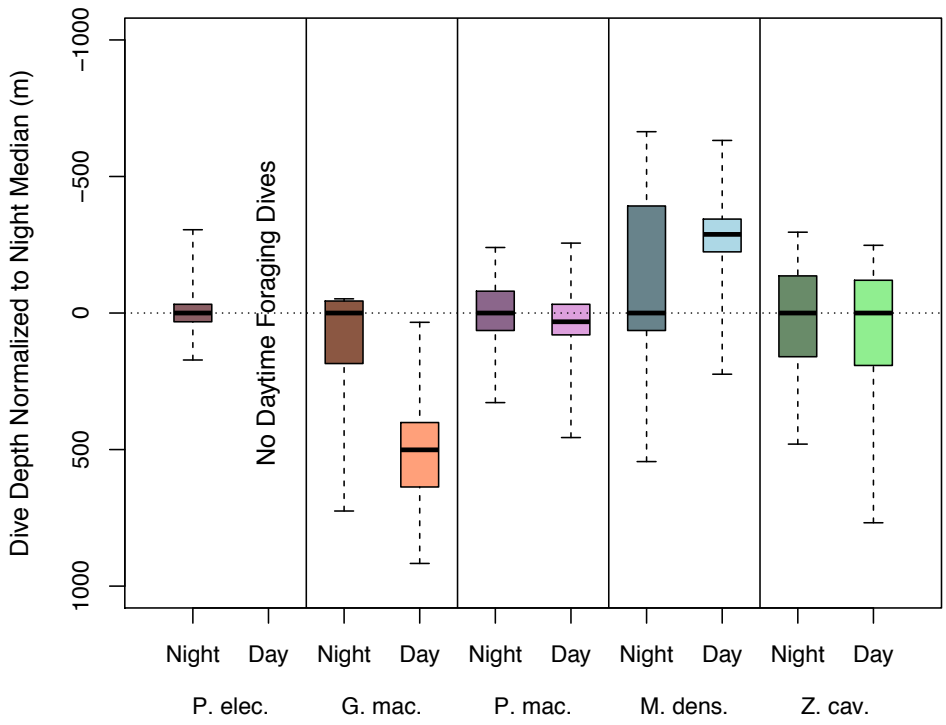

Figure 2-9. The variation from shallowest to deepest diving species in the difference between daytime and nighttime foraging dives normalized to the median depth of nighttime dives. Positive values indicate that daytime dives were on average deeper than nighttime dives. Although the species-specific patterns of responsiveness to light are complex there is a general trend, from arguably the largest, completely binary, response of the shallowest diving species *P. electra*, to the non-response of the deepest diving species *Z. cavirostri*

Figure 2-10. Predictions from a continuous time correlated random walk model fitted to Argos estimates of tag locations. These points are overlain on the distribution of benthic habitats that within the observed foraging dive ranges (blue shading) for each species delineated in Fig. 2. Overall the shallower diving species *Peponocephala electra*, *Globicephala macrorhynchus*, and sub-adult male *Physeter macrocephalus* show less consistent spatial overlap with benthic habitats within their dive ranges than do deeper diving adult female *Physeter macrocephalus*, *Mesoplodon densirostris*, *Ziphius cavirostris*. The percent overlap scores shown on each map also quantitatively demonstrate this difference.

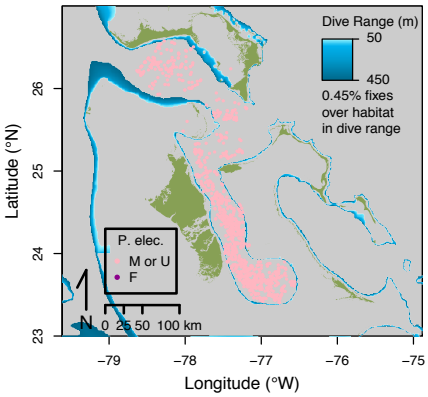
Dive Range (m)
50
450
0.45% fixes
over habitat
in dive range
P. elec.
M or U
F
N
0 25 50 100 km
Latitude (°N)
Longitude (°W)

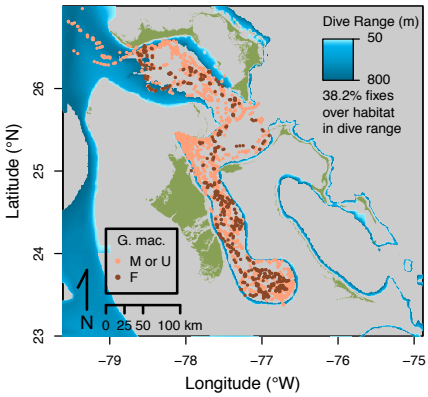
Dive Range (m)
50
800
38.2% fixes
over habitat
in dive range
G. mac.
M or U
F
N
0 25 50 100 km
Latitude (°N)
Longitude (°W)

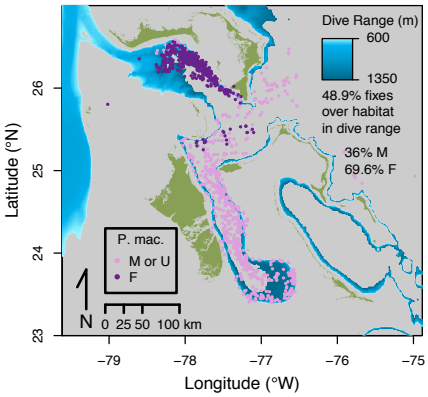
Dive Range (m)
600
1350
48.9% fixes
over habitat
in dive range
36% M
69.6% F
P. mac.
M or U
F
N
0 25 50 100 km
Latitude (°N)
Longitude (°W)

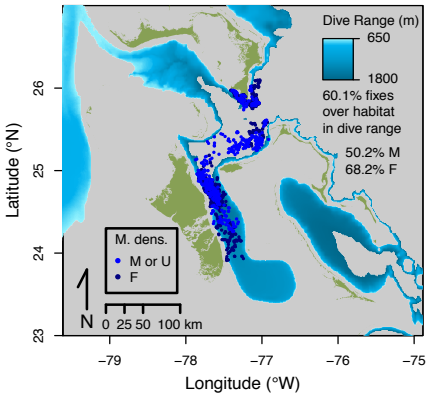
Dive Range (m)
650
1800
60.1% fixes
over habitat
in dive range
50.2% M
68.2% F
M. dens.
M or U
F
N
0 25 50 100 km
Latitude (°N)
Longitude (°W)

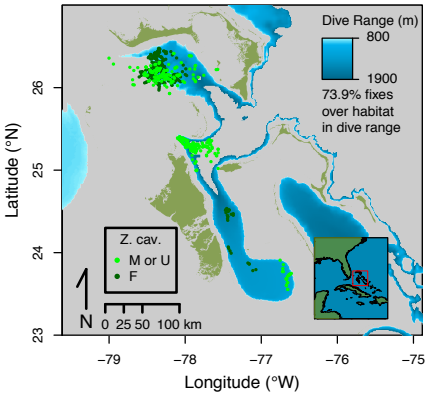
Dive Range (m)
800
1900
73.9% fixes
over habitat
in dive range
Z. cav.
M or U
F
N
0 25 50 100 km
Latitude (°N)
Longitude (°W)

CHAPTER 3:

Estimates of foraging depth using blubber fatty acid proxies in a sympatric assemblage of deep-diving toothed-whales from the Bahamas

TREVOR W. JOYCE, GINA YLITALO, DAVID HERMAN ,JOHN W. DURBAN,
HOLLY FEARNBACH, DIANE CLARIDGE, LISA T. BALLANCE

Abstract

We evaluated the use of fatty acid (FA) relative abundance as a proxy of cetacean foraging depth based on extensive satellite tag dive data (N_{tag} = 75) and blubber biopsy sampling (N_{biopsy} = 205) from six species of toothed whales (Suborder: Odontoceti) inhabiting the oceanic North Atlantic waters surrounding the Bahamas archipelago. Tagged and biopsied species included the melon-headed whale (*Peponocephala electra*, N_{tag} = 13), rough toothed dolphin (*Steno bredanensis*, N_{tag} = 1), short-finned pilot whale (*Globicephala macrorhynchus*, N_{tag} = 15), sperm whale (*Physeter macrocephalus*, N_{tag} = 27), Cuvier's beaked whale (*Ziphius cavirostris*, N_{tag} = 7), and Blainville's beaked whale (*Mesoplodon densirostris*, N_{tag} = 12). Previous research has shown substantial depth variation in the relative abundance of polyunsaturated FA (PUFA) and odd-chain-length FA (associated with heterotrophic bacteria) in the particulate organic matter constituting the base of marine trophic webs. We likewise found a strong relationship of PUFA relative abundance in blubber with the depth of cetacean foraging dives. Generalized linear models (GLM) with a tobit-censored distribution showed highly significant declines in PUFA with increasing dive depth when analyzed at both the mean species level (GLM_{tobit}, df = 191, z = -14.79, $p < 0.0001$) and at the individual level (GLM_{tobit}, df = 21 , z = -4.572, $p < 0.0001$) in the limited cases where the same individual had been both tagged and

biopsied ($N_{tag,biopsy}$ = 28). The proportional representation of odd-chain length FA was not significantly correlated with dive depths ($P > 0.05$). However a subsequent exploratory data analysis revealed that foraging depths were highly significant predictors of ratios between some odd-chain length FA, and in particular, the ratio between the two most abundant FA in this class: C15:0 and C17:1n8. Back-calculating from models relating PUFA and [C15:0]/[C17:1n8] to dive depth, we estimated mean foraging depth of a biopsied but not tagged species, the Gervais' beaked whale (*Mesoplodon europaeus*), at 1108 m and 1072 m, respectively. Overall this approach shows substantial promise for the use of archival and novel biopsy and necropsy sampling of blubber to estimate the foraging depths in many cryptic cetacean species that have yet to be electronically tagged.

Introduction

Foraging depth is fundamental to the ecological interactions, evolutionary biology, and vulnerabilities of marine mammals. Dive depth and duration have been hypothesized as important drivers of morphology, physiology, and behavior (Noren and Williams 2001, Halsey et al. 2006, Mirceta et al. 2013) based on a range of energetic tradeoffs (Houston and Carbone 1992, Carbone and Houston 1996, Mori 1999, 2002, Joyce et al. *in review*). Dive depth range also influence habitat overlap between marine mammal species (*e.g.*, Friedlaender et al. 2010), impacts of marine mammals on depth-specific prey communities (*e.g.*, Clarke 1996), roles of marine mammals in nutrient cycling (*e.g.*, Lavery et al. 2010), and marine mammal spatial

distribution patterns (*e.g.*, Forney et al. 2012). Foraging depth is also an important component of evaluating exposure to anthropogenic impacts, including noise (McCarthy et al. 2011, Pirotta et al. 2012), chemical pollutants (Peterson et al., 2015), and vessel strike risk (Laist et al. 2001).

The development of electronic biologging technologies has vastly expanded scientific knowledge of dive behavior and foraging depths in many marine mammal species (Hooker and Baird 2001, Johnson et al. 2009, Joyce et al. 2016). The early time-depth recording (TDR) tags required the capture of marine mammals for instrument deployment and recovery (Kooyman 1965). The development of suction cup-mounted TDR and multi-instrument tags have enabled the deployment of archival electronic instruments on a wider array of free ranging marine mammal species (e.g., Hooker and Baird 1999, Johnson and Tyack 2003, Aoki et al. 2015). In particular, digital acoustic recording tags (DTAG; Johnson and Tyack 2003) have enabled descriptions of not only where time was spent vertically, but also where search and prey capture attempts occurred in both toothed whales (Madsen et al. 2002, Miller et al. 2004, Tyack et al. 2006, Watwood et al. 2006, Aguilar de Soto et al. 2008, Teloni et al. 2008) and baleen whales (Goldbogen et al. 2006, Ware et al. 2011). The recent development of medium-duration (e.g., weeks to months) satellite transmitting tags (Andrews et al. 2008) that can be projected using cross-bows or air guns and attached using small implantable darts, have further expanded the range of species for which detailed dive depth information can be obtained (Baird *et al.* 2011, Schorr *et al.* 2014, Durban and Pitman 2012, Joyce et al. 2016).

Despite these tagging advances substantial knowledge gaps remain, particularly for many oceanic cetacean species, which are not accessible to researchers from terrestrial or ice platforms, and which are often sparsely and patchily distributed in remote offshore habitats. To date researchers have only succeeded in deploying depth-sensing instruments on a minority ($N_{spp,tagged} \cong 27$) of the 90 currently recognized cetacean species (Hooker and Baird 2001, Mirceta et al. 2013, Committee on Taxonomy 2014). Deep diving habits of many beaked whales (Family: Ziphiidae) and minimal time spent at the surface between dives (Tyack et al. 2006, Arranz et al. 2011, Joyce et al. *in review*) have further limited the ability of researchers to successfully deploy tags on many ziphiid species. However, beaked whale dive behavior is of particular concern, due to their apparent vulnerability to Navy sonar and seismic exploration activities (McCarthy et al. 2011, Pirotta et al. 2012, New et al. 2013).

Fatty acids (FA) are a diverse class of organic molecules that have been extensively applied as tracers of diet (Ackman and Eaton 1966, Smith et al. 1996, Iverson et al. 1997, 2001, Falk-Petersen et al. 2004). Many marine mammal species deposit substantial layers of sub-cutaneous fat, or blubber, which is readily collected in biopsy and/or necropsy sampling for a variety of purposes (Barrett-Lennard *et al.* 1996, Ylitalo et al. 2001, Kellar et al. 2006). If natural depth gradients in FA composition exist in oceanic trophic webs, then measurements of the FA relative abundance in commonly collected blubber samples could potentially be used as proxies of foraging depths in cetaceans that currently lack electronic tagging

information. Within the broad class of FA molecules, particular groups of FA, defined by chain lengths, numbers and positions of double bonds, and the presence-absence of branching or cyclic structures, often share characteristics that lend themselves to their application as integrated signals of prey composition (Smith et al. 1996, Iverson et al. 2001, Hooker et al. 2001, Falk-Petersen et al. 2004, Budge et al. 2006), or as accumulated signals of animal age (Møller 1999, Herman et al. 2008, 2009). These properties include: 1) a unique biosynthetic origin in a specific class of autotroph or heterotroph (Perry et al. 1979, Dalsgaard et al. 2003), and 2) deposition in body tissues with minimal chemical modification and in ratios reflective of prey FA composition (Cook 1991, Iverson et al. 2004, Budge et al. 2006).

Based on these properties, poly-unsaturated fatty acids (PUFA) represent an intriguing potential tracer of depth. Jones et al. (2008) has documented substantial decreases in the proportional representation of PUFA in suspended particulate organic matter (POM) over the epipelagic and mesopelagic zones in the Southern California Bight. Jones et al. (2008) further demonstrated an increase in the proportional representation of odd-chain length and branched FAs (e.g., iso-C15:0, C15:0, cyc-C17:0) between POM samples collected at the surface and POM collected below 100m. These odd-chain length and branched FAs are thought to originate uniquely in heterotrophic bacterial biosynthesis pathways (Perry et al. 1979, Ackman 1989).

PUFA and odd-chain-length FA also represent potentially valuable tracers of foraging depth in blubber samples, because the tissues of consumers may more faithfully reflect their proportional representations in prey, relative to other classes of

FA (Budge et al. 2006). PUFA and odd-chain-length FA can both be catabolized by oxidation (Budge et al. 2006). However, if these FA are deposited in adipose tissues instead of being oxidized, their proportional representations are likely to undergo minimal modification. Most chain length modification pathways in mammals are restricted to even-numbered chain length saturated fatty acids (SFA) and mono-unsaturated fatty acids (MUFA; Budge et al. 2006). The endogenous biosynthesis of new FA in mammals also primarily yields SFA and MUFA (Volpe and Vagelos 1973, Cooper 2004, Budge et al. 2006). If the latter process represented a major pathway, it could substantially modify the proportional representation of PUFA and odd-chain length FA in blubber tissues. However, in consumers of lipid rich diets, such as marine mammals, most lipid reserves are accumulated through the deposition of exogenously produced lipids, rather than through *de novo* biosynthesis (Budge et al. 2006). Overall these findings point to the potential value of PUFA and odd-chain length classes of FA as tracers of depth in blubber samples.

To test whether the relative abundance of PUFA and odd-chain length FA could be used as quantitative tracers of foraging depths in marine mammal blubber samples, we collected and analyzed large biopsy and electronic tagging datasets consisting of six toothed whale species (Sub-order: Odontoceti) that occupied a wide range of depths in the sub-tropical oceanic waters of the Bahamas archipelago. Herman et al. (2008, 2009) also showed empirically that applying ratios of specific fatty acids instead of overall proportions could have a normalizing effect, controlling for inter-individual variation in overall FA composition based on diet, condition,

gender, and stratification in blubber. Therefore we also examined the empirical covariance between depth and a variety of concentration ratios between specific odd-chain length FA compounds. Finally, we used derived relationships between various FA and depth from the tagged species to predict the approximate foraging depth of a species, the Gervais' beaked whale (*Mesoplodon europaeus*), which was not successfully tagged in this study. We go on to discuss the implications of this estimated foraging depth for the ecology and biology of this species, which has been involved in prior mass stranding events (Fernandez et al. 2005).

Methods

Study Area

Biopsy samples and tag data were collected in the Great Bahama Canyon region of the Bahamas Archipelago in the sub-tropical western North Atlantic Ocean, between 23ºN and 27ºN, and 76ºW and 79ºW (Fig. 1). This study area was situated between the Antilles Current and the Florida Current with an east to west flow of 0.9-1.3 Sv (10^6 m^3/s) through the steep and convoluted bathymetric topography the northern half of the study area (Wang and Mooers 1997, Hamilton *et al.* 2005, Beal *et al.* 2008). Bathymetric depths of cetacean habitats ranged from <50m on the slopes of shallow banks to the edge of the abyssal plain at >3000m (Fig. 1).

Tagging and Biopsy Sampling

Cetaceans were detected using both visual and acoustic search from ship and small boat platforms (see Joyce et al. 2016). In total six species were successfully tagged and biopsied: melon-headed whale (*Peponocephala electra*), short-finned pilot whale (*Globicephala macrorhynchus*), rough-toothed dolphin (*Steno bredanensis*), sperm whale (*Physeter macrocephalus*), Cuvier's beaked whale (*Ziphius cavirostris*), and Blainville's beaked whale (*Mesoplodon densirostris*). One additional species Gervais' beaked whale (*Mesoplodon europaeus*) was biopsied but was not successfully tagged. Some individuals were successfully tagged and biopsied simultaneously. Identification of tagged and biopsied individuals from photographs allowed subsequent matching of several tag deployments and biopsy samples for the same individuals encountered on separate occasions.

Two types of Argos satellite-linked instruments were deployed: the SPOT model (AM-S240A-C, Wildlife Computers Inc.; *e.g.*, Andrews *et al.* 2008) and the SPLASH model (Mk-10, Wildlife Computers Inc.; *e.g.*, Schorr *et al.* 2014). While both tag types were similar in the telemetry information transmitted via the Argos satellite system, each tag type bore different sensors and provided different dive behavior data outputs. SPLASH dive data was collected from a pressure sensor and a wet-dry sensor in two formats. A behavior log summarized sequences of dives as a series of maximum depths and dive durations, as well as the durations of any surface intervals. An additional time series log recorded depth observations at either 2.5 or 5 minute intervals. Dive data from SPOT tags was received in the form of time-at-temperature (TAT) histograms summarized at 6-hr intervals from a temperature

sensor only (i.e., no direct measure of pressure or depth). Interpreting TAT as a proxy for the distribution of dive depths required the assimilation and interpolation of external temperature sampling from a variety of research vessels, profiling floats, and animal-borne sensors as described in Joyce *et al*. (2016).

Based on the results of previous DTAG studies involving the four deepest diving species in this study (*G. macrorhynchus*, *P. macrocephalus*, *Z. cavirostris*, and *M. densirostris*), not all dive activity could be interpreted as foraging activity (Tyack et al. 2006, Watwood et al. 2006, Aguilar de Soto et al. 2008, Arranz et al. 2011). We used these DTAG studies to define species-specific threshold depths (Table 1) below which activity was considered foraging (see more detailed description in Joyce et al. *in review*). Mean foraging depth for SPLASH-tagged individuals was calculated as the arithmetic mean of time series observations recorded below the species-specific foraging threshold depth. The number of time series data points received by the Argos satellites varied substantially between individuals, therefore species-specific mean foraging depths were calculated as a grand mean of individual foraging depths using only the SPLASH data. Mean foraging depths for SPOT-tagged individuals were calculated by simulating 1000 depth "observations" from each TAT histogram based on the depth estimated for the mid-point of each temperature bin using external temperature-depth profile information (see Joyce et al. 2016). An mean was then calculated for each SPOT-tagged individual by taking the mean of the simulated depth observations falling within the species-specific foraging depth ranges described above.

Biopsy Sample Collection and Preservation

Biopsy samples used in chemical tracer and genetic sexing analyses were collected from adult and sub-adult individuals from the six tagged species, as well as *M. europaeus*, using a remote dart biopsy technique (*e.g.,* Barrett-Lennard *et al.* 1996, Parsons *et al.* 2003). Subcutaneous blubber samples were initially preserved by freezing in liquid nitrogen at ≤ -190ºC, followed by shipping in dry ice (-79ºC) and storage in -80ºC freezer. Blubber samples ranged from 5 to 30mm below the epidermis. Because of the known potential for stratification of fatty acids with blubber depth (Kloopman et al. 1996), we analyzed only blubber tissue in the upper 12mm layer (3mm-15mm from the sample surface). Lipid liquefaction and loss to the surrounding water during the interval between biopsy dart sampling and dart recovery could potentially skew FA ratios. Thus blubber samples consisting of <5% lipid content were excluded from subsequent FA analyses for all species with the exception of *P. macrocephalus*. Over half of the biopsy samples from this species (34 of 55) had <5% total lipid content, thus we used a lower threshold of <1% total lipid content so as to maintain a robust sample size.

We used epidermis tissue from these same biopsy samples to determine genetic sex. These skin samples were frozen in a solution of salt-saturated dimethyl sulfoxide (DMSO) up to the time of DNA extraction. Silica-based filter membrane (Qiagen, Valencia, CA) or lithium chloride (Gemmell and Akiyama 1996) extraction methods were used to isolate total genomic DNA from subsamples of skin tissue and

a PCR amplification of the SRY and ZFX genes following methods detailed by Rosel (2003) indicated genetic sex.

Fatty Acid Extraction and Quantification

The concentrations of 83 different FA constituents in cetacean blubber samples were measured following methods for extraction, esterification, separation, and measurement via gas chromatography and mass spectrometry as previously described in Krahn et al. (2004) and Herman et al. (2005). Batches of 14 blubber samples were analyzed in conjunction with a standard reference material (*i.e.*, fish tissue homogenate, SRM 1946) from National Institute Standards and Technology for quality control following procedures detailed in Herman et al. (2005) and Sloan et al. (2006). Abbreviated names of the measured FA were reported in the International Union of Pure and Applied Chemistry n-number nomenclature system, which describes the carbon (C) chain length and number of C-C double bonds separated by a colon, followed by an "n" and the C position of first double bond counting from the terminal methyl group on the end of the aliphatic chain portion of the FA molecule (e.g., C18:2n6 which represents $CH_3(CH_2)_4CH{=}CHCH_2CH{=}CH(CH_2)_7COOH$).

Statistical Analyses

We first developed models of % PUFA by weight as functions of the mean foraging depths of different cetaceans in our tagging dataset. Percent PUFA by weight was calculated by dividing the total mass of fatty acids with two or more

double bonds in their aliphatic chains (C*X*:2 to C*X*:6) by the total mass of fatty acids in each blubber sample. Since % PUFA represented continuous proportional data, generalized linear models (GLM) with a beta distribution and a logit link function were used to describe the relationship of % PUFA to mean foraging depth using the function *betareg* in the *betareg* library in R (Cribari-Neto and Zeileis 2009). Male and female cetaceans differ substantially in size in many cetacean species (particularly *P. macrocephalus* and *G. macrorhynchus*, see Joyce et al. *in review*), and also exhibit different patterns in the deposition and remobilization of fat reserves over the course of their lives. Therefore we also considered beta GLM models describing % PUFA that included mean foraging depth and a factor variable denoting gender. As an alternative to the beta distribution which provided a curvilinear fit in real number space, we also developed similarly structured linear tobit GLMs with identity link functions, which were fitted between % PUFA and mean foraging depth using the function *vglm* in the *VGAM* library in R (Yee et al. 2010). Because of the proportional nature of % PUFA values, the response variable in this case was modeled as a tobit distribution with a lower bound of 0 and an upper bound of 1. Tobit models were also developed which included gender as a factor. Beta and tobit GLM were fitted to both species-mean data and individual-mean foraging depth data (the latter using the limited number of individuals where both tagging and biopsy data were available). Models with and without gender were compared based on Akaike's information criterion (AIC, Akaike 1974).

We subsequently developed analogous beta and tobit GLM models describing the relationship of % odd-numbered chain length FA to species- and individual-specific mean foraging depth. The % abundance of odd-numbered chain length FA by weight was calculate by summing the total mass of fatty acids with odd numbers of carbon atoms (e.g. C11:0, C11:1, 4812-Me-C13:0, iso-C15:0, anteiso-C15:0, C15:0, C15:1n5, 261014-Me-C15:0, iso-C17:0, anteiso-C17:0, C17:0, C17:1ne, C17:1n7, C19:0) that were found in measurable quantities, and dividing this sum by the total mass of fatty acids in each blubber sample. These beta and tobit GLM were then also compared on the basis of AIC scores.

We also ran an exploratory data analysis to look at which ratios of odd-chain length FA showed strong predictive relationships with species- and individual-specific mean foraging depths. Odd-chain length FA on average constituted only 2.9% of the total FA weight per sample, and many specific odd-chain-length FA were substantially rarer. To avoid division-by-zero errors in constructing ratios, we examined only the ratios between the six most abundant odd-chain length FA. We estimated a series of tobit GLM relating species-specific mean foraging depths with the 18 different possible ratios of odd-chain length FA as response variables. Models were then systematically ranked and compared on the basis of their pseudo-coefficients of determination, pseudo-R^2, which represented the proportion of variance explained by the models.

$$pseudo\ R^2 = 1 - \frac{var_{residuals}}{var_{total}} \qquad (1)$$

Depth Predictions and Morphometrics

We used models of % PUFA and ratios of fatty acids to back calculate the mean foraging depth of *M. europaeus*, a species which we were unable to tag. To discuss the implications of this predicted foraging depth for the ecology and biology of *M. europaeus* we also estimated a median body mass for this species following Joyce et al. (*in review*). Briefly, body mass and standard length data used in estimating the median body mass of *M. europaeus* were extracted from the National Museum of Natural History (NMNH) whale collection database (downloaded from http://collections.nmnh.si.edu/search/mammals/ on July 13, 2015) and from (Mead 1989). A log-log linear model of body mass and standard length measurements was fitted using *lm* command from the R library *stats*. Median adult standard length was then used to predict median mass from the estimated log-log (i.e., power law) functional relationship.

Results

Foraging Depths and Fatty Acid Values

A total of 75 satellite tags (n= 75) were deployed on six odontocete cetacean species; they yielded 1268 and 9115 h of SPLASH time series and SPOT TAT data, respectively (Table 1). Mean foraging depths ranged from 56 m in *S. bredanensis* to 1176 m (s.d.: 231 m) in *Z. cavirostris* (Table 2). Foraging depths in *P. electra* (mean: 103 m; s.d.: 125 m) and *P. macrocephalus* (mean: 779 m; s.d.: 98 m) were relatively consistent when compared with the greater depth variability exhibited by *G.*

macrorhynchus (mean: 159 m; s.d.: 188 m) and *M. densirostris* (mean: 981 m; s.d.: 237 m; Table 2).

A total of 409 biopsy samples were collected over the period 2002 to 2014, and of these biopsies 205 samples yielded FA information. In total 24 individuals from four species were tagged and biopsied simultaneously, and 15 more individuals were tagged and biopsied on separate occasions but linked through photo-identification. However blubber samples were not obtained from all 39 tagged and biopsied individuals. Both FA and dive depth information was obtained from 28 samples, representing 37.3% of the tagging dataset and 13.6% of the FA dataset.

Overall SFA and MUFA represented the largest components of total fatty acids in odontocete blubber samples, constituting 16.9% (s.d.: 5.0%) and 74.1% (s.d.: 8.6%) by weight. On average PUFA made up 5.8 % (s.d.: 4.4%) of total fatty acids by weight, although this component of FA varied substantially from 24.3 % in the shallowest diver *S. bredanensis*, to a mean of 2.0% (s.d.: 0.8%) in the deepest diver *Z. cavirostris* (Table 2). The proportion of MUFA in blubber samples varied approximately inversely with the proportion of PUFA (Table 2). On average the odd-chain length component represented 2.9% (s.d.: 1.7%) of total FA composition, however this value also varied widely between species (Table 2). The mean percent odd-chain length FA was lower in the two species of *Mesoplodon*, *M. densirostris* (1.41%; s.d.: 0.31) and *M. europaeus* (1.85%; s.d.: 0.48), relative to the mean among the other five species (3.33%; s.d.: 1.67).

Models of PUFA

Percent PUFA decreased with increasing foraging depth (Fig. 2). The beta GLM yielded significant intercept and negative trend parameter terms when modeled as functions of mean species-specific (GLM_{beta}, df = 191, z = -15.72, $p < 0.0001$) and mean individual-specific foraging depth (GLM_{beta}, df = 21, z = -4.711, $p < 0.0001$). Tobit GLM also produced significant intercept and negative trend parameters with respect to mean foraging depth for species (GLM_{tobit}, df = 191, z = -14.79, $p < 0.0001$) and individuals (GLM_{tobit}, df = 21 , z = -4.572, $p < 0.0001$). For both species and individual levels the beta GLM provided a closer fit to the observed % PUFA data (Table 3). Also, models that included mean foraging depth only, were favored over models that also included gender on the basis of Akaike's weights, although beta GLM for species were nearly equivalent in terms of wAIC (Table 3).

Models of Odd-length FA

Neither beta GLM nor tobit GLM yielded significant trend parameters when modeling the % of odd-chain-length FA as functions of foraging depth at the species ($GLM_{beta, tobit}$, $p > 0.05$) and individual levels ($GLM_{beta, tobit}$, $p > 0.05$). However, exploratory data analyses (Table 4) examining the relationship between species- and individual specific foraging depths and ratios between the six most abundant odd-length FA, yielded significant trend parameters in 13/18 models based on a Bonferroni-corrected α of 0.003. Of these models, the ratio of two most abundant odd-length FAs (C15:0 and C17:1n8) yielded the strongest predictive relationship

with mean foraging depths (pseudo-$R^2 = 0.58$, Table 4). Tobit GLMs relating the ratio [C15:0]/[C17:1n8] to foraging depth were significant at both the species-(GLM_{tobit}, df = 191 , z = -8.499, $p < 0.0001$) and individual-specific levels (GLM_{tobit}, df = 21 , z = -5.588, $p < 0.0001$).

Depth Predictions and Morphometrics

Back calculating from the species-mean GLM_{tobit} models of % PUFA and [C15:0]/[C17:1n8], yielded a predicted mean foraging depths of 1102 m (Fig. 2) and 1076 m (Fig. 3) for *M. europaeus*, based on mean % PUFA and [C15:0]/[C17:1n8] values of 2.18% (s.d.: 1.00%) and 0.26 (s.d.: 0.06), respectively. The estimated body mass of *M. europaeus* based on the power-law relationship of standard length to body mass shown in Figure 4, was 680 kg in males and 724 kg in females.

Discussion

Although blubber % PUFA showed relatively high residual variability compared to ratios of [C15:0] to [C17:1n8], the overall decline in % PUFA between cetaceans feeding near the surface (*S. bredanensis*) and in the upper bathypelagic (*Z. cavirostris*), corresponded strongly with declines in % PUFA documented in POM within the Southern California Bight (Jones et al. 2008). Moreover, some of the large inter-individual variability in % PUFA exhibited in particular by *G. macrorhynchus*, was consistent with the wide range of daytime and nighttime foraging depths

exhibited by this species, as well as the apparent targeting of vertically migratory deep scattering layer prey (Aguilar de Soto et al. 2008, Joyce et al. *in review*). The similarity of the % PUFA pattern between two distinct marine ecosystems in different ocean basins provides a preliminary suggestion that a generalized mechanism might account for the fractionation of PUFA with depth. The biosynthesis of PUFAs with an n-number <9, which make up on average 94.5% of PUFA in blubber samples by weight, is thought to occur almost exclusively among photosynthetic autotrophs within the euphotic zone (Cook and McMaster 2002, Dalsgaard et al. 2003). Furthermore, Wakeham (1995) and others have suggested that PUFA is preferentially consumed and/or degraded, relative to SFA and MUFA, as POM sinks and is re-mineralized by heterotrophic consumers below the euphotic zone (Wakeham 1995, Harvey and Macko 1997, Wakeham et al. 1997, Jones et al. 2008). It is plausible therefore that these source and sink dynamics might combine to establish general gradients of % PUFA at the respective bases of trophic webs in different depth zones of the water column. These underlying gradients may in turn translate to the lipid reserves of high trophic level consumers through transfer up the food chain. However, the purely correlational results of this study obviously cannot exclude alternative hypotheses for the observed overall decline in blubber % PUFA with depth. PUFA are important dietary compounds both as precursors for a variety of synthesis pathways (e.g., arachidonic acid C20:4n-6 to prostaglandin; Cook and McMaster 2002) and also in maintaining the phospholipid bilayer pliability (Cook and McMaster 2002, Dalsgaard et al. 2003). Deeper diving cetaceans may thus have

different metabolic demands for PUFA, and specifically incorporate less PUFA in blubber based on endogenous processes instead of through trophically-acquired ratios.

The non-significant relationship of % odd-chain length FAs with depth was also consistent with the results of Jones et al. (2008). These authors found large increases in the relative abundance of the "bacterial" component of FA (specifically *iso*-C15:0, C15:0, *cyc*-C17:0) from the surface to 100m, but then a relatively consistent proportion of bacterial FA from 100m to the depth of benthos, which ranged from ~600-900m in their study. Heterotrophic bacteria are active at all depths, however in terms of relative abundance these bacterially-derived FA were likely swamped by even-numbered chain length and unbranched FA from autotrophs and other non-bacterial heterotrophic consumers within the euphotic zone. Given that 5 of the 6 tagged species in our study dove to foraging depths significantly below 100m, at least during the day, it is therefore not surprising that we did not find a significant relationship of % odd-chain length FAs with depth. Interestingly, however, the ratio of [C15:0] to [C17:1n8] did show an even tighter relationship with foraging depth than % PUFA. Given that this was an empirically derived relationship, we do not have a specific biological hypothesis for why the abundance of C15:0 may decrease relative to C17:1n8 with depth. However, both of these bacterial FAs are not thought to play important roles in the metabolic pathways of mammals, and therefore we had no reason to suspect that this pattern would not have been reflective of an underlying environmental gradient. Moreover, examining these FA as ratios instead of

proportions may have allowed us to factor out variation in the overall proportion of diet ultimately derived from bacterial sources, and/or the differential stratification of fatty acid classes within the blubber, improving the identification of the underlying gradient.

Based on the proxy estimates of *M. europaeus* dive depth and median body mass, we can infer that *M. europaeus* likely experienced constraints on its dive duration and dive depth similar to those exhibited by other small and medium beaked whale species (e.g., *M. densirostris* and *Z. cavirostris*; Joyce et al. *in review*). Based on the mass, inter-deep dive interval, dive duration, and dive depth relationships detailed in Joyce et al. (*in review*), we hypothesize that *M. europaeus* likely extended foraging durations beyond aerobic dive limits (ADL; Kooyman et al. 1983) in order access lower mesopelagic and bathypelagic prey with sufficient time to make the energy invested in each foraging dive profitable. As a tradeoff this partial reliance on anaerobic metabolism to sustain muscular function over extended foraging dive durations would also imply a substantially lower proportion of its time budget available for foraging, relative to other aerobically diving cetacean species (e.g., *P. macrocephalus* and *G. macrorhynchus*; Kooyman 1980, Tyack et al. 2006, Joyce et al. *in review*). This reduction in time available for foraging results from the need to aerobically metabolize lactic acid accumulations, necessitating greater time spent near the surface relative to the time needed for the exchange of gases (Kooyman 1980, Kooyman 1983). This depth estimate also pointed to a relatively high overlap in foraging depth between *M. europaeus* and its congener *M. densirostris*. Based on the

overlapping distribution of *M. densirostris* Argos position fixes and *M. europaeus* biopsy and encounter locations these species also overlapped in the spatial dimension of habitat. This three dimensional habitat overlap raised intriguing questions of whether competitive interactions and/or niche partitioning may influence other aspects of their respective niche-spaces such as prey selection.

The close correspondence in *M. europaeus* foraging depth estimates derived from the % PUFA and [C15:0]/[C17:1n8] tracers also suggested that if the relationships demonstrated in this analysis can be empirically validated for other regions and ecosystems, then FA techniques could have quite wide applicability in estimating the foraging depths of many cryptic cetacean species that have yet to be electronically tagged. With the proxy estimate of *M. europaeus* foraging depth obtained in this study, the dwarf and pygmy sperm whales (*Kogia sima* and *Kogia breviceps*, Family: Kogiidae) represent the only commonly encountered deep-diving cetacean species in the Bahamas for which dive information is currently lacking. The extreme shyness and difficulty of approaching *K. breviceps* and *K. sima* have to date hampered the ability of researchers to directly measure dive parameters in free ranging kogiids. Archival blubber tissues from necropsies of stranded *K. breviceps* and *K. sima* individuals may however yield FA composition for these reclusive species. Proxy foraging depth estimates for these two species would enable a more complete analysis of habitat overlap within the diverse Bahamas odontocete assemblage. More broadly, the highly significant relationships of both % PUFA and [C15:0]/[C17:1n8] with foraging depth, also corroborated the dive depth patterns

observed in the tagging dataset using the much larger biopsy sample sizes.

Finally, biopsy sampling is logistically simpler, far less expensive, and less invasive than tagging, and has a wide range of additional applications including genetic sampling (e.g., Parsons et al. 2003), contaminant analyses (e.g., Ylitalo et al. 2001), and stress/reproductive hormone measurement (e.g., Kellar et al. 2006). The development of these fatty acid tracers of foraging depth could, if verified, add a substantial complementary dimension to ongoing research using new and archival biopsy sampling.

Acknowledgements

We appreciate the large contribution of Charlotte Dunn and Leigh Hickmott at the Bahamas Marine Mammal Research Organisation (BMMRO) to the field research and planning of this project. Brice Semmens, Lynne Talley, and Paul Dayton all provided valuable input on this manuscript. We would also like to thank the many biologists, including Robert Pitman, Olivia Patterson, Aaron Banks, Marie Guilpin, Kendria Ferguson, Eric Lewallen and Edward Adderley who contributed to the field efforts. We would also like to acknowledge the captains and crews of the R/V *Walton Smith* and M/V *Slumber Venture* for their support of these research efforts. Funding for tagging efforts in the Bahamas and FA analyses at the NOAA-NMFS Northwest Fisheries Science Center were supported by the US Navy Office of Naval Research (grant N000140710120), NAVFAC (grants N002441110021, N002441210007 and contract N6660413P2671), and the Strategic Environmental Research and

Development Program (award RC-2114). All tagging was conducted under Bahamas Marine Mammal Protection Permit #12A. Tag types, methods of deployment, and sample sizes were all reviewed and approved by BMMRO's Institutional Animal Care and Use Committee (IACUC).

Chapter 3, in full, has been submitted for publication of the material. Joyce, Trevor W.; Durban, John W.; Claridge, Diane E.; Ylitalo, Gina; Fearnbach, Holly; Ballance, Lisa T. The dissertation author was the primary investigator and author of this material.

References

Ackman, R.G. (1989) Fatty acids. *Marine biogenic lipids, fats and oils*, **1**, 103–137.

Ackman, R.G. and Eaton, C.A. (1966) Lipids of the fin whale (Balaenoptera physalus) from north Atlantic waters. III. Occurrence of eicosenoic and docosenoic fatty acids in the zooplankter Meganyctiphanes norvegica (M. Sars) and their effect on whale oil composition. *Canadian Journal of Biochemistry,* 44, 1561–1566.

Aguilar Soto, N., Johnson, M.P., Madsen, P.T., Díaz, F., Domínguez, I., Brito, A. & Tyack, P. (2008) Cheetahs of the deep sea: deep foraging sprints in short-finned pilot whales off Tenerife (Canary Islands). *Journal of Animal Ecology*, **77**, 936–947.

Akaike, H. (1974) A new look at the statistical model identification. *IEEE transactions on automatic control*, **19**, 716–723.

Andrews, R.D., Pitman, R.L. & Ballance, L.T. (2008) Satellite tracking reveals distinct movement patterns for Type B and Type C killer whales in the southern Ross Sea, Antarctica. *Polar Biology*, **31**, 1461–1468.

Aoki, K., Amano, M., Mori, K., Kourogi, A., Kubodera, T. & Miyazaki, N. (2012) Active hunting by deep-diving sperm whales: 3D dive profiles and maneuvers during bursts of speed. *Marine Ecology Progress Series*, **444**, 289–301.

Arranz, P., De Soto, N.A., Madsen, P.T., Brito, A., Bordes, F. & Johnson, M.P. (2011) Following a foraging fish-finder: Diel habitat use of Blainville's beaked whales revealed by echolocation. *PloS one*, **6**, e28353.

Baird, R.W., Schorr, G.S., Webster, D.L., Mahaffy, S.D., McSweeney, D.J., Hanson, M.B. & Andrews, R.D. (2011) Open-Ocean Movements of a Satellite-Tagged Blainville's Beaked Whale (Mesoplodon densirostris): Evidence for an Offshore Population in Hawai'i? *Aquatic Mammals*, **37**, 506.

Barrett-Lennard, L., Smith, T.G. & Ellis, G.M. (1996) A cetacean biopsy system using lightweight pneumatic darts, and its effect on the behavior of killer whales. *Marine Mammal Science*, **12**, 14–27.

Beal, L.M., Hummon, J.M., Williams, E., Brown, O.B., Baringer, W. & Kearns, E.J. (2008) Five years of Florida Current structure and transport from the Royal Caribbean Cruise Ship Explorer of the Seas. *Journal of Geophysical Research: Oceans*, **113**.

Budge, S.M., Iverson, S.J. & Koopman, H.N. (2006) Studying trophic ecology in marine ecosystems using fatty acids: a primer on analysis and interpretation. *Marine Mammal Science*, **22**, 759–801.

Carbone, C. & Houston, A.I. (1996) The optimal allocation of time over the dive cycle: an approach based on aerobic and anaerobic respiration. *Animal Behaviour*, **51**, 1247–1255.

Clarke, M.R. (1996) Cephalopods as prey. III. Cetaceans. *Philosophical Transactions of the Royal Society B: Biological Sciences*, **351**, 1053–1065.

Committee on Taxonomy (2014) List of marine mammal species and subspecies. Society for Marine Mammalogy, www.marinemammalscience.org, consulted on 16 July, 2016.

Cook, H.W. (1991) Fatty acid desaturation and chain elongation in eucaryotes. *New Comprehensive Biochemistry*, **20**, 141–169.

Cook, H.W. & McMaster, C.R. (2002) Fatty acid desaturation and chain elongation in eukaryotes. *New comprehensive biochemistry*, **36**, 181–204.

Cooper, M.H. (2004) *Fatty acid metabolism in marine carnivores: Implications for quantitative estimation of predator diets*. PhD thesis, Dalhousie University, Halifax, Canada.

Cribari-Neto, F. & Zeileis, A. (2009) Beta regression in R.

Dalsgaard, J., John, M.S., Kattner, G., Müller-Navarra, D. & Hagen, W. (2003) Fatty acid trophic markers in the pelagic marine environment. *Advances in marine biology*, **46**, 225–340.

Durban, J.W. & Pitman, R.L. (2011) Antarctic killer whales make rapid, round-trip movements to subtropical waters: evidence for physiological maintenance migrations? *Biology Letters*, rsbl20110875.

Falk-Petersen, S., Haug, T., Nilssen, K.T., Wold, A. & Dahl, T.M. (2004) Lipids and trophic linkages in harp seal (Phoca groenlandica) from the eastern Barents Sea. *Polar Research*, **23**, 43–50.

Fernández, A., Edwards, J.F., Rodriguez, F., De Los Monteros, A.E., Herraez, P., Castro, P., Jaber, J.R., Martin, V. & Arbelo, M. (2005) "Gas and fat embolic syndrome" involving a mass stranding of beaked whales (family ziphiidae) exposed to anthropogenic sonar signals. *Veterinary Pathology Online*, **42**, 446–457.

Forney, K.A., Ferguson, M.C., Becker, E.A., Fiedler, P.C., Redfern, J.V., Barlow, J., Vilchis, I.L. & Ballance, L.T. (2012) Habitat-based spatial models of cetacean density in the eastern Pacific Ocean. *Endangered Species Research*, **16**, 113–133.

Friedlaender, A.S., Lawson, G.L. & Halpin, P.N. (2009) Evidence of resource partitioning between humpback and minke whales around the western Antarctic Peninsula. *Marine mammal science*, **25**, 402–415.

Gemmell, N.J. & Akiyama, S. (1996) An efficient method for the extraction of DNA from vertebrate tissues. *Trends in Genetics*, **12**, 338–339.

Goldbogen, J.A., Calambokidis, J., Shadwick, R.E., Oleson, E.M., McDonald, M.A. & Hildebrand, J.A. (2006) Kinematics of foraging dives and lunge-feeding in fin whales. *Journal of Experimental Biology*, **209**, 1231–1244.

Halsey, L.G., Butler, P.J. & Blackburn, T.M. (2006) A phylogenetic analysis of the allometry of diving. *The American Naturalist*, **167**, 276–287.

Hamilton, P., Larsen, J.C., Leaman, K.D., Lee, T.N. & Waddell, E. (2005) Transports through the Straits of Florida. *Journal of physical oceanography*, **35**, 308–322.

Harvey, H.R. & Macko, S.A. (1997) Kinetics of phytoplankton decay during simulated sedimentation: changes in lipids under oxic and anoxic conditions. *Organic Geochemistry*, **27**, 129–140.

Herman, D.P., Burrows, D.G., Wade, P.R., Durban, J.W., Matkin, C.O., LeDuc, R.G., Barrett-Lennard, L.G. & Krahn, M.M. (2005) Feeding ecology of eastern North Pacific killer whales Orcinus orca from fatty acid, stable isotope, and organochlorine analyses of blubber biopsies. *Marine Ecology Progress Series*, **302**, 275–291.

Herman, D.P., Matkin, C.O., Ylitalo, G.M., Durban, J.W., Hanson, M.B., Dahlheim, M.E., Straley, J.M., Wade, P.R., Tilbury, K.L., Boyer, R.H. & others. (2008) Assessing age distributions of killer whale Orcinus orca populations from the composition of endogenous fatty acids in their outer blubber layers. *Marine Ecology Progress Series*, **372**, 289–302.

Herman, D.P., Ylitalo, G.M., Robbins, J., Straley, J.M., Gabriele, C.M., Clapham, P.J., Boyer, R.H., Tilbury, K.L., Pearce, R.W. & Krahn, M.M. (2009) Age determination of humpback whales Megaptera novaeangliae through blubber fatty acid compositions of biopsy samples. *Marine Ecology Progress Series*, **392**, 277–293.

Hooker, S.K. & Baird, R.W. (1999) Deep–diving behaviour of the northern bottlenose whale, Hyperoodon ampullatus (Cetacea: Ziphiidae). *Proceedings of the Royal Society of London B: Biological Sciences*, **266**, 671–676.

Hooker, S.K. & Baird, R.W. (2001) Diving and ranging behaviour of odontocetes: a methodological review and critique. *Mammal Review*, **31**, 81–105.

Hooker, S.K., Iverson, S.J., Ostrom, P. & Smith, S.C. (2001) Diet of northern bottlenose whales inferred from fatty-acid and stable-isotope analyses of biopsy samples. *Canadian Journal of Zoology*, **79**, 1442–1454.

Houston, A.I. & Carbone, C. (1992) The optimal allocation of time during the diving cycle. *Behavioral Ecology*, **3**, 255–265.

Iverson, S.J., Field, C., Don Bowen, W. & Blanchard, W. (2004) Quantitative fatty acid signature analysis: a new method of estimating predator diets. *Ecological Monographs*, **74**, 211–235.

Iverson, S.J., Frost, K.J. & Lowry, L.F. (1997) Fatty acid signatures reveal fine scale structure of foraging distribution of harbor seals and their prey in Prince William Sound, Alaska. *Marine Ecology Progress Series*, **151**, 255–271.

Iverson, S.J., McDonald, J.E. & Smith, L.K. (2001) Changes in the diet of free-ranging black bears in years of contrasting food availability revealed through milk fatty acids. *Canadian Journal of Zoology*, **79**, 2268–2279.

Johnson, M., de Soto, N.A. & Madsen, P.T. (2009) Studying the behaviour and sensory ecology of marine mammals using acoustic recording tags: a review. *Marine Ecology Progress Series*, **395**, 55–73.

Johnson, M.P. & Tyack, P.L. (2003) A digital acoustic recording tag for measuring the response of wild marine mammals to sound. *IEEE journal of oceanic engineering*, **28**, 3–12.

Jones, A.A., Sessions, A.L., Campbell, B.J., Li, C. & Valentine, D.L. (2008) D/H ratios of fatty acids from marine particulate organic matter in the California Borderland Basins. *Organic Geochemistry*, **39**, 485–500.

Joyce, T.W., Durban, J.W., Fearnbach, H., Claridge, D. & Ballance, L.T. (2016) Use of time-at-temperature data to describe dive behavior in five species of sympatric deep-diving toothed whales. *Marine Mammal Science*, **32**, 1044–1071.

Kellar, N.M., Trego, M.L., Marks, C.I. & Dizon, A.E. (2006) Determining pregnancy from blubber in three species of delphinids. *Marine Mammal Science*, **22**, 1–16.

Koopman, H.N., Iverson, S.J. & Gaskin, D.E. (1996) Stratification and age-related differences in blubber fatty acids of the male harbour porpoise (Phocoena phocoena). *Journal of Comparative Physiology B*, **165**, 628–639.

Kooyman, G.L. (1965) Techniques used in measuring diving capacities of Weddell seals. *Polar Record*, **12**, 391–394.

Kooyman, G.L., Castellini, M.A., Davis, R.W. & Maue, R.A. (1983) Aerobic diving limits of immature Weddell seals. *Journal of Comparative Physiology B: Biochemical, Systemic, and Environmental Physiology*, **151**, 171–174.

Kooyman, G.L., Wahrenbrock, E.A., Castellini, M.A., Davis, R.W. & Sinnett, E.E. (1980) Aerobic and anaerobic metabolism during voluntary diving in Weddell seals: evidence of preferred pathways from blood chemsitry and behavior. *Journal of Comparative Physiology B: Biochemical, Systemic, and Environmental Physiology*, **138**, 335–346.

Krahn, M.M., Herman, D.P., Ylitalo, G.M., Sloan, C.A., BURROwS, D.G., Hobbs, Roderic.C., Mahoney, B.A., Yanagida, G.K., Calambokidis, J. & Moore, S.E. (2004) Stratification of lipids, fatty acids and organochlorine contaminants in blubber of white whales and killer whales. *Journal of Cetacean Research and Management*, **6**, 175–189.

Laist, D.W., Knowlton, A.R., Mead, J.G., Collet, A.S. & Podesta, M. (2001) Collisions between ships and whales. *Marine Mammal Science*, **17**, 35–75.

Lavery, T.J., Roudnew, B., Gill, P., Seymour, J., Seuront, L., Johnson, G., Mitchell, J.G. & Smetacek, V. (2010) Iron defecation by sperm whales stimulates carbon export in the Southern Ocean. *Proceedings of the Royal Society of London B: Biological Sciences*, rspb20100863.

Madsen, P.T., Payne, R., Kristiansen, N.U., Wahlberg, M., Kerr, I. & Møhl, B. (2002a) Sperm whale sound production studied with ultrasound time/depth-recording tags. *Journal of Experimental Biology*, **205**, 1899–1906.

Madsen, P., Wahlberg, M. & Møhl, B. (2002b) Male sperm whale (Physeter macrocephalus) acoustics in a high-latitude habitat: implications for echolocation and communication. *Behavioral Ecology and Sociobiology*, **53**, 31–41.

McCarthy, E., Moretti, D., Thomas, L., DiMarzio, N., Morrissey, R., Jarvis, S., Ward, J., Izzi, A. & Dilley, A. (2011) Changes in spatial and temporal distribution and vocal behavior of Blainville's beaked whales (Mesoplodon densirostris) during multiship exercises with mid-frequency sonar. *Marine Mammal Science*, **27**, E206–E226.

Mead, J.G. (1989) *Beaked Whales of the Genus Mesoplodon*. Handbook of marine mammals.

Miller, P.J., Johnson, M.P. & Tyack, P.L. (2004a) Sperm whale behaviour indicates the use of echolocation click buzzes "creaks" in prey capture. *Proceedings of the Royal Society of London B: Biological Sciences*, **271**, 2239–2247.

Miller, P.J., Johnson, M.P. & Tyack, P.L. (2004b) Sperm whale behaviour indicates the use of echolocation click buzzes "creaks" in prey capture. *Proceedings of the Royal Society of London B: Biological Sciences*, **271**, 2239–2247.

Mirceta, S., Signore, A.V., Burns, J.M., Cossins, A.R., Campbell, K.L. & Berenbrink, M. (2013) Evolution of mammalian diving capacity traced by myoglobin net surface charge. *Science*, **340**, 1234192.

Møller, P. (1999) Distinguishing between foraging patterns and sexual maturity of harbour porpoise (Phocoena phocoena) utlilising blubber fatty acid signature and classification regression analysis. MSc thesis, University of Aarhus, Denmark.

Mori, Y. (1999) The optimal allocation of time and respiratory metabolism over the dive cycle. *Behavioral Ecology*, **10**, 155–160.

Mori, Y. (2002) Optimal diving behaviour for foraging in relation to body size. *Journal of Evolutionary Biology*, **15**, 269–276.

New, L.F., Moretti, D.J., Hooker, S.K., Costa, D.P. & Simmons, S.E. (2013) Using energetic models to investigate the survival and reproduction of beaked whales (family Ziphiidae). *PloS one*, **8**, e68725.

Noren, S.R. & Williams, T.M. (2000) Body size and skeletal muscle myoglobin of cetaceans: adaptations for maximizing dive duration. *Comparative Biochemistry and Physiology Part A: Molecular & Integrative Physiology*, **126**, 181–191.

Parsons, K.M., Durban, J.W., Claridge, D.E., Balcomb, K.C., Noble, L.R. & Thompson, P.M. (2003) Kinship as a basis for alliance formation between male bottlenose dolphins, Tursiops truncatus, in the Bahamas. *Animal Behaviour*, **66**, 185–194.

Perry, G.J., Volkman, J.K., Johns, R.B. & Bavor, H.J. (1979) Fatty acids of bacterial origin in contemporary marine sediments. *Geochimica et Cosmochimica Acta*, **43**, 1715–1725.

Peterson, S.H., Ackerman, J.T. & Costa, D.P. (2015) Marine foraging ecology influences mercury bioaccumulation in deep-diving northern elephant seals. *Proc. R. Soc. B*, p. 20150710. The Royal Society.

Pirotta, E., Milor, R., Quick, N., Moretti, D., Di Marzio, N., Tyack, P., Boyd, I. & Hastie, G. (2012) Vessel noise affects beaked whale behavior: results of a dedicated acoustic response study. *PLoS One*, **7**, e42535.

Rosel, P.E. (2003) PCR-based sex determination in Odontocete cetaceans. *Conservation Genetics*, **4**, 647–649.

Sloan, C.A., Brown, D.W., Ylitalo, G.M., Buzitis, J., Herman, D.P., Burrows, D.G., Tanagida, G., Pearce, R.W., Bolton, J.L., Boyer, R.H. & others. (2006) *Quality Assurance Plan for Analyses of Environmental Samples for Polycyclic Aromatic Compounds, Persistent Organic Pollutants, Fatty Acids, Stable Isotope Ratios, Lipid Classes, and Metabolites of Polycyclic Aromatic Compounds*.

Smith, R.J., Hobson, K.A., Koopman, H.N. & Lavigne, D.M. (1996) Distinguishing between populations of fresh-and salt-water harbour seals (Phoca vitulina) using stable-isotope ratios and fatty acid profiles. *Canadian Journal of Fisheries and Aquatic Sciences*, **53**, 272–279.

Teloni, V., Mark, J.P., Patrick, M.J. & Peter, M.T. (2008) Shallow food for deep divers: Dynamic foraging behavior of male sperm whales in a high latitude habitat. *Journal of Experimental Marine Biology and Ecology*, **354**, 119–131.

Tyack, P.L., Johnson, M., Soto, N.A., Sturlese, A. & Madsen, P.T. (2006) Extreme diving of beaked whales. *Journal of Experimental Biology*, **209**, 4238–4253.

Volpe, J. J., and P. R. Vagelos (1973) Saturated fatty acid biosynthesis and its regulation. *Annual Review of Biochemistry* 42, 21–60.

Wakeham, S.G. (1995) Lipid biomarkers for heterotrophic alteration of suspended particulate organic matter in oxygenated and anoxic water columns of the ocean. *Deep Sea Research Part I: Oceanographic Research Papers*, **42**, 1749–1771.

Wakeham, S.G., Hedges, J.I., Lee, C., Peterson, M.L. & Hernes, P.J. (1997) Compositions and transport of lipid biomarkers through the water column and surficial sediments of the equatorial Pacific Ocean. *Deep Sea Research Part II: Topical Studies in Oceanography*, **44**, 2131–2162.

Wang, J. & Mooers, C.N. (1998) Three-dimensional perspectives of the Florida Current: transport, potential vorticity, and related dynamical properties. *Dynamics of atmospheres and oceans*, **27**, 135–149.

Ware, C., Friedlaender, A.S. & Nowacek, D.P. (2011) Shallow and deep lunge feeding of humpback whales in fjords of the West Antarctic Peninsula. *Marine Mammal Science*, **27**, 587–605.

Watwood, S.L., Miller, P.J., Johnson, M., Madsen, P.T. & Tyack, P.L. (2006) Deep-diving foraging behaviour of sperm whales (Physeter macrocephalus). *Journal of Animal Ecology*, **75**, 814–825.

Yee, T.W. & others. (2010) The VGAM package for categorical data analysis. *Journal of Statistical Software*, **32**, 1–34.

Ylitalo, G.M., Matkin, C.O., Buzitis, J., Krahn, M.M., Jones, L.L., Rowles, T. & Stein, J.E. (2001) Influence of life-history parameters on organochlorine concentrations in free-ranging killer whales (Orcinus orca) from Prince William Sound, AK. *Science of the Total Environment*, **281**, 183–203

Tables

Table 3-1. Data types and sample sizes by species, 2002-2014. N = number of individuals. SPOT and SPLASH refer to different models of Argos satellite tags. Time Series refers the number of hours of time-depth recorder dive information returned by SPLASH tags. The number of hours of time-at-temperature histograms (TAT Histo.) returned by SPOT tags is also noted. Also indicated are the daytime and nighttime dive depth thresholds used to distinguish foraging from non-foraging dive activity.

Species	**N_{biopsy}**	**$N_{biopsy\ \&\ tag}$**	**$N_{fatty\ acid}$**	**N_{tag}**		**Time Series (h)**	**TAT Histo. (h)**	**Foraging Depth Threshold (m)**
				SPOT	**SPLASH**			
Rough-toothed dolphin *Steno bredanensis*	2	0	1	1	0	0	225	0 (Day) 0 (Night)
Melon-headed whale *Peponocephala electra*	42	0	29	9	4	15	1605	50 (Day) 0 (Night)
Short-finned pilot whale *Globicephala macrorhynchus*	62	3	46	12	3	278	3639	100 (Day) 0 (Night)
Sperm whale *Physeter macrocephalus*	131	16	54	21	6	140	3340	600 (Day) 600 (Night)
Blainville's beaked whale *Mesoplodon densirostris*	96	3	34	3	9	695	167	650 (Day) 650 (Night)
Gervais' beaked whale *Mesoplodon europaeus*	15	0	12	0	0	0	0	-
Cuvier's beaked whales *Ziphius cavirostris*	61	4	29	1	6	140	139	800 (Day) 800 (Night)

Table 3-2. Mean (and standard deviation) foraging depths and percent fatty acid composition by species. Fatty acids (FA) were classified as either saturated fatty acids (SFA), mono-unsaturated fatty acids (MUFA), poly-unsaturated fatty acids (PUFA), or odd-chain length fatty acids (including saturated, unsaturated, and branched FA with chain lengths of C11, C13, C15, C17, C19, and C21). *Mean foraging depth of *Steno bredanensis* calculated from TAT histogram simulations.

Species	**Foraging Depth**	**% SFA**	**% MUFA**	**% PUFA**	**% odd-chain FA**
Rough-toothed dolphin *Steno bredanensis*	56.1 (2.9)*	17.9 (-)	54.2 (-)	24.3 (-)	3.5 (-)
Melon-headed whale *Peponocephala electra*	103.3 (125.8)	18.8 (1.8)	66.1 (3.4)	12 (2.7)	2.7 (0.4)
Short-finned pilot whale *Globicephala macrorhynchus*	159.3 (187.9)	21 (3.6)	67.3 (5.6)	8.2 (3.8)	3.2 (1.9)
Sperm whale *Physeter macrocephalus*	779.4 (98)	19.3 (4.2)	72.8 (6.9)	4.4 (2.9)	3.2 (0.7)
Blainville's beaked whale *Mesoplodon densirostris*	980.9 (237)	11.3 (1.3)	83.9 (2.1)	3.2 (1.3)	1.4 (0.3)
Gervais' beaked whale *Mesoplodon europaeus*	- (-)	12.3 (1.8)	83.4 (2.4)	2.2 (1)	1.8 (0.5)
Cuvier's beaked whales *Ziphius cavirostris*	1176.6 (231.6)	12.7 (3.7)	80.6 (4.2)	2 (0.8)	4.4 (2.6)

Table 3-3. Section (a) compares beta and tobit generalized linear models (GLM_{beta} and GLM_{tobit}) fits relating % poly-unsaturated fatty acids (PUFA) with mean foraging depth and gender using species-specific mean estimates of foraging depth (Z_{forage}). Section (b) compares GLM_{beta} and GLM_{tobit} fits using individual-specific Z_{forage} for the limited subset of individuals that were both tagged and biopsied. The term *k* indicates the number of parameters estimated in each model fit. Models were selected on the basis of absolute and relative Akaike's Information Criterion scores (AIC and ΔAIC). Also shown are Akaike's weights (*w*AIC), which provides a measure of the relative probability that each model represents best model from a defined set of candidate models (Burnham and Anderson 2002).

Model Formula	**Level**	***k***	**AIC**	**ΔAIC**	**wAIC**
Mod. 1a (GLM_{beta}): PUFA ~ Z_{forage}	Species	1	-900.966	0	0.531
Mod. 2a (GLM_{beta}): PUFA ~ Z_{forage} + Gender	Species	2	-900.714	0.252	0.469
Mod. 3a (GLM_{tobit}): PUFA ~ Z_{forage}	Species	1	-797.036	103.93	0
Mod. 4a (GLM_{tobit}): PUFA ~ Z_{forage} + Gender	Species	2	-801.041	99.925	0
Mod. 1b (GLM_{beta}): PUFA ~ Z_{forage}	Individual	1	-119.613	781.353	0.722
Mod. 2b (GLM_{beta}): PUFA ~ Z_{forage} + Gender	Individual	2	-117.622	783.344	0.267
Mod. 3b (GLM_{tobit}): PUFA ~ Z_{forage}	Individual	1	-110.646	790.32	0.008
Mod. 4b (GLM_{tobit}): PUFA ~ Z_{forage} + Gender	Individual	2	-108.655	792.311	0.003

Table 3-4. Comparison of the proportion of variance explained (pseudo-R^2 or pseudo coefficients of determination) by tobit generalized linear models (GLM_{tobit}) relating ratios of different odd-chain length fatty acids with individual- and species-specific mean foraging depths (Z_{forage}). This exploratory data analysis examined ratios between the six odd-chain length fatty acids that were on average most abundant by weight. Whether each specific ratio was positively or negatively correlated with Z_{forage} is indicated by + and – signs, respectively.

Model Formula	**Individual Level**		**Species Level**	
	R^2	**(+/-)**	**R^2**	**(+/-)**
[C15:0]/[C17:1n8] ~ Z_{forage}	0.58	-	0.39	-
[iso.C15:0]/[C17:1n8] ~ Z_{forage}	0.58	-	<0	-
[iso.C17:0]/[C17:1n8] ~ Z_{forage}	0.56	-	0.35	-
[C17:0]/[C17:1n8] ~ Z_{forage}	0.56	-	0.48	-
[C17:0]/[C15:0] ~ Z_{forage}	0.40	-	0.15	-
[C19:0]/[C17:1ne] ~ Z_{forage}	0.40	-	0.17	-
[iso.C15:0]/[C15:0] ~ Z_{forage}	0.21	-	0.86	-
[iso.C17:0]/[iso.C15:0] ~ Z_{forage}	0.15	+	0.54	+
[iso.C17:0]/[C15:0] ~ Z_{forage}	0.11	-	<0	+
[C19:0]/[C17:0] ~ Z_{forage}	0.10	+	0.18	+
[C19:0]/[iso.C15:0] ~ Z_{forage}	0.10	+	0.40	+
[iso.C17:0]/[C17:0] ~ Z_{forage}	0.04	+	0.05	+
[C19:0]/[C15:0] ~ Z_{forage}	0.04	-	0.09	+
[C19:0]/[iso.C17:0] ~ Z_{forage}	0.01	+	0.12	+
[iso.C15:0]/[C17:0] ~ Z_{forage}	0.00	+	<0	-

Figures

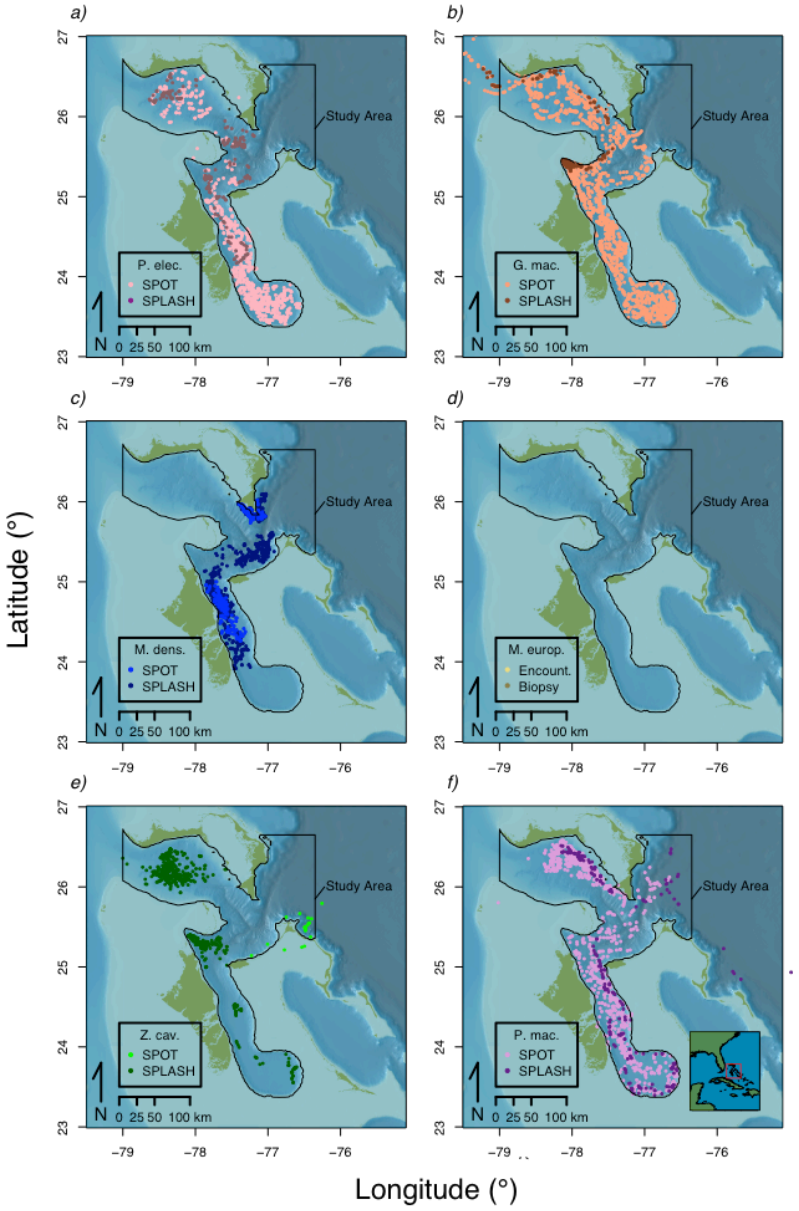

Figure 3-1. Position fix locations from Argos transmitter tags deployed on five species of cetaceans in the Great Bahama Canyon study area: *a*) melon-headed whale (*Peponocephala electra*, N_{SPOT}=9, N_{SPLASH}=4), *b*) short-finned pilot whale (*Globicephala macrorhynchus*, N_{SPOT}=12, N_{SPLASH}=3), *c*) Blainville's beaked whale (*Mesoplodon densirostris*, N_{SPOT}=3, N_{SPLASH}=9) and *e*) Cuvier's beaked whale (*Ziphius cavirostris*, N_{SPOT}=1, N_{SPLASH}=6) *f*) sperm whales (*Physeter macrocephalus*, N_{SPOT}=21, N_{SPLASH}=6). The locations of *d*) Gervais' beaked whale (*Mesoplodon europaeus*) biopsy samples and other encounters with this species are also shown.

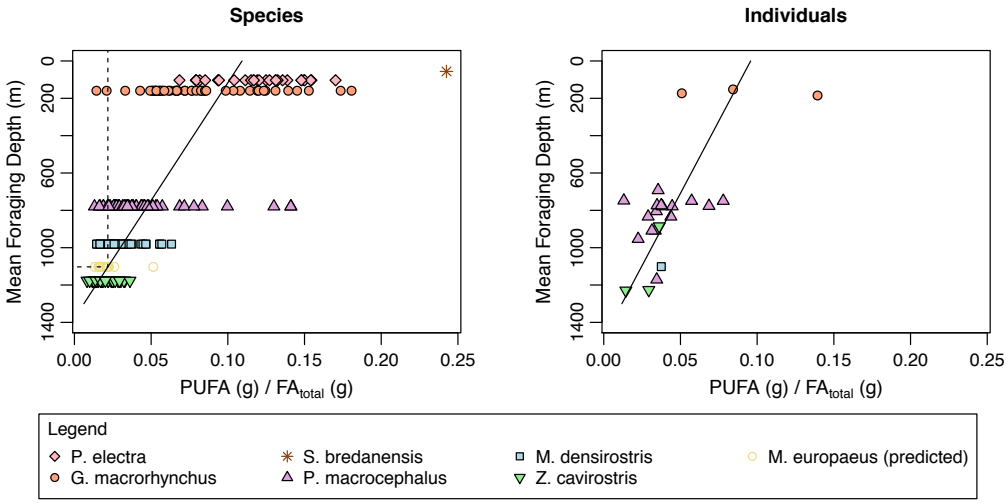

Figure 3-2. Distribution of % poly-unsaturated fatty acid (PUFA) values by a) species-specific mean foraging depth (Z_{forage}) and b) individual-specific mean Z_{forage} (where individuals were both tagged and biopsied). Trend lines indicate predicted % PUFA values from tobit generalized linear models (GLM_{tobit}) at the species (pseudo-$R^2 = 0.53$, formula: $\%PUFA = -7.9x10^{-5} Z_{forage} + 0.11$) and individual levels (pseudo-$R^2 = 0.48$, formula: $\%PUFA = -6.5x10^{-5} Z_{forage} + 0.1$). A predicted mean foraging depth of 1102.8m for the Gervais' beaked whale (*Mesoplodon europaeus*) was back-calculated (stippled lines) from the species-level GLM_{tobit} based on a mean percent %PUFA value of 2.18% (s.d.: 1.00%). The distribution of *M. europaeus* % PUFA values are shown as open circles at this depth.

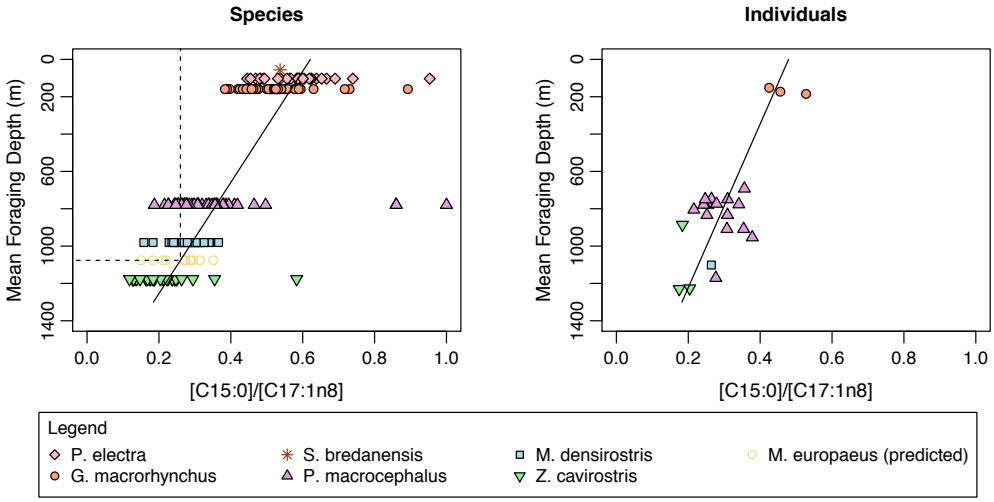

Figure 3-3. Distribution of the ratio of [C15:0] to [C17:1n8] values by a) species-specific mean foraging depth (Z_{forage}) (where individuals were both tagged and biopsied). Trend lines indicate predicted [C15:0]/[C17:1n8] values from tobit generalized linear models (GLM_{tobit}) at the species (pseudo-R^2 = 0.39, formula: [C15:0]/[C17:1n8] = -3.4×10^{-4} Z_{forage} + 0.62) and individual levels (pseudo-R^2 = 0.58, formula: [C15:0]/[C17:1n8] = -2.3×10^{-4} Z_{forage} + 0.48). A predicted mean foraging depth of 1076.3m for the Gervais' beaked whale (*Mesoplodon europaeus*) was back-calculated (stippled lines) from the species-level GLM_{tobit} based on a mean percent %PUFA value of 0.26 (s.d.: 0.06). The distribution of *M. europaeus* [C15:0]/[C17:1n8] values are shown as open circles at this depth.

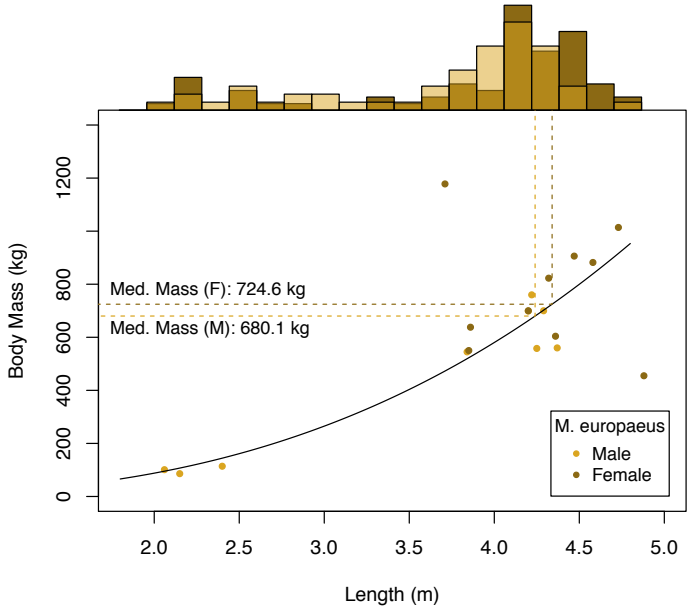

Figure 3-4. The relationship of body mass and standard length in male (lighter) and female (darker) Gervais' beaked whale (*Mesoplodon europaeus*). Histograms at top of the plot show the distributions of male ($N_{length, male} = 56$) and female ($N_{length, male} = 68$) standard lengths in stranding data from the National Museum of Natural History Cetacean Database and Mead (1989). Based on median male and female adult standard lengths (vertical dashed lines) of 4.24 m and 4.34 m we predicted median masses (horizontal dashed lines) of 680.1 kg and 724.6 kg, respectively, based on the log-log linear model (i.e., power law; $R^2 = 0.879$) illustrated by the trendline (formula: $\log M = 2.723 \log L + 1.124$).

CHAPTER 4:

Estimates of Hawaiian Petrel (*Pterodroma sandwichensis*) and Newell's Shearwater (*Puffinus newelli*) abundance based on data collected at sea, 1998-2011

TREVOR W. JOYCE, ROBERT L. PITMAN & LISA T. BALANCE

Abstract

This study estimated the abundance of the Newell's Shearwater (*Puffinus newelli*) and the Hawaiian Petrel (*Pterodroma sandwichensis*) within oceanic areas of the Central and Eastern Tropical Pacific sampled during National Oceanic and Atmospheric Administration (NOAA) research cruises. The objective of this effort was to inform species status assessments for these endangered endemic Hawaiian seabirds by providing climatological estimates of at-sea abundance and density distribution over the sampling period 1998-2011. Abundances estimates employed both 1) simple stratification analogous to previous published efforts (e.g., Spear et al. 1995); and 2) maximum likelihood based generalized additive models (GAM). The latter methods enabled the estimation of seabird densities across sampling units, or strata, that varied in survey design (i.e., randomized vs. systematic) and in sampling density. The GAM models covering the greatest proportion of the respective species ranges, yielded estimates of 52,186 Hawaiian Petrels (Bootstrap 95% Percentile, 39,823 - 67,379) and 27,011 Newell's Shearwaters (Bootstrap 95% Percentile, 18,254 - 37,125). These estimates did not encompass the entire oceanic range of either species, and therefore did not provide comprehensive estimates of total Hawaiian Petrel and Newell's Shearwater population sizes. However these estimates can be interpreted as minima of the average global populations of each species over the

sampling period 1998-2011.

Introduction

The Newell's Shearwater, or A'o (*Puffinus newelli*, Family: Procellariidae), and the Hawaiian Petrel, or Ua'u (*Pterodroma sandwichensis*, Family: Procellariidae) are listed species under the U.S. Endangered Species Act (ESA) criteria, with the former classified as threatened and the latter as endangered. The International Union for the Conservation of Nature (IUCN) Red List also lists both species, although the designations are reversed with *P. newelli* listed as endangered and *P. sandwichensis* listed as vulnerable. The relative abundance and population trends of both species are currently being monitored using proxy metrics such as coastal radar surveys and fallout recoveries. However, the only available estimates of overall abundance or population size for these species are based on at-sea surveys that only partially covered the oceanic range of each species, and also date to sampling conducted in the central and eastern tropical Pacific between 1980 and 1994 (Spear et al. 1995). Based on radar surveys, we know that the population *P. newelli* has undergone a substantial decline since the 1980-1994 period (Day et al. 2003). The absence of more recent and more comprehensive abundance estimates currently impedes decision-making regarding the population status and future conservation resource allocation for both species. Here, seabird strip transect surveys conducted by the Southwest and Pacific Islands Fisheries Science Centers (SWFSC and PIFSC) within the National Oceanographic and Atmospheric Administration, National Marine Fisheries Service (NOAA-NMFS) may provide novel information that could improve the status

assessment and management of both species.

However, it is important to consider that as a general approach to estimating seabird populations, data collected from visual surveys at sea faces several important limitations. First, the distribution patterns of seabirds at sea are typically dispersed, dynamic, and patchy relative to their more concentrated and static distributions on breeding colonies. Moreover, the strip transect survey methods used to measure seabird at sea distribution and abundance, are also a comparatively inefficient techniques for capturing patterns of animal abundance relative to line-transect distance sampling methods, particularly in sparsely distributed taxa (Buckland et al. 2001). To successfully meet the strip transect survey assumption of perfect detectability within the survey strip necessitated the use of a relatively narrow transect strip widths (≤300 m). Birds outside this narrow strip, although often detectable, were ignored in this case for the purposes of density estimation (Ballance 2007). Line-transect distance sampling, in which detection probability is modeled as a function of perpendicular distance from the track line, does not rely on this assumption of perfect detection and can thus include more distant observations of rare seabirds in estimating densities (Buckland et al. 2001). However, implementing a full line transect sampling protocol for seabirds has been generally found to be impractical, even considering the comparatively low seabird densities in the tropical latitudes, because of the rapid movements of seabirds and their relatively high abundance (i.e., often there are too many individuals observed simultaneously to record a distance and direction to each seabird, Ballance, pers. comm.). Because of

this restricted (≤300 m) strip width and the vast geographic scope of the NOAA-NMFS sampling strata, the directly sampled area represented a small fraction of total marine habitat within the study area.

Given these considerations, it is important to examine why the use of data collected at sea was warranted for the estimation of abundance in *P. newelli* and *P. sandwichensis*. Colony-based methods have been applied in estimating population size for a range of species. These include the direct counting of surface-nesting seabirds on colonies (e.g., Cuthbert et al. 2003), the quantification density and occupancy for burrow-nesting species (e.g., Rayner et al. 2007), and the application of mark-recapture sampling (e.g., Jones et al. 2007). However these approaches are impractical for both the *P. newelli* and *P. sandwichensis* because of their cryptic breeding behaviors. Important breeding habitats for both species are inaccessible because of steepness, remoteness, and/or high disturbance-sensitivity. Many portions of the species breeding ranges are also on privately owned land, and have not been made accessible to researchers. Where nesting habitat has been accessed, the ability of researchers to detect nests or birds on the ground even at very short distances (<5m) has been significantly limited by the cryptic situation of burrow entrances under dense sub-tropical vegetative cover, and due to the crepuscular or nocturnal activity patterns of both species while on their colonies. Densities of nests for both species are also typically sparse and patchily distributed relative to other colonially breeding procellariid seabirds. Finally no method of capturing a representative sample of either species has been validated for the application of mark-recapture methods of

estimating population size.

Given these limitations, data collected at sea may provide the best available basis for the estimation of *P. newelli* and *P. sandwichensis* abundance. Moreover, this approach has been extensively applied in a broad range of marine ecosystems and in a wide variety of seabird species (Ainley, O'Conner and Boekelheide 1984, Stahl and Bartle 1991, Piatt and Ford 1993, Spear et al. 1995, van der Meer and Leopold 1995, Clarke et al. 2003, Renner et al. 2013). Specifically, Spear et al. (1995) developed the only previous estimates of *P. newelli* and *P. sandwichensis* abundance based on sampling conducted using a continuous vector strip transect survey technique described in Tasker et al. (1984) over the period 1980 and 1994. These authors used a simple grid-based sub-division of their study area into sampling strata, and then estimated the average density of each species within each stratum. They then multiplied the grand mean of these stratum level densities by the total area within each species range to arrive at abundance estimates. Clarke et al. (2003) applied a somewhat more advanced approach of fitting spatial habitat generalized additive models (GAM) to the strip transect data, and then using the predicted densities surfaces from these models to derive estimates of oceanic abundance in several seabird species. This model based approach allowed 1) flexible non-linear relationships between counts and covariates, 2) non-normal error distributions, and 3) departures from a purely random or systematic sampling designs (Clarke et al. 2003). In addition, these authors validated their estimates by comparing at-sea abundance estimates with independent colony-based estimates of abundance for several

populations easily quantified, surface-nesting seabirds (Clarke et al. 2003). The close correspondence, in terms of both total abundance and trends between the at-sea estimates and colony-based estimates provided strong justification for the use of at-sea survey data to estimate abundance of our study species.

In this study we have attempted to provide more comprehensive and more precise estimates of *P. newelli* and *P. sandwichensis* abundance using recent NOAA-NMFS sampling covering the period 1998-2011. To improve the basis for assessing the status of each species and making future management decisions we have applied both 1) simple stratification and 2) maximum likelihood GAM methods of deriving robust estimates of abundance. We also devote substantial attention to the quantification of the uncertainty surrounding these estimates.

Methods

Study Area

NOAA seabird strip transect surveys have been conducted in the three study areas of the Central and Eastern Tropical Pacific Ocean: the Eastern Tropical Pacific (1998, 1999, 2000, 2003, 2006), the Hawaii Exclusive Economic Zone (2002, 2010), and the Palmyra and Johnston Atoll Exclusive Economic Zones and surrounding waters (2005, 2011). Sampling was conducted from August to November, with the exception of 2011 in which sampling was conducted only from October to November. The sampling schema of the NOAA strip transect datasets were not specifically designed to assess the abundance of these rare and endangered seabirds; they instead

were laid out with the intent of representatively sampling cetacean abundance distributions. Thus sampling was conducted employing approximately randomized (Stenella Abundance Research=STAR) or systematic (Hawaii Cetacean and Ecosystem Assessment Survey=HICEAS, Pacific Islands Cetacean and Ecosystem Assessment Survey=PICEAS) sampling designs (Fig. 1).

Field Methods

NOAA SWFSC seabird strip transect data were collected employing a "continuous vector" strip transect survey method as defined by Tasker et al. (1984) and Spear et al. (1992). This method involves the continuous recording of all seabird observations within a 90˚ arc forward of the vessel to either port or starboard, and of a variable radius between 100 and 300m depending on observation conditions. Radial distance to each seabird was categorized into three 100m ordinal bins using a range finder adapted from Equation 1 in Heinemann (1981), which relates both the observer's height above the water surface and distance to the horizon, to the radial distance to the ocean surface beneath the seabird. In addition, the flight direction and seabird behavior (eg. directional flight, milling, feeding, circling, sitting on the water) were also recorded for later flux correction (Gaston et al. 1987, Spear et al. 1992a). Strip transect observations were conducted continuously from sunrise to sunset as weather conditions allowed and were recorded in real-time by a single observer using the custom computer program SeeBird http://swfsc.noaa.gov/textblock.aspx?Division=PRD&ParentMenuId=147&id=1446. Daily

survey effort was broken up into transects, defined as segments of pre-defined survey track with unchanging weather conditions, observer, ship course (±10°), and ship speed. Any change in this suite of variables resulted in stopping the current transect and starting a new transect, thus transects varied in length over several orders of magnitude from <1km to >50km. In the modeling and stratification portions of this analysis, transects were aggregated by day-of-cruise in order to reduce inter-transect variability in sampled area.

All seabirds observed within the survey strip were identified to the lowest taxonomic grouping, gender, and age class possible using visual cues based on Onley and Scofield (2008), Harrison (1983), and other primary literature sources (Force et al. 2007, Howell et al. 1996, Howell et al. 1994, Spear et al. 1992a). Visual differentiation of Hawaiian Petrels from Galapagos Petrels (*Pterodroma phaeopygia*) at sea is based on very subtle interspecific differences in axillary shading, wing shape, and the demarcation of white on the forehead (Tomkins and Milne 1991, Force et al. 2007, Pyle et al. 2012). Prior to 2002 (Banks et al. 2002) Hawaiian and Galapagos petrels were considered con-specifics, and were thus recorded as "Dark-Rumped Petrels" in more than half of the NOAA dataset. To estimate abundance for the Hawaiian Petrel I applied the same geographic demarcation between the two species (130°W, Fig. 2) that was applied by Spear et al. (1995). This longitude also corresponds to a pronounced density minimum (Fig. 3). The Newell's Shearwater does not present the same challenges of identification at sea (Onley and Scofield 2008), and all but 4 of the 282 combined observations of *P. newelli* and its closest

congeneric, the Townsend's Shearwater (*Puffinus auricularis*), were identified to the species level.

Spatial and Habitat Covariates

The spatial distributions of abundance of the *P. newelli* and *P. sandwichensis* were modeled as functions of geographic, static, and dynamic habitat covariates. The analyses presented in this study employed remotely sensed, as opposed to, *in situ* dynamic habitat covariates because *in situ* measurements were not available for all cruises. The use of geographic variables such as Latitude and Longitude, and/or Distance-to-Colony as covariates can be biologically justified as descriptors of the central place foraging distribution patterns (Orians 1989) exhibited by both species during the breeding portion of the sampling period (Deringer 2009). However, Latitude and Longitude also served as powerful, though ecologically uninformative, proxies for spatial and ecological processes that were poorly quantified by the other available static and dynamic environmental covariates. To standardize the extraction of these covariates, transects with lengths > 5km were cut into segments of 5km or less. Covariate values were then calculated or extracted from raster datasets at the midpoint of these segments as described below. As noted in Section 2.2, transects were aggregated by day-of-cruise to create the data table used in both stratification and model construction. To index covariate values by day-of-cruise, average covariate values over all segments within a day of cruise effort were calculated.

Surface chlorophyll concentration (CHL) and sea surface temperature (SST) values for each segment were extracted from remotely sensed datasets by taking the mean of all pixel values falling within a 0.2˚ by 0.2˚ bounding box centered on the midpoint of each segment using an R script (xtractomatic_bdap.R version 1.0.3, http://coastwatch.pfel.noaa.gov/xtracto/R/code/xtractomatic_bdap.R) . For surveys between the years 1998 and 2006, mean remotely sensed values were drawn from both 8-day and monthly composite raster datasets of SeaWiFs CHL and Pathfinder SST version 5.2 with spatial resolutions of 9.0km and 5.5km, respectively. For the 2010 and 2011 surveys, SeaWiFs datasets became unavailable because of failure of the satellite instrument in 2010, and NOAA Pathfinder data only becomes available after several years of reprocessing and integration with *in situ* measurements (most recent data currently available is 2009). Therefore, comparable CHL and SST data from the Aqua MODIS instrument with 8- and 14-day composite temporal resolutions and 9.0km spatial resolution were used for these years. Where extraction at the 8-day temporal resolution returned an NA value (i.e. no pixels with real data values within the 0.2˚x0.2˚ bounding box attributed to glint and/or cloud cover), the mean values from the 14-day or monthly composite datasets were substituted. Mean bottom depths (BATHY) within a 2.5km radius around segment midpoints were extracted from the ETOPO1 1 arc-minute global relief model (http://www.ngdc.noaa.gov/mgg/global/) using the *extract* function from the R tool package *raster*. Latitude (LAT_MID) and Longitude (LONG_MID) were calculated for each segment at the mean of start and end point latitudes and longitude. Distance-to-colony (DIST_COL_SHNE and

DIST_COL_PEDR) was calculated as the shortest geodesic distance from the midpoint of each segment to the centroid of Kauai (159.5˚W, 22.08˚N) for the Newell's Shearwater, and the centroids of Kauai (159.5˚W, 22.08˚N), Maui (156.20˚W, 20.75˚N), Lanai (156.89˚W, 20.83˚W), Hawaii (155.49˚W, 19.43˚N) for the Hawaiian Petrel, using the *gdist* function in the R package *Imap*.

To incorporate these covariates in model predictions, a grid of 1˚ by 1˚ polygons was established covering the study area, and was clipped to the boundaries of the sampling strata. For the purpose of model prediction, dynamic covariates such as SST and CHL were represented as seasonal climatology layers (i.e., a raster image of long-term average values over a specified temporal window) that were assembled by calculating the mean raster values from four monthly Aqua MODIS 9km resolution SST and CHL climatology layers (2002-present, http://oceancolor.gsfc.nasa.gov/cgi/l3) covering the sampling period months of August, September, October, and November. The mean climatological SST and CHL values, as well as BATHY values, were then extracted within each prediction grid cell using the *extract* function. LAT_MID and LONG_MID were calculated as the centroid coordinate of each prediction grid cell, and DIST_COL_SHNE, and DIST_COL_PEDR were each calculated using *gdist* and the same colony coordinates as applied with the transect data.

Calculation of Density

The response variable and target for prediction in this analysis were counts of seabirds, normalized by the area of ocean surface sampled or used for prediction (ie. birds/km^2 or density). Buckland et al. (2001) define strip transect survey methods as an extension of quadrat sampling methods in which density is measured by simply dividing counts by the area sampled.

$$Density_i = \frac{Count_i}{Width_i \cdot Length_i} \quad (1)$$

However, in continuous vector strip transect sampling, birds that moved directionally through the sampling area relative the observer introduced a potentially large positive bias (Tasker et al. 1984, Spear et al. 1992b). Intuitively this makes sense as a moving bird could be counted in a greater number of possible transects over a fixed period of time relative to a stationary bird. Gaston et al. (1987) and Spear et al. (1992b) proposed an adjustment to the basic calculation of density in Equation 1 to account for the movement of seabirds relative to a moving survey platform by introducing what they termed a "flux correction" constant, K^{-1} (Fig. 4). The unitless constant K^{-1} was calculated by estimating the difference between the velocity vectors of the bird and the ship, and then normalizing by the ship's velocity or displacement vector (Fig. 4). Calculating this ratio necessitates measuring or estimating both the velocities of the ship and the directionally flying seabird, as well as the relative angle (θ) between the bird's and ship's courses. The ship's velocity vector (A) was measured by calculating the geodesic distance between the start and stop coordinates of each transect using the function *gdist*, and dividing by the transect duration. The seabird's velocity vector B was not measured directly but was estimated using published

empirical relationships of wind velocity and flight-speed-over-water (Spear et al. 1997). In this paper a separate linear regression relationship of wind speed and flight velocity was estimated for each functional taxonomic grouping (e.g., large *Pterodroma* petrel and Manx-type shearwater) and relative wind direction category (e.g., headwind, crosswind, or tailwind: Spear et al. 1997). For taxonomic groupings and relative wind direction categories where Spear et al. (1997) did not find a significant relationship between flight velocity and wind speed (Table 2 in Spear et al. 1997), I substituted the mean flight velocity (Table 3 in Spear et al. 1997), in the estimate of flight speed for correcting movement bias. The flight direction of birds relative to the ship course was directly estimated to the nearest 10˚ by seabird observers. The constant K^{-1} is indexed to j^{th} individual seabird observation, therefore to calculate the weighted average value of K^{-1} (AVG_K_SHNE and AVG_K_PEDR) for higher index levels such as transects or day-of-cruise, the sum of the flux-corrected (or absolute) counts was divided by the sum of the raw (or apparent) counts (see Fig. 4).

Abundance Estimation

In this analysis abundance estimation proceeded by estimating seabird density within a series of grid cells or strata, then multiplying each estimated density by the surface area of its respective grid cell or stratum, and summing the products across the study area of interest. Density estimation methods employed in this analysis fall into two general categories: stratification and modeling/interpolation methods.

Seabird densities were estimated within both randomly and systematically sampled strata by summing the birds counted and dividing by the total sampled area, which is equivalent to calculating the average density across all transects within a stratum. To estimate abundance within a given stratum, the j^{th} mean density was then multiplied by its surface area, which was calculated in ArcGIS 10.0 using a World Cylindrical Equal Area projection and the World Geodetic Survey 1984 (WGS84) datum. These estimated abundances were then summed over all strata (Equation 2). Stratification represents the simplest approach and gets around the stochastic nature of highly variable individual counts by taking an average over a large sample of counts. However, this approach relies on the assumption of perfectly representative sampling of the underlying unknown population density, and is highly sensitive to inevitable departures from sampling design. Using this approach would also require excluding from the analysis several important areas of habitat for the Newell's and Hawaiian Petrel, which were only sampled during transits to and from Hawaii, and not with any regular sampling design (see HICEAS and STAR Transits, Fig. 1).

$$Abundance = \sum_{j=1}^{n} \overline{Density_j} \cdot Area_j \qquad (2)$$

Spear et al. (1995) applied a variant of this stratification approach by calculating an overall density across the approximate range of each species, first estimating density within 5˚ by 5˚ degree strata, allowing for some deviation around the North Equatorial Counter Current, and then deriving a weighted average density, with weights corresponding to the respective surface area of each stratum. To estimate

abundance Spear et al. (1995) then multiplied this overall average density by the total surface area of the approximate species range (Equation 3), including some 5° by 5° strata that were excluded from the calculation of overall mean density because of insufficient sampling (i.e., less than 75 linear kilometers of transect per stratum). Importantly the approximate species ranges that were used to calculate abundance in this study encompassed only the areas sampled in this study, and did not include known areas of Newell's Shearwater and Hawaiian Petrel habitat to the North and West of the Hawaiian Islands.

$$Abundance = \overline{Density} \cdot \sum_{j=1}^{n} Area_j \tag{3}$$

Generalized Additive Models

The alternative approach to stratification explored in this analysis, involves the use of Generalized Additive Models (GAM) (Hastie and Tibshirani, 1986) to estimate the distribution of Newell's Shearwater and Hawaiian Petrel densities over a regular grid of unsampled locations, using static (BATHY), geographic (LAT, LONG, DIST_COL), and dynamic covariates (SST, CHL). These GAM models were then used to predict the expected counts within each prediction grid cell of the study area. These predicted counts were then summed to derive an estimate of abundance (Equation 5).

$$Abundance = \sum_{j=1}^{n} \widehat{Count}_j \tag{4}$$

A GAM is a semi-parametric variant of the Generalized Linear Model (GLM) (Nelder and Wedderburn 1970). It uses an iteratively re-weighted lease squares (IRLS) algorithm to estimate both the parametric distribution parameters, such as the mean and dispersion parameters of the negative binomial distribution, and the shape of non-parametric smooth functions for each covariate, which are defined by "knots" (or inflection points in a non-linear curve). To fit GAMs to the day-of-cruise scale strip transect count data and covariates, I used the R package *mgcv* ("Mixed GAM Computation Vehicle") which employs a recursive "leave-one-out" cross-validation algorithm to assess whether the addition or adjustment of a knot improves the predictive power of the model. Like standard GLMs, GAMs employ a link function that allows for a non-normal error distribution of the residuals. In this case raw counts of Newell's Shearwaters and Hawaiian Petrels showed greater variance than would be expected in the canonical Poisson distribution for count data in which count variance is expected to equal the mean. Therefore a negative binomial distribution with a log link function was used in fitting GAM models. The model-fitting algorithm was allowed to search for the negative binomial dispersion parameter θ over the range 1 to 2, with a parameter value of 1 indicating no overdispersion (i.e. Poisson error distribution), and a parameter value of 2 indicating moderate overdispersion, which is related to the spatial aggregation or patchiness of seabirds at-sea.

Following the approach of Clarke et al. (2003) I initially fitted negative binomial GAM models composed of one-dimensional cubic shrinkage spline smooth functions of either LAT and LONG, or DIST_COL, as well as CHL, SST, and

BATHY, each with a limit of 4 degrees of freedom (k). The area surveyed (AREA) and average flux correction constant (AVG_K), were each included in the offset term to account for variable survey effort between days, and to convert the discrete response variable, apparent counts (APP_COUNTS), to standardized units of flux corrected density. The entire offset term was logged because this term modifies the response variable, which is related to the covariates through a log link function $g(\cdot)$. The cubic shrinkage splines used in this analysis are identical to the cubic regression spline smooth functions used in Clarke et al. (2003), with the exception that their effective degrees of freedom (EDF) can be "penalized" (i.e. reduced) by the model fitting algorithm all the way to zero, which yields a line with a slope of zero and effectively removes the term from the model. This obviates the need for a stepwise forwards and backwards covariate selection process (Wood 2006), allowing the efficient incorporation of model selection variability in bootstrap estimates of uncertainty surrounding the abundance estimates (see Section 2.6). I subsequently experimented with replacing univariate spatial terms with a bivariate interaction term of LAT and LONG. I also refitted models using to the same combinations of covariates, but allowing mgcv to choose an appropriate number of effective degrees freedom by generalized cross validation, rather than artificially capping them at 4 d.f. (mgcv sets default caps on k of 9 for univariate terms and 29 for bivariate terms). In generalized cross validation mgcv uses Akaike's Information Criterion (AIC) as the metric of whether model fit is improved by increasing effective degrees of freedom (i.e. number of parameters).

To compare the predictive performance of the different candidate models, and assess the potential for "overfitting" (i.e. believing too strongly in the particular configuration of data generated by a stochastic process), which may have been introduced by allowing mgcv greater latitude to fit patterns in the data I performed a 10-fold cross validation exercise. Observations were assigned randomly to 10 subsets evenly distributed across all sampling strata in the dataset to maintain the spatial structure of the sampling effort. To compare candidate models, 1 of 10 subsets ("test" data) was excluded and the models were then refitted to the remaining 9 subsets ("training" data). The training models were then used to predict counts using the covariates of the test data. The model fitted values were compared to the observed values based on the 1) Mean Squared Prediction Error (MSPE) (Becker et al. 2010), 2) Pearson Correlation Coefficient (r) (Oppel et al. 2012), and 3) the intercept of a log-transformed linear model of the fitted and observed values (Oppel et al. 2012). The intercept is interpreted by Oppel et al. (2012), as a metric of bias representing the deviation of the best fit line relating observed and fitted values from the origin. Since this relationship is fitted in a log-transformed space (very small number 0.0000001 added to avoid imaginary number errors), large negative number represents a very small deviations from the origin. This process was repeated such that each of the 10 subsets was used once as test data, and nine times as part of the training dataset, and mean values of MSPE, r, slope, and intercept were calculated for each model. I primarily selected the optimal model from this set of non-nested candidate models, based on maximizing predictive performance represented by minimum MSPE and log

intercept values, and maximum r values. However, I also report the sample size-corrected Akaike's Information Criterion (AICc) score and deviance explained. I also compared the abundances estimates derived from each model with the stratification estimate within the subset of strata that were either randomly or systematically sampled (all strata except HICEAS and STAR Transits, see Fig. 1). Finally the resulting models were also checked for biological credibility by using ArcGIS 10.0 to overlay the observed spatial distribution of Newell's Shearwater and Hawaiian Petrel on the GAM predicted density surfaces.

Uncertainty Estimation

To estimate the uncertainty surrounding both the stratification and GAM based abundance estimates, a non-parametric bootstrap re-sampling procedure was performed (Efron and Tibshirani 1993). In parallel with the cross-validation exercise, a bootstrap sample with replacement was drawn within each strata and then recombined to created that a bootstrap dataset of the same size as the original dataset while maintaining the spatial structure of the original sampling. This procedure differed slightly from the semi-parametric moving-blocks bootstrap procedure of Clarke et al. (2003), which was performed to incorporate dependence between sequential data values in the estimate of uncertainty (Clarke et al. 2003). The unit of analysis was a day of survey effort that was geographically and temporally separated from other days of survey effort by night-time transiting of the research vessel. This unit corresponds to that used in Clarke et al. (2003) where the block size at which

independence was assumed was one day of survey effort which corresponds to the unit of analysis in this study. The non-parametric bootstrap randomly resamples the original dataset (i.e. empirical distribution function) with replacement, requiring fewer assumptions than the parametric (or semi-parametric) analogue, which generates a bootstrap sample from the residuals and fitted values of a parametric (or semi-parametric) model (Efron and Tibshirani 1993). GAM models for Hawaiian Petrel and Newell's Shearwater with the greatest predictive performance were refitted to each of the iterations of the bootstrap dataset. Abundance was then re-estimated for each bootstrap dataset using both stratification and GAM approaches, over both the entire study area and within each stratum. To describe the uncertainty surrounding the Newell's Shearwater and Hawaiian Petrel abundance estimates, the 2.5% and 97.5% quantiles were reported. Bootstrap bias was calculated as the difference between the abundance estimates using the original dataset and the bootstrap median.

Results

Sampling

Between 1998 and 2011, sampling across all strata yielded 378 observations of Hawaiian Petrels and 177 observations of Newell's Shearwaters within 71,394.93 km^2 of strip transect survey effort. Note however that these counts excluded two large outlying counts for the Newell's Shearwater of 40 and 70 individuals respectively and one large outlying count for the Hawaiian Petrel of 31 individuals, which may have

resulted from either unflagged typographic errors or the survey strip intersecting with a feed flock. The sampled area represented 0.23% of the 32,005,929 km^2 of ocean surface area within the study area, however this proportion varied over more than an order of magnitude from 0.75% in the core area of the HICEAS cruises surrounding the main Hawaiian Islands, to <0.07% in the northern transit stratum between the US West Coast and Hawaii.

Abundance Estimates

Comparing the *P. sandwichensis* spatial habitat models detailed in Table 2, no single GAM was clearly optimal in all model summary and cross-validation metrics (Table 2). Of the candidate models, Model 1b was selected as the best predictive model for the purpose of abundance estimation on the basis of minimizing MSPE and the log-linear model intercept parameter, while also maximizing Pearson's correlation coefficient (r). This model also produced a biologically credible model fit (Fig. 5). Using this model to predict overall abundance, yielded an estimate of 52,186 Hawaiian Petrels within the entire study area. Within the strata where the stratification and the model-based approaches could both be applied, the model based estimate differed from the stratification based estimate by -7.1% (Table 3). The upper and lower bounds of the 95% quantile surrounding the bootstrap median of 52,205, were 39,823 and 67,379 respectively (Table 2). There was also a slight right skew to the bootstrap distribution (Fig. 6) lending greater confidence to the lower bound of the 95% quantile than the upper bound.

As was the case with models of *P. sandwichensis*, no single model optimally described the observed distribution of *P. newelli* based on all the model summary and cross-validation metrics (Table 5). Of the candidate models, Model 3b was selected as the best predictive model for the purpose of abundance estimation, based on minimizing MSPE and the log-linear model intercept. Although Model 3b had a somewhat lower Pearson's correlation coefficient than Model 1b, it yielded a more biologically credible model fit (Fig. 7). The difference in abundance estimates between Models 1b and 3b was <4% (Table 6). This model predicted an overall abundance estimate of 27,011 *P. newelli* within the study area. Within the strata where there was sufficiently sampling to estimate abundance using the stratification approach, the model-based estimate differed from the stratification estimate by 9.0% (Table 6). The upper and lower bounds of the 95% quantile surrounding the bootstrap median of 26,407, were 18,254 and 37,125 respectively (Table 2). Similar to the bootstrap distribution of *P. sandwichensis*, there was a slight right skew to the model-based *P. newelli* bootstrap distribution lending greater confidence to the lower bound of the 95% quantile than the upper bound (Fig. 8).

Discussion

The goal of the analyses presented in this study was to provide unbiased estimates of the unknown population parameter, abundance, for *P. sandwichensis* and *P. newelli*, along with estimates of the uncertainty surrounding these parameters. To assess whether unbiased estimation was achieved we first need to

consider two potential sources of bias: 1) biases associated with sampling, and 2) biases associated with stratification and modeling.

Potential Sampling Biases

Unbiased sampling using strip transect methods would require 1) perfect detection of all seabirds within the survey strip, 2) birds being neither attracted to nor averted from the research vessel, 3) equal probability of detecting a seabird in all areas of the survey strip, and 4) appropriate correction of the known biasing effect of bird movement relative to observer. Foremost among these assumptions is that all seabirds entering survey strip are detected. Relative to marine vertebrates, seabirds are readily visually detected and counted within moderate distances of a moving survey platform, and NOAA strip transect sampling has been consistently conducted by highly skilled seabird observers. The assumption of perfect detection within the survey strip is likely subject to small violations because 1) some seabirds may have been missed at the outer edges of the strip due to slightly declining detectability as a function of perpendicular distance from the trackline (Ronconi and Burger 2009), and 2) some seabirds may also have been missed while briefly entering data or while scanning other areas of the survey arc (Spear et al. 2004). Ronconi and Burger (2009) found some bias within a 300m strip transect, particularly in diving seabirds sitting on the water. However shearwaters and petrels of comparable size were regularly recorded well beyond the 300m-strip width in presence-absence logs from this study. Missed birds due to data-entry and imperfect-scanning were likely greater potential sources of detection bias. Spear et

al. (2004) found a 21.7% increase in overall counts between simultaneous single and dual observer counts, and an additional 4.8% increase between dual and triple observer counts. However, this aggregate effect across all species is somewhat misleading. Most of the observed negative bias occurred in the small and low-flying storm-petrels, auks, gulls, small gadfly petrels, diving petrels and penguins. Large gadfly petrels (shearwaters were not measured) showed a negative bias of <10% (Figure 3A in Spear et al. 2004). Moderate to large size and high flight height, both exhibited by Newell's Shearwaters and Hawaiian Petrel, were both negatively related to total bias (Spear et al. 2004).

The second area of potential bias is due to effects of research vessels on seabird behavior. Specifically, diving and diversion of seabirds in response to the presence of the research vessel are likely to induce a negative bias (Hyrenbach et al. 2007, Ronconi and Burger 2009, Clarke et al. 2003), whereas attraction of seabirds to the research vessel may result in oversampling (Clarke et al. 2003). In the case of NOAA strip transect sampling seabird observers directly correct for the potential ship attraction bias by recording any indication of ship attraction with a specific behavior code (Ballance 2007). Diversion bias is more difficult to detect, as it requires the seabird observer to estimate where the seabird would have gone in the absence of the ship, although there are procedures in the sampling protocol to include these seabirds in the sampling arc. *P. sandwichensis* and *P. newelli* are not known to exhibit ship attraction or aversion behavior, and *P. newelli* are only observed to dive during foraging bouts, which have not been recorded within the

300m sampling arc.

The third and fourth areas of potential sampling bias are related and can be tested using relatively simple simulations. The NOAA strip transect sampling protocol employs an arc-shaped sampling area, with the result that there is slightly lower search effort in the outer distance bins perpendicular to the trackline relative to the inner distance bins. If the world were composed of stationary seabirds then the effect of this difference in sampling area would be non-existent, and a bird would have an equal probability of being counted in each perpendicular distance bin. In reality most tropical seabirds spend a large proportion of their time in flight. This implies that some birds just skirting the outside border of the arc shaped sampling area, would be counted in a sampling protocol that equally samples all distance bins (e.g. a 300m x 300m square sampling area of 22% greater surface area than the arc). Hence a stochastic simulation demonstrates that when sampling a randomly distributed field of moving simulated seabirds of known density and realistic flight velocity, the use of an arc shaped sampling area results in a moderate (-12.9%) and statistically significant (One sample T-test, $t=-14.45$, $d.f.=98$, $p<0.0001$) negative bias after applying flux correction. Applying the flux correction constant to the sampling conducted within a square shaped sampling area results in 10.0% deviation (Fig. 9) from the programmed density in the simulation. However, in reality not all birds are observed in directional flight thus this effect is likely even smaller than that suggested by this simulation. In summary, as with any sampling regime, the assumptions of strip transect sampling are not perfect.

However variants of this sampling method have been applied consistently in NOAA seabird surveys since the 1980s, and have been published in numerous peer reviewed publications, including Spear et al. (1995) and Clarke et al. (2003). Moreover with the exception of flux correction, which is directly addressed in the models, all these other potential sources of bias are small and in the negative direction, yielding conservative abundance estimates.

Potential Estimation Biases

Applying the mean estimates within each stratum to predict abundance relies on the assumption of representative sampling of the underlying spatial process. This makes stratification approaches highly sensitive to departures from purely randomized and/or systematic sampling designs. For example, the inclusion of transits to and from port in Honolulu, Hawaii in the HICEAS and PICEAS strata, has the effect of concentrating survey effort in highest density areas for the *P. sandwichensis* and *P. newelli* near breeding colonies, and thus may lead to overestimates of abundance within these strata. To address this potential bias, stratification abundance estimates were calculated without the inclusion of transits. Another potential source of deviations from sampling design were the breaks in survey effort because of diversions from the track-line to pursue marine mammal sightings.

The modeling approach avoids stratification's sensitivity to uneven sampling by fitting a model to the actual spatial process, rather than estimating a

single mean parameter, and soaking up the remaining scatter as error. Nevertheless, particularly where there is little pattern in the data and large count variances, the choice between different classes of models, and different combinations of covariates can result in disparate predictions of density, as shown in model 2b in Table 3 and 1a in Table 6. Reassuringly, however most of the configurations of covariates in the GAM models, as well as the different constraints on the smoothing parameters, showed remarkably little effect on the overall estimated abundance (Tables 3 and 6) and spatial distribution pattern of abundance. In general, these model-based estimates also converged with the stratification estimates, though the model based estimates were consistently 6-14% higher for *P. newelli* (Tables 3 and 6).

Overall Interpretation

In the preceding two sections it was demonstrated that 1) violations of the assumptions of unbiased sampling, if present, have been small and in the negative direction, and 2) that both GAM model and stratification methods yield similar abundance estimates. These suggest an interpretation of the stratification and GAM abundance estimates as conservative estimates of *P. sandwichensis* and *P. newelli* abundance within the sampled areas of the ETP and CTP. However, accumulating sufficient sampling to achieve model convergence required pooling surveys between 1998 and 2011 into a single dataset, reducing the temporal resolution of these abundance estimates. Proxy indicators of *P. newelli* population

trends, including coastal radar surveys on Kauai (Day et al. 2003, DOFAW Unpublished data), fallout recovery trends (Day et al. 2003, DOFAW unpublished data), and the extirpation of historically documented colonies (DOFAW unpublished data) suggest recent declines in populations between 1993 and the present (Day et al. 2003). It is critical to note that the abundance estimates presented in this study represent average at-sea abundance over the entire sampling period (1998-2011), not current abundance.

Furthermore, the NOAA strip transect sampling effort from 1998 to 2011 greatly expanded on the area of habitat covered by the Spear et al. (1995) estimate. That said it does not encompass the entire oceanic ranges of either species based on telemetry studies. Hence these abundance estimates do not provide comprehensive estimates of either the total Hawaiian Petrel and Newell's Shearwater abundance, and instead represent minima of the global populations. ARGOS satellite telemetry (Adams and Flora 2010) indicates that chick-provisioning adult Hawaiian Petrels forage across a broad swath of the temperate and sub-tropical North Pacific, from the Ogasawara (Bonin) Islands, to the Aleutian Islands, and the outer California Current (Adams and Flora 2010, Adams unpublished data). Preliminary tracking studies of the Newell's Shearwater also suggest that chick provisioning adults forage outside of the HICEAS sampling area (Fig. 10; Joyce et al. unpublished data).

Overall this analysis provided updated abundance estimates that were analogous though not identical in survey area and methodology to the abundance

estimates published in Spear et al. (1995). Because of these differences, population trends cannot be inferred by directly comparing the current estimates with those reported in Spear et al. (1995). The abundance estimates represented in these two studies differ in both area covered and in timing with respect to the breeding phenology (Deringer 2009), and also diverge slightly in survey and analytical methodology. It can be demonstrated from telemetry studies that an unknown percentage both species' oceanic populations likely fell outside the sampled areas of both studies. Because the relative size of this unsampled portion of the population is unknown and likely differs between the two studies, differences in abundance estimates may reflect either changes in the underlying population size or in the proportion of the total population sampled. Differentiating between these two alternative hypotheses requires expanding at-sea sampling coverage, or achieving greater resolution of habitat use through telemetry studies. In the future it may be possible to make these estimates more comparable and evaluate trends in abundance. This analysis would necessitate sub-sampling the spatially and temporally overlapping portions of the current and Spear et al. datasets and subsequently applying consistent analytical framework to both. However this type of analysis would still face the caveat that seabird oceanic distributions are dynamic in space and time. Hence, changes in the abundance estimates could still be attributable to either changes in distribution at inter-annual or sub-annual scales, or changes in the underlying population size, or both.

Acknowledgements

We would like to acknowledge the many people who contributed their time, resources, and talents to this project. The chief-scientists, seabird and marine mammal observers, officers, and crews of the NOAA research vessels R/V Macarthur II, R/V David Star Jordan, R/V who contributed years of sea-time to create these amazing datasets. In particular I would like to acknowledge Mike Force and Annette Henry for their patience and good nature in helping me learn the strip transect data collection. Jeff Laake, Tim Gerrodette, Lynn Shepherd, and Adam Vorsino all provided invaluable feedback on drafts of this manuscript. Also, Jessica Redfern, Tomo Eguchi, Stuart Sandin, Bryce Semmens, and Charles Perretti gave very helpful statistical advice. Funding support was provided by the Kauai Island Utility Cooperative's Temporary Short-term Habitat Conservation Plan. Finally I would like to thank Lisa Ballance for her continuing support and for providing me valuable feedback at all stages of this project.

Chapter 4, in full, is currently being prepared for submission for publication of the material. Joyce, Trevor W.; Pitman, Robert L.; Ballance, Lisa T. The dissertation author was the primary investigator and author of this material.

References

Adams, J. & Flora, S. (2010) Correlating seabird movements with ocean winds: linking satellite telemetry with ocean scatterometry. *Marine Biology*, 157, 915–929.

Ainley, D.G., O'Connor, E.F. & Boekelheide, R.J. (1984) The marine ecology of birds in the Ross Sea, Antarctica. *Ornithological monographs*, iii–97.

Ballance, L.T. (2007) Understanding seabirds at sea: why and how. *Marine Ornithology*, 35, 127–135.

Banks, R.C., Cicero, C., Dunn, J.L., Kratter, A.W., Rasmussen, P.C., Remsen Jr, J.V., Rising, J.D. & Stotz, D.F. (2002) Forty-Third Supplement to the American Ornithologists' Union Check-List of North American Birds. *The Auk*, 897–906.

Becker, E.A., Forney, K.A., Ferguson, M.C., Foley, D.G., Smith, R.C., Barlow, J. & Redfern, J.V. (2010) Comparing California Current cetacean–habitat models developed using in situ and remotely sensed sea surface temperature data. *Mar Ecol Prog Ser*, 413, 163–183.

Buckland, S.T., Anderson, D.R., Burnham, K.P. & Laake, J.L. (2005) Distance Sampling. Encyclopedia of Biostatistics, Wiley Online Library, John Wiley & Sons, http://dx.doi.org/10.1002/0470011815.b2a16019

Clarke, E.D., Spear, L.B., McCracken, M.L., Marques, F.F.C., Borchers, D.L., Buckland, S.T. & Ainley, D.G. (2003) Validating the use of generalized additive models and at-sea surveys to estimate size and temporal trends of seabird populations. *Journal of Applied Ecology*, 40, 278–292.

Cuthbert, R., Ryan, P.G., Cooper, J. & Hilton, G. (2003) Demography and population trends of the Atlantic yellow-nosed albatross. *The Condor*, 105, 439–452.

Day, R.H., Cooper, B.A., Telfer, T.C. & Powell, A. (2003) Decline of Townsend's (Newell's) shearwaters (Puffinus auricularis newelli) on Kauai, Hawaii. *The Auk*, 120, 669–679.

Deringer, C.V. (2009) *Breeding Phenology of Hawaiian Petrels (Pterodroma Sandwichensis) and Newell's Shearwaters (Puffinus Auricularis Newelli) on Kaua'i, Hawai'i: Using Ornithological Radar, Auditory, and Visual Surveys*. University of Hawai'i at Hilo.

Efron, B. & Tibshirani, R.J. (1993) *An introduction to the bootstrap*. Chapman & Hall. New York, USA.

Force, M.P., Webb, S.W. & Howell, S.N.G. (2007) Identification at sea of Hawaiian and Galapagos petrels. *Western Birds*, 38, 242–248.

Gaston, A.J., Collins, B.L. & Diamond, A.W. (1987) The“ snapshot” count for estimating densities of flying seabirds during boat transects: a cautionary comment. *The Auk*, 336–338.

Harrison, P. (1983) *Seabirds, an Identification Guide*. Houghton Mifflin, Boston, Massachusetts, USA.

Hastie, T. & Tibshirani, R. (1986) Generalized additive models. *Statistical science*, 297–310.

Heinemann, D. (1981) A range finder for pelagic bird censusing. *The Journal of Wildlife Management*, 45, 489–493.

Howell, S.N., Spear, L.B. & Pyle, P. (1994) Identification of Manx-type shearwaters in the eastern Pacific. *Western Birds*, 25, 169–177.

Howell, S.N., Webb, S. & Spear, L.B. (1996) Identification at sea of Cook’s, De Filippi’s, and Pycroft’s Petrels. *Western Birds*, 27, 57–64.

Hyrenbach, K.D., Henry, M.F., Morgan, K.H., Welch, D.W. & Sydeman, W.J. (2007) Optimizing the width of strip transects for seabird surveys from vessels of opportunity. *Marine Ornithology*, 35, 29–37.

Jones, I.L., Hunter, F.M., Robertson, G.J., Williams, J.C. & Vernon Byrd, G. (2007) Covariation among demographic and climate parameters in whiskered auklets Aethia pygmaea. *Journal of Avian Biology*, 38, 450–461.

van der Meer, J. & Leopold, M.F. (1995) Assessing the population size of the European storm petrel (Hydrobates pelagicus) using spatial autocorrelation between counts from segments of criss-cross ship transects. *ICES Journal of Marine Science: Journal du Conseil*, 52, 809–818.

Nelder, J.A. & Wedderburn, R.W.M. (1972) Generalized linear models. *JR Statist. Soc. A,* 135, 370-384.

Onley, D.J., & R P. Scofield (2007) *Albatrosses, Petrels, and Shearwaters of the World*. Princeton University Press, Princeton, New Jersey, USA.

Oppel, S., Meirinho, A., Ramírez, I., Gardner, B., O'Connell, A.F., Miller, P.I. & Louzao, M. (2012) Comparison of five modelling techniques to predict the spatial distribution and abundance of seabirds. *Biological Conservation*, 156, 94–104.

Orians, G.H. & Pearson, N.E. (1979) *On the theory of central place foraging*. *Analysis of ecological systems.* pp. 155–177 Ohio State University Press, Columbus, Ohio, USA.

Piatt, J.F. & Ford, R.G. (1993) Distribution and abundance of marbled murrelets in Alaska. *Condor*, 662–669.

Pyle P., Webster D.L., & Baird R.W. (2011) Notes on Petrels of the Dark Rumped Petrel Complex in Hawaiian Waters. *Western Birds*, 65, 364-367

Rayner, M.J., Clout, M.N., Stamp, R.K., Imber, M.J., Brunton, D.H. & Hauber, M.E. (2007) Predictive habitat modelling for the population census of a burrowing seabird: a study of the endangered Cook's petrel. *Biological Conservation*, 138, 235–247.

Renner, M., Parrish, J.K., Piatt, J.F., Kuletz, K.J., Edwards, A.E. & Hunt Jr, G.L. (2013) Modeled distribution and abundance of a pelagic seabird reveal trends in relation to fisheries. *Marine Ecology Progress Series*, 484, 259–277.

Ronconi, R.A. & Burger, A.E. (2009) Estimating seabird densities from vessel transects: distance sampling and implications for strip transects. *Aquatic Biology*, 4, 297–309.

Spear, L.B. & Ainley, D.G. (1997) Flight behaviour of seabirds in relation to wind direction and wing morphology. *Ibis*, 139, 221–233.

Spear, L.B., Ainley, D.G., Hardesty, B.D., Howell, S.N. & Webb, S.W. (2004) Reducing biases affecting at-sea surveys of seabirds: use of multiple observer teams. *Marine Ornithology*, 32, 147–157.

Spear, L.B., Ainley, D.G., Nur, N. & Howell, S.N. (1995) Population size and factors affecting at-sea distributions of four endangered procellariids in the tropical Pacific. *Condor*, 613–638.

Spear, L.B., Howell, S.N. & Ainley, D.G. (1992a) Notes on the at-sea identification of some Pacific gadfly petrels (Genus: Pterodroma). *Colonial Waterbirds*, 202–218.

Spear, L., Nur, N. & Ainley, D.G. (1992b) Estimating absolute densities of flying seabirds using analyses of relative movement. *The Auk*, 109, 385–389.

Stahl, J. & Bartle, J.A. (1991) Distribution, abundance and aspects of the pelagic ecology of Barau's Petrel (Pterodroma baraui) in the south-west Indian Ocean. *Notornis*, 38, 211–225.

Tasker, M.L., Jones, P.H., Dixon, T. & Blake, B.F. (1984) Counting seabirds at sea from ships: a review of methods employed and a suggestion for a standardized approach. *The Auk*, 567–577.

Tomkins, R.J. & Milne, B.J. (1991) Differences among Dark-rumped Petrel (Pterodroma phaeopygia) populations within the Galapagos Archipelago. *Notornis*, 38, 1–35.

Wood, S.N. (2006) *Generalized Additive Models: An Introduction with R*. CRC Press, Boca Raton, Florida, USA.

Tables

Table 4-1. Apparent and absolute counts of Newell's Shearwater (*Puffinus newelli*) and Hawaiian Petrel (*Pterodroma sandwichensis*) within 10 sampling strata and within the overall study area. See Fig. 1 and 4 for definitions of sampling strata, and calculation of apparent and absolute counts, respectively.

Stratum	Surface Area (km^2)	Sampled Area (km^2)	App. Count *P. newelli*	Abs. Count *P. newelli*	App. Count *P. sandwichensis*	Abs. Count *P. sandwichensis*
HICEAS - Core	974362.62	7321.09	127	54.12	293	162.10
HICEAS - Outer	1499670.04	6106.99	6	3.07	13	5.66
HICEAS - Transits	5128137.72	3686.38	0	0.00	8	3.30
PICEAS - Johnston	1936505.24	3187.21	4	2.52	38	19.93
PICEAS - Palmyra	358409.43	1577.24	12	10.61	3	2.49
STAR - Coastal	731010.06	4263.93	0	0.00	0	0.00
STAR - Core	6031817.21	25805.85	6	4.59	0	0.00
STAR - Outer North	4783474.88	8270.70	19	15.28	5	3.59
STAR - Outer South	9865491.51	9926.86	0	0.00	0	0.00
STAR - Transit	697050.83	1178.65	3	1.78	18	10.38
All Strata	32005929.54	71324.92	177	91.97	378	207.45

Table 4-2. Model summaries statistics and 10 fold cross-validation results from six candidate models of Hawaiian Petrel (*Pterodroma sandwichensis*) counts considered in this analysis. Deviance explained and AICc were calculated based on the overall dataset. The remaining metrics are average values calculated from ten cross validation subsets of the overall dataset.

GAM Model	Deviance Explained	AICc	MSPE	r	Coefficient	Intercept
Model 1a: APP_COUNT ~ s(LAT,k=4)+s(LONG,k=4) +s(SST,k=4)+s(BATHY,k=4) +offset(log(AREA/AVG_K))	0.71	826.3	0.73	0.52	0.12	-10.41
Model 2a: APP_COUNT ~ s(DIST_COL,k=4)+s(SST,k=4) +s(BATHY,k=4)+offset(log(AREA/AVG_K))	0.67	855.8	0.55	0.55	1.06	-6.11
Model 3a: APP_COUNT ~ s(LAT,LONG,k=10)+s(SST,k=4) +s(BATHY,k=4)+offset(log(AREA/AVG_K))	0.74	799.2	0.73	0.53	0.55	-8.54
Model 1b: APP_COUNT ~ s(LAT)+s(LONG)+s(SST) +s(BATHY)+offset(log(AREA/AVG_K))	0.74	791.9	0.64	0.60	0.15	-10.34
Model 2b: APP_COUNT ~ s(DIST_COL)+s(SST) +s(BATHY)+offset(log(AREA/AVG_K))	0.71	834.3	0.63	0.55	0.11	-10.35
Model 3b: APP_COUNT ~ s(LAT,LONG)+s(SST) +s(BATHY)+offset(log(AREA/AVG_K))	0.76	785.5	0.70	0.61	0.20	-9.88

Table 4-3. Comparisons of Hawaiian Petrel (*Pterodroma sandwichensis*) abundance estimates predicted by the six candidate generalized additive model specifications (1a-3b) as well as stratification. For comparability the overall estimates are calculated based only on the strata that were sampled sufficiently to derive an abundance estimate using the stratification approach (i.e. excluding STAR and HICEAS Transits).

Stratum	Model 1a	Model 2a	Model 3a	Model 1b	Model 2b	Model 3b	Stratification
HICEAS - Core	16428	18716	17651	19143	21393	20144	23577
HICEAS - Outer	3777	8294	1786	2314	7792	1402	1390
PICEAS - Johnston	11692	13653	13968	10649	14977	12419	13021
PICEAS - Palmyra	264	654	636	477	352	532	567
STAR - Coastal	0	5	0	0	0	0	0
STAR - Core	0	69	0	0	0	0	0
STAR - Outer North	6496	1788	4592	5097	4594	5679	2075
STAR - Outer South	94	114	26	82	149	24	0
All Strata	38750	43292	38659	37762	49257	40200	40629

Table 4-4. This table shows the bootstrap variability (median and 95% quantile boundaries) in estimates of Hawaiian Petrel (*Pterodroma sandwichensis*) abundance in the overall study area as well as within individual strata. Model-based and stratification-based estimates are presented, however stratification based estimates were only calculated within strata that were sufficiently sampled. Hence the overall confidence bounds (bottom row) represent different geographic areas.

	GAM Estimates			Stratification Estimates		
Stratum	95% Lower Bound	Median	95% Upper Bound	95% Lower Bound	Median	95% Upper Bound
HICEAS - Core	15203	20044	26123	17282	23500	30775
HICEAS - Outer	900	2162	4128	250	1331	2894
HICEAS - Transits	3152	6769	13216	-	-	-
PICEAS - Johnston	6303	11019	16707	5121	12288	22985
PICEAS - Palmyra	43	338	837	0	550	1328
STAR - Coastal	0	0	4	0	0	0
STAR - Core	0	0	29	0	0	0
STAR - Outer North	1600	4084	7230	449	2118	4228
STAR - Outer South	0	5	165	0	0	0
STAR - Transit	3133	6872	13752	-	-	-
All Strata	39823	52205	67379	23102	39787	62210

Table 4-5. Model summaries statistics and 10 fold cross-validation results from six candidate models of Newell's Shearwater (*Puffinus newelli*) counts considered in this analysis. Deviance explained and AICc were calculated based on the overall dataset. The remaining metrics are average values calculated from 10 cross validation subsets of the overall dataset.

GAM Model	Deviance Explained	AICc	MSPE	r	Coefficient	Intercept
Model 1a: APP_COUNT ~ s(LAT,k=4)+s(LONG,k=4) +s(SST,k=4)+s(BATHY,k=4) +offset(log(AREA/AVG_K))	0.45	606.4	0.17	0.41	0.04	-12.95
Model 2a: APP_COUNT ~ s(DIST_COL,k=4)+s(SST,k=4) +s(BATHY,k=4)+offset(log(AREA/AVG_K))	0.46	601.1	0.17	0.42	0.03	-13.01
Model 3a: APP_COUNT ~ s(LAT,LONG,k=10)+s(SST,k=4) +s(BATHY,k=4)+offset(log(AREA/AVG_K))	0.50	589.9	0.19	0.39	0.04	-12.96
Model 1b: APP_COUNT ~ s(LAT)+s(LONG)+s(SST) +s(BATHY)+offset(log(AREA/AVG_K))	0.65	496.6	0.22	0.54	0.07	-12.68
Model 2b: APP_COUNT ~ s(DIST_COL)+s(SST) +s(BATHY)+offset(log(AREA/AVG_K))	0.60	533.4	0.45	0.51	0.07	-12.72
Model 3b: APP_COUNT ~ s(LAT,LONG)+s(SST) +s(BATHY)+offset(log(AREA/AVG_K))	0.71	488.2	0.23	0.46	0.05	-12.86

Table 4-6. This table compares the Newell's Shearwater (*Puffinus newelli*) abundance estimates predicted by the six candidate generalized additive model specifications (1a-3b) as well as stratification. For comparibility, the overall estimates are calculated based only on the strata that were sampled sufficiently to derive an abundance estimate using the stratification approach (i.e. excluding STAR and HICEAS Transits).

Stratum	Model 1a	Model 2a	Model 3a	Model 1b	Model 2b	Model 3b	Stratification
HICEAS - Core	6771	7094	7411	5663	8493	7701	8438
HICEAS - Outer	5658	5387	2630	1113	1872	2006	755
PICEAS - Johnston	5538	7142	4402	5057	2453	3768	1671
PICEAS - Palmyra	1389	969	1081	2629	1254	1377	2412
STAR - Coastal	32	84	5	161	30	16	0
STAR - Core	1250	1865	1507	1511	1661	1288	1072
STAR - Outer North	12777	3931	7394	9984	8207	7566	8839
STAR - Outer South	3081	600	1978	412	752	1753	0
All Strata	36497	27072	26407	26529	24722	25475	23187

Table 4-7. This table shows the bootstrap variability (median and 95% quantile boundaries) in estimates of Newell's Shearwater (*Puffinus newelli*) abundance within the overall study area and also within individual strata. Model-based and stratification-based estimates are presented, however stratification based estimates were only calculated within strata that were sufficiently sampled. Hence the overall confidence bounds represent different geographic areas.

	GAM Estimates			Stratification Estimates		
Stratum	95% Lower Bound	Median	95% Upper Bound	95% Lower Bound	Median	95% Upper Bound
HICEAS - Core	4034	7574	12345	4288	8302	13472
HICEAS - Outer	778	1633	3059	0	670	2045
HICEAS - Transits	103	331	697	-	-	-
PICEAS - Johnston	1797	3666	6709	0	1546	4526
PICEAS - Palmyra	457	1361	2909	856	2353	4487
STAR - Coastal	0	8	33	0	0	0
STAR - Core	416	1291	2400	305	1074	2103
STAR - Outer North	3465	7370	13242	3286	8412	15126
STAR - Outer South	669	1624	3412	0	0	0
STAR - Transit	159	900	2272	-	-	-
All Strata	18254	26407	37125	8735	22356	41759

Figures

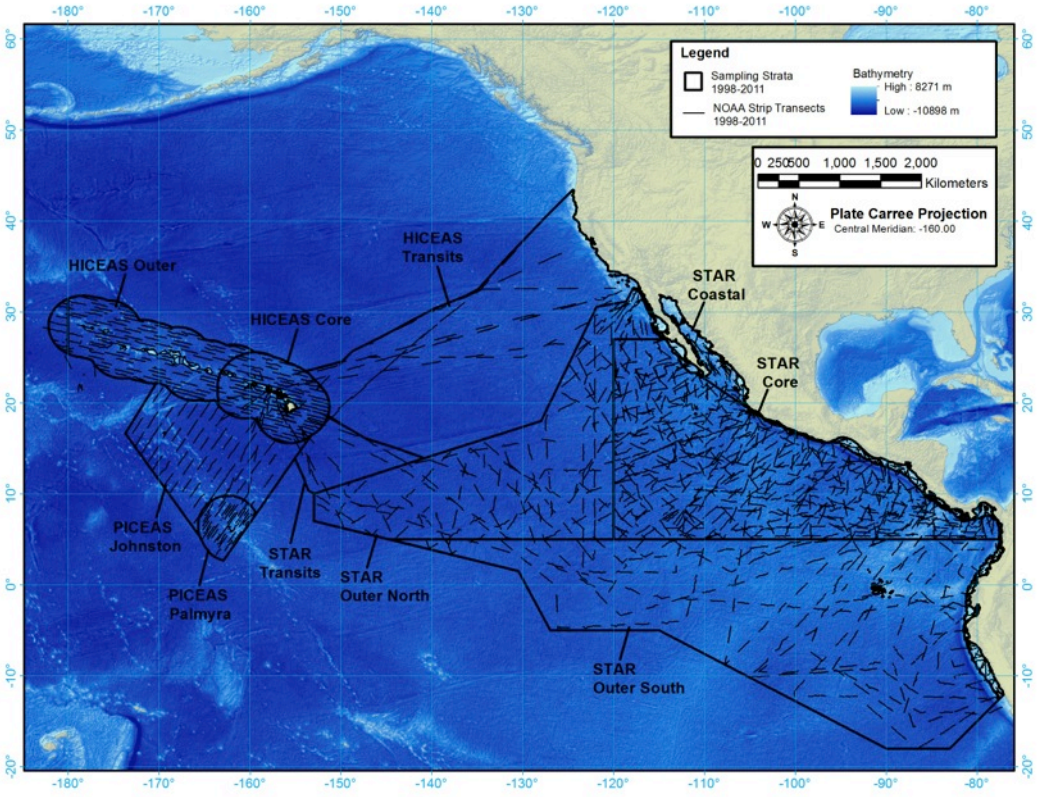

Figure 4-1. Seabird survey effort aboard NOAA research vessels in the Eastern Tropical Pacific (STAR), Hawaii Exclusive Economic Zone (HICEAS), and Johnston and Palmyra Atoll Exclusive Economic Zones and surrounding waters (PICEAS) between 1998 and 2011. The dark bordered polygons represent strata that were sampled at different levels of intensity.

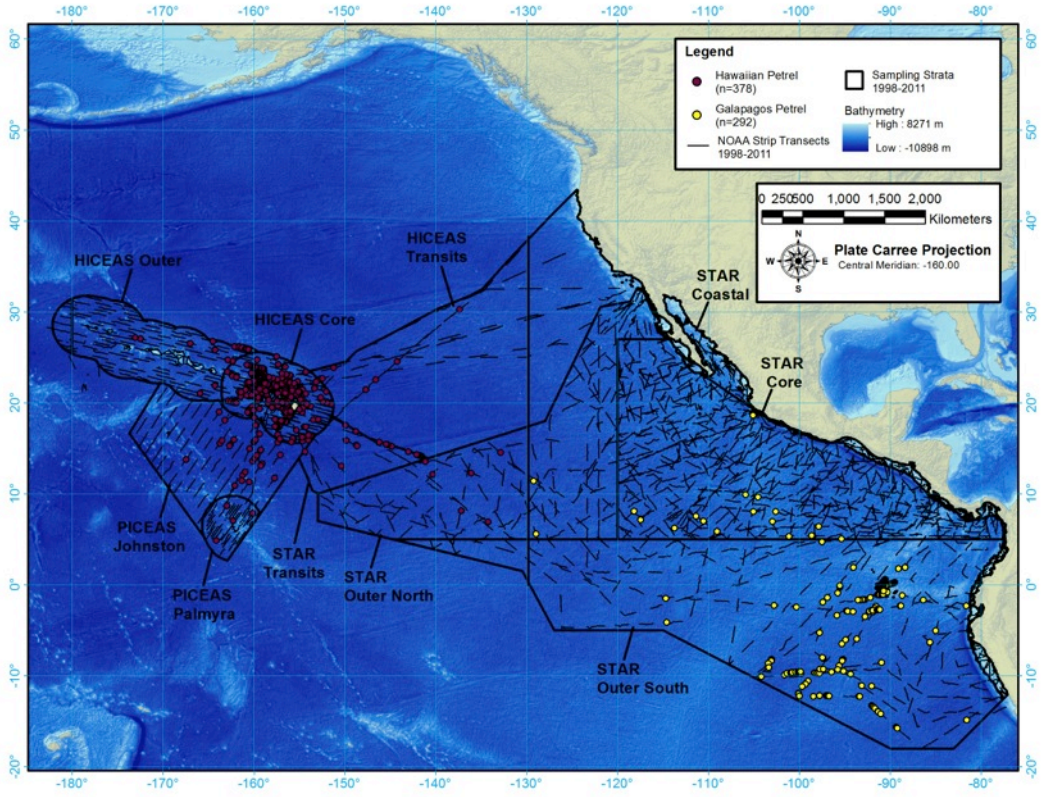

Figure 4-2. Detections of Dark-rumped Petrels classified as either Hawaiian Petrel (*Pterodroma sandwichensis*; purple points), and Galapagos Petrel (*Pterodroma phaeopygia*; yellow points). All sightings west of 130˚W longitude were considered to be *P. sandwichensis*.

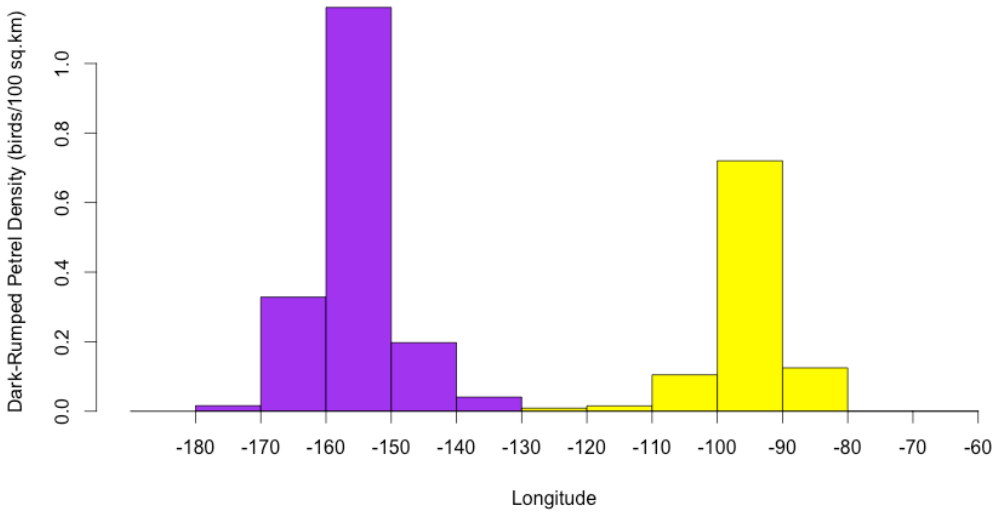

Figure 4-3. Histogram of Dark-rumped Petrel density in 10-degree longitude bins. Dark-rumped Petrels is a historic taxonomic classification that in this plot includes undifferentiated Dark-rumped Petrels, Hawaiian Petrels, and Galapagos Petrels. The lowest density of Dark-rumped Petrels corresponds to the bin between 130 and 120 degrees W. For the purposes of the analysis in this report Dark-rumped Petrels observed west of 130 were considered Hawaiian Petrels.

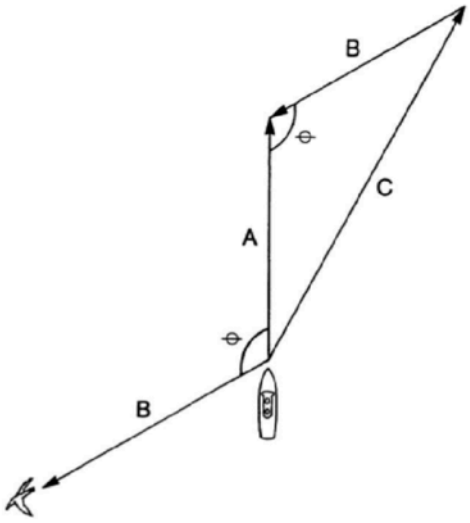

$$Count_{apparent,i} = \sum_{j=1}^{m} Observation_j$$

$$C_j = \sqrt{A_j^2 + B_j^2 - 2A_jB_j \cdot cos(\ominus_j)}$$

$$K_j^{-1} = \frac{A_j}{C_j}$$

$$Count_{absolute,i} = \sum_{j=1}^{m} Observation_j \cdot K_j^{-1}$$

$$Density_{absolute,i} = \frac{Count_{absolute,i}}{Length_i \cdot Width_i}$$

Figure 4-4. Diagram and associated equations detailing the calculation of absolute density within the i^{th} transect or day-of-cruise through the incorporation of the flux correction constant (K^{-1}), to adjust the apparent count for the effect of bird movement. The ship's velocity or displacement vector is denoted by A, while the bird's velocity motion over a unit of time is denoted by B. The difference between these two vectors is given by C. Diagram reproduced from Spear et al. (1992).

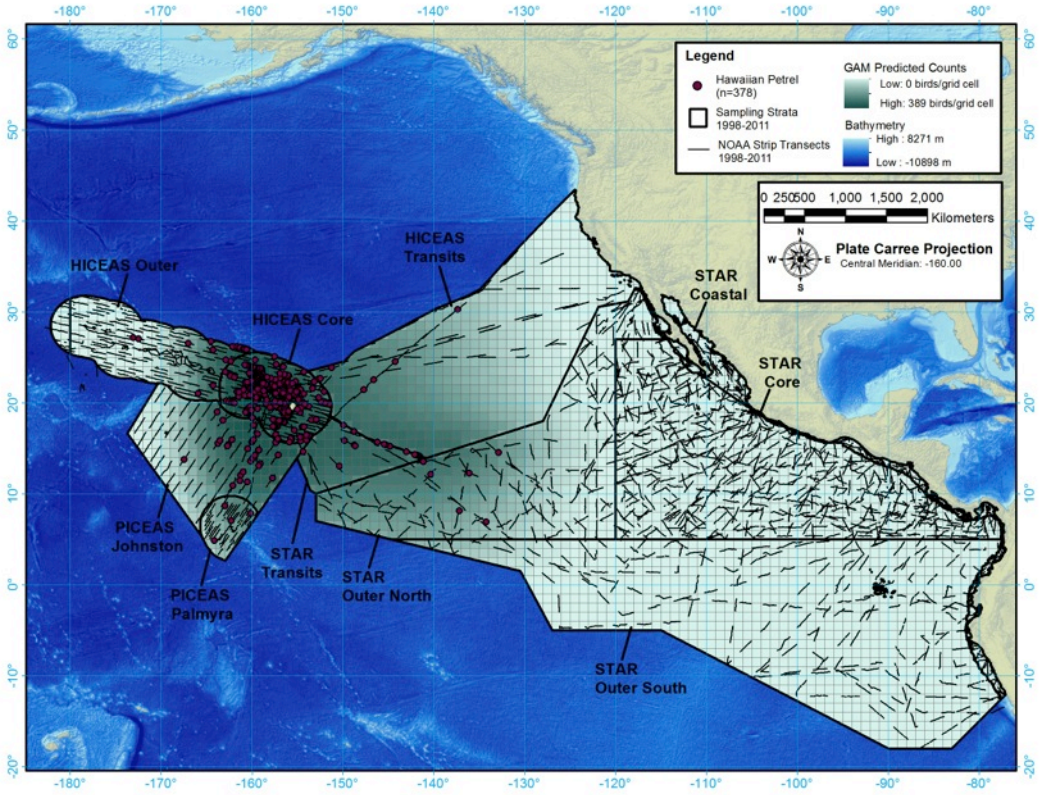

Figure 4-5. The distribution of Hawaiian Petrel observations, overlaid on the gridded predicted densities from GAM Model 1b.

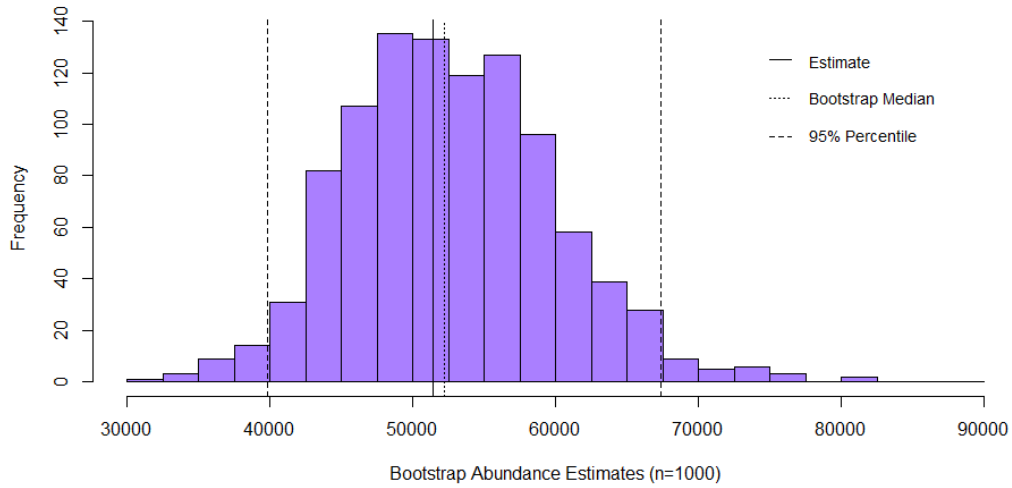

Figure 4-6. Histogram of Hawaiian Petrel bootstrapped abundance estimates within the study area. Dashed lines indicate boundaries of the 95% quantile surrounding the stippled line indicating the bootstrap median; the solid line indicates the abundance estimate based on the original dataset. Note that there is a slight right skew to the distribution.

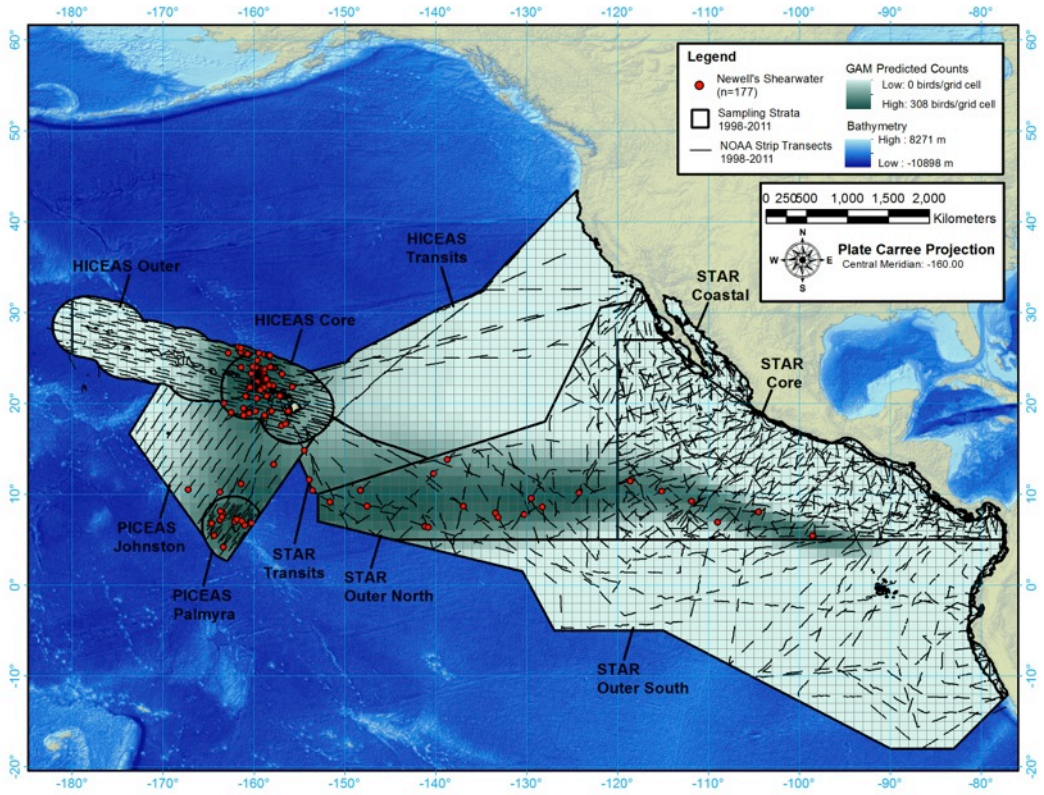

Figure 4-7. The distribution of Newell's Shearwater (*Puffinus newelli*) sightings, overlaid on the gridded predicted densities from GAM Model 3b.

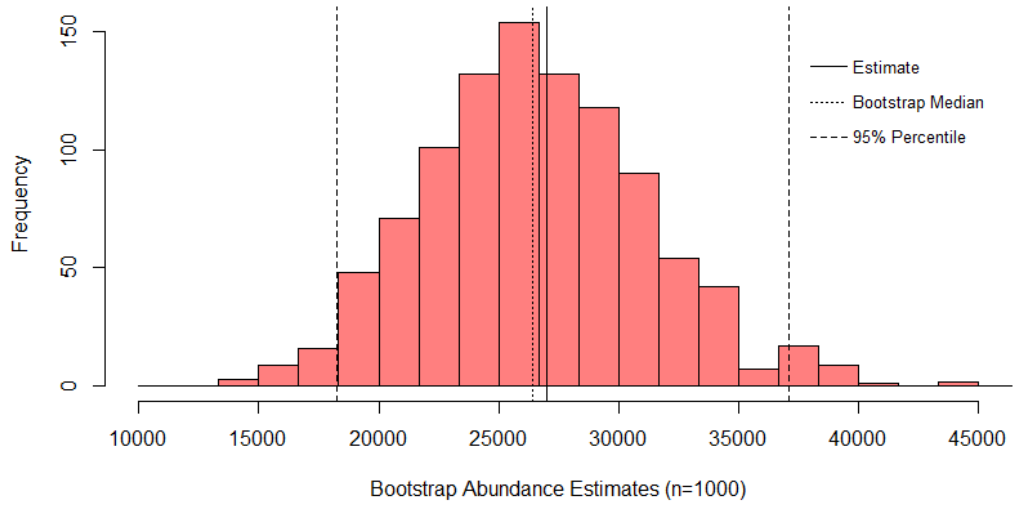

Figure 4-8. Histogram of Newell's Shearwater (*Puffinus newelli*) bootstrapped abundance estimates within the study area. Dashed lines indicate boundaries of the 95% quantile surrounding the stippled line indicating the bootstrap median; the solid line indicates the abundance estimate based on the original dataset. Note that there is a slight right skew to the distribution.

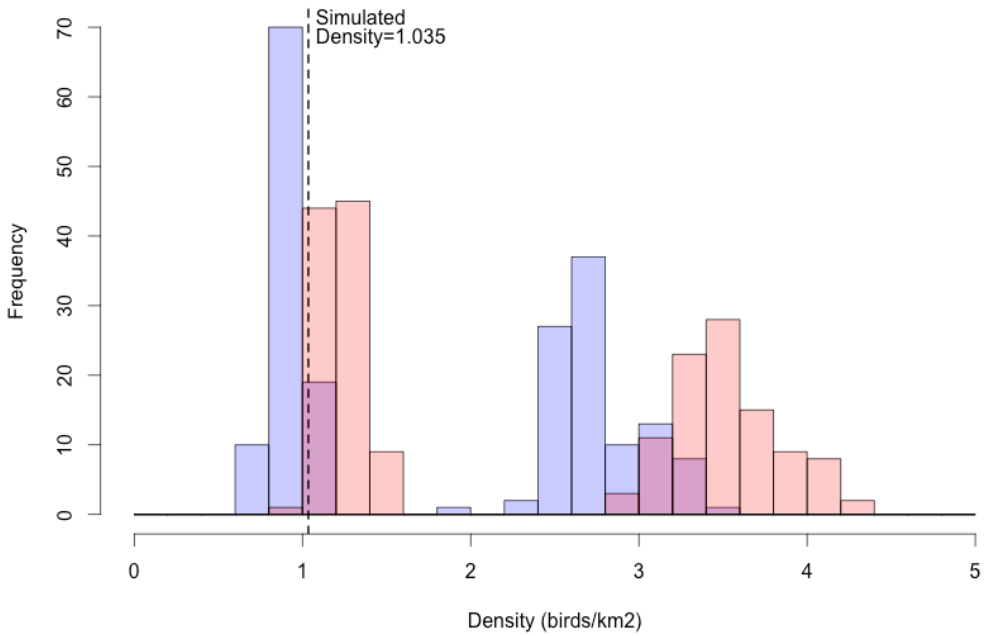

Figure 4-9. This histogram shows the density estimates derived from simultaneous sampling with arc (blue) and square (red) shaped simulated sampling areas. The peaks at the right show the positive bias in apparent density introduced by the movement of simulated birds relative to a moving observer. The peaks at the left show the distributions of absolute density estimates per sampling iteration (60 simulated transects), after applying flux correction.

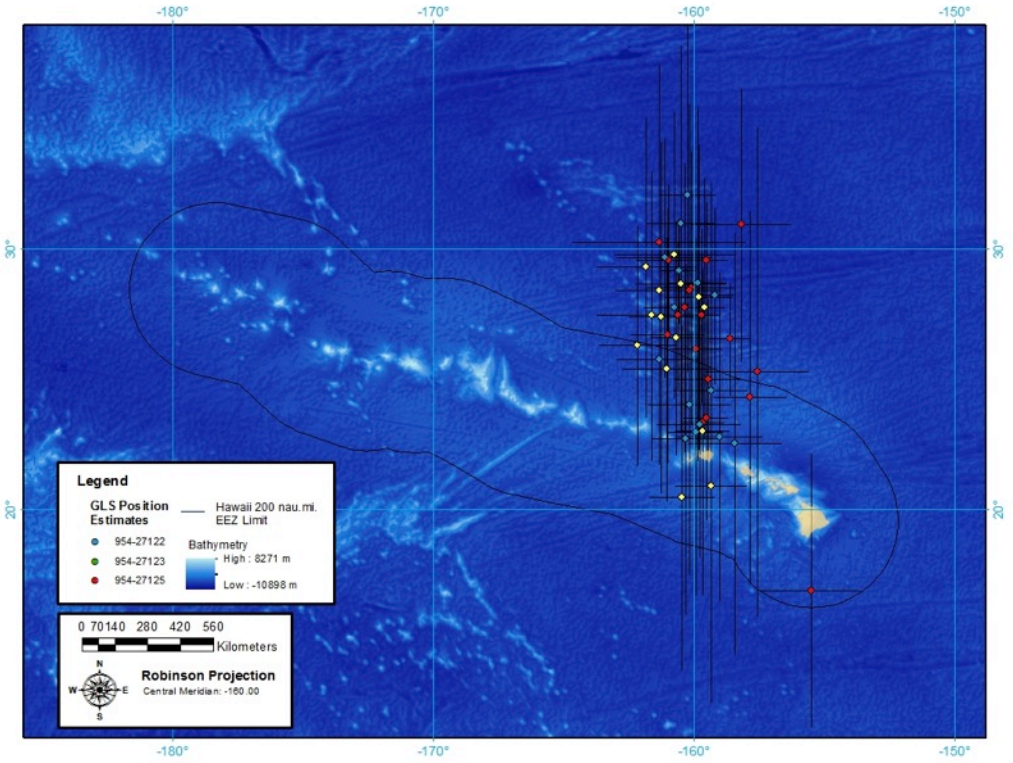

Figure 4-10. Lotek Global Location System (GLS) telemetry positions of three chick-provisioning adult Newell's Shearwaters (*Puffinus newelli*) tracked from Upper Limahuli Preserve, Kaua'i, Hawai'i over a 16-21 day period from August 12-September 11, 2011. Joyce et al. (unpublished data).

CHAPTER 5:

Estimating abundance and trends of procellariiform seabirds using Bayesian state-space models and at-sea data

TREVOR W. JOYCE, JEFFREY E. MOORE, ROBERT L. PITMAN,
AND LISA T. BALLANCE

Abstract

Long-lived and slow-reproducing storm-petrels (*Hydrobatidae*) and petrels (*Procellariidae*) experience among the highest rates of endangerment within the class *Aves*. Many hydrobatid and procellariid species also favor cryptic breeding strategies and inaccessible breeding habitats that may hinder the use of colony-based data to estimate population growth rate (*r*) and abundance (*N*), two parameters that are critical in assessing extinction risk. Here we evaluate the use of a hierarchal Bayesian state-space model to simultaneously estimate posterior probability distributions of *r* and *N* using strip transect count data. Data were gathered aboard oceanic research surveys in the central and eastern Pacific Ocean over 17 field seasons spanning a 26-year period from 1988 to 2014. Case study species included the Townsend's shearwater (*Puffinus auricularis*), black-vented shearwater (*Puffinus opisthomelas*), black storm petrel (*Oceanodroma melania*), and ashy storm petrel (*Oceanodroma homochroa*). Despite considerable interannual variance in point estimates of abundance due to both the sampling process and underlying population variation, 82.8% of the *P. auricularis* posterior distribution of *r* fell below zero providing considerable evidence of a decline in this species from a median initial abundance estimate of 61,295 individuals. By contrast, 99.0% of the *r* posterior distribution in *P. opisthomelas* exceeded zero, yielding strong evidence of population increases in this

species. Inferences in the two *Oceanodroma* species exhibited lower certainty but were consistent with increases in both populations. Overall, the hierarchal Bayesian state-space models developed in this study yielded useful information for the management of these species.

Introduction

The avian families Hydrobatidae (storm-petrels) and Procellariidae (petrels and shearwaters), experience particularly high rates of population endangerment, with 31% and 45% of species, respectively, listed by the International Union for Conservation of Nature (IUCN) Redlist with a status of Vulnerable to Critically Endangered (IUCN Redlist 2016). With the exception of a few species breeding in extreme continental habitats (e.g., *Oceanodroma markhami* and *Oceanodroma hornbyi* breeding in the Atacama desert; García-Godos et al. 2002) the vast majority of small and medium hydrobatid and procellariid seabirds have co-evolved life history and breeding ecology characteristics with oceanic island habitats (Gaston 2004). These families therefore generally lack lengthy evolutionary histories of co-existence with terrestrial mammals, making their populations particularly susceptible to the anthropogenic introductions of mammalian predators (e.g., cats, rats, dogs, mongooses, pigs) and habitat modifiers (e.g., rabbits, goats, pigs) (Spatz et al. 2014). Specifically, these species are highly accessible and susceptible to mammalian predators due to 1) small and medium body sizes, 2) burrow, crevice, and/or ground nesting habits associated with high wing loading and the posterior placement of legs (Gaston 2004), and 3) behavior patterns often naïve to the threat of terrestrial

predators (e.g., ground calling; Keitt and Tershy 2003, Hervias et al. 2013). Demographically these populations are also highly vulnerable to elevated rates of adult and chick depredation due to 1) extended lifespans, 2) late recruitment to breeding populations, and 2) low annual reproductive outputs (Lavers et al. 2010, Croxall et al. 2012).

Given these vulnerabilities, accurate empirical assessments of the key demographic parameters, abundance and population trends, play critical roles in assessing risk of extinction for listing decisions (IUCN 2001), and strategically targeting limited conservation resources for these vulnerable seabirds (Spatz et al. 2014, Dawson et al. 2015). However, several breeding ecology characteristics shared by many small and medium hydrobatid and procellariid species make it extremely challenging to apply rigorous random sampling and statistical methods in the breeding colony assessments of these key demographic parameters. Specifically, many procellariid and hydrobatid species have adopted 1) cryptic burrow or crevice entrances, 2) nocturnal or crepuscular patterns of colony attendance (Day and Cooper 1995, Brooke 2013), and 3) steep or heavily vegetated breeding habitats (Rayner et al. 2007, Troy et al. 2016), likely in response to long co-evolutionary histories with traditional avian predators (Lockley 1932, Howell and Cade 1954, Harris 1974, Olson and James 1982, 1991, Jehl and Parkes 1983, Watanuki 1986, Martinez-Gomez and Curry 1995). These breeding ecology characteristics make many important areas of breeding habitat inaccessible to researchers due to precipitousness, remoteness, or disturbance-sensitivity. Where habitats are accessible, researchers often face

additional challenges in terms of detecting cryptic burrow or crevice entrances and definitively establishing occupancy for quadrat sampling (Rayner et al. 2003). Finally, in long-lived, late-maturing hydrobatid and procellariid seabirds, a potentially substantial non-breeding component of the population may go unsampled by colony based assessments (Brooke 2013).

Considering these limitations, the rigorous sampling of seabird density patterns from oceanic transect surveys may provide opportunities to resolve some of the challenges associated with colony-based estimation of abundance and population trend parameters in these species. First, in terms of accessibility, oceanic habitats present few barriers to research vessel access, allowing comparatively unbiased randomized or systematic sampling of underlying seabird density distributions (e.g., Wade and Gerrodette 1993, Barlow and Forney 2007). Additionally in terms of detectability, non-diving seabirds are relatively conspicuous, and thus readily counted and identified within reasonable distances from a research vessel or aircraft during daylight periods (Spear et al. 2004). Also, with the exception of egg- and early chick-rearing phases of the breeding cycle when one incubating/brooding adult is generally present on the nest, the entire breeding and non-breeding population is typically represented in the oceanic habitat (Spear et al. 1995).

However, the strength of seabird abundance, and particularly trend inferences from at-sea data, are often constrained by several substantial and potentially confounded sources of count variance. First, at-sea seabird sampling often contains substantial scatter due to the inherently stochastic process of encountering seabirds

during transect surveys (Tasker et al. 1984), as well as the relatively small proportion of the ocean surface area that can be effectively sampled (Spear et al. 2004), even with extensive transect survey effort. Second, seabird oceanic density distributions are also typically dynamic and patchy at multiple space and time scales (Hunt and Schneider 1987). These can range from general habitat associations, such as central place distributions around colonies (Orians and Pearson 1979) and/or neritic foraging habitats along continental shelf margins, down to highly concentrated but short-lived and small-scale foraging features, such as mixed-species foraging aggregations associated with tuna schools. Third, due to real variation in the underlying population processes, there is year-to-year variation around the central tendencies of abundance and population trend parameters,. Finally, if only a portion of the species range has been sampled (i.e., an open population) then movement between the sampled and unsampled portions of the range (i.e., immigration and emigration) may also contribute to variation in abundance and trend parameters (Moore and Barlow 2014).

One approach to the estimation abundance and trends that has been applied to seabird transect data entails a two-step process in which abundance is first estimated within survey years, followed by subsequently fitting a generalized additive model (Hastie and Tibshirani 1986) to these point estimates of abundance across multiple years (Clarke et al. 2003). However, as shown in cetacean line transect data, the reduction of sampling information to a set of annual point abundance estimates can limit the statistical power for detecting trends (Taylor et al. 2007, Jewell et al. 2012). Moreover, individual abundance estimates are not ultimately independent of each

other; observations in any specific year not only provide information related to that year, but also joint information about the overall population process through time. Finally, this approach also fails address the distinction between true variation in the underlying population process and nuisance scatter associated with the sampling technique.

In this study we estimated abundance and trend parameters in two procellariid and two hydrobatid species using Bayesian hierarchal (or mixed-effects) state-space models (e.g., Moore and Barlow 2011, 2013, 2014) based on a modification of the framework delineated in Moore and Barlow (2014). Case study species included the Townsend's shearwater (*Puffinus auricularis*, Critically Endangered, IUCN Redlist 2016), the black-vented shearwater (*Puffinus opisthomelas*, Near Threatened, IUCN Redlist 2016), the ashy storm-petrel (*Oceanodroma homochroa*, Endangered, IUCN Redlist 2016) and the black storm-petrel (*Oceanodroma melania*, Least Concern, IUCN Redlist 2016). These study species were selected because each represents a breeding endemic species, for which the sampled area of the Eastern Pacific Ocean covered *circa* 95-100% of their oceanic range, thereby reducing variation due to interannual range fluctuations (i.e., immigration and emigration). This model framework allowed substantial flexibility in how the underlying population abundance process was represented through time. In these models we implemented two representations: a Markov process with exponential growth between years and a log-linear regression (i.e. exponential) process. This framework also allowed for the addition of randomly distributed process error to account for true variation around

these average population processes (Moore and Barlow 2014). However, the underlying population dynamics could only be observed through a sampling process, which introduced additional sources of stochastic error. These observation processes were described in models relating the underlying population abundance parameters to the observed transect count data at multiple scales (e.g., rate of encounter with groups of one or more seabirds, and the size of each group). This study simultaneously estimated Bayesian posterior distributions of both the population dynamics (i.e., process model) and observation model parameters using Markov Chain Monte Carlo (MCMC) algorithms (Lunn et al. 2000). The posterior distribution of the growth rate parameter in this framework provided a relatively easily interpreted inference of population growth or decline, based on the proportion of posterior probability falling above or below zero, a value which would indicate no population change with time (Gerrodette 2011, Moore and Barlow 2011, 2013, 2014).

Methods

Data

The models of seabird abundance and trends developed in this study employed seabird strip transect data collected on research cruises run by NOAA Southwest Fisheries Science Center in the Eastern Tropical Pacific (ETP: 1988, 1989, 1990, 1998, 1999, 2000, 2003, and 2006) and the California Current ecosystems (CCE: 1996, 2001, 2005, 2008, and 2014). Sampling in both ecosystems was conducted simultaneously from two or more vessels over the period August to November in each sampling year for the ETP and from one or two vessels in different

years of CCE sampling. Seabird strip transect sampling was conducted on surveys that were designed to assess population status and trends of a variety of cetacean species in each ecosystem (Wade and Gerrodette 1993, Kinzey et al. 2000, Barlow & Forney 2007). Based on these objectives the sampling designs differed between the CCE and ETP. The CCE was sampled using a systematic grid design repeated across multiple years of sampling (all except 1996 which used a slightly different grid pattern; Barlow & Forney 2007), while the ETP was sampled using semi-randomized pattern that varied in the layout of transects between sampling years. Despite these major differences, both sampling designs were laid out with the overarching goal of representatively sampling the underlying distribution and density patterns of broadly and patchily distributed marine predator populations over large geographic areas. Thus seabird surveys conducted opportunistically from these research cruises can be used to implement so-called "design-based" abundance estimation procedures, where animal density in given sampling area or stratum can be estimated by dividing the count by the area sampled.

Sampling in the ETP was subdivided into two strata with 1) a more densely sampled core stratum from the Central American coast out to 120°W between 5°N and 27°N, and 2) a less densely sampled outer stratum extending in a wedge shape from the core area out to 153 °W between 18°S and 32.6°N (Fig. 1). Sampling in the CCE was treated as a single stratum that extended to approximately 556 km (300 nautical miles) from the West Coast of the US mainland between 30°N and 48.5°N. Explicitly incorporating these distinct strata in subsequent abundance trend analyses

was important, both because each ecosystem was sampled in separate years and because the density of survey effort differed substantially among strata. In total, across all years, on-effort transect sampling summed to approximately 1) 127,283.5 km in the ETP core strata, 2) 104442.9 km in the ETP outer strata, and 3) 70229.6 km in the CCE strata (Fig. 1). Many of the case study species examined in this analysis were closely associated with either the narrow continental shelf along the Pacific Coast or the shelf slope zone (Fig. 2). Therefore small year-to-year variation in the proportional representation of these habitats in the sampling of the broader ETP core, ETP outer, and CCE strata could potentially increase the year-to-year variance of abundance estimates. To more directly account for these potential variations in sampling distribution, we subdivided the ETP and CCE strata into four geographic bins based on geodesic distances (<200km, 200-400km, 400-800km, >800km) from the edge of the continental shelf margin (i.e., the 200m isobath).

Seabird surveys followed a "continuous vector" strip transect method (Spear et al. 1992), which involves the continuous recording of all individuals and groups of seabirds entering a 90˚ arc to either port or starboard of the vessel heading. The radius of this arc varied between 100 and 300m depending on an assessment of the observation conditions (e.g., Beaufort conditions, visibility, glare) and the size-class of the observed seabird (e.g., small: auklets and storm-petrels vs. large: all other seabirds). For each individual or group encountered, the number of individuals entering the strip, as well as the flight direction and behavior (e.g. directional flight,

milling, feeding, circling, sitting on the water) were recorded for the subsequent calculation of a "flux correction" parameter (see Spear et al. 1992).

Population Trend Model (Process Model)

Based on the approach of Moore and Barlow 2014, we developed two representations of population growth both describing change through time as an exponential process (i.e. where growth of the population, N, between time, t and t+1, varies in proportion to the size of the population, N_t, at time, t). In a closed animal population where the entire range has been sampled (e.g., *P. auricularis*), emigration and immigration contribute little to the rate of population change through time. The size of the population can therefore be described by a Markov process, where the size of the population, N_t, at time, t (t_{ETP} = 1, 2, ... 18 for years 1988, 1989, ... 2006; t_{CCE} = 1, 5, ... 18 for years 1996, 2001... 2014), depends on the size of the population at the previous time step, $t - 1$. An exponential Markov model with a growth rate parameter, r, (r is the natural log of the λ parameter specified in other models of population growth, e.g., Ainley et al. 2001), describing this population change through time is detailed in the following system of equations:

$$N_1 = N_0\, e^r e^{\varepsilon_t}$$

$$N_t = N_{t-1}\, e^r e^{\varepsilon_t}$$

$$\varepsilon_t \sim Normal(0, {\sigma_{process}}^2) \qquad (1)$$

Here, N_0 is the population at t = 0 (i.e., 1-year prior to first year of sampling), while ε_t is a random effect process error term, representing variation in the population, N_t,

based on idiosyncratic deviations from the average demographic processes captured in *r*. The growth rate parameter, *r*, is typically defined as the total of the birth rate – death rate + immigration rate – emigration rate.

We also considered a simpler exponential (i.e., log-linear) regression model. While nearly the entire ranges of *P. opisthomelas*, *O. homochroa*, and *O. melania* were contained by the CCE and ETP sampling areas collectively, neither stratum captured the entire ranges of these species at the same time. Thus year-to-year northward or southward shifts in the distribution of these species across the boundary dividing the CCE and ETP sampling areas (due to for example El Niño Southern Oscillation) could have resulted in population variation unaccounted for by birth and death processes. This exponential regression model was specified as:

$$N_t = N_0\, e^{r \cdot t} e^{\varepsilon_t}$$

$$\varepsilon_t \sim Normal(0, {\sigma_{process}}^2) \qquad (2)$$

with a random effect process error term, ε_t, analogous to the term described in Eq. 1.

Because the sampling included in each model was conducted across multiple sampling strata, the population N_t was sub-divided into *j* number of strata. The proportion of the overall population within each stratum was defined by a Dirichlet distribution, with parameters u_1 to u_j, following the approach of Moore and Barlow 2014.

$$N_{jt} = N_t\, \varphi_j$$

$$\varphi_j \sim Dirichlet(u_j) \qquad (3)$$

Finally, the density of individual seabirds (D) contributing to the expected and observed counts in stratum j at time t, was defined as:

$$D_{jt} = \frac{N_{jt}}{A_{jt}} \quad (4)$$

where A_j represents the total ocean surface area within each stratum polygon.

Encounter Rate Model (Observation Model)

In addition to the stochasticity in underlying population dynamics denoted by ε_t, these population processes could only be observed through a sampling process, which introduced additional sources of stochastic variability. In the state-space model framework, this strip transect sampling was defined by an observation model describing the expected rate at which observers encountered groups of one or more seabirds within the survey strip, n_{jt}. The expected number of groups encountered, μ_{jt}, was defined as:

$$\mu_{jt} = \frac{D_{jt}}{\gamma} \cdot a_{jt} \cdot \bar{k}^{-1} \quad (5)$$

based on 1) the underlying density of individual seabirds D_{jt}, 2) the area sampled, a_{jt}, 3) seabird group size, γ, and 4) a correction factor for the effect of seabird movement, $\bar{k}^{-1}$ (Gaston et al. 1987, Spear et al. 1992). This observation model was adapted from an expected encounter rate model for line-transect abundance estimation defined in equations 5-9 of Moore and Barlow (2014). Because seabird sampling applied a strip transect methodology instead of a line transect methodology, a_{jt} was simply calculated by summing the products of segment length and variable strip width (100-300m; see description in Data subsection) at the transect level, instead of applying the

more complex line transect estimation of effective strip width as calculated by Moore and Barlow (2014).

Earlier iterations of this model framework (e.g., Moore and Barlow 2011, 2013) assumed that the number of observed encounters with groups of seabirds, n_{jt}, was a Poisson distributed variable where mean and variance both equaled μ_{jt}.

$$n_{jt} \sim Poisson(\mu_{jt}) \quad (6)$$

To meet this Poisson assumption of mean and variance equality, the underlying spatial distribution of seabird groups would have to resemble a uniform random field. Given the known underlying heterogeneity and patchiness of seabird distribution patterns, a more realistic description of the encounter rate process required the inclusion of extra-Poisson sampling variance. One approach considered in this analysis added a normally distributed random effect term, τ_{jt}, to the observation portion of the model, allowing sampling variance to exceed the mean (Link and Sauer 2002, Kéry et al. 2009, Moore and Barlow 2014).

$$n_{jt} \sim Poisson(\mu_{jt} \cdot e^{\tau_{jt}})$$

$$\tau_{jt} \sim Normal(0, {\sigma_{obs}}^2) \quad (7)$$

However, estimating random effects in both the process and observation portions of the model had the potential to confound these two distinct sources of variance (Moore and Barlow 2014), potentially leading to underestimates of the true process variance and over-estimates of certainty in the posterior distributions of r, N_0, and N_t. Based on the approach of Moore and Barlow (2014), we therefore estimated models using a generalized Poisson distribution (Famoye 1993, Famoye et al. 2004),

$$n_{jt} \sim gPoisson(\mu_{jt}, \alpha_{jt}) \quad (8)$$

as an alternative approach to handle Poisson overdispersion. Unlike the negative binomial and quasi-Poisson distributions, in which overdispersion is estimated directly within the model, the generalized Poisson distribution can incorporate an external empirical estimate of a "variance inflation factor" (*VIF*) in its overdispersion parameter, α_{jt}, (Famoye 1993, Famoye et al. 2004). The *VIF* was calculated by taking the average of encounter rate variance to mean ratios from 1000 bootstrap re-samples with replacement of the underlying strip transects (Moore and Barlow 2014). This permitted the introduction an external estimate of extra-Poisson sampling variance, and facilitated a more realistic description of process variance and posterior uncertainty surrounding estimates of r, N_0, and N_t.

Group Size Model (Observation Model)

In this model framework the expected number of groups encountered, μ_{jt}, represented processes affecting broad-scale distribution and density patterns (e.g., central place foraging). By contrast, seabird group size, s_{jt}, was primarily affected by localized processes such as the formation of flocks over prey aggregations. This resulted in a vast majority of encounters with solitary individuals or groups of two individuals, but occasional stochastic encounters with flocks of 10s to 1000s of individuals. This situation resulted in substantial overdispersion with respect to a Poisson distribution, for which ver Hoef and Boveng (2007) recommended the use of

the negative binomial distribution. We modeled observed group sizes, *g*, as a truncated negative binomial distribution,

$$g_{trunc.} = g - 1$$

$$\gamma = \gamma_{trunc.} + 1$$

$$g_{trunc.} \sim NegBinom(\gamma_{trunc.}, \kappa) \quad (9)$$

where the truncated expected group size, $\gamma_{trunc.}$, was related to the truncated observed group size, $g_{trunc.}$, to account for the lack of zeros in observed group sizes. The negative binomial overdispersion parameter, κ, defined group size variance as multiplicatively (as opposed to proportionally, e.g., quasi- and generalized Poisson) related to the group size mean (ver Hoef and Boveng 2007).

To account for the possibility that cetacean group size changed over time as a function of population growth or decline, Moore and Barlow (2014) modeled group size "as a random effect variable, generating estimates of s_{2jt} [group size] that are intermediate between a grand mean and the individual data means [in *j* strata and *t* years]". We also initially developed analogous models of γ_{jt} with random effects in *j* stratum and *t* year, but the processes generating seabird and cetacean groups are substantially biologically divergent. Seabird groups are generally ephemeral associations likely to vary in size on a time-scale of minutes to hours (Hoffman et al. 1981), whereas cetacean groups (particularly among toothed whales) are generally stable social and familial associations lasting from weeks to decades (Whitehead 2003). As such we might expect long-term change in cetacean group sizes as a function of population growth or decline, however the short-term variability in

seabird group size would likely swamp any ability to detect a coherent trend with time. We thus opted to model expected group size with only random effects of stratum, j.

Parameter Estimation

We implemented models in the *JAGS* 3.4.0 language (Plummer 2004; analogous to WinBUGS and OpenBUGS, Lunn et al. 2000), and these models were run from an R interface using the library *R2jags* (Su and Yajima 2012). We sampled the posterior distributions of the model parameters r, N_0, and N_t from 3 MCMC chains. Each chain consisted to 500,000 simulations, with the first 100,000 iterations discarded in the burn-in phase. The remaining 400,000 iterations were thinned by 50, leaving 4000 samples from each chain, and a total of 12,000 in the overall estimated posterior distribution. Convergence and mixing of the three chains was evaluated visually and confirmed using the $\hat{R}$ convergence metric (Gelman and Rubin 1992). Priors for all model parameters were defined using uniform distributions (Moore and Barlow 2014).

Results

Townsend's Shearwaters (Puffinus auricularis)

Overall, both the exponential regression and exponential Markov process models suggested a decline in *P. auricularis* population over the study period 1988 to 2006. Median estimates of trend parameter (r) posterior distributions in the

exponential regression and Markov models were -0.037 and -0.080, respectively. However the precision of *r* posterior distributions in these two models differed substantially, with much narrower 95% credible intervals for the exponential regression model (Tables 1 and 2). More than 82.8% of the *r* posterior distribution for *P. auricularis* fell below $r = 0$ in the exponential regression model (Fig. 3, *inset*). The Markov model also provided evidence of a decline, with 68.2% of the *r* posterior probability distribution falling below zero. Over the 18 year study period in the ETP, the growth rate parameter in the exponential model resulted in a 65.2% decline from a median posterior estimated population size of 61,295 in the first three years of sampling (e.g., 1988,1989, 1990), to a median estimate of 21,333 in the last year of sampling (e.g., 2006). The process model random effect variance was similar between the exponential regression model (0.74) and the Markov model (0.78). This magnitude of process error resulted in year-to-year changes in the median posterior estimate of abundance ranging from - 46.1% to -0.73%.

Black-vented Shearwaters (Puffinus opisthomelas)

Hierarchical state-space models of *P. opisthomelas* abundance supported positive trends in this population based on estimates of *r* in both the ETP and CCE segments of this species' range (Fig. 2). The exponential regression and Markov models showed close agreement in posterior estimates of the *P. opisthomelas* annual rate of change parameter (*r*), with median growth rates of 0.145 and 0.142 in the ETP, and 0.113 and 0.100 in the CCE, respectively. These estimates of *r* in excess of 0.100

implied a doubling of population in <7 years. The precision of *P. opisthomelas r* posterior distributions in the ETP were substantially greater in the exponential regression model with 95% CRI ranging from 0.04 to 0.35, relative to 95% CRI -0.19 to 0.51 in the Markov model (Tables 1 and 2). Despite these wide credible intervals, 89-99% of the *r* posterior distribution in both models from the ETP exceeded zero (Fig. 4, *insets*), suggesting growth in the *P. opisthomelas* population over the ETP study period (1988-2006). The CCE study area, which was outside the breeding range of *P. opisthomelas* (Keitt et al. 2003) and on average represented only 35.6% of the estimated population, showed greater variability in estimates of *r* than the ETP, with 95% CRI ranging from -0.11 to 0.36 in the exponential regression model and -0.46 to 0.63 in the Markov model. Markov and exponential regression models in the CCE also suggested an increase in *P. opisthomelas* population, with 71-84% of *r* posterior probability exceeding zero. These growth rate parameters corresponded with a 13-fold increase in the abundance of *P. opisthomelas* in the ETP study area, with median posterior estimates of N_t increasing from 24,470 in the first three years of sampling (e.g., 1988,1989, 1990) to 324,134 in the last year of sampling (e.g., 2006). The median process variance for this species was comparable to *P. auricularis* in exponential model ($\sigma_{exp.\ process} = 0.73$) but substantially lower in the Markov model ($\sigma_{mark.\ process} = 0.42$) from the ETP.

Black Storm-petrel (Oceanodroma melania)

The exponential regression and Markov configurations of *O. melania*

hierarchical state- space models diverged in their estimates of abundance trend parameters and provided substantially different inferences on population change in the ETP portion of *O. melania*'s species range (Fig. 2). The exponential regression model version of *O. melania* abundance in the ETP, yielded a positive median trend parameter, median(r) = 0.135, with a comparatively narrow posterior distribution of r (Fig. 5a, inset), and an estimated >99.9% of the posterior probability > 0. However the process variance for this model was extremely large ($\sigma_{exp.\ process}$ = 1.34), resulting in year-to-year changes in the median posterior estimate of abundance ranging from -70% to +34%. The Markov model of *O. melania* abundance in the ETP also estimated a median positive trend, but exhibited substantially lower precision and more equivocal evidence of a population increase with only 64% of the r posterior falling above zero (Table 2). It appears that the exponential regression inference of an increasing trend in the ETP was heavily influenced by the high rate of encounters with *O. melania* in the 1998 year of sampling. Refitting these models without the year 1998 sampling, brought closer alignment of the median trend parameters 0.141 and 0.078 in the exponential regression and Markov models, respectively. Positive trends from both models in the ETP also diverged from the essentially flat trend estimate in the CCE portion of *O. melania*'s range (Fig. 5). However, on average the CCE only represented 2.8% of the population (Fig. 2), and estimates of r in this region were also highly variable with the widest spread of 95% CRI of any species or region (Table 1 and 2).

Ashy Storm Petrel (Oceanodroma homochroa)

Finally, exponential regression and Markov models both pointed to an increase in *O. homochroa* abundance over the study period in the CCE region (1996 to 2014). Median estimates of trend parameter (*r*) posterior distributions in the exponential regression and Markov models were 0.070 and 0.088, respectively. As was the case in the models reported above, the precision of trend parameter (*r*) inference in the Markov formulation (95% CRI: -0.47 - 0.65; Table 2) was substantially lower than the precision for the exponential regression model (95% CRI: -0.16 - 0.27; Table 1). In both formulations 71-78% of the *r* posterior sample for *O. homochroa* was distributed above $r = 0$ (Fig. 6, *inset*). Over the 18 year study period in the CCE, these growth rate parameters resulted in a 3.3-fold increase from a median posterior estimate population size of 1474 in the first year of sampling (e.g., 1996), to a median estimate of 4820 in the last year of sampling (e.g., 2014) based on the exponential regression model. The process model random effect variance was substantially greater 1.66 in the exponential regression model when compared to the process variance 1.17 in the Markov model. This magnitude of process error resulted in changes in the median posterior estimate of abundance between survey years ranging from -70% (over to 3 years 2005-2008) to + 315% (over to 6 years 2008-2014).

Discussion

Townsend's Shearwaters (Puffinus auricularis)

The earliest years of sampling in this study (1988-1990) overlapped the sampling period (1980-1994) of the only previous study to estimate *P. auricularis* abundance (Spear et al. 1995). Median *P. auricularis* abundance estimates in these first three years of sampling, fell within the 95% confidence intervals of Spear et al. (1995) abundance estimates. However, the median of the N_t posterior distributions across these three years was 32.2% higher than the reported estimate of 46,378 from Spear et al. (1995). The 95% credible intervals in 1988-1990 estimates of *P. auricularis* abundance are considerably wider (19,508-160,519) than the 95% confidence intervals (17,522-89,008) of Spear et al. (1995) estimates, thus this discrepancy possibly resulted from a lack of precision in the present estimates. However, a portion of this discrepancy could also have potentially resulted from differences in sampling areas considered by these two studies. Spear et al. (1995) estimates did not include areas within the Gulf of California north of Cabo San Lucas (22.9°N), due to a lack of sampling. The present study extended sampling further into the Gulf of California to the latitude of Midriff Island group (28.5°N). This area of the Gulf of California, while small relative in geographic area when compared with the overall sampling areas of both studies, is an important habitat of *P. auricularis* and could thus have accounted for the larger estimates of abundance in the present study.

The relatively tight clustering of the *P. auricularis* posterior distribution of *r,* as well as the substantial proportion falling below zero, provided comparatively strong evidence of a decline in the abundance of this species over the study period.

These estimates of decline were also consistent with 1) the reported extirpation of *P. auricularis* from Clarion Island, 2) reductions in the extent of breeding habitat on Socorro Island, and 3) extensive records of depredation by feral cats (*Felis silvestris catus*) and native Socorro red-tailed hawk (*Buteo jamaicensis socorroensis*) documented during the field surveys conducted between 1986-2000 (Martinez-Gomez and Jacobsen 2004). Applying median estimated *r* to either the 1988-1990 estimates of abundance from the present study or to the Spear et al. (1995) estimates would both result in declines of this species to extinction within 150 years based on the population model developed by Martinez-Gomez and Jacobsen (2004). All of these estimates support the classification of this single-island endemic species under Critically Endangered status based on IUCN criteria (IUCN 2001).

Black-vented Shearwaters (Puffinus opisthomelas)

Estimates of *P. opisthomelas* abundance prior to the research of Keitt et al. (1998, 2003) were generally based on "cursory burrow counts or best guesses based on numbers of birds observed at sea around known colonies." With that caveat in mind, previous island-specific estimates include 1) 500-2500 pairs breeding on islets surrounding Guadalupe Island (Jehl and Everett 1985) 2) 150 pairs (Delong and Crossin 1968) to 250–500 pairs (Everett and Pitman 1993) on San Benito and surrounding islands, and 3) between 5000 burrows (Delong and Crossin 1968) and 5000-10,000 burrows (Everett 1988) on Natividad Island. Keitt et al. (1998, 2003)

provided the first rigorous estimate of 76,570 (SD: 18,411) breeding pairs at Natividad Island based on quadrat sampling of burrow densities and burrow occupancy measurements using an infrared camera probe conducted in 1997 and 1998. Although *P. opisthomelas* breeding has been reported on the island groups described above and in very low numbers in the Coronado Island group, the preponderance of evidence points to Natividad Island as containing the vast majority of global breeding *P. opisthomelas* (Keitt et al. 2003). If the estimate of 76,570 breeding pairs were approximately doubled to 150,000 breeding adults as applied in Keitt et al. (2002), and if breeding adults represented approximately 56% of the total population as described by Spear et al. (1995), then this would imply a population of 267,857 from Natividad Island in 1997-98 with the addition of smaller populations on and around Guadalupe Island, San Benito Island, and the Coronado Islands. This total substantially exceeds median estimates of abundance from at sea data in the present study, which ranged from 88,474 in 1998 to 109,606 in 1999 in the ETP, with an additional 11,428 to 12,865 from the CCE in 1998 and 1999, respectively.

Both the exponential regression and Markov models of *P. opisthomelas* population changes with time provided strong indications of increasing population trends. The fact that positive trends were indicated in independent sampling conducted in both the breeding (ETP) and non-breeding (CCE) segments of *P. opisthomelas* range, further strengthens the inference of increases in this population over the study period. This increasing trend, particularly between sampling conducted in 1988-1990 and 1998-2000, is intriguing. It appears to run counter to the estimated

population growth rate from the Keitt et al. (2002) population viability analysis (PVA), which suggests a negative population growth rate in the absence of feral cat eradication on Natividad Island. If borne out, the increasing trends in *P. opisthomelas* population appears to pre-date the eradication of feral cats on Natividad Island, which was conducted in 1998-1999 and confirmed successful in 2001. The median trend parameters estimated in both the ETP and CCE also substantially exceeds the PVA estimate of growth rate parameter, $\lambda = 1.006$ (with $\lambda = 1$ indicating population stability) estimated by Keitt et al. (2002) for the scenario of cat eradication. This increasing trend parameter and the estimated changes in median abundance detailed in this study, could also potentially go some distance to explaining the disparity between the early burrow counts of Delong and Crossin 1968 and Everett 1988, and the substantially higher estimates of burrow numbers detailed by Keitt et al. (1998, 2003). Overall the results of this study support the 2000 downgrading of *P. opisthomelas* IUCN status from Vulnerable to Near Threatened.

Black Storm-petrel (Oceanodroma melania)

The most recent edition of the IUCN Redlist classifies *O. melania* as a species of Least Concern on the basis of extensive range, lack of a strongly negative population trend, and substantial population size (IUCN 2016). This species assessment drew heavily on the *O. melania* species account in Brooke (2004), which suggested a global population of approximately 500,000 individuals with a suspected declining trend due to invasive predators affecting several breeding colonies.

However, estimates of *O. melania* abundance and trends based on rigorous sampling methods have been lacking to date. In this modeling exercise, *O. melania* median posterior estimates of abundance fluctuated unrealistically from year-to-year considering the breeding biology of this relatively long-lived and slow-reproducing (i.e., one potential offspring per year) species. However, with the exception of the 1998 sampling, in which uniquely high *O. melania* encounter rates were recorded, median estimates of abundance in both the Markov and exponential regression models all fell below 500,000 individuals. We interpret this as an indication that the true population likely also fell below Brooke's (2004) estimate, although it remained within the same order of magnitude.

Unlike the results of *P. auricularis* and *P. opisthomelas* hierarchical state-space models, the modeling of *O. melania* abundance failed to provided strong evidence of either population increases or declines. As noted above, the process error component of *O. melania* models varied to an unrealistic extent given that *O. melania* represented an essentially a closed population within our combined CCE and ETP study areas and also considering aspects of the breeding biology of this species. One potential explanation for this lack of coherent trend could be shifts in the distribution of *O. melania*, due potentially to oceanographic variability in the region (e.g., ENSO; Tershy et al. 1991). Small shifts in spatial distribution, particularly with respect to a distribution of sampling transects that also varied from year-to-year in the ETP, may have resulted in substantial variation in abundance estimates and weak trend inferences. However, despite this large variance and wide credible intervals,

population trends in the ETP, which contained the vast majority of *O. melania* population, were still generally positive even after testing the removal of the potentially problematic 1998 sampling. This weakly supported inference of an increasing population trend, while differing from the suggestion of Brooke (2004), would be consistent with the eradication of invasive feral cats on known breeding colonies at Santa Barbara Island (Channel Islands, California, USA), Coronado Norte Island (Baja California, Mexico), and in the San Benito Island group (Baja California, Mexico; McChesney and Tershy 1998), as well as the eradication of black (*Rattus rattus*) and Norway rats (*Rattus norvegicus*) at Rasa Island in the Gulf of California (Donlan et al. 2000). Overall the results presented in this analysis support the classification of *O. melania* as a species of Least Concern under IUCN Redlist criteria (IUCN 2001).

Ashy Storm Petrel (Oceanodroma homochroa)

Previous island-specific estimates of *O. homochroa* abundance based on capture-recapture studies conducted in the Farallon and Channel Islands have yielded estimated population sizes of 1) 4690 at southeast Farallon lsland (Sydeman et al. 1998) 2) 3460 at San Miguel Island (Nur et al. 1999), 3) 1700 at Santa Cruz and Anacapa Islands (Nur et al. 1999), and 2430 at Santa Barbara Island (Nur et al. 1999). The sampling contributing to these estimates was conducted in 1994 on Southeast Farallon Island and over the period 1991-1997 in the Channel Islands (Sydeman et al. 1998, Nur et al. 1999). The median posterior

estimates of abundance within the CCE sampling area from this study were clearly substantially lower than any of these individual estimates. In fact, they were more than an order of magnitude lower than the estimated 12,280 individuals across these major breeding colonies, which also do not include smaller known breeding locations such as Steamboat Rock on the Humboldt County coast, Casket Rock on the Mendocino Coast near Fort Bragg, and Coronado Norte Island off Baja California Norte (Carter et al. 2016). This species was distributed widely over the California Current at distances up to ~556km from the coast (Fig. 2), thus making insufficient sampling close to shore due to the draft considerations of large research vessels to be an unlikely explanation for this larger disparity. Other potential explanations may include ship avoidance or problems with detection within the strip, however we lack the means to draw any firm conclusions on these conjectures at present.

Setting aside these disparities in absolute abundance, the inference from the posterior distribution of the trend parameter *r* yielded moderate evidence of an increase in the relative abundance of *O. homochroa* over the 1996-2014 study period in the CCE. The population of *O. homochroa* is thought to have undergone a decline on Southeast Farallon Island between 1972 and 1994 incidental to an increase in avian predation by burrowing owls (*Athene cunicularia*) attracted to the island by invasive house mouse (*Mus musculus*) populations (Sydeman et al. 1998). Additional historic declines in the Channel Islands have been attributed to depredation by invasive mammals (Carter et al. 2016) and eggshell thinning from

organochlorine pollution in the Southern California Bight (Fry 1994). However many of these threats have been mitigated in recent years through invasive mammal eradications, reductions in pollution, and active colony restoration efforts (Harvey et al. 2016, McIver et al. 2016). Carter et al. (2016) conclude that populations of *O. homochroa* are likely increasing which would be consistent with the inference from this study.

Management Implications

Although information on the abundance of several study species has existed at the level of colonies or island groups, the population estimation component of this analysis provide the first range-wide estimates of abundance for many of our case study species. However, given the wide credible intervals derived for most species, it is unclear how effectively these estimates can be applied in management decision-making.

The trends inferred from hierarchical state-space models of *P. auricularis*, *P. opisthomelas*, and *O. homochroa* abundance represent novel information that is invaluable from a management perspective. In particular, the three species (e.g., *P. opisthomelas*, *O. melania*, and *O. homochroa*) showing some indications of positive population trends all reproduce, at least over a portion of their breeding ranges, on islands where invasive predators have been eradicated in recent decades (McChesney and Tershy 1998). By contrast, the fourth case study species, *P. auricularis*, which exhibited a declining trend over the study period (1988-2006),

breeds on an island where feral cats persist to date. We would contend that the results from this limited number of case studies support the value of invasive mammal eradications as a tool to preserve and restore island ecosystems, and in particular to improve the population status of vulnerable seabird populations.

Nevertheless, some caution is warranted in attributing causation of population increases/declines to eradication efforts or the lack thereof. In particular, the beginning of apparent increases in *P. opisthomelas* abundance preceded the eradication of cats on their major breeding site, Natividad Island. This finding does not negate the substantial post-eradication increases in *P. opisthomelas* abundance, although it does suggest that other underlying dynamics may also have contributed to abundance changes in this species. In the coming decades, it will be intriguing to observe how populations of *P. auricularis*, respond to on-going feral cat eradication efforts on Socorro Island, which has also recently undergone a feral sheep (*Ovis aries*) eradication. It will also be intriguing to observe how the currently proposed eradication of *M. musculus* on SE Farallon Island will affect the future trajectory of *O. homochroa* abundance. In both cases, the continuing collection of at-sea strip transect data, along with application of advances in hierarchical state-space modeling techniques, will likely provide novel insights into ongoing population changes.

Use of Bayesian Hierarchical Framework

The Bayesian hierarchical state-space approach developed in this study to

model seabird strip transect time series provided several benefits. First, to describe population processes, it allowed us to partition the underlying population variation from a noisy observation process by including external empirical estimates of encounter rate variability in the generalized Poisson distribution and normally distributed random effects error (Moore and Barlow 2014). Second, this model framework allowed the specification of more complex models of underlying population change through time, such as the Markov process model. Third, it enabled the simultaneous optimization of parameters across models for population processes, encounter rates, and group sizes (Moore and Barlow 2014).

Previous approaches (e.g., Clarke et al. 2003) obtained estimates from each sampling year independently. For many rarer species such as *P. auricularis* and *O. homochroa,* this would have forced a reliance on a small number of data points to estimate encounter rate and group size parameters in any given survey year, making these estimates more sensitive to random stochastic variation in year-to-year counts. In this formulation, the time-dependence encoded in the process models "formalized an assumption that abundance within the survey area was related through time" (Moore and Barlow 2014). This has the important effect of "limiting the extent to which individual abundance estimates can vary" and "shrinking stand-alone estimates toward a modeled expectation" (Moore and Barlow 2014). Altogether this increases the precision of abundance and trend parameter estimates. However, as shown by the unrealistically large random-effects process-error variance particularly in *O. melania,* this model still faces challenges where the sampling distribution and underlying

species distribution may both vary in space and time. Finally, fitting these models using a Bayesian MCMC approach, enabled the estimation of posterior probability distributions for the trend parameter, *r*, that were relatively simple to interpret in terms the probability of an increase or decline, as well as the uncertainty of estimates based on the shape of this posterior distribution.

Acknowledgements

We would like to acknowledge the many people who contributed their time, resources, and talents to this project. The chief scientists, seabird and marine mammal observers, officers, and crews of the NOAA research vessels *R/V McArthur II* and *R/V David Starr Jordan* who contributed years of sea-time to create these amazing datasets. In particular I would like to acknowledge Mike Force and Annette Henry for their patience and good nature in helping me learn the strip transect data collection. Lynn Shepherd also provided invaluable feedback on a draft of this manuscript. Also, Martin Renner, and Arliss Winship who gave very helpful statistical advice. Funding support was provided by the National Science Foundation Graduate Research Fellowship Program. Finally I would like to thank Lisa Ballance for her continuing support and for providing me valuable feedback at all stages of this project.

Chapter 5, in full, is currently being prepared for submission for publication of the material. Joyce, Trevor W.; Moore, Jeffrey E.; Pitman, Robert L.; Ballance, Lisa T. The dissertation author was the primary investigator and author of this material.

References

Ainley, D.G., Podolsky, R., DeForest, L., Spencer, G. & Nur, N. (2001) The status and population trends of the Newell's shearwater on Kauai: insights from modeling. *Studies in Avian Biology*, 22, 108–123.

Barlow, J. & Forney, K.A. (2007) Abundance and population density of cetaceans in the California Current ecosystem. *Fishery Bulletin*, 105, 509–526.

Brooke, M. (2013) *The Manx Shearwater*. A&C Black Publishers, London, UK.

Carter, H.R., Ainley, D.G., Wolf, S.G. & Weinstein, A.M. (2016) Range-wide conservation and science of the Ashy Storm-Petrel *Oceanodroma homochroa*. *Marine Ornithology*, 44, 53–62.

Croxall, J.P., Butchart, S.H., Lascelles, B.E.N., Stattersfield, A.J., Sullivan, B.E.N., Symes, A. & Taylor, P. (2012) Seabird conservation status, threats and priority actions: a global assessment. *Bird Conservation International*, 22, 1–34.

Dawson, J., Oppel, S., Cuthbert, R.J., Holmes, N., Bird, J.P., Butchart, S.H.M., Spatz, D.R. & Tershy, B. (2015) Prioritizing islands for the eradication of invasive vertebrates in the United Kingdom overseas territories. *Conservation Biology*, 29, 143–153.

Day, R.H. & Cooper, B.A. (1995) Patterns of movement of Dark-rumped Petrels and Newell's Shearwaters on Kauai. *Condor*, 97, 1011–1027.

Day, R.H., Cooper, B.A., Telfer, T.C. & Powell, A. (2003) Decline of Townsend's (Newell's) shearwaters (Puffinus auricularis newelli) on Kauai, Hawaii. *The Auk*, 120, 669–679.

Donlan, C.J., Tershy, B.R., Keitt, B.S., Wood, B., Sánchez, J.Á., Weinstein, A., Croll, D.A. & Alguilar, J.L. (2000) Island conservation action in northwest Mexico. *Proceedings of the Fifth California Islands Symposium*, pp. 330–338.

García-Godos, I., Goya, E. & Jahncke, J. (2002) The diet of Markham's Storm Petrel *Oceanodroma markhami* on the central coast of Peru. *Marine Ornithology*, 30, 77–83.

Gaston, A.J. (2004) *Seabirds: A Natural History*. Yale University Press, New Haven, Connecticut, USA.

Gelman, A. & Rubin, D.B. (1992) Inference from iterative simulation using multiple sequences. *Statistical science*, 457–472.

Gerrodette, T. (2011) Inference without significance: measuring support for hypotheses rather than rejecting them. *Marine Ecology*, 32, 404–418.

Gómez, J.E.M. & Curry, R.L. (1995) First description of the nest and eggs of the Socorro Mockingbird. *The Wilson Bulletin*, 107, 551–555.

Harris, S.W. (1974) Status, chronology, and ecology of nesting storm petrels in northwestern California. *The Condor*, 76, 249–261.

Harvey, A.L., Mazurkiewicz, D.M., McKown, M.W., Barnes, K.W. & Parker, M.W. (2016) Changing breeding status of the Ashy Storm-Petrel *Oceanodroma homochroa* on Anacapa Island, California. *Marine Ornithology*, 44, 93–97.

Hastie, T. & Tibshirani, R. (1986) Generalized additive models. *Statistical Science*, 1, 297–310.

Hervías, S., Henriques, A., Oliveira, N., Pipa, T., Cowen, H., Ramos, J.A., Nogales, M., Geraldes, P., Silva, C., de Ybáñez, R.R. & others. (2013) Studying the effects of multiple invasive mammals on Cory's shearwater nest survival. *Biological invasions*, 15, 143–155.

Hoffman, W., Heinemann, D. & Wiens, J.A. (1981) The ecology of seabird feeding flocks in Alaska. *The Auk*, 98, 437–456.

Howell, T.R. & Cade, T.J. (1954) The birds of Guadalupe Island in 1953. *The Condor*, 56, 283–294.

Hunt Jr, G.L. & Schneider, D.C. (1987) Scale-dependent processes in the physical and biological environment of marine birds. *Seabirds: feeding ecology and role in marine ecosystems*, (ed. J.P. Croxall), pp. 7–41. Cambridge University Press, Cambridge, UK.

IUCN, S.S.C. (2001) IUCN red list categories and criteria: version 3.1. *Prepared by the IUCN Species Survival Commission*. www.iucnredlist.org

Jehl Jr, J.R. & Parkes, K.C. (1983) Replacements of landbird species on Socorro Island, Mexico. *The Auk*, 100, 551–559.

Jewell, R., Thomas, L., Harris, C.M., Kaschner, K., Wiff, R., Hammond, P.S. & Quick, N.J. (2012) Global analysis of cetacean line-transect surveys: detecting trends in cetacean density. *Marine Ecology Progress Series*, 453, 227–240.

Keitt, B.S. & Tershy, B.R. (2003) Cat eradication significantly decreases shearwater mortality. *Animal Conservation*, 6, 307–308.

Keitt, B.S., Tershy, B.R. & Croll, D.A. (2003) Breeding biology and conservation of the Black-vented Shearwater *Puffinus opisthomelas*. *Ibis*, 145, 673–680.

Keitt, B.S., Wilcox, C., Tershy, B.R., Croll, D.A. & Donlan, C.J. (2002) The effect of feral cats on the population viability of black-vented shearwaters (*Puffinus opisthomelas*) on Natividad Island, Mexico. *Animal Conservation*, 5, 217–223.

Lavers, J.L., Wilcox, C. & Donlan, C.J. (2010) Bird demographic responses to predator removal programs. *Biological Invasions*, 12, 3839–3859.

Lockley, R.M. (1932) On the breeding habits of the Storm Petrel, with special reference to its incubation and fledging periods. *British Birds*, 25, 206–211.

Lunn, D.J., Thomas, A., Best, N. & Spiegelhalter, D. (2000) WinBUGS-a Bayesian modelling framework: concepts, structure, and extensibility. *Statistics and computing*, 10, 325–337.

Martínez-Gómez, J.E. & Jacobsen, J.K. (2004) The conservation status of Townsend's shearwater *Puffinus auricularis auricularis*. *Biological Conservation*, 116, 35–47.

McChesney, G.J. & Tershy, B.R. (1998) History and status of introduced mammals and impacts to breeding seabirds on the California Channel and northwestern Baja California Islands. *Colonial Waterbirds*, 21, 335–347.

McIver, W.R., Carter, H.R., Harvey, A.L., Mazurkiewicz, D.M. & Mason, J.W. (2016) Use of social attraction to restore Ashy Storm-Petrels *Oceanodroma homochroa* at Orizaba Rock, Santa Cruz Island, California. *Marine Ornithology*, 44, 99–112.

Olson, S.L. & James, H.F. (1982) Fossil birds from the Hawaiian Islands: Evidence for wholesale extinction by man before Western contact. *Science (Washington)*, 217, 633–635.

Olson, S.L. & James, H.F. (1991) Descriptions of thirty-two new species of birds from the Hawaiian Islands: Part I. Non-Passeriformes. *Ornithological Monographs*, 45, 1–88.

Orians, G.H. & Pearson, N.E. (1979) On the theory of central place foraging. *Analysis of ecological systems,* pp. 155-177. Ohio State University Press, Columbus, Ohio, USA..

Plummer, M. & others. (2003) JAGS: A program for analysis of Bayesian graphical models using Gibbs sampling. *Proceedings of the 3rd international workshop on distributed statistical computing*, p. 125. Vienna, Austria.

Rayner, M.J., Clout, M.N., Stamp, R.K., Imber, M.J., Brunton, D.H. & Hauber, M.E. (2007) Predictive habitat modelling for the population census of a burrowing seabird: a study of the endangered Cook's petrel. *Biological Conservation*, 138, 235–247.

Spatz, D.R., Newton, K.M., Heinz, R., Tershy, B., Holmes, N.D., Butchart, S.H.M. & Croll, D.A. (2014) The biogeography of globally threatened seabirds and island conservation opportunities. *Conservation Biology*, 28, 1282–1290.

Spear, L.B., Ainley, D.G., Hardesty, B.D., Howell, S.N. & Webb, S.W. (2004) Reducing biases affecting at-sea surveys of seabirds: use of multiple observer teams. *Marine Ornithology*, 32, 147–157.

Su, Y.-S. & Yajima, M. (2012) R2jags: A Package for Running jags from R. *R package version 0.03-08, URL http://CRAN. R-project. org/package= R2jags*.

Sydeman, W.J., Nur, N., McLaren, E.B. & McChesney, G.J. (1998) Status and trends of the Ashy Storm-petrel on Southeast Farallon Island, California, based upon capture-recapture analyses. *Condor*, 100, 438–447.

Tasker, M.L., Jones, P.H., Dixon, T. & Blake, B.F. (1984) Counting seabirds at sea from ships: a review of methods employed and a suggestion for a standardized approach. *The Auk*, 101, 567–577.

Taylor, B.L., Martinez, M., Gerrodette, T., Barlow, J. & Hrovat, Y.N. (2007) Lessons from monitoring trends in abundance of marine mammals. *Marine Mammal Science*, 23, 157–175.

Tershy, B.R., Bréese, D. & Alvarez-Borrego, S. (1991) Increase in cetacean and seabird numbers in the Canal de Ballenas during an El Nino-Southern Oscillation event. *Marine ecology progress series*, 69, 299–302.

Troy, J.R., Holmes, N.D., Joyce, T., Behnke, J.H. & Green, M.C. (2016) Characteristics associated with Newell's Shearwater (*Puffinus newelli*) and Hawaiian Petrel (*Pterodroma sandwichensis*) burrows on Kauai, Hawaii, USA. *Waterbirds*, 39, 199–204.

Ver Hoef, J.M. & Boveng, P.L. (2007) Quasi-Poisson vs. negative binomial regression: how should we model overdispersed count data? *Ecology*, 88, 2766–2772.

Wade, P.R. & Gerrodette, T. (1993) Estimates of cetacean abundance and distribution in the eastern tropical Pacific. *Report of the International Whaling Commission*, 43, 477-494.

Watanuki, Y. (1986) Moonlight avoidance behavior in Leach's Storm-Petrels as a defense against Slaty-backed Gulls. *The Auk*, 103, 14–22.

Whitehead, H. (2003) *Sperm Whales: Social Evolution in the Ocean*. University of Chicago Press, Chicago, Illinois, USA.

Tables

Table 5-1. A summary of the posterior distributions from hierarchal exponential regression state space models of four seabird species in the Eastern Tropical Pacific and California Current ecosystems. The population growth rate *r*, abundance in the first ($N_{t=1}$) and last ($N_{t=max}$) survey years are reported as medians and 95% credible intervals (0.025 and 0.975 quantiles) based on 12,000 samples of the posterior distribution. The posterior probability that the growth rate was less than zero, P(r<0) is also reported.

Species	**Region**	***r*** med. (95% CI)	**P(*r*<0)**	$N_{t=1}$ med. (95% CI)	$N_{t=max}$ med. (95% CI)
Townsend's Shearwaters *(Puffinus auricularis)*	Eastern Tropical Pacific	-0.037 (-0.11-0.07)	0.828	83254 (34716-183843)	21333 (1607-267409)
Black-vented Shearwaters (*Puffinus opisthomelas*)	Eastern Tropical Pacific	0.145 (0.04-0.35)	0.007	18052 (478-72741)	324134 (26177-4758189)
	California Current	0.113 (-0.11-0.36)	0.157	5055 (442-20945)	33786 (559-2158082)
Black Storm-petrel (*Oceanodroma melania*)	Eastern Tropical Pacific	0.135 (0.04-0.27)	0.005	207928 (54622-517902)	638248 (23348-20977779)
	California Current	-0.004 (-0.28-0.21)	0.514	934 (168-2902)	575 (3-45181)
Ashy Storm Petrel (*Oceanodroma homochroa*)	California Current	0.07 (-0.16-0.27)	0.218	1474 (194-4570)	4820 (64-237210)

Table 5-2. A summary of the posterior distributions from hierarchal exponential Markov state- space models of four seabird species in the Eastern Tropical Pacific and California Current ecosystems. The population growth rate *r*, abundance in the first ($N_{t=1}$) and last ($N_{t=max}$) survey years are reported as medians and 95% credible intervals based on 12,000 samples of the posterior distribution. The posterior probability that the growth rate was less than zero, P(r<0) is also reported.

Species	**Region**	***r*** med. (95% CI)	**P(*r*<0)**	$N_{t=1}$ med. (95% CI)	$N_{t=max}$ med. (95% CI)
Townsend's Shearwaters *(Puffinus auricularis)*	Eastern Tropical Pacific	-0.08 (-0.6 - 0.45)	0.682	81520 (35048-176727)	6716 (267-60194)
Black-vented Shearwaters (*Puffinus opisthomelas*)	Eastern Tropical Pacific	0.142 (-0.19 - 0.51)	0.106	19374 (1194-69191)	282576 (33163-1249473)
	California Current	0.100 (-0.46 - 0.63)	0.288	5221 (471-20963)	36666 (1143-653879)
Black Storm-petrel (*Oceanodroma melania*)	Eastern Tropical Pacific	0.073 (-0.42 - 0.59)	0.364	153476 (49166-435743)	166782 (11452-1887160)
	California Current	0.022 (-0.66 - 0.65)	0.46	1005 (196-3047)	1804 (64-62117)
Ashy Storm Petrel (*Oceanodroma homochroa*)	California Current	0.088 (-0.47 - 0.65)	0.294	1495 (201-4545)	7167 (502-115218)

Figures

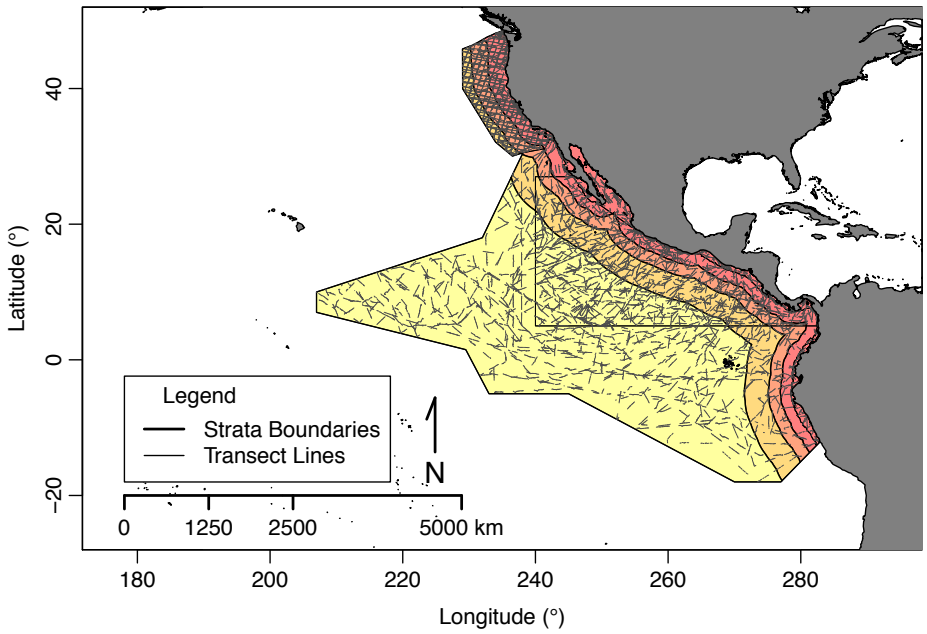

Figure 5-1. Seabird strip survey effort from NOAA ecosystem assessment cruises in the Eastern Tropical Pacific (ETP) and California Current ecosystems (CCE) conducted between 1988 and 2014. The heavier lines show the sampling areas or stratum polygons that were sampled in each ecosystem. The ETP was subdivided into a more densely sampled core stratum roughly corresponding to the Western Pacific Warm Pool, a less densely sampled outer stratum, and a coastal stratum with water depths <1000m. Strata in the ETP and CCE were further sub-divided into four bins based on geodesic distances (<200km, 200-400km, 400-800km, >800km) from the edge of the continental shelf margin (i.e., 200m isobath).

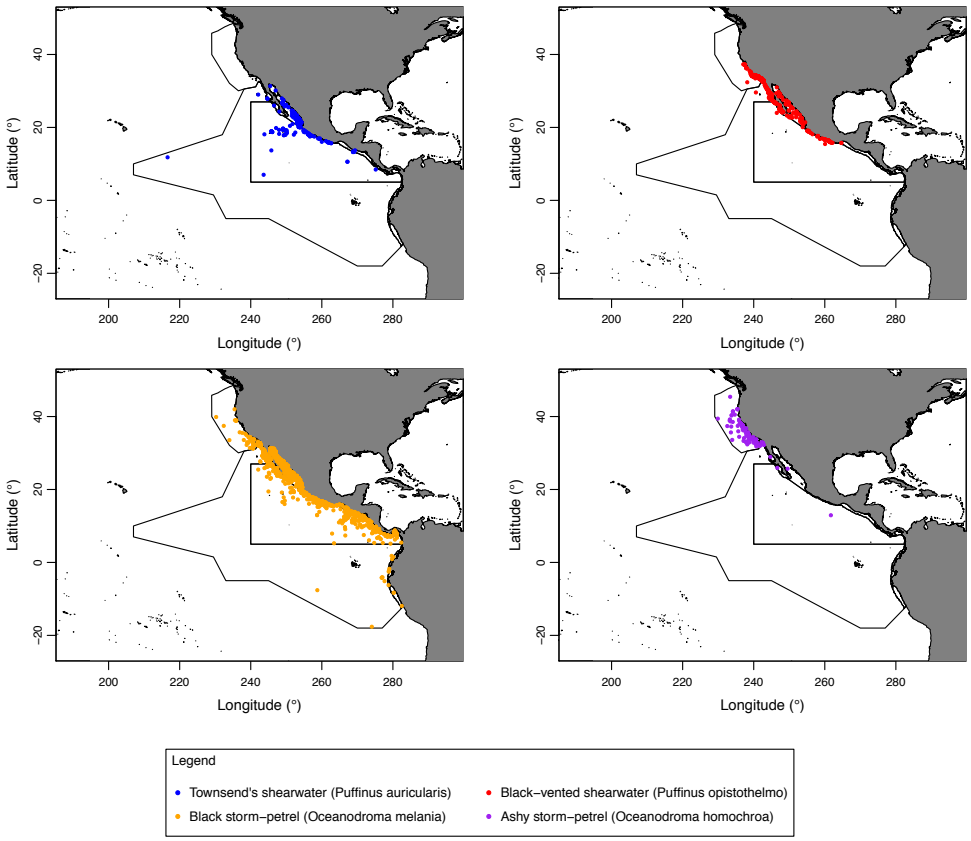

Figure 5-2. Geographic distribution of strip transect observations of a) Townsend's Shearwater (*Puffinus auricularis*), b) Black-vented Shearwater (*Puffinus opisthomelas*), c) Black Storm-petrel (*Oceanodroma melania*), and d) Ashy Storm-petrel (*Oceanodroma homochroa*). The ranges of both *Puffinus opisthomelas* and *Oceanodroma melania* encompassed areas of both the Eastern Tropical Pacific (ETP) and California Current ecosystems (CCE) sampling areas. Separate models of abundance and trends were estimated for these species in the ETP and CCE. Although, *Oceanodroma homochroa* is known to breed (Carter et al. 2016) in both the CCE and ETP, the number of observations was too low (n=4) to effectively estimate abundance or trends in the ETP.

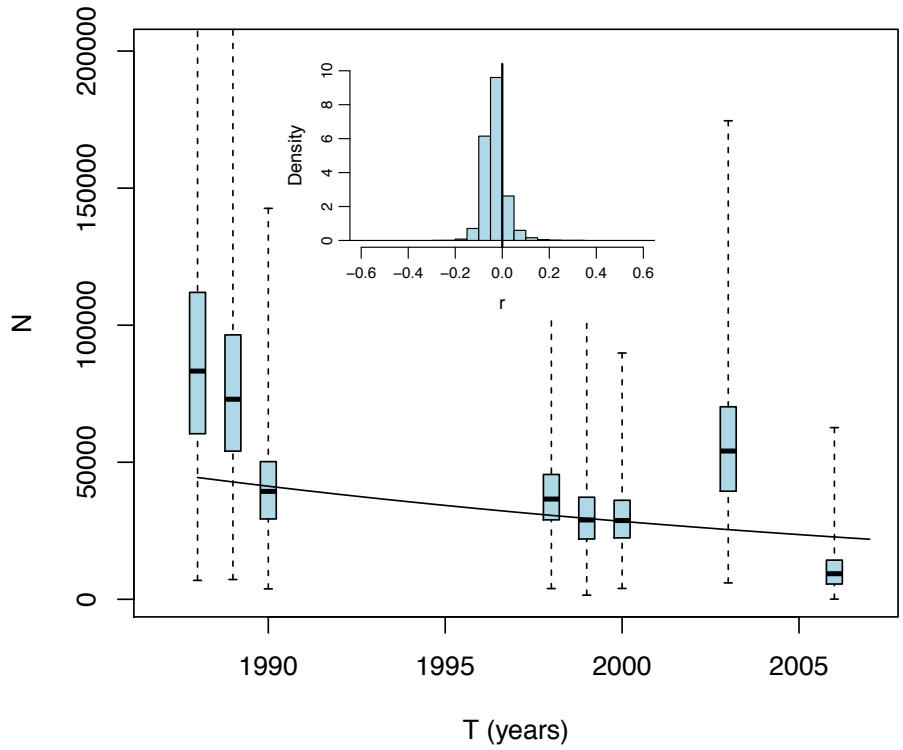

Figure 5-3. Boxplots indicate the distributions of posterior probability samples (n=12,000) from the hierarchal exponential regression state-space model of Townsend's Shearwater (*Puffinus auricularis*) abundance, N_t. The version of the model shown in this plot did not include group size random effects for year or stratum. Posterior estimates are shown in the years when surveys were conducted in the Eastern Tropical Pacific ecosystem (e.g., 1988, 1989, 1990, 1998, 1999, 2000, 2003, and 2006). The trendline shows predictions from the exponential regression model (eq. 2) based on posterior median values of the initial population parameter, N_0, and the growth rate parameter, r. The inset histogram shows the posterior probability distribution of r from this model of *P. auricularis*.

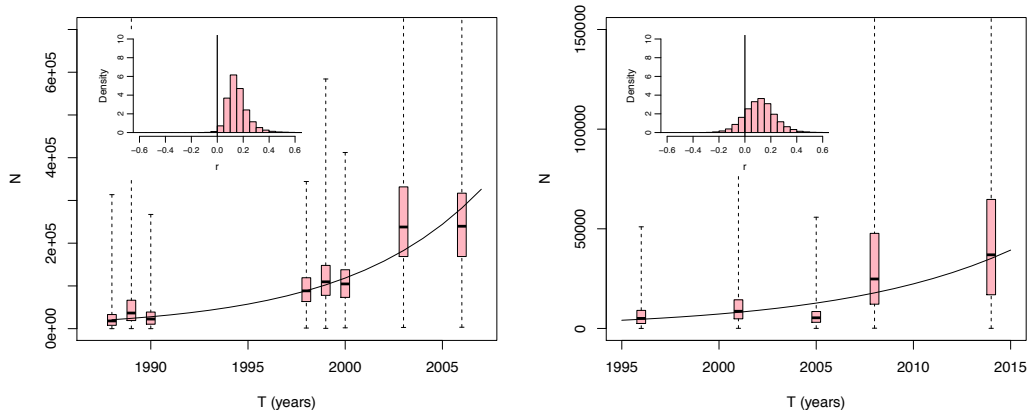

Figure 5-4. Boxplots display posterior probability distributions (n=12,000) of the abundance parameter, N_t, for the Black-vented Shearwater (*Puffinus opisthomelas*). See description of model and trend line in Fig. 3. Posterior estimates are shown for a) the Eastern Tropical Pacific (1988, 1989, 1990, 1998, 1999, 2000, 2003, and 2006) and b) the California Current (1996, 2001, 2005, 2008, and 2014). The inset histogram showing the posterior probability distribution of the growth rate parameter, r.

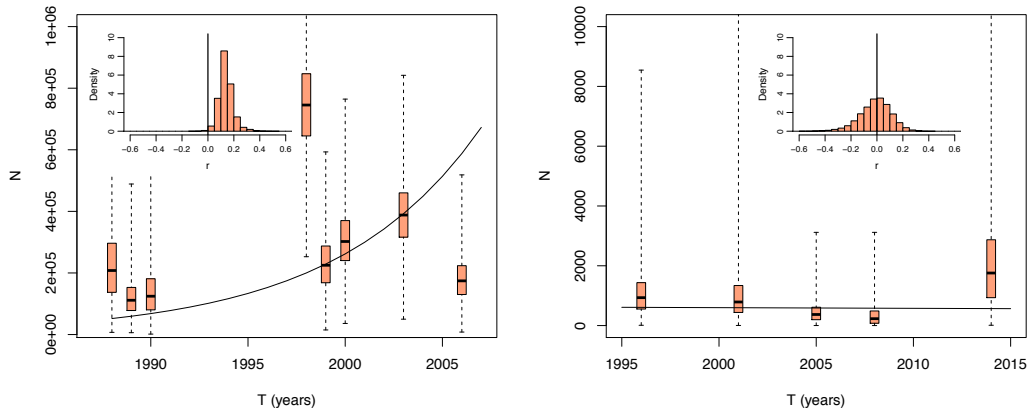

Figure 5-5. Boxplots show the posterior probability distributions (n=12,000) of the Black Storm-petrel (*Oceanodroma melania*) abundance parameter, N_t, from the exponential regression version of the hierarchal state space model, fitted in the Eastern Tropical Pacific (ETP) and California Current (CCE) study areas. See description of model and trend line in Figs. 3 and 4. The posterior probability distributions of the growth rate parameter, r, shown in the inset histograms in panels a and b.

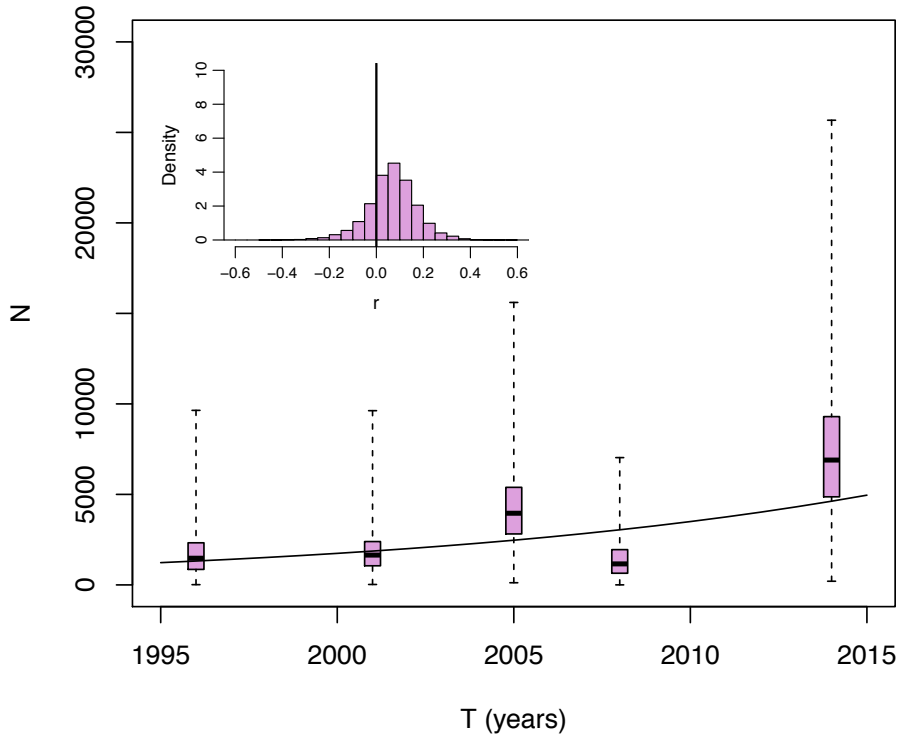

Figure 5-6. Boxplots show the posterior probability distributions (n=12,000) of the abundance parameter, N_t, for the Ashy Storm-petrel (*Oceanodroma homochroa*). See description of model and trend line in Fig. 3. Posterior estimates are shown in the years when surveys were conducted in the California Current ecosystem (e.g., 1996, 2001, 2005, 2008, and 2014). The posterior probability distribution of the growth rate parameter, r, shown in the inset histogram, suggest that *O. homochroa* is undergoing a moderate increase in population within the CCE. The Markov version of this model (not shown) yielded a similar inference of an increase in the population of *O. homochroa* over the study period, though with lower precision.